Rational Design and Synthesis of Novel Firefly Luciferin Analogues for Bioluminescence

by

Chia-Hao Chang

A thesis submitted in partial fulfilment of the requirement for the degree of

Doctor of Philosophy

Department of Chemistry

University College London

Declaration

I, Chia-Hao Chang, confirm that the work presented in this thesis is my own. Where information has been derived from other sources, I confirm that this has been indicated in the thesis.

Signed: .....
Date: .....

Abstract

Firefly luciferin, also called D-luciferin, is the natural compound that bioluminesces in certain beetles and flies. This small molecule has been used for bioluminescence imaging (BLI), for example in preclinical cancer research. This thesis concerns the synthesis of novel D-luciferin analogues and the investigation of their bioluminescence and photophysical properties to explore the development of red shifted and brighter analogues. Chapter one presents the history and background of D-luciferin, and the synthesis of D-luciferin and its analogues. The second chapter presents basic photophysical principles. The third chapter discusses the synthesis of boron-chelated rigid luciferin analogues. The fourth chapter begins by discussing the concept of excited state intramolecular proton transfer (ESIPT) and then moves onto the design and synthesis of potential ESIPT type rigid luciferin based on the skeleton of infra-luciferin (iLH_2). The fifth chapter starts with a brief introduction of BODIPY and then discusses the development of BODIPY luciferin *via* a convergent synthetic route. The sixth chapter gives the basic idea of intramolecular charge transfer (ICT) and then demonstrates the synthesis of an ICT enhanced 4',6'-hydroxybenzothiazole luciferin. The seventh chapter begins with the design of novel V-shaped benzo[1,2-d:4,3-d']bis(thiazole) core structure according to our computational study and then describes the synthesis of V-shaped luciferin analogues *via* an S_NAr reaction. The eighth chapter summarises the results and suggests some future work plans. The final chapter includes experimental procedures and characterisation data. The thesis is fully referenced to the primary literature.

Statement of Impact

Bioluminescence imaging (BLI) is a non-invasive technique for tracing and monitoring biological activities in cells or in live bodies. With firefly luciferase or its mutants, D-luciferin and its analogues gave a wide range of emission from visible light to near-infrared (nIR) region. The nIR imaging market has been increasing from USD 416 million in 2018 and estimated to reach USD 822 million by 2023. Therefore, the firefly luciferin analogues in this thesis are important to academic and industrial areas.

This study explores the synthesis of nIR luciferin analogues and attempts to solve the conflict between emission wavelength and quantum yield. In general, longer wavelength emission has better penetration through tissues, but is often of a weaker light intensity. Balancing emission wavelength and light output intensity is an interesting topic in scientific research. According to basic photophysical principles, the design and synthesis of 4 types of new D-luciferin analogues with various emissions have been delivered. These new types of probes will provide more opportunities for medical and biological researchers to understand microscopic behaviours non-invasively and in real time. Moreover, the new convergent synthetic methods are beneficial to synthesize new bioluminescent compounds in the future.

Acknowledgements

I am very grateful to my supervisor, Prof. Jim Anderson for his guidance, enthusiasm, and encouragement over the past four years. He lets me know how the beauty of organic chemistry is. My PhD research journey was enjoyable, but also full of challenges. Without his inspiration and kind help, no fruitful result could have been achieved. It is really my honor to be his PhD student.

I would like to thank our analytical staffs at UCL: Dr. Abil Aliev for his support with NMR, Dr. Kersti Karu for her help with mass spectroscopy, Dr. Martin Rosillo-Lopez for his help with XPS analysis, and Dr Merina Corpinot for the single crystal X-ray structure determination. I also would like to thank Prof. Helen Hailes, Prof. Alethea Tabor, and Prof. Stefan Howorka groups for providing access and expertise to HPLC and the uv-vis spectrophotometer. Moreover, I would like to thank our collaborator Dr Amit Jathoul at the University of Cardiff for the bioluminescence studies.

Thanks also to the past and current members of Anderson group- Dr. Helen Allan, Dr. Steven Packman, Dr. Oliver Ware, Dr. Xiangyu Zhang, Dr. Aisha Syed, Dr. Boyuan Deng, Anand Patel, Mikhail Pumpianskii, Panagiotis Fikas, Minyan Lyu, Jasper Fairchild, Chia-Hung Huang, Sultaan Yousaf, Helen Chen, Jiayi Zhang, for their friendship. You all really make my life colourful in London.

Finally, I must thank my parents for their unlimited support throughout my education. Importantly, I must express my gratitude to I-Hsuan Wang for her love and backing during my study. It is to them that I dedicate this thesis.

Abbreviations

Ac	= Acetyl
ACQ	= Aggregation caused quenching
Aq.	= Aqueous
Ac_2O	= Acetic anhydride
AMP	= Adenosine diphosphate
ATP	= Adenosine triphosphate
Ar	= Aryl
Bn	= Benzyl
BLI	= Bioluminescence imaging
n-Bu	= *n*-Butyl
t-Bu	= *tert*-Butyl
Bz	= Benzoyl
BPO	= Benzyl peroxide
BOP	= (Benzotriazol-1-yloxytris(dimethylamino)phosphonium hexafluorophosphate)
BRET	= Bioluminescence resonance energy transfer
BODIPY	= Boron dipyrromethene
BioLet	= Bioluminescent enzyme-induced electron transfer
CCD	= Charge-coupled device
CIEEL	= Chemically-initiated electron exchange luminescence
$\emptyset_Y$	= Chemical yield
CTIL	= Charge transfer induced luminescence
DAST	= Diethylaminosulphur trifluoride
DCM	= Dichloromethane
D-cys	= D-cysteine
D-cys·HCl	= D-cysteine hydrochloride
DIPEA	= *N*,*N*-diisopropylethyl amine

DLSA	=5'-*O*-(*N*-(dehydroluciferyl)sulfamoyl)adenosine
D-LH_2	= D-luciferin
DFT	= Density functional theory
DMF	= *N*,*N*-Dimethylformamide
DMAP	= 4-Dimethylaminopyridine
DMSO	= Dimethylsulfoxide
DeT	= Dexter electron transfer
e.e.	= Enantiomeric excess
eT	= Electron transfer
$\emptyset_E$	= Excitation efficiency
ET	= Energy transfer
E_{S1}	= Excitation energy
EDG	= Electron donating group
EDC	= 1-Ethyl-3-(3-dimethylaminopropyl) carbodiimide
EGL	= Energy gap law
EWG	= Electron withdrawing group
ESIPT	= Excited state intramolecular proton transfer
f	= Oscillator strength
HOBt	= 1-Hydroxybenzotriazole
Hoveyda -Grubbs 2nd Gen catalyst	= (1,3-Bis-(2,4,6-trimethylphenyl)-2-imidazolidinylidene)dichloro(*o*-isopropoxyphenylmethylene)ruthenium
HOMO	= Highest occupied molecular orbital
HMRS	= High-resolution mass
HPLC	= High performance liquid chromatography
FRET	= Forster resonance energy transfer
GFP	= Green fluorescent protein
GSIPT	= Ground state intramolecular proton transfer
Im	= Imidazole
IC	= Internal conversion

ICT	= Intramolecular charge transfer
ISC	= Intersystem crossing
LUMO	= Lowest unoccupied molecular orbital
Luc	= Firefly luciferase
LiHMDS	= Lithium bis(trimethylsilyl)amide
LE	= Local excited state
iLH_2	= infra-luciferin
MOMCl	= Methoxymethyl chloride
MEMCl	= 2-Methoxyethoxymethyl chloride
MRI	= Magnetic resonance imaging
*m*CPBA	= *meta*-chloroperoxybenzoic acid
nIR	= Near Infrared
NBS	= *N*-Bromosuccinimide
NIS	= *N*-Iodosuccinimide
OFETs	= Organic field-effect transistors
Para/ortho/meta (*p*-, *o*-, *m*-)	= (1,4)/(1,2)/(1,3)-Substitution on benzene
PG	= Protective group
Ph	= Phenyl
PP	= pyrophosphate
Py	= Pyridine
PyHCl	= Pyridine hydrochloride
PLE	= Pig liver esterase
P/C	= Palladium on carbon
quant.	= Quantitative
$\emptyset$	= Quantum yield
$\emptyset_B$	= Quantum yield of bioluminescence
$\emptyset_f$	= Quantum yield of fluorescence
rac	= Racemic
rt	= Room temperature
SET	= Single electron transfer
S_NAr	= Nucleophilic aromatic substitution

SAR	= Structure-activity relationship
S_0	= Ground state
S_1	= Excited state
T_1	= Triplet state
TBAF	= Tetra-*n*-butylammonium fluoride
TBDMS/TBS	= *tert*-Butyldimethylsilyl
TD-DFT	= Time-dependent density functional theory
TEA	= Triethylamine
TLC	= Thin layer chromatography
THF	= Tetrahydrofuran
Tf_2O	= Trifluoromethanesulfonyl anhydride
TfOH	= Trifluoromethanesulfonic acid
TFA	= Trifluoroacetic acid
TFAA	= Trifluoroacetic anhydride
THF	= Tetrahydrofurane
TIPS	= Triisopropylsilyl
Trt	= Trityl, triphenylmethyl
UV	= Ultraviolet
WT	= Wide type
XPS	= X-ray photoelectron spectroscopy

Table of Contents

1. Introduction

1.1 History of Bioluminescence

Bioluminescence is considered as a “cold light” which is generated by bioluminescent organisms rather than normal heat radiation such as sun, and fire from combustion. Therefore, bioluminescence has been a fantastic and mysterious phenomenon observed by human beings for a long time. The cold luminescence could be found in living organs, decaying leaves, dead fish, sea water and so on. In the past, people believed that the emission of cold light from living creatures had various purposes. For example, to attract a mate, prey, or to startle predators for different survival reasons. [1] This natural phenomenon has been recorded and observed in ancient Greece, China, Africa and South America. In the 19th century, the famous biologist Charles Darwin (1809-1882) observed both bioluminescence and bioelectricity in marine species and wrote: [2]

“*The luminous organs which occur in few insects, belonging to widely different families, and which are situated in different parts of the body, offer under our present state of ignorance, a difficulty almost exactly parallel with that of the electric organs*”

Moreover, by the role of natural selection in the evolution of bioluminescent creatures, Darwin also questioned why certain natural species are luminous but their close relatives are not. In this point of view, bioluminescence is a fascinating natural phenomenon and there remain a lot of mysteries for scientists to solve.

In 1916, a French pharmacologist Raphaël Horace Dubois (1849-1929) demonstrated the explanation of the modern bioluminescence mechanism. [3] An important experiment called the “luciferin-luciferase experiment.” was conducted. Dubois extracted luminous materials from fireflies and divided them into two portions. Both portions exhibited bioluminescence. One portion was kept cool and the other was boiled. The cold extract still showed bioluminescence, but the heated one did not. Once the cold extract had stopped glowing, the boiled extract was cooled and mixed with the cold extract. The light was generated again. This key result supported the hypothesis that at least two components were involved in the chemical reaction leading to bioluminescence. We now understand that the light was produced by mixing heat-stable “luciferin” and heat-unstable “luciferase” from

luminous organisms together. Dubois also found that luciferin was able to give visible emission when small amounts of oxidising reagents, such as H_2O_2, or permanganate, were added without luciferase. This phenomenon is known as chemiluminescence.

The 2008 Nobel Prize winner, Osamu Shimomura, was a leading pioneer in the chemical and biochemical aspects of bioluminescence. [4] He developed the techniques of chemical and biochemical analyses to determine the structures of green fluorescent proteins (GFP). Nowadays, with sophisticated equipment such as NMR, X-ray diffraction, cryo-electron microscopy and mass spectrometers, more and more protein structures have been solved accurately. A greater understanding of bioluminescence has led to many new applications for scientific studies.

1.2 Different Luciferins

Bioluminescent organisms have been found in around 800 genera of *ca*. 13 phyla and probably over 10,000 species in the world. To date, the chemical structures of natural luciferins and luciferases have been isolated and identified for luciferin chemistry research and other applications. [5] According to luciferin chemistry, several types of luciferin have been categorized: firefly luciferin (**1**) also named D-luciferin (D-LH_2) with yellow emission was structurally elucidated in 1961. [6] Coelenterazine-type luciferin (**2**) emitting blue light were isolated from crystal jellyfish. [7] Krill luciferin (**3**) and dinoflagellate luciferin (**4**) that also emit blue light were found in the sea and they share similar skeletons which have a tetrapyrrole structure. [8] *Latia* luciferin (**5**) isolated from a fresh-water snail gives shining green light. [9] Fungal luciferin (**6**) [10] and earthworm luciferin (**7**) [11] have yellow green light output. Cypridina luciferin (**8**) was found in deep-sea fish and gives a blue emission. [12] Bacterial luciferin (**9**) has a long chain and emits blue light (Figure 1). [13] Each group utilizes a unique bioluminescent system to produce various wavelengths of light. Among different luciferin-luciferase substrates, firefly luciferin (**1**) has been regarded as the most important luciferin with wide applications, especially in the life sciences, as an analytical tool for bioluminescence imaging.

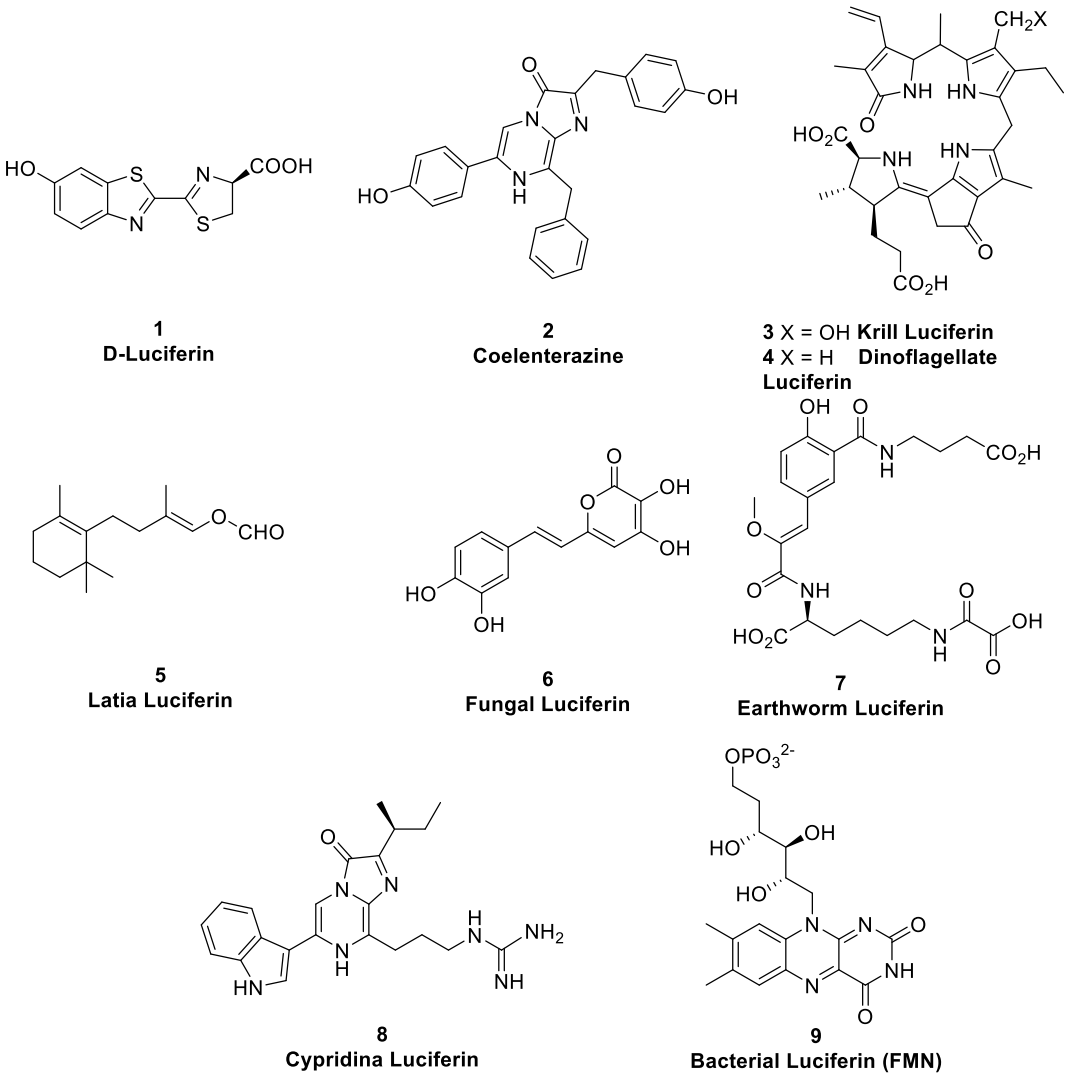

Figure 1 Different Luciferins

1.3 The Mechanism Studies of Firefly Bioluminescence in 1950s

Bioluminescence is the generation of visible light *via* a series of chemical reactions in luminous living organism. In 1947, McElroy supposed that adenosine triphosphate (ATP) mixed with Mg^{2+} was the main energy source providing bioluminescent emission. [14] However, this hypothesis was not complete. According to Plank's Law, the photon energy of yellow firefly emission (about 550 nm) requires around 52 kcal/mol. That was far higher than standard ATP hydrolysis which is equal to 7 kcal/mol. The latter research showed that oxygen is one of the factors to drive the chemical reaction because oxidation is highly exothermic, which gives enough energy to overcome the energy barrier.

The firefly luciferase (Luc) from *Photinus pyralis* was isolated by crystallization in 1956. [15] The single crystal X-ray structure and the electrophoretic pattern suggested that the

luciferase protein was homogeneous, and it could bind to luciferin and adenosine monophosphate (AMP), which was generated from ATP hydrolysis as a stoichiometric product. After several years, the luciferase was characterised as a monomer with a single binding site with a mass calculated to be around 62 kDa. In 1957, 9 mg of crystalline firefly luciferin was obtained from 15,000 fireflies. The neutral solution showed an absorption peak at 327 nm and fluorescence emission at 530 nm, which is close to the bioluminescence emission at 550 nm from *in vitro* studies. As ^{1}H NMR spectroscopy was unavailable at that time, the detailed chemical structure of luciferase was not identified until 1996. In 1996, the crystal structure of firefly luciferase (Figure 2) was defined at 2.0 Å resolution by Conti *et al*. [16] The protein is folded into two domains which included a C-terminal domain (yellow) portion and an N-terminal domain (blue, purple and green). The C-terminal was distinct from the N-terminal by a wide cleft. The N-terminal domain consisted of two β-sheets (blue and purple) and a β-barrel (green). The β-sheets are flanked by α-helices to generate an αβαβα five layered structure.

Figure 2 The Structure of Firefly Luciferase [16]

In 1961, the structure of firefly luciferin (**1**) was further verified by total synthesis reported by Emil White and Frank McCapra at Johns Hopkins University. [6] The structure could

have two optical configurations D (-) and L (+). Both forms could undergo the adenylation with ATP and then release of pyrophosphate (PP) in the presence of Mg^{2+}, oxygen and luciferase. However, only the D-luciferin showed bioluminescence.

After these studies, more research started to focus on the mechanism of light output. In general, the reaction is an oxidation process where luciferin molecules are oxidized by various kinds of luciferases under oxygen with metal ions such as Mg^{2+}, Fe^{2+}, Ca^{2+}. [17] Taking firefly luciferin as an example (Scheme 1), the reaction involves two steps: first, the luciferase and Mg^{2+} facilitates an adenylation where D-luciferin reacts with ATP to give the D-LH_2-AMP ester **10**, second, the adenyl ester **10** is oxidized by O_2 to produce the excited state oxy-luciferin **11***. The electronically excited oxyluciferin returns to its ground state **11**, resulting in the emission of visible light. [18]

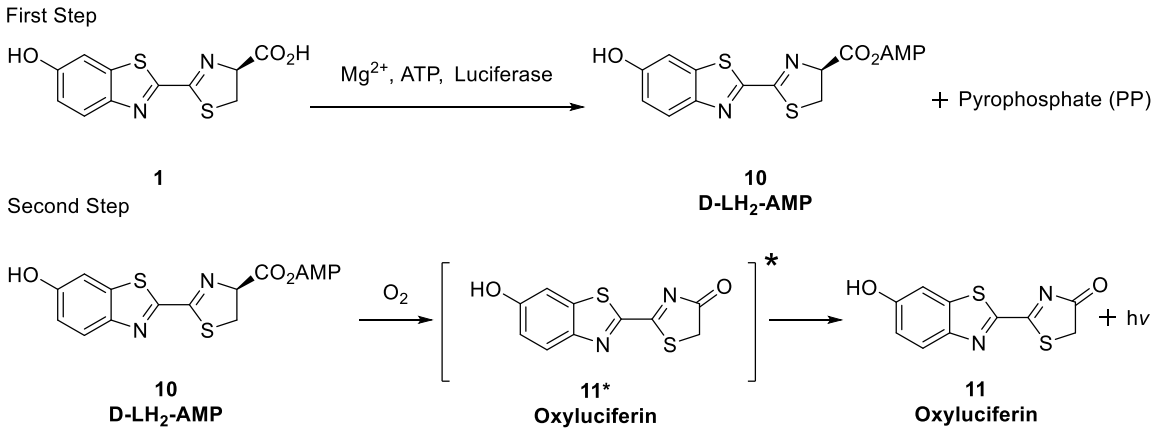

Scheme 1 The Mechanism of Firefly Bioluminescence

The second step of the oxidation was interesting and investigated further. The original mechanism was proposed by White and co-workers according to their chemiluminescence model studies. [19] Once D-LH_2-AMP **10** was produced, the proton at C_4 was deprotonated by a base from the luciferase to form an enolate. The anion **12** reacts with oxygen to give a peroxy anion species **13** which rapidly attacks the carboxyl group followed by the elimination of AMP to generate the high energy unstable dioxytenone intermediate **14** (Scheme 2 (a)). However, White's mechanism was problematic because the peroxide was formed from the spin forbidden $^1O_2$ rather than $^3O_2$. In 2015, a radical mechanism was proposed by Branchini and co-workers (Scheme 2 (b)). [20] Reaction of anion **12** with $^3O_2$ gave the peroxide anion **13** *via* single electron transfer (SET). This mechanism is more acceptable because the electron transfer proceeds without electron spin change.

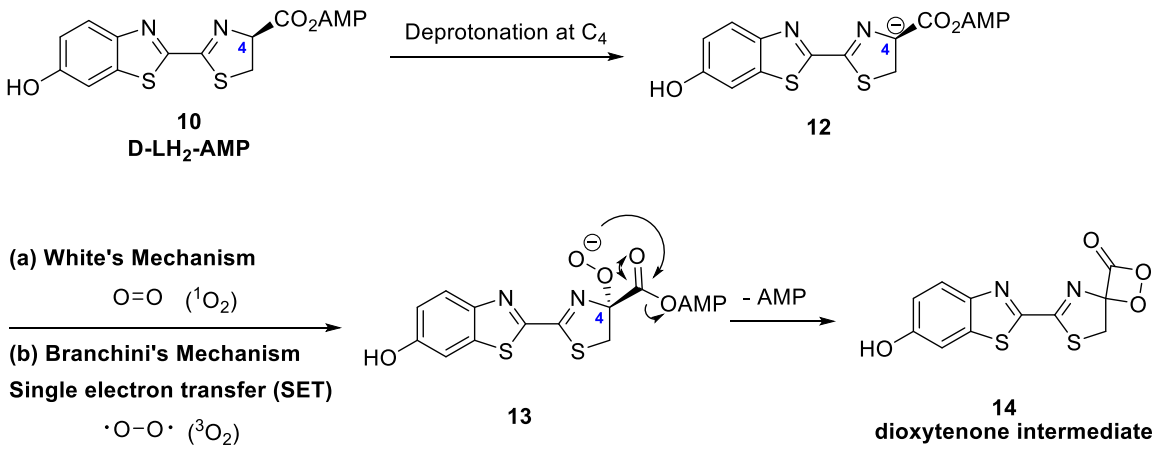

Scheme 2 The Generation of High Energy Dioxytenone Intermediate

To date, there are two generally accepted decarboxylation mechanism for the collapse of the dioxytenone **14**. The first mechanism (Scheme 3) is step-wise chemically-initiated electron exchange luminescence (CIEEL). [20] The anion dioxytenone **15** is an electron rich species from which an intramolecular electron transfer (eT) takes place from the phenolate moiety to the 4-membered ring O-O sigma anti-bonding orbital to give a radical ion product **16** which then undergoes a back-electron transfer to yield the excited phenolate oxyluciferin **11a**. It is possible that the highly reactive radical **15** undergoes side reactions such as spontaneous proton transfer.

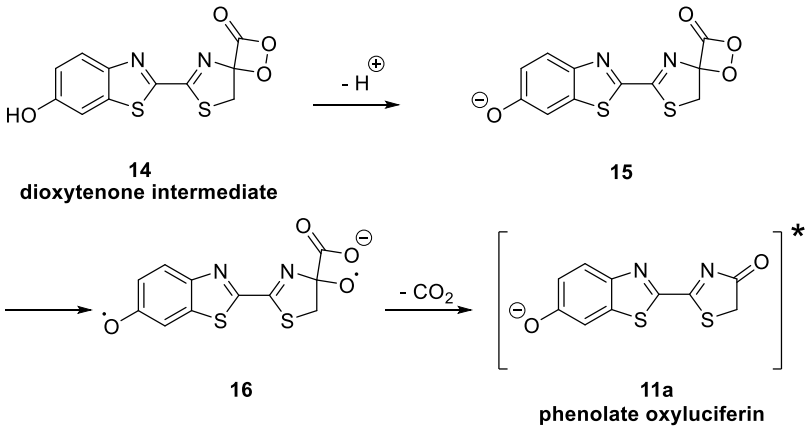

Scheme 3 The Mechanism of CIEEL

The second mechanism (Scheme 4) is called charge transfer induced luminescence (CTIL). The anion compound **15** directly decomposes without a radical anion intermediate. [21]

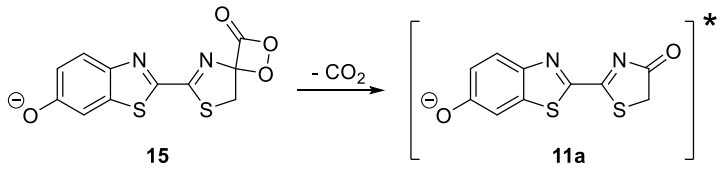

Scheme 4 The Mechanism of CTIL

In addition, it is worth noting that D-LH$_2$-AMP **10** can be oxidised by O_2 to form its dehydro product **17** (Scheme 5) and H_2O_2. [22] This dehydro-luciferyl-adenylate **17** is a notorious inhibitor of the luciferase. As a result, the efficiency of bioluminescence emission was decreased by this unwanted dark reaction.

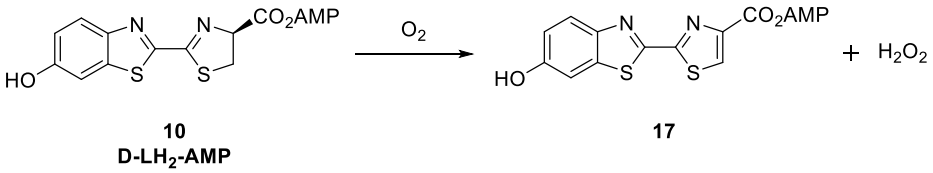

Scheme 5 The Formation of Inhibitor **17**

1.4 Emission Wavelength Modulation

Different beetles exhibit different wavelengths of emission even though they use the same chemical compound D-luciferin. The D-luciferin has a wide range of bioluminescence emission ranging from yellow green to red light (530 – 635 nm). [23] These various colours of light arise from the surrounding environment in the active pocket of the luciferases, the temperature, pH value, and metal ions such as Hg^{2+}, Zn^{2+}, and Cd^{2+}.

In 1989, Wood and co-workers reported that the emission of D-luciferin could be tuned by four types of luciferases. [24] By reverse transcription from mRNA from the bioluminescent click beetle, *Pyrphorus plagiophthalamus*, eleven complementary DNA clones based on four clone codes were produced. When these DNAs were expressed in *Escherichia coli,* four distinguishable bioluminescence emissions (green (λ_{max} = 546 nm), yellow-green (λ_{max} = 560 nm), yellow (λ_{max} = 578 nm), and orange (λ_{max} = 593 nm)) were observed (Figure 3). The amino acid sequences of each of the luciferases are 95 to 99 percent similar, but about 48 percent was different from the native firefly, *Photinus pyralis* luciferase.

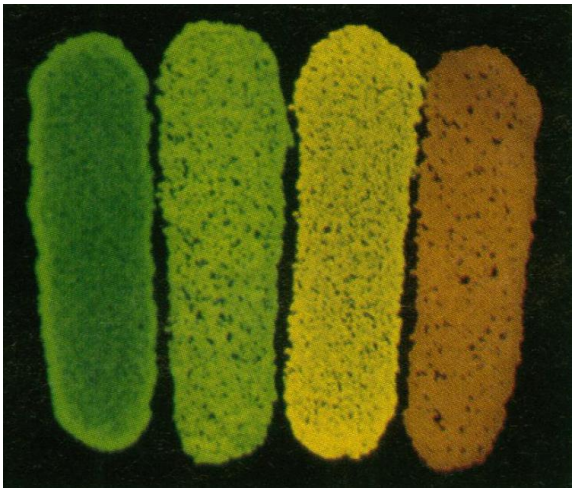

Figure 3 The Clone DNAs Expressed in *Escherichia coli* [24]

Additionally, different emissions can come from the different protonated or deprotonated states of excited state oxyluciferin. At different pH values, oxyluciferin has six possible structures **11**, **11a**, **18**-**21** (Figure 4). [25] The phenol group on the benzothiazole can be deprotonated to form an anion and the ketone on the thiazoline ring has enol tautomers which also can be deprotonated to give enolate structures. The high energy structure **21** is also possible. The emission maxima of these oxyluciferins have been studied by computational and theoretical researchers. The common conclusions suggested that the

emission wavelengths were affected by the active pocket of luciferases which could stabilize either of the exited state oxyluciferins.

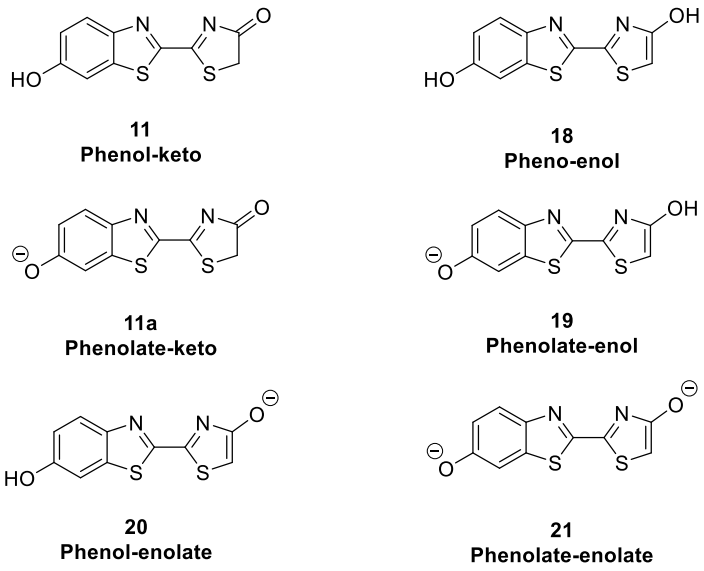

Figure 4 Six States of Oxyluciferin

1.5 Bioluminescence imagine *in-vitro* and *in-vivo*

In 1995, Contag and co-workers demonstrated that bioluminescent bacteria could be used to monitor cells in live mice by utilizing an ultrasensitive charge-coupled device (CCD) camera. [26] Based on this technique, non-invasive bioluminescence imaging (BLI) has attracted much attention in biogenetics, microbiological process investigations and disease tracing such as growth of tumours.

In preclinical cancer research, BLI with firefly luciferase (Luc) and D-luciferin is regarded as a standard method to trace biological processes including the localization, detection and the quantification of cells non-invasively and in real time within living system. [27] Mouse cells are labeled with the genes for tumor cells that have been transduced with the genes for luciferase expression. These substrates can not only be applied to *in-vitro* cell assays but can also be injected back into the rodent for *in-vivo* imaging. Upon tumor growth, luciferase is expressed, and the diseased cells can be traced and quantified by BLI upon injection of luciferin. The light output is proportional to the amount luciferase generated and in turn the number of transduced cancer cells (Figure 5).

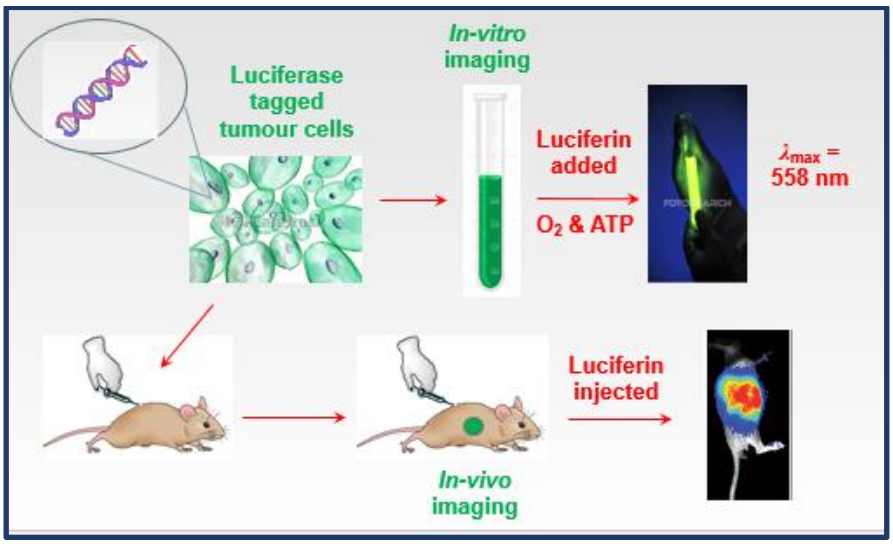

Figure 5 The Bioluminescence imaging in live mice [27]

Although fluorescent pigments are regarded as a powerful tool and have been used as diagnostic probes in bioimaging, they still have some limitations and drawbacks in practical research. [28] For example, external excitation, such as by lasers, is required to generate excited state molecules. Phototoxicity depends on the dose of the incident light. This process can generate free radicals resulting in cell damage. Additionally, extra radiation leads to unnecessary light scattering resulting in poor resolution of bioimaging. There are many species such as haemoglobin in living samples that can autofluorescence upon light irradiation, thus confusing the desired fluorescence signal. Aggregation of fluorescent proteins can form a potential toxicity *in vivo* study or induce cytotoxic effects. Connecting a fluorescent dye to a protein and sugar might lead to fluorescence quenching.

Unlike fluorescent probes, bioluminescence imaging does not need additional incident radiation such as x-ray, laser and ultra-visible light to generate light. Therefore, it has an extremely high signal to noise ratio. Due to its less harmful characteristics, non-invasive bioluminescence imaging (BLI) using luciferins provides a practical approach to cancer imaging and disease detection.

Unfortunately, the BLI techniques using D-luciferin have several limitations. For example, the visible light emission (λ_{max} = 558 nm) is easily absorbed and scattered by haemoglobin and tissue, which means that the D-luciferin-Luc substrate is not suitable for deep-tissue imaging. Using D-luciferin as a substrate for BLI leads to a restriction of image resolution and signal due to attenuation and scatter. As a result, the development of BLI with more-

red shifted emission has been regarded as a possible solution to resolve this problem and has received much attention (Figure 6). [29] This has been achieved to some extent by mutating luciferases and/or modifying the structure of the luciferin.

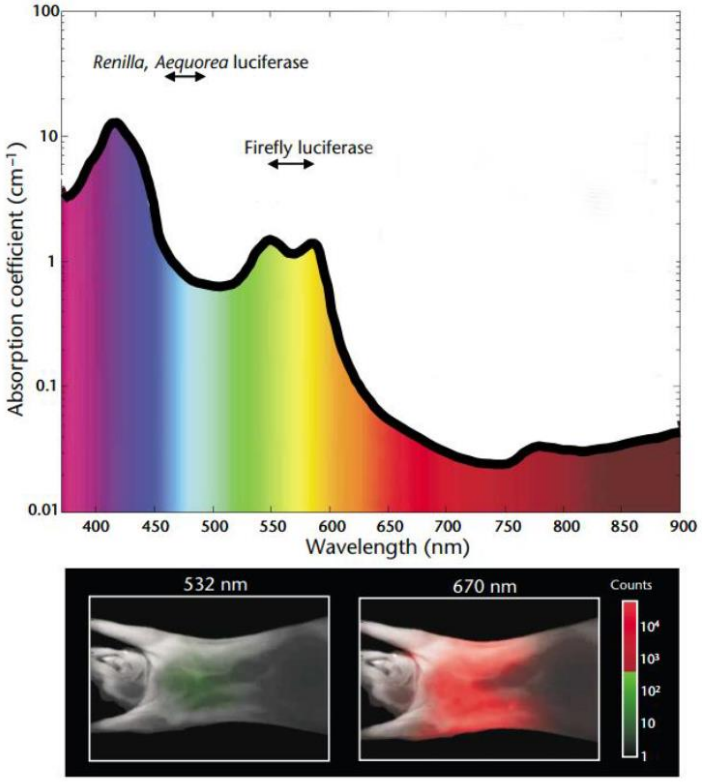

Figure 6 Different Bioluminescence Wavelengths Passes through Mouse Bodies [29]

Moreover, radioactive studies using ^{14}C-labelled D-luciferin substrates demonstrated the inhomogeneous bio-distribution in rodents because D-luciferin showed modest cell permeability. [30] In addition, some organs such as brain have poor uptake of bioluminescence probes *in vivo*. [31] As a result, a large amount of D-luciferin was required for *in vivo* experiments. These limitations restrict the applications of BLI using D-luciferin as the probe.

1.6 Firefly Luciferase Mutants

Early stage bioluminescence studies used natural luciferases-like enzyme from mealworm *Tenebrionidae* (λ_{max} = 619 nm) or rail-road worms *Phengodidae* (λ_{max} = 623 nm). [32] The rapid development of genetic techniques enabled mutant luciferases to be investigated for enhanced properties. Over the years, many artificial luciferases have been designed and produced (Table 1). [33] These unnatural luciferases with D-luciferin were able to give light output at different wavelengths successfully. Moreover, some of these luciferases showed better thermal stabilities and greater solvent tolerance than firefly luciferase (Luc). However, these mutants still could not push the emission wavelength to near infrared (nIR) region which is a crucial key point for tissue penetration, because of the inherent emission properties of oxyluxiferin reaching its limit. In view of this point, the development of novel nIR D-luciferin analogues is regarded as an alternative area for deeper tissue BLI.

Mutant Luciferases	Properties
Q283R, S284G	$\lambda_{max} \approx$ 605 nm in *Escherichia coli*.
S293P	$\lambda_{max} \approx$ 600 nm in *Escherichia coli*. $\lambda_{max} \approx$ 560 nm at pH = 8.0 $\lambda_{max} \approx$ 610 nm at pH = 5.5
F14R/ L35Q/ V182K/ I232K/ F465R	6 times more thermal stable than Luc at 43 °C
T214A/ I232A/ F295L/ E354K	2 times more thermal stable than Luc at 35 °C
T214A/ A215L/ I232A/ V241I/ G246A/ F250S/ F295L/ E354K	$\lambda_{max} \approx$ 546 nm, 40 times more thermal stable than Luc at 37 °C
T214A/ A215L/ I232A/ S284T/ F295L/ E354K	$\lambda_{max} \approx$ 610 nm, 34 times more thermal stable than Luc at 37 °C
I423L/ D436G/ L530R	At low ATP levels, 10 times more luminescence activity than Luc
R337Q/ R337M	Good thermal stability and resistance to trypsin degradation
S239T/ D357Y/ A532T	Stable in $CHCl_3$, Surfactants, EtOH

Table 1 Synthetic Mutants of the North Firefly

1.7 Synthesis of D-luciferin and Relevant Analogues

Since firefly luciferase (Luc) has been mutated by genetic editing technology to give suitable characteristics for bioluminescent expression, the organic synthesis for the development of novel D-luciferin analogues became a new hot spot in bioluminescence research.

1.7.1 Biosynthesis of D-Luciferin

The biosynthesis study of D-luciferin was first reported by Okada and co-workers in 1974. [34] The injection of ^{14}C-labelled 2-cyano-6-hydroxybenzothiazole (**22**) into the lantern of firefly, *Luciola cruciata* gave the corresponding ^{14}C labelled D-luciferin (Scheme 6). This result supposed that ^{14}C labelled compound **22** might be the precursor of D-luciferin in the biosynthetic process. This result was interesting because 2-cyano-6-hydroxybenzothiazole has not been detected directly in fireflies. Therefore, there is still uncertainty whether compound **22** is involved in the biosynthetic pathway.

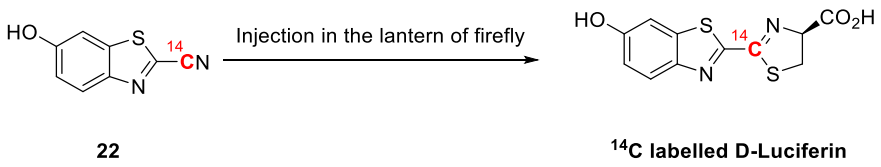

22 **^{14}C labelled D-Luciferin**

Scheme 6 ^{14}C labelled Study in The Biosynthetic Study in 1974

In 2016, Knaie and co-workers published the first one pot biosynthesis of firefly luciferin in a buffer without enzymes or synthetic reagents (Scheme 7). [35] This gave a clue that 1,4-benzoquinone (**23a**) could be a precursor in the biosynthetic pathway. In 2018, the same group detected the key intermediate deuterium labelled 2-cysteinyl hydroquinone (**25**) which was synthesized by reacting deuterium labelled 1,4-benzoquinone (**23b**) with L-cystine (**24**). [36] Synthetic compound **25** was injected into living firefly, *Luciola lateralis*, which then produced racemic luciferin *in vivo*. When deuterated molecule **25** was treated with L-cysteine *in vitro*, only L-luciferin (**26**) was isolated. Decarboxylation of compound **25** was a key step for the formation of the benzothiazole ring in the biosynthetic route. These studies suggested that firefly luciferin could be developed from benzoquinone *via* non-enzymatic synthesis. However, the reasons for racemization of luciferin *in-vivo* should be further investigation.

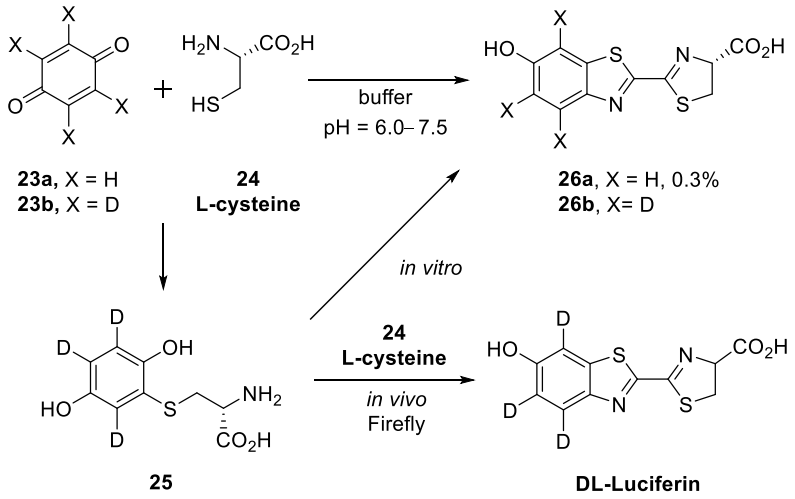

Scheme 7 Biosynthetic Pathway by 1,4-benzoquinone (**23a**)

1.7.2 Total Synthesis of D-Luciferin and Its Derivatives

The first total synthesis of D-luciferin was demonstrated by White and co-workers in 1961.[6] The synthetic route consisted of 9 steps and gave an overall yield of 9% (Scheme 8). The reaction started from *p*-anisidine (**27**) which was condensed with ethyl oxalate to produce amino oxoacetate **28** in 58% yield. Treatment of compound **28** with phosphorous(V) pentasulfide (P_2S_5) gave thioamide **29**. The ester of **29** was saponified by NaOH to form the corresponding carboxylic acid and the formation of the benzothiazole ring was achieved by treatment with $K_2Fe(CN)_6$ *via* oxidative cyclisation. The carboxyl group of benzothiazole **30** was esterified with diazomethane to give the methyl ester **31** which was further condensed with anhydrous NH_3 to afford the amide **32** in 40% yield over 4 steps. Dehydration of amide **32** with $POCl_3$ gave the nitrile benzothiazole **33** in 62% which was followed by demethylation with pyridine hydrochloride (Py·HCl) to yield 2-nitrile-6-hydroxyl benzothiazole (**34**) in 62% yield. Finally, the condensation of nitrile **34** with D-cysteine gave the desired D-luciferin (**1**) in 94%. The condensation between D-cysteine and suitable nitrile moieties to construct a thiazoline ring is a vital step which can be found in the synthesis of most D-luciferin analogues.

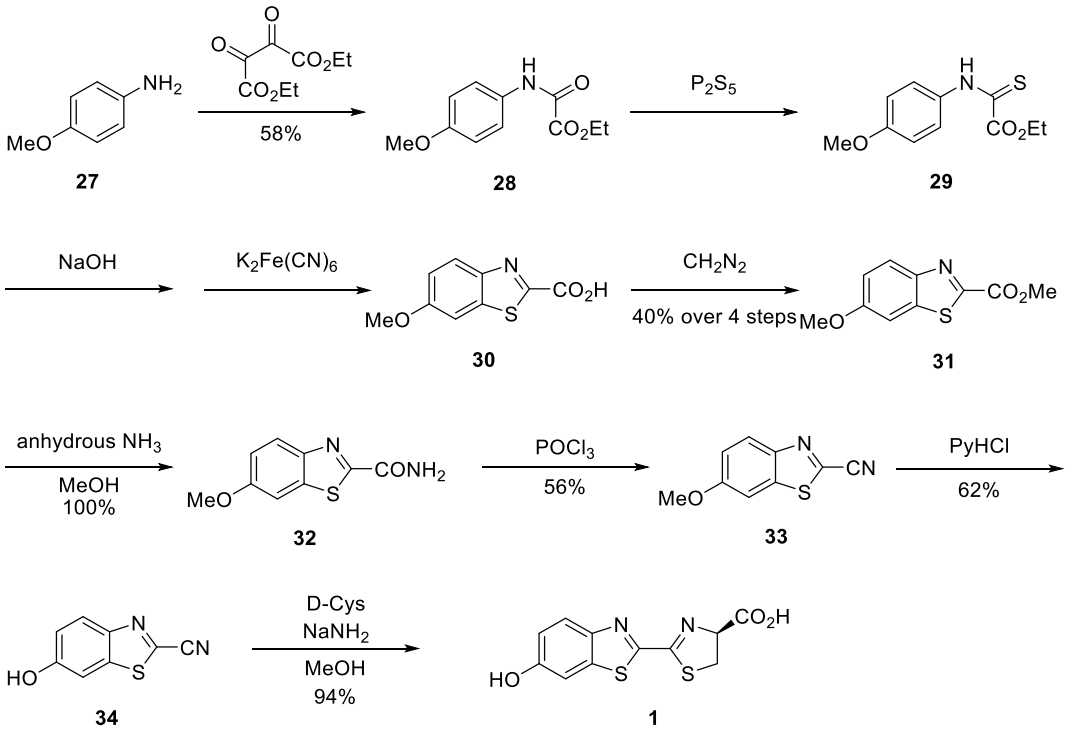

Scheme 8 The First Total Synthesis of D-luciferin Reported in 1961

The synthesis of 2-nitrile benzothiazole derivatives was challenging. The original method (Scheme 8) required 6 steps to deliver the key intermediate 2-cyano-6-methoxy-benzothiazole (**33**). In 2000, Besson and co-workers reported that Appel's salt chemistry [37] for the preparation 2-cyanobenzothiazole derivatives was applicable and rapid. [38] Condensation of *o*-bromo primary aromatic amine **35** with 4,5-dichloro-1,2,3-dithiazolium chloride (**36**, Appel's salt) gave readily stable bromo compound **37** in 61% yield *via* nucleophilic attack. Under CuI catalysis and microwave conditions, the corresponding 2-cyano benzothiazole rings **38** was formed in 70% yield.

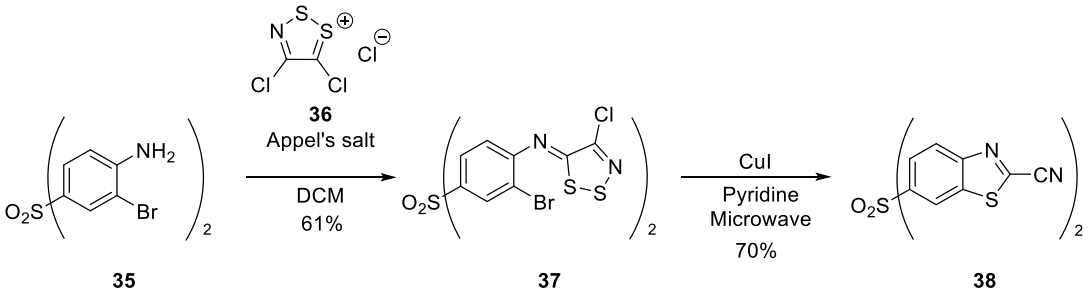

Scheme 9 The New Synthesis Towards 2-Cyanobenzothiazole Product

Using the Appel's salt chemistry, Prescher's group in 2012 reported a novel method to synthesize the important intermediate **33** *via* C-H activation (Scheme 10). [39] To begin with, *p*-anisidine (**27**) was treated with Appel's salt to form the expected dithiazole **39** in 99%. Treatment of compound **39** with excess DBU gave thioamide **41** in 97% yield and then 2-cyano-6-methoxybenzothiazole (**33**) could be achieved in 87% yield using a palladium and copper (I) mediated cyclisation. This new synthesis is 4 steps shorter in comparison to the original route reported by White in 1916.

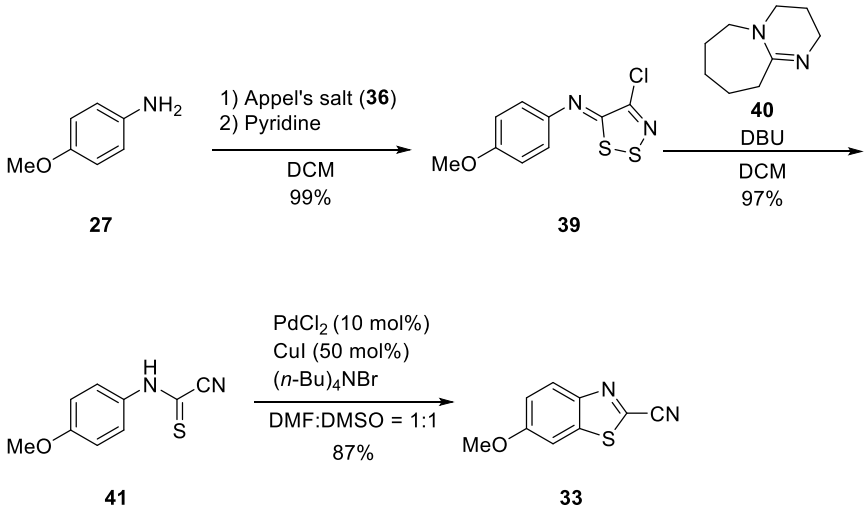

Scheme 10 The Synthesis of Compound **33** via C-H Activation

In 2015, Prescher's group demonstrated a one pot condensation/fragmentation synthesis which boosted the formation of 2-nitrile-6-hydroxybenzothiazole (**34**) (Scheme 11). [40] This improved route allowed access to D-luciferin precursor **34** on 20 g scale without any isolation during the process. Through the same intermediates as before (Scheme 10), but in a one pot reaction, *p*-anisidine (**27**) was condensed with Appel's salt (**36**), followed by pyridine at rt, then heated in sulfolane at 180 °C, and then mixed with pyridine hydrochloride (Py·HCl) in order to give the desired product **34** in 51% overall yield. This route gave D-luciferin in 44% overall yield.

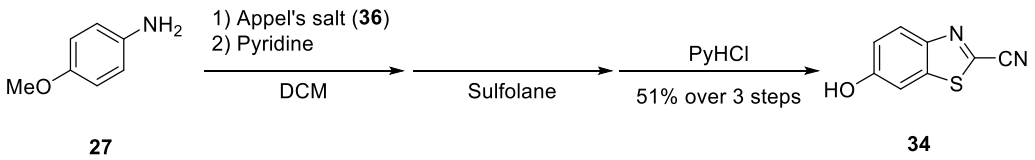

Scheme 11 A One Pot Synthesis of 2-Nitrile-6-hydroxybenzothiazole **34**

With the precursor 2-nitrile-6-hydroxybezothiazole (**34**) in hand, D-luciferin (**1**) and its potassium salt **42** could be synthesized in high yield (Scheme 12). The nitrile **34** was treated with D-cysteine hydrochloride (D-Cys·HCl) and K_2CO_3 in a co-solvent system of MeOH:H_2O = 2:1 at rt for 30 mins. After acid workup by HCl, the free carboxylic acid form of D-luciferin was afforded. The thiazoline ring of D-luciferin could also be furnished when the solvent system was changed to MeCN: H_2O = 4:1 at rt for 20 mins. This allowed the potassium salt **42** to precipitate out due to the less polar co-solvent system. The potassium salt **42** can give different bio-activities and bioluminescent results for *in vitro* and *in vivo* studies compared to **1**. [40]

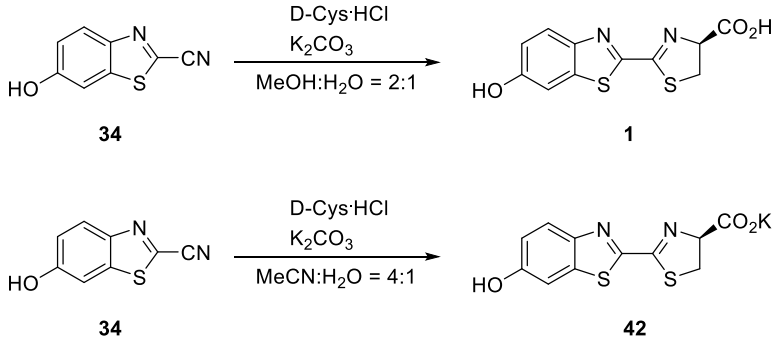

Scheme 12 The Synthesis of D-luciferin **1** and Its Potassium Salt **42**

D-Luciferin methyl ester **43** was first synthesised by White in 1971. [19b] D-luciferin esters have been employed in living mice and cells for cancer studies. The ester group can be hydrolyzed by specific enzymes *in vivo* and *in vitro*. However, the location of hydrolysis and the enzymes that facilitate hydrolysis have not been unambiguously assigned. [41] In addition to bioluminescence, the D-luciferin esters can give chemiluminescence. In the presence of alkaline DMSO in an oxygen rich atmosphere, light can be emitted without firefly luciferase. The methyl ester **43** was formed in quantitative yield by treatment of D-luciferin (**1**) with TMS-diazomethane in a co-solvent system MeOH:toluene = 9:1 (Scheme 13). [42]

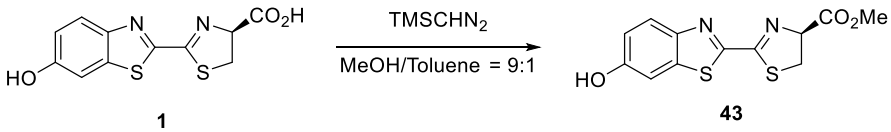

Scheme 13 The Synthesis of D-luciferin Methyl Ester **43**

1.7.3 The Synthesis of D-Luciferin Analogues

Soon after the first total synthesis of D-luciferin, the stereospecificity of D-luciferin bioluminescence was studied by Seliger in 1961. [6] Following the same synthesis of D-luciferin (Scheme 8), but by using L-cysteine, L-luciferin was prepared and was found to act as an inhibitor of the luciferase enzyme and did not emit light. The structure of L-luciferin **26** has been depicted in Scheme 7 with its deuterated form. There have since been many modifications of D-luciferin (Figure 7). [43]

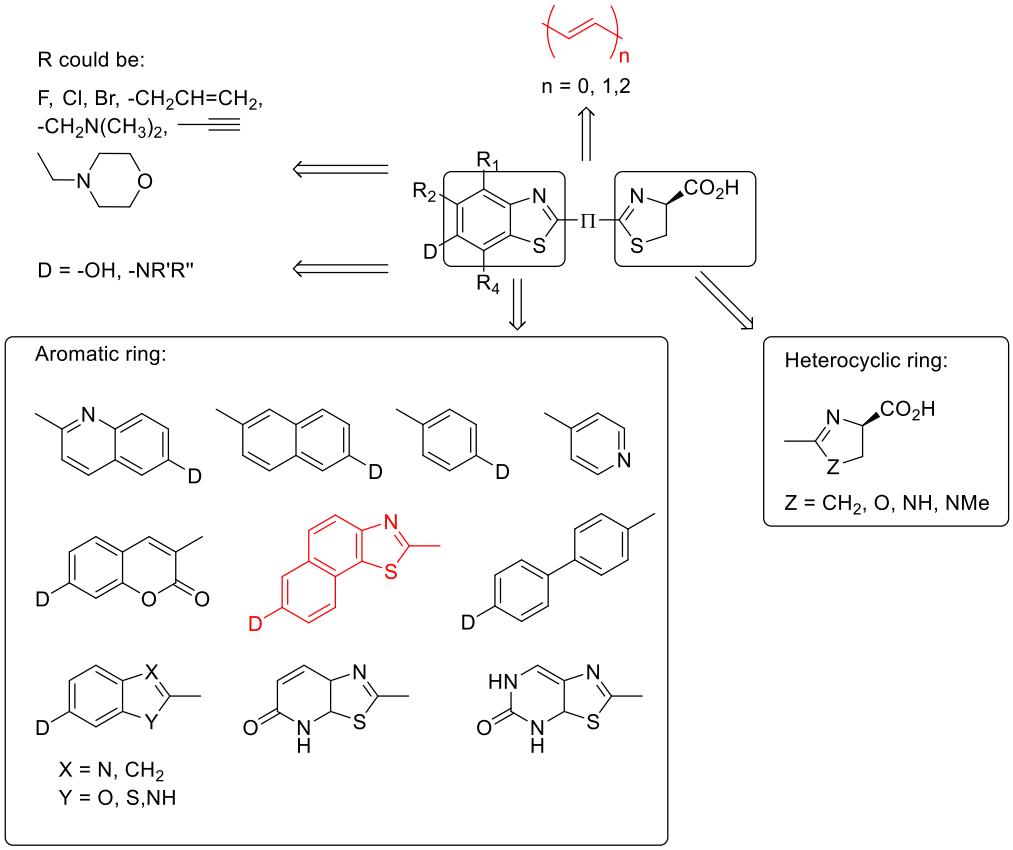

Figure 7 Published Modifications for Luciferin Analogues

The first modification was substitution of the hydroxyl group by different amino groups, halogens, alkyl, alkenyl and alkynyl groups. Second, the replacement of the benzothiazole or thiazoline ring by the combinations of heterocyclic or aromatic moieties opened a new synthetic field to construct luciferin analogues. Third, the introduction of additional conjugation between the benzothiazole and thiazoline moieties has been achieved. However, most of these modifications (Figure 7) showed only slight wavelength shifts (< 100 nm) compared to D-luciferin. The synthesis and relevant bioluminescent properties of these analogues are detailed in the following context.

In 1965 White's group reported several D-luciferin analogues (Figure 8) produced by following their synthetic route to D-luciferin. [44] Condensation of the corresponding nitrile compounds with D-cysteine at the final step gave *o*-methoxyluciferin **44**, 5,5'-dimethylluciferin **45**, decarboxyluciferin **46** and pyridyl luciferin **47**. However, none of the analogues showed bioluminescence. We can understand that compound **46**, without the carboxyl group, is unable to form the excited state ketone through the oxidation mechanism with luciferase.

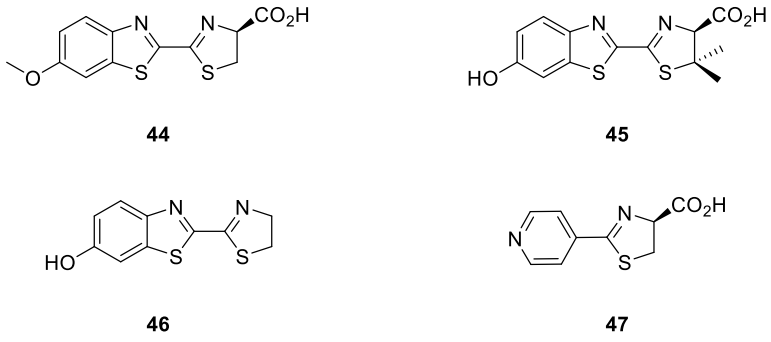

Figure 8 D-Luciferin Analogues in 1965

In 1966, the development of novel D-luciferin analogues based on a structure-activity relationship (SAR) was investigated by White and co-workers. [45] In this study, the hydroxyl group(s) were positioned on different carbons of the benzothiazole ring (Figure 9). Only luciferin **51** showed "red light", none of the other analogues **48**-**50** were bioluminescent. The actual wavelength of the "red light" of compound **51** was not reported.

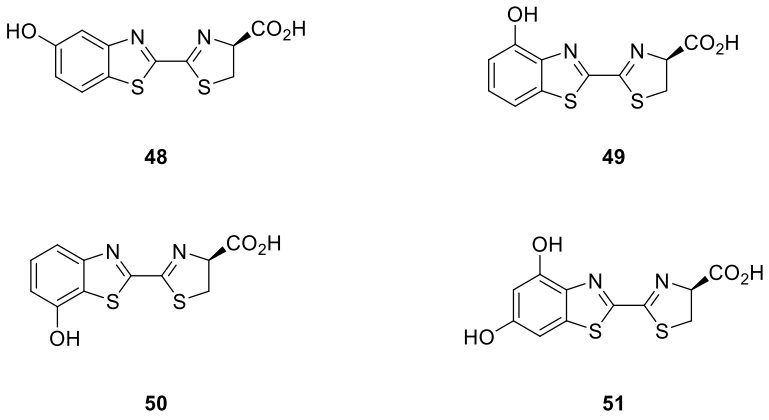

Figure 9 Different Hydroxyl Luciferins in 1966

1.7.3.1 First Modification: The Synthesis of Substituted Analogues

White and coworkers also discovered that the 6-hydoxyl group of D-luciferin can be replaced by an amino group (Scheme 14) to give red-shifted bioluminescence over 590 nm, but with a much lower intensity of light output, about 90% less than D-luciferin. [46] By reacting 2-chlorobenzothiazole derivatives **52a-c** with NaCN, the nitrile precursors **53a-c** were obtained. These were condensed with racemic cysteine to yield the corresponding amino-luciferins **54a-c**. Amino-luciferin **54a** is pH independent giving a bioluminescent emission at 605 nm with *P. plagiophthalamus dosal* organ luciferase. Other *N*-acetylamino analogues did not emit light with the luciferase. This study opened extensively a new concept to synthesize novel amino-luciferins which has been ongoing for the last 50 years.

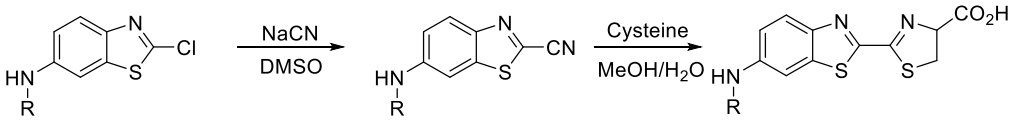

52a, R = H
52b, R = CH_3O
52c, R = CF_3O

53a, R = H
53b, R = CH_3O
53c, R = CF_3O

54a, R = H
54b, R = CH_3O
54c, R = CF_3O

Scheme 14 The Synthesis of Amino-Luciferins **54a-c** in 1966

In 2010, Reddy successfully synthesized alkyl (Scheme 15) and cyclic (Scheme 16) amino-luciferins showing bioluminescence emissions λ_{max} > 600 nm. [47] Starting material **52a** is an important intermediate for the development of new amino-luciferins. Preparation of 6-amino-2-chlorobenzothiazole (**52a**) could be delivered in two consecutive steps involving nitration and reduction from 2-chlorobenzothiazole (**55**). Reductive alkylation of **52a**

followed by S_NAr reaction with KCN and then condensation with D-cysteine provided **MeNHLH$_2$**, **58a** (609 nm) and **6'-Me$_2$NLH$_2$**, **58b**. These *N*-methylated amino luciferins gave bioluminescent emissions at 609 and 623 nm with railroad worm beetle luciferase *Pxh*Re.

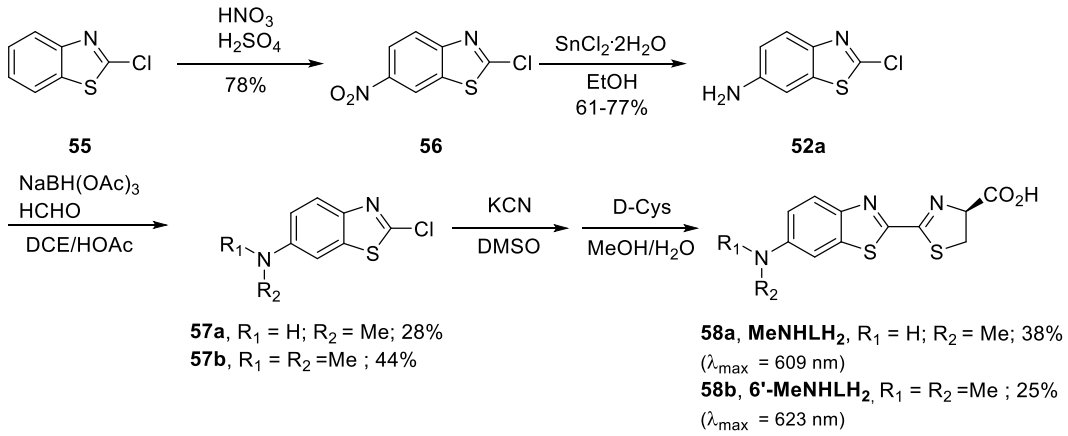

Scheme 15 Synthesis of MeNHLH$_2$ and 6'-Me$_2$NLH$_2$

The conformationally restricted fused cyclic amine chlorobenzothiazole core structure **64a** was prepared by protection of **59** with trifluoroacetic anhydride (TFAA), reduction of the nitro group, formation of the benzothiazole, diazotisation of the 2-amino group and substitution by chlorine, and reductive deprotection of the TFA protecting group. Reductive alkylation of **64a** gave another *N*-methylated intermediate **64b**. Introduction of the 2-cyano group to precursors **64a** and **64b** *via* nucleophilic substitution, followed by condensation of D-cysteine provided the cyclic analogues **CycLuc1 65a** (599 nm) and **CycLuc2 65b** (607 nm) with wild type luciferase. Although the emissions of cyclic amino-luciferins were slightly blue-shifted than alkyl amino luciferins **MeNHLH$_2$** (**58a**) and **6'-Me$_2$NLH$_2$** (**58b**), their intensity of light outputs were 5.7-fold higher. As a result, the restriction of conformational flexibility around the aryl-nitrogen bond is a method to enhance the bioluminescence quantum yield.

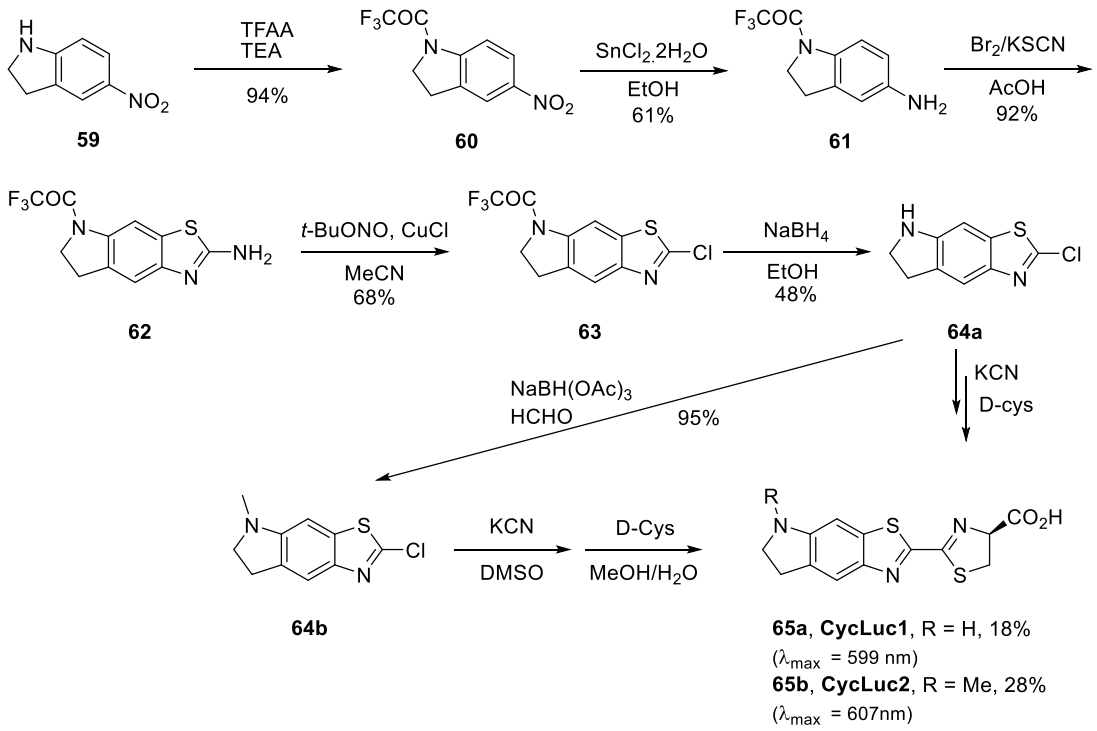

Scheme 16 The Synthesis of Cyclic Amino Luciferins **CycLuc1** and **CycLuc2**

In 2014, Mofford and co-workers designed more cyclic amino-luciferins to create orthogonal luciferin assays (Scheme 17). [48] Their syntheses started from amines **66-69** to give the corresponding cyclic amino-luciferins **CycLuc3-10** by following the same general synthetic routes which have been described (Scheme 16). The secondary amines and *N*-methylated final products required 7 and 8 steps to achieve respectively. Many of these analogues provided more red-shifted bioluminescence emission than previously reported **CycLuc1** and **CycLuc2** with mutant firefly luciferases. Among them, **CycLuc10** gave the most red-shifted emission (642 nm) in this study.

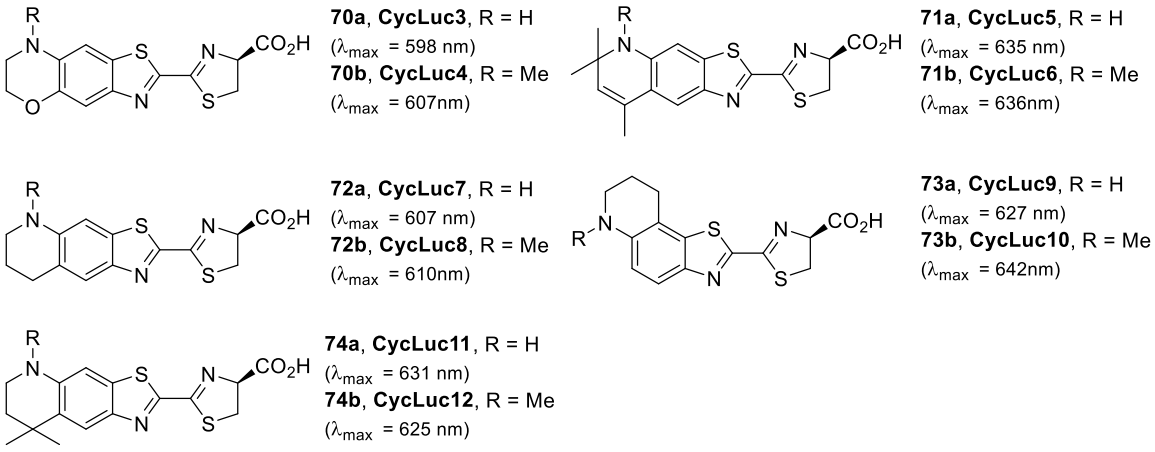

Scheme 17 The Synthesis of Cyclic Aminoluciferins **CycLuc3-10**

In 2011, Takakura and co-workers reported an alternative alkylation method to modify amino moiety of 6-amino-2-cyanobenzothiazole (**53a**). [49] Reductive alkylation with the appropriate aldehydes in the presence of H_2SO_4 and $NaBH_4$ in THF gave the *N*-functionalised benzothiazoles **75a-d** which were converted into their corresponding amino-luciferins **76a-d** by condensation with D-cysteine (Scheme 18). All derivatives gave bioluminescence over 600 nm. The length of the alkyl chains contributed to cell membrane permeability by introduction of hydrophobic or hydrophilic functional groups for outside or inside cellular studies.

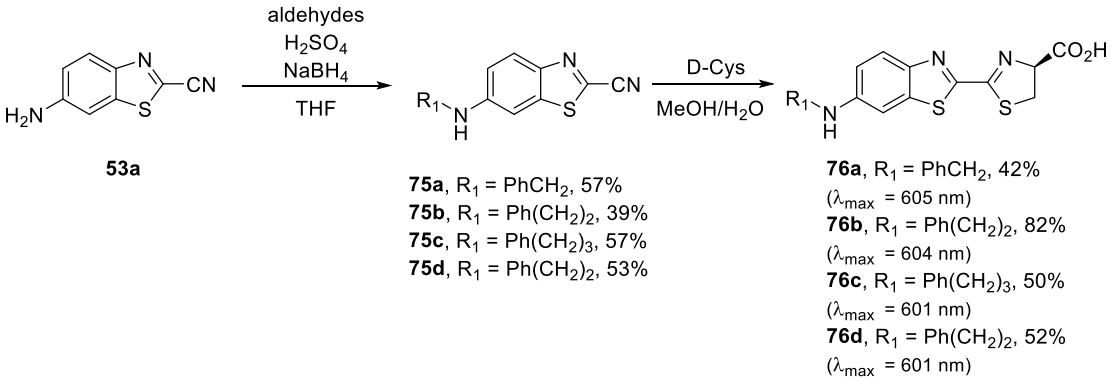

Scheme 18 The Synthesis of Alkylated Amino-luciferins **76a-d**

In this study, it is worthy to note that a cyanine (Cy5) nIR dye was linked to the amino-luciferin skeleton *via* this successful alkylation approach. It was hoped to increase the emission wavelength by Bioluminescence Resonance Energy Transfer (BRET). The nIR emission of **Cy5 COOH-AL 77** (Figure 10) was 673 nm and was proven to be due to BRET. It suggested that the highly efficient energy transfer from AL to Cy occurred (Figure 10). This result indicates that amino-luciferin can give the non-radiative energy to excite the BRET acceptor and could be used for a range of functional fluorophores to give BRET emissions for *in vivo* and *in vitro* studies.

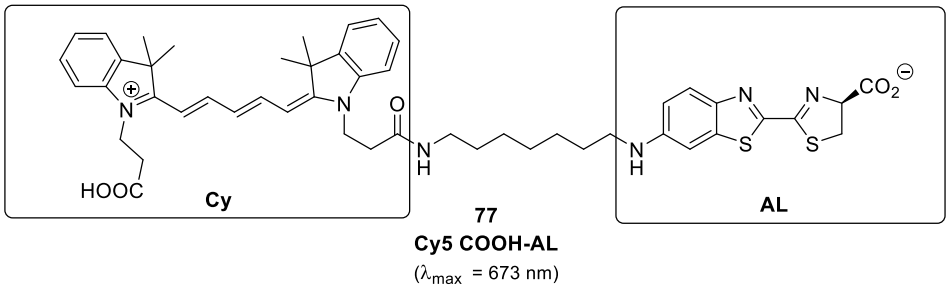

Figure 10 The structure of **Cy5 COOH-AL**

In 2013, Kojima and co-workers created a series of BRET-based luciferins by linking amino-luciferin **54a** to nIR fluorophores (Figure 11) in an attempt to lengthen the emission wavelength. [50] All the novel compounds **78-82** showed nIR emission over 650 nm. The luciferin **Cy7 indolenine Me-AL 82** showed the longest intramolecular BRET emission around 800 nm. However, its light intensity was only 0.65% of amino luciferin **54a**. This was the first report of nIR bioluminescence obtained in living mice and living cells with natural firefly luciferase from *Photinus pyralis*. However, some drawbacks were observed in that the compounds have poor *in-vivo* bioavailability due to the size of the molecule and its non-polar nature, and it had to be administrated intravenously.

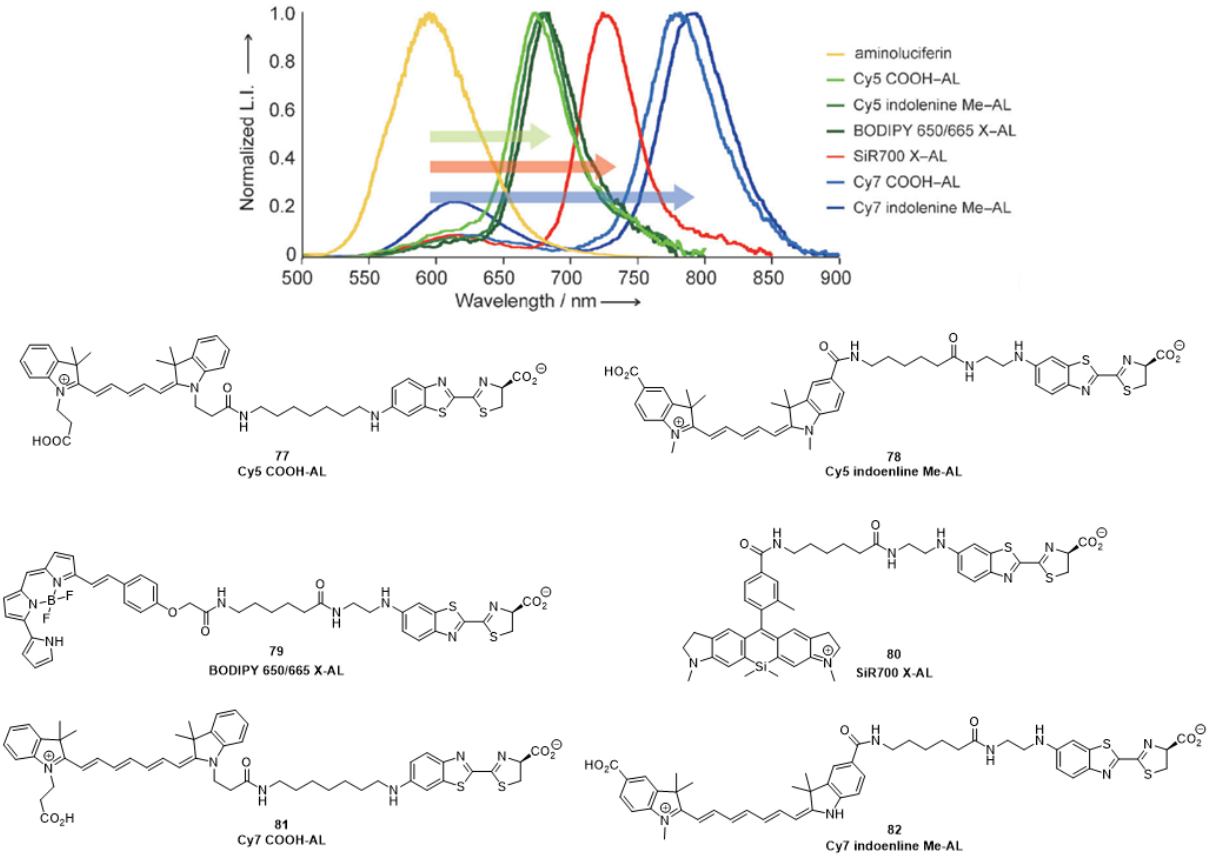

Figure 11 BRET-Based Amino-luciferins

In 2017, Wu and co-workers reported *N*-cycloalkylated amino-luciferins **83a-c** for deep bioluminescence imaging. [51] These compounds were prepared efficiently by the reductive amination of key intermediate **53a** with the corresponding cyclanones and condensation with D-cysteine (Scheme 19). These derivatives were found to be suitable candidates for *in vitro*, *in cellulo*, and *in vivo* studies. Compared with amino-luciferin **54a** (591 nm), a small bathochromic effect (603 nm and 607 nm) was found in these *N*-cycloalkylated luciferins with native firefly luciferase. In the *in vivo* study, **cybLuc 83b** was more sensitive to detect brain tumors in the living mice and could be extended to other deep tissue imaging.

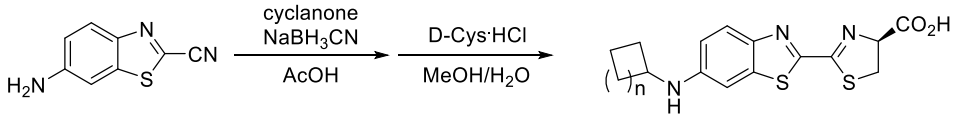

53a

83a, **cybLuc,** n=1 (λ_{max} = 603 nm)
83b, **cypLuc,** n=2 (λ_{max} = 603 nm)
83c, **cyhLuc,** n=3 (λ_{max} = 607 nm)

Scheme 19 The Synthesis of *N*-cycloalkylated Amino-luciferins **83a-c**

In 2017, a rapid synthesis of amino-luciferin analogues was reported by Sharma and co-workers. [52] Their two steps synthesis was devised to quickly explore synthetic 6'-substituted luciferin analogues containing amine or alkylamine donors. A wide variety of amines could be introduced to 6-bromo-2-cyanobenzothiazole (**84**) *via* a Buchwald-Hartwig reaction [53] with xantphos as a ligand (Scheme 20). The amine groups of the precursors **85-90** included morpholine derivative **85a**, thiomorpholine derivative **85b**, thiomorpholine dioxide derivative **85c**, Boc-piperazine derivative **85d**, arylamino derivatives **86a-l** and **87a-b**, amide derivatives **88a-e**, 2-oxazolidone **89,** benzyl carbamate **88f** and, urea derivative**s 88g-h**, and secondary amines **90a-c**.

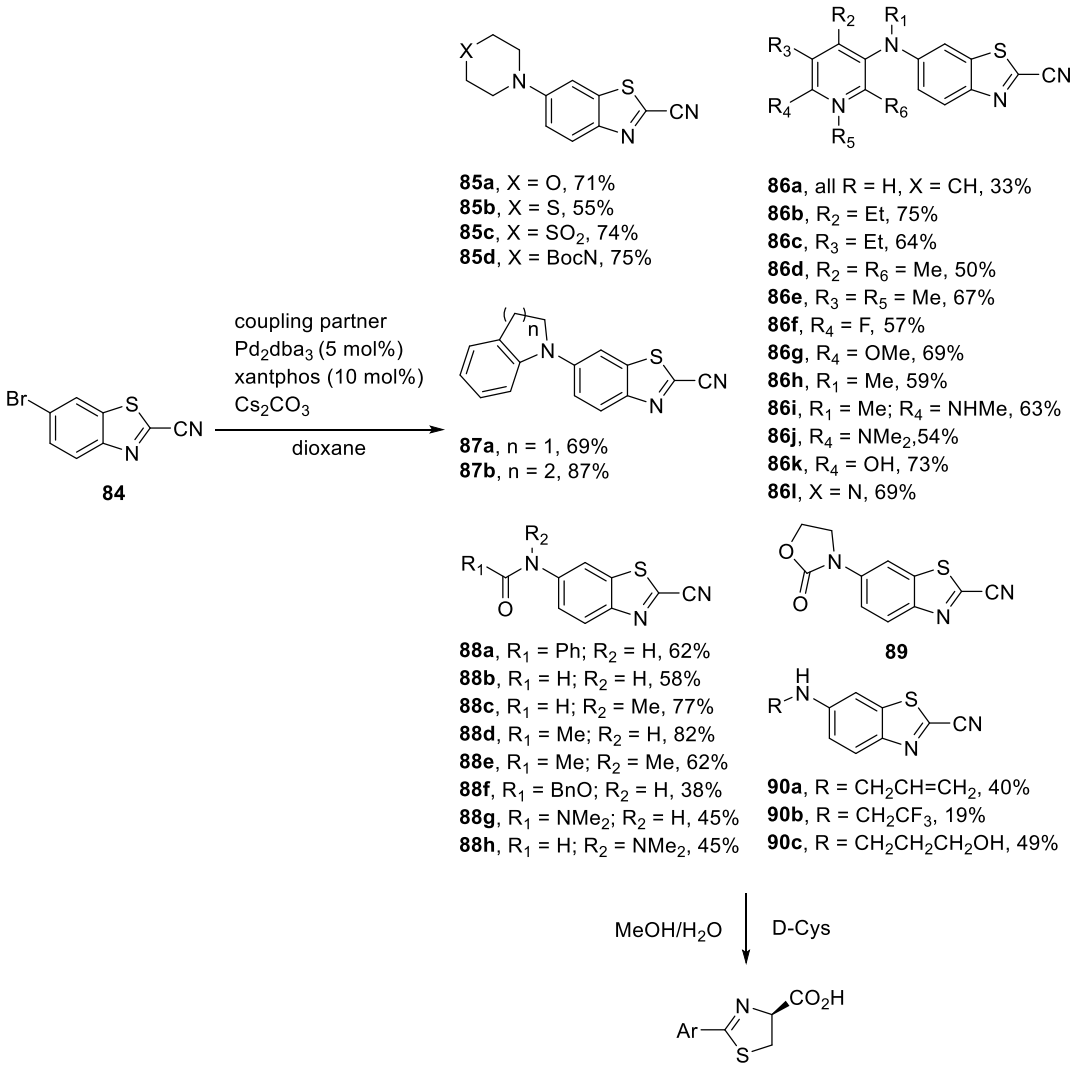

Scheme 20 Rapid Synthesis of Amino-luciferins *via* Buchwald-Hartwig Amination

In this study, it also mentioned the preparation of 6'-thiol-substituted-2-cyanobenzothiazole intermediates for the development of thiol-luciferin analogues. Replacement of fluoride at 6' position by methanethiol or thiophenol provided thiol moieties **92a-b** *via* S_NAr. The thiol-benzothiazoles could be further oxidized by Oxone (Potassium peroxymonosulfate) or *meta*-chloroperoxybenzoic acid (*m*CPBA) to give the corresponding sulfoxide **93a** and sulfone **93b** derivatives (Scheme 21). These groups of new nitriles **85-90** and **92-93** were further condensed with D-cysteine to give their amino-luciferin products. The bioluminescence of these luciferins was performed by using wide type luciferase (WT) and mutant luciferase (R218K).

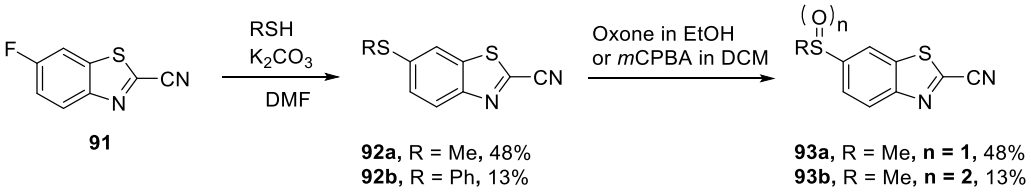

Scheme 21 The Synthesis of Thiol **92a-b**, sulfoxide **93a** and sulfone **93b**

Several examples **94a-i** showed bioluminescent emissions from 547 to 614 nm with WT or R218K enzymes (Figure 12). However, two compounds **94j** and **94k** were inhibitors without light output.

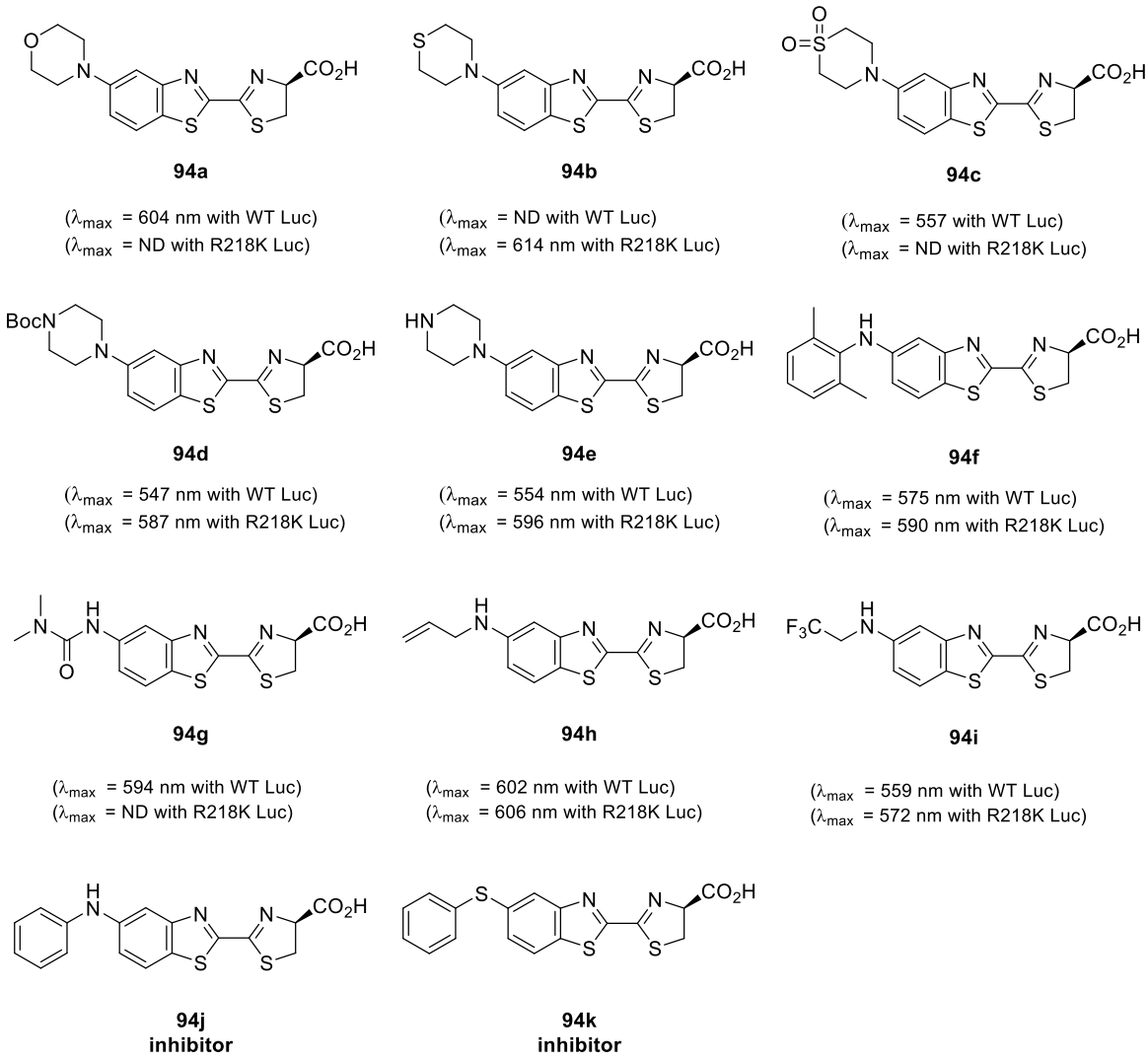

Figure 12 6'-Substituted Firefly Luciferin Emitters and Inhibitors; ND: not determined

In 2019, Sharma and co-workers synthesized a class of amino luciferins functionalized with sulfonamides. [54] The general procedure includes two steps where a series of sulfonamides were installed *via* Buchwald-Hartwig reaction followed by amide condensation with D-cysteine to give the desired sulfonamide luciferins **95a-e** and **96a-d** (Scheme 22). The elongated aliphatic chains of derivatives **95** were expected to fit into the active pocket of enzyme for tuning the wavelengths. The derivatives **96** with bulky groups were those at the extreme limit of steric bulk accepted by the coupling methodology. With these analogues in hand, several *in vitro* assays were collected to investigate their bioluminescent performances. For the elongated chain luciferins, **95a** exhibited the longest emission at 642 nm, **95c** dropped off in luminescent activity with the weakest intensity at 628 nm, and **95e** gave the strongest light output at 547 nm in this class. For bulky luciferins **96a-d**, higher photon fluxes than **95a-e** were observed in general. Additionally, the highest emission intensity of **96c** is about 10% of that achieved with D-luciferin at 554 nm with native firefly luciferase. Compounds **95a** and **96c** were the brightest substrates and showed the similar photo flux in living cell study.

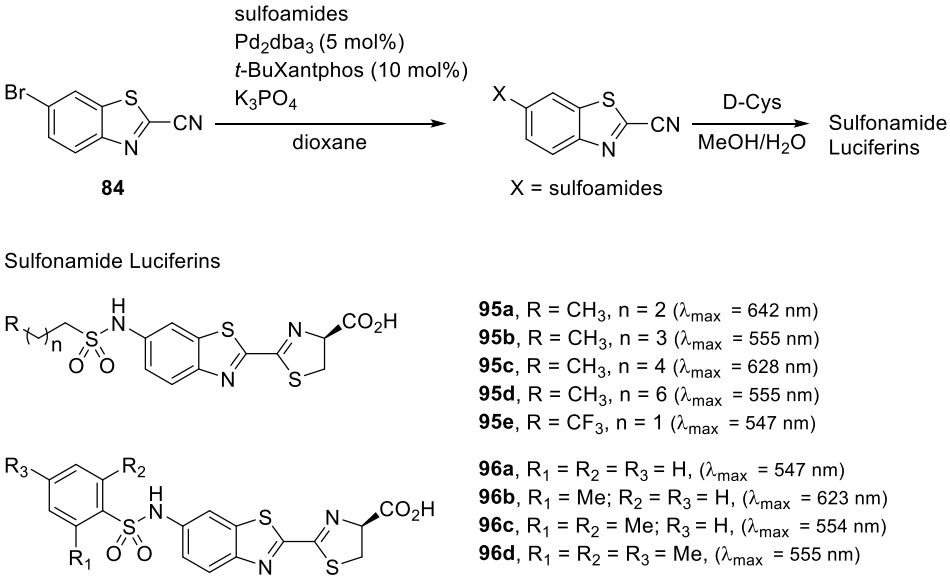

Scheme 22 The Class of Sulfonamide Luciferins

Compared with amino luciferin **54a**, modification of the amino group by introducing alkyl, aryl, heterocyclic, thiol, sulfone, and bulky groups is capable of giving longer wavelengths of emission, but simultaneously diminishes the bioluminescence quantum yield.

In addition to the modification of amino luciferin *N*-substituents, the introduction of additional substituent(s) to the benzothiazole ring has been a noteworthy method to expand the scope of novel luciferin analogues for red-shifted emission.

In 1990, Farace and co-workers synthesised 4-methyl-D-luciferin **98** by following White's procedure [6] (Scheme 8) starting from 4-methoxy-2-methylaniline (**97**) in low yield over 7 steps (Scheme 23). [55] In this study, the wavelength of bioluminescence was not recorded but fluorescence results showed that methylated luciferin **98** and D-luciferin have similar fluorescent wavelengths at 535 nm 532 respectively.

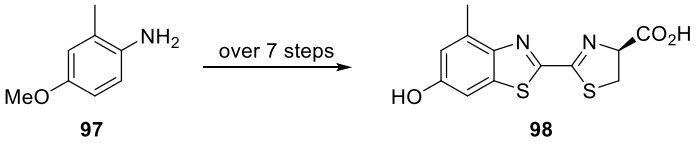

Scheme 23 Brief Synthesis of 4-Methyl-D-luciferin **98**

In 2014, Pirrung and co-workers synthesized a difluoro-luciferin **103**. [56] The acidity of the phenol group would be increased due to the additional fluorine atoms and may have an effect on the character of the phenolate of the light emitting species. To begin with, 2,6-difluoro-*p*-anisidine (**99**) was treated with Br_2 and KSCN to form the amino benzothiazole **100** which was converted into bromo benzothiazole **101** *via* a modified Sandmeyer reaction. The methyl ether cleavage of compound **101** was achieved by BBr_3 to give hydroxyl benzothiazole **102**. The final product **103** was produced through the standard two step S_NAr reaction with NaCN and condensation by with D-cysteine (Scheme 24). Difluoro-luciferin **103** has lower (pKa = 6.4) than D-luciferin (pKa = 8.7) due to two fluorides attached. The bioluminescence results showed that difluoro-luciferin **103** is sensitive when to the pH of its environment. The wavelength of emission was over 600 nm in acidic conditions (pH = 5), and around 570 nm in basic conditions (pH = 8).

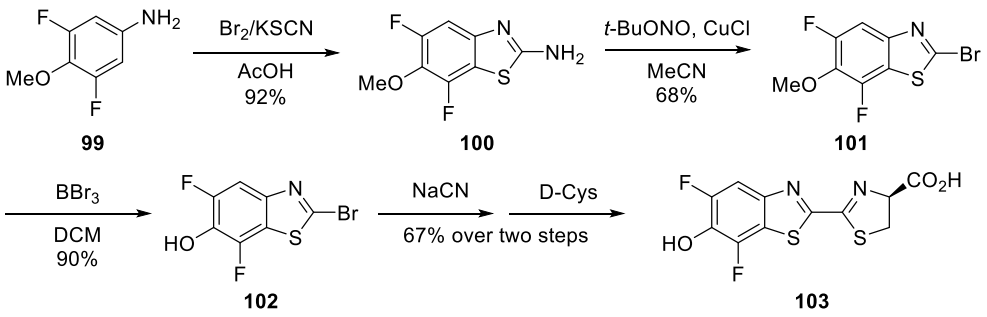

Scheme 24 The Synthesis of Difluoro-luciferin **103**

In 2016, the synthesis of the first alkynyl luciferin was reported by Steinhardt and co-workers. [57] The synthesis began with 2-bromo-4-nitrophenol (**104**) (Scheme 25). Protection of the phenol group with a methanesulfonyl group followed by treatment with ethynyltrimethylsilane produced alkynyl substrate **106** *via* standard Sonogashira reaction. Reduction the nitro group of **106** using iron in glacial acetic acid provided amino **107** which was condensed with Appel's salt followed by pyridine to form the diimine product **108**. However, attempted ring closing reaction from compound **108** to **110** by thermal cyclization failed. As a result, another approach was developed to form the ring. Compound **108** underwent fragmentation by using resin-linked nucleophile PPh_3 to give thioamide **109**. The formation of the benzothiazole ring from compound **109** was achieved by palladium/copper catalysed C-H activation. The protecting groups were removed by treatment with LiHMDS and TMSCl, followed by condensation with D-cysteine to form alkynyl luciferin **111**. With HEK293 cells, this novel luciferin was cell permeant and gave more red-shifted emission at 610 nm than D-luciferin at 565 nm.

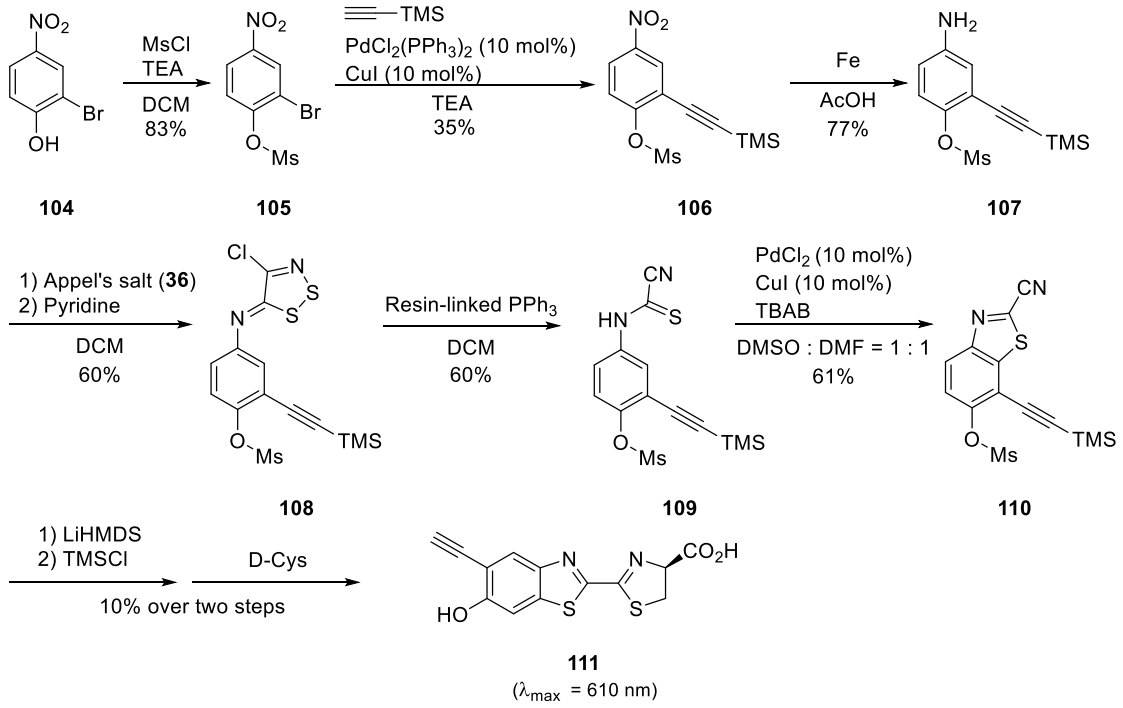

Scheme 25 The Synthesis of Alkynyl Luciferin **111**

In 2017, Steinhardt and co-workers developed three brominated D-luciferin analogues as bioluminescent probes (Scheme 26). [58] The sterically modest bromo substitution at the 4'; 5'; or 7 positions on benzothiazole were expected to fit into the active pocket of firefly

luciferase to different degrees. They were good candidates for the orthogonal mutant enzymes and gave robust light outputs. The procedure for the preparation of these mono-brominated D-luciferins started from suitable anilines **112a-c** which were treated with Appel's salt for the formation of diimine moieties **113a-c**. The next steps were fragmentation with DBU followed by cyclization using palladium/copper catalysis to give 2-cyanobenzothiazoles **114a-c**. After reaction with *N*-bromosuccinimide (NBS), benzothiazole **114c** was converted into 7-bromo-2-cyanobenzothiazole (**114d**). Treatment of mono-brominated **114a**, **114b** and **114d** with BCl_3 gave the corresponding hydroxyl benzothiazoles which were condensed with D-cysteine to provide brominated D-luciferins **115a-c**. Among these novel luciferins, only the 5'- substituted luciferin gave robust emission over 600 nm, but the intensity of emission was still lower than D-luciferin during *in vivo* study. However, the bromo-benzothiazole substrates could prove useful for the introduction of an additional aromatic heteroaromatic ring with palladium catalysis in the future.

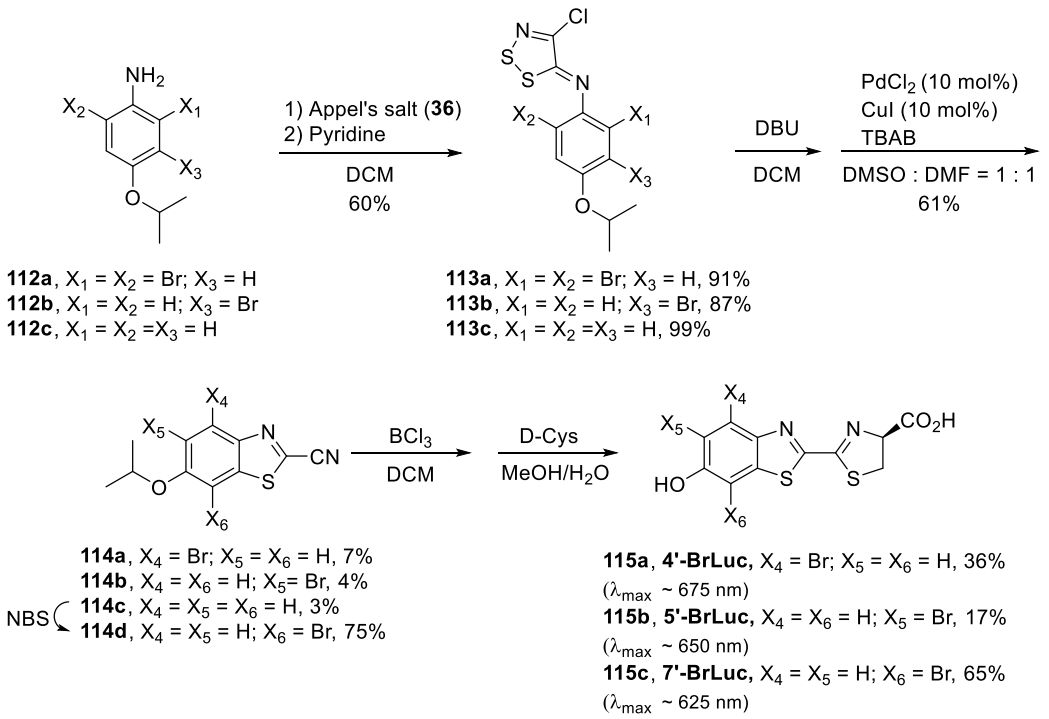

Scheme 26 The Synthesis of Mono-brominated D-Luciferins

In 2017, Jones and co-workers reported a strategy for the production of orthogonal luciferase-luciferin pairs. [59] This is useful because a modified luciferin can be matched to a mutant luciferase to maximize light output or wavelength shift. Several 4' and 7'-

substituted luciferin analogues were synthesized using either of two synthetic routes. The first route capitalized on the availability of the 7-methyl benzotihiazole derivative **116** (Scheme 27(a)). Benzylic bromination was achieved by using NBS and the radical initiator benzyl peroxide (BPO) in the dark. Replacement of bromide with morpholine yielded intermediate 2-cyanobenzothiazole **117**, which was condensed with D-cysteine to give product **118**. Other derivatives were synthesized *via* a Mannich-type reaction (Scheme 27 (b)) between the electron-rich 2-cyano-6-hydroxylbenzothiazole (**34**) and iminium ions formed in situ to give the 4-aminomethylene 2-cyano intermediates **119a-c**. The desired 7'-substituated products **120a-c** were delivered after standard treatment with D-cysteine. These sterically modified luciferins were then subjected to libraries of mutant luciferases to identify orthogonal pairs. All the novel luciferins gave bioluminescence over 600 nm and product **118** produced the longest wavelength at 628 nm. Product **120a** possessed the greatest total photon flux value in this class, but the value was still far lower than D-luciferin. Interestingly, chemiluminescence with luciferin analogues were also performed and all the products gave comparable intensity of emission to D-luciferin. The results were different from their bioluminescence.

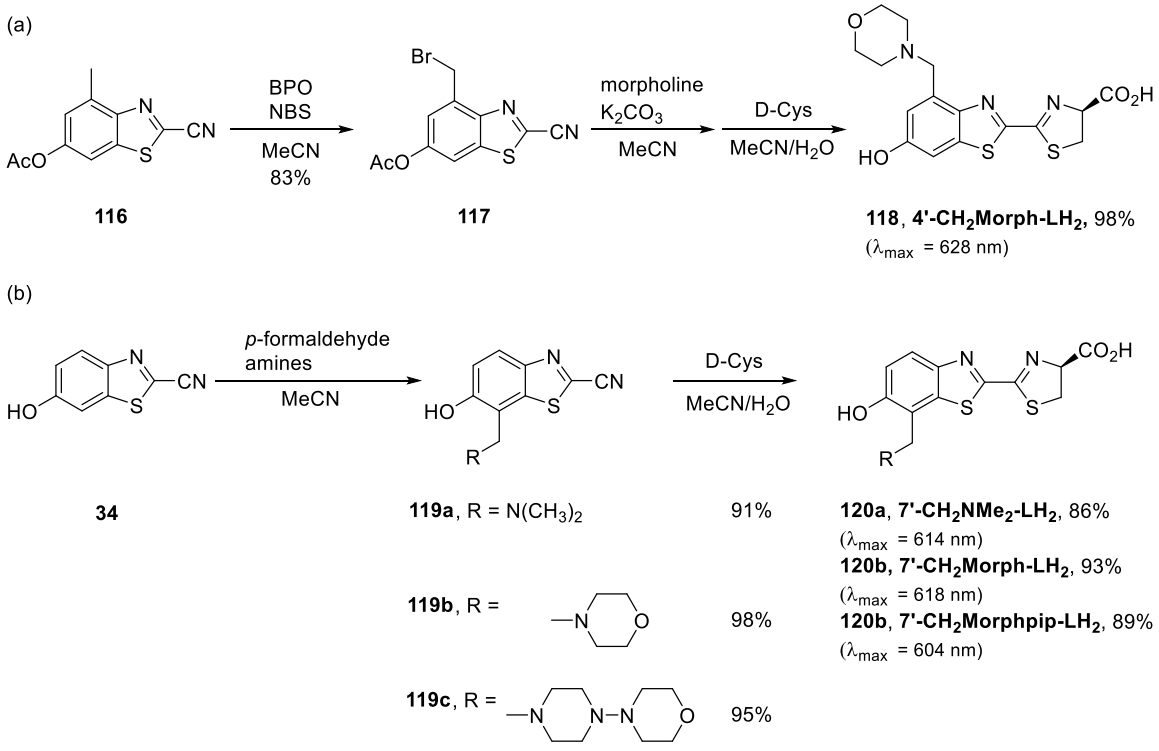

Scheme 27 The Synthesis of 4' and 7'-Substituted Luciferins for Orthogonal Pairs

D-Luciferin is pH sensitive so it is not suitable to be used in acidic conditions where cancer and Alzheimer's diseases are usually observed. In 2012, Takakura and co-workers developed a series of acid-tolerant 5'- halo, and 7'- substituted luciferins (Scheme 28). [60] The 7-susbtituent was introduced by a Claisen type reaction. Reaction of 6-hydroxyl benzothiazoles **121a-b** with allyl bromide provided 6-allyloxybenzothiazole-2-carbonitrile derivatives **122a-b** which were subjected to the Claisen rearrangement for the formation of the corresponding 5-substituted **123a-b** in very poor yields. Conversion to the 5-hydroxymethyl group was achieved by chemical ozonolysis of allyl compounds **123a-b** followed by reduction of the aldehydes **124a-b** to give **125a-b**. The final step was standard condensation between the nitriles and D-cysteine to produce the expected 5'- and 7'-substituted luciferin analogues **126a-f**. In bioluminescence investigations, the wavelength of emissions was over 600 nm at pH = 6. Additionally, the analogues have a bulky group at the 5'-position which rendered their bioluminescence pH-independent because of the loss of the interaction between the 6-hydroxyl group and the basic amino acid residue in active pocket. Among these analogues, **126e**, **7'F5'HM-LH$_2$** (pKa = 6.9) showed a better acid-tolerance than D-luciferin (pKa = 8.5). At pH = 7.4, both luciferins had similar luminescence intensities. At pH =6.5, the luminescence intensity of D-luciferin dropped down to one-sixth of its at pH = 7.4 but **126e** maintained its intensity.

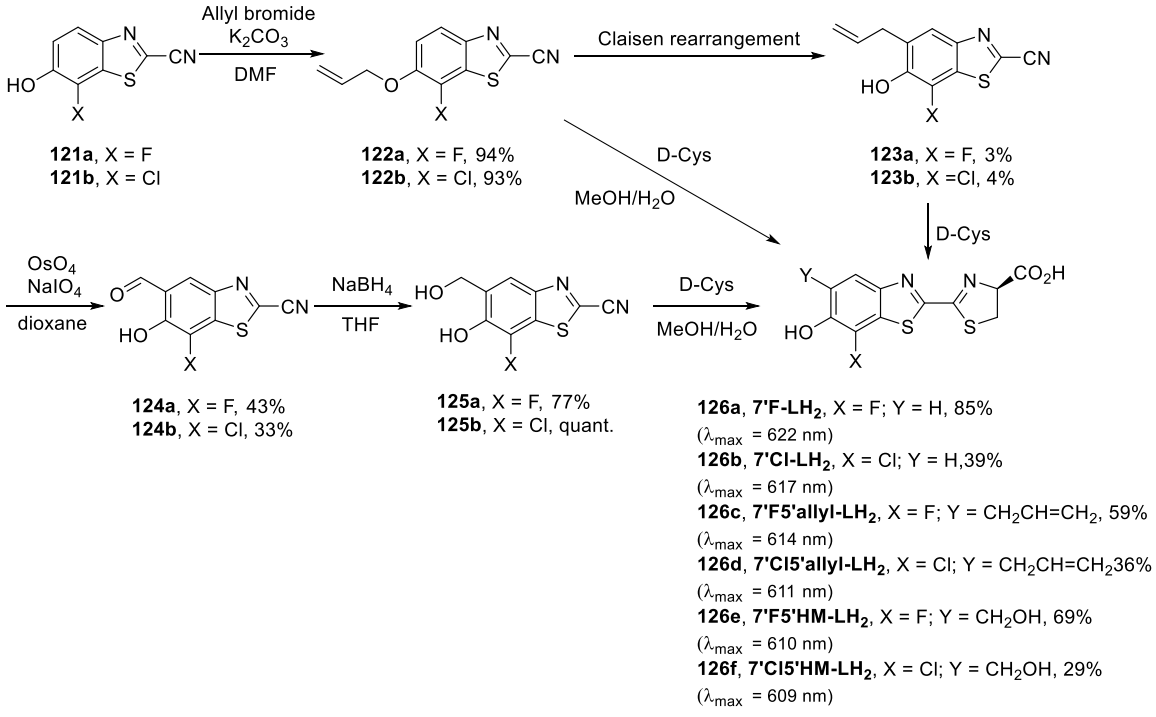

Scheme 28 The Synthesis of acid-tolerant 5'- and 7'- Luciferins

In 2018, Ikeda and co-workers reported a high yielding synthesis of 7'-allylated firefly luciferin (Scheme 29). [61] The allyl modification at the 7'-position is able to occupy the hydrophobic microenvironment in the active pocket. The synthesis started from commercially available 2-cyano-6-hydroxybenzothiazole (**34**). The hydroxyl group of benzothiazole **34** was allylated and then a regioselective Claisen rearrangement led to the formation of the 7'-allyated product **128**. Standard condensation with D-cysteine provided the desired product **129**. This luciferin showed a bioluminescent emission at 605 nm with ~10% of luminous efficiency with wild type luciferase compared to the native D-luciferin substrate. Moreover, the *ee* value of **129** was determined to be 99% by chiral HPLC.

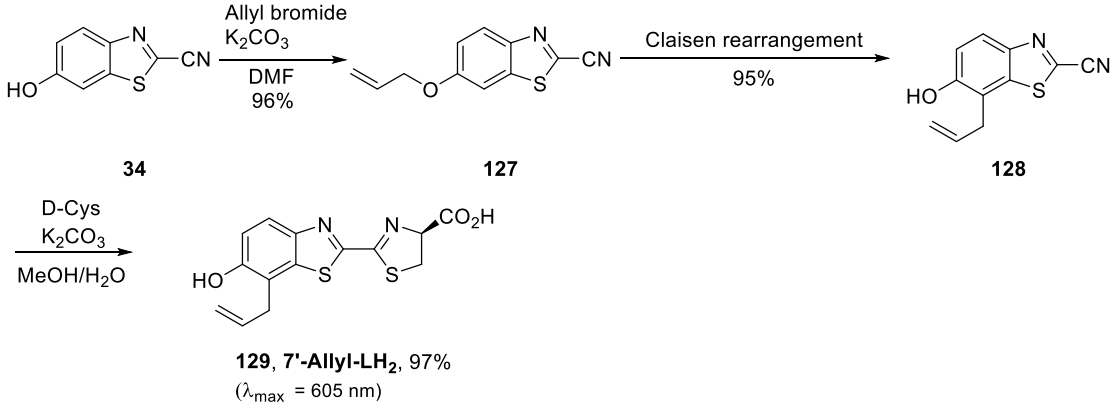

Scheme 29 The Synthesis of 7'-allylated Luciferin

1.7.3.2 Second Modification: Replacement of Benzothiazole or Thiazoline Ring

Replacement of benzothiazole or thiazoline moiety by other aromatic or heterocyclic rings has paved a way to synthesize novel luciferin analogues. In 2012, Woodroofe and co-workers synthesized a class of novel non-benzothiazole based luciferin analogues. [62] The benzothiazole was replaced by five different aromatic rings including benzimidazole, benzofuran, benzothiophene, benzoxaole and indole (Scheme 30) *via* different synthetic routes. Primary amide formation of 6-methoxy-indole-2-carboxylic acid (**130**) with NH_4Cl followed by dehydration with $POCl_3$ gave indole **132a**. Starting material 2-hydroxy-4-methoxybenzaldehyde (**133**) was used for the development of benzofuran **132b** and benzothiophene **132c**. Reaction of compound **133** with bromoacetonitrile followed by intramolecular condensation of the activated methylene with the aldehyde gave benzofuran **132b**. Treatment of compound **133** with thiocarbamoyl chloride to yield O-aryl thiocarbamate **135** then underwent a Newman–Kwart rearrangement in toluene at 180 °C to provide S-aryl thiocarbamate **136**. Thiocarbamate **136** was hydrolysed and then alkylated with chloroacetonitrile under basic condition which allowed spontaneous condensation to give the desired benzothiophene **132c**. Methylation and oxidation of compound **137** followed by substitution of the resultant methansulfone with KCN gave 2-cyano-6-methoxybenzothiazole (**132d**).

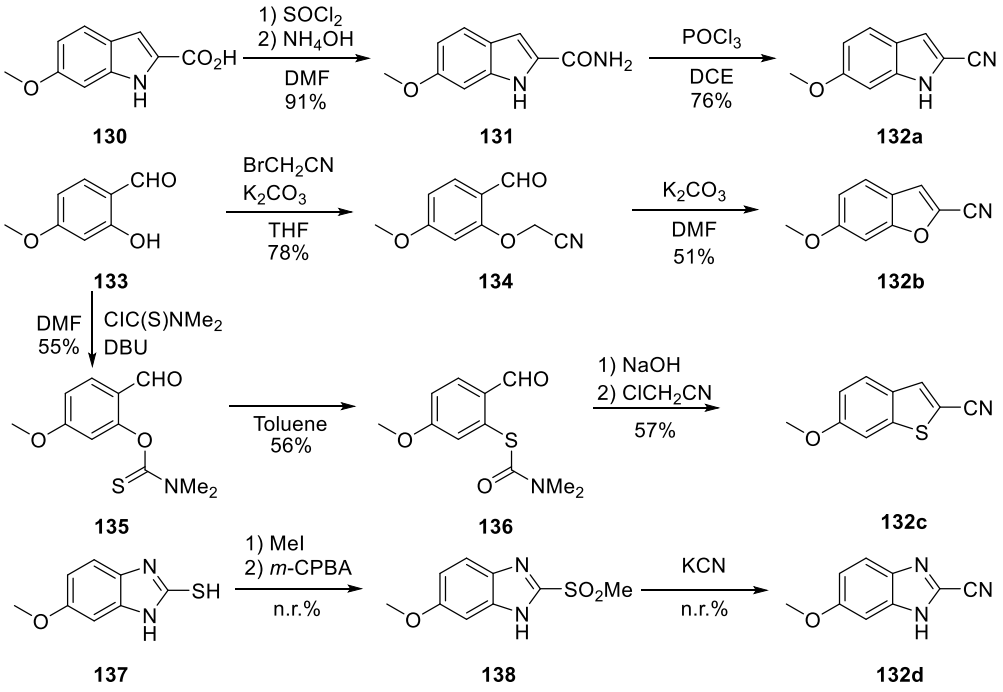

Scheme 30 The Synthesis of 2-Nitrile Heterocyclic Precursors **132a-d**

The 6-hydoxyl-2-cyano heterocyclic precursors **133a-e** were delivered by two methods (Scheme 31). The first method was protodemethylation of methoxy compounds **132a-d** with pyridine hydrochloride and the second was the reaction of 4-aminobenzene-1,3-diol (**139**) with Appel's salt to provide compound **133e**, but in poor yield. All the nitrile compounds **133a-e** were transformed into their corresponding luciferins **140a-e** by standard condensation with D-cysteine hydrochloride. From the bioluminescence results, compound **140a** was an inhibitor which did not give any emission and only imidazole-based **140d** gave more red-shifted emission than D-luciferin within pH = 6.2 and 9.4. The other analogues gave slightly blue-shifted light compared to D-luciferin. Unfortunately, the authors did not attach any NMR spectra, and high-resolution mass (HRMS) data in this study. The procedure for the synthesis of compound imidazole **132d** was not detailed and the yields of some intermediates were absent.

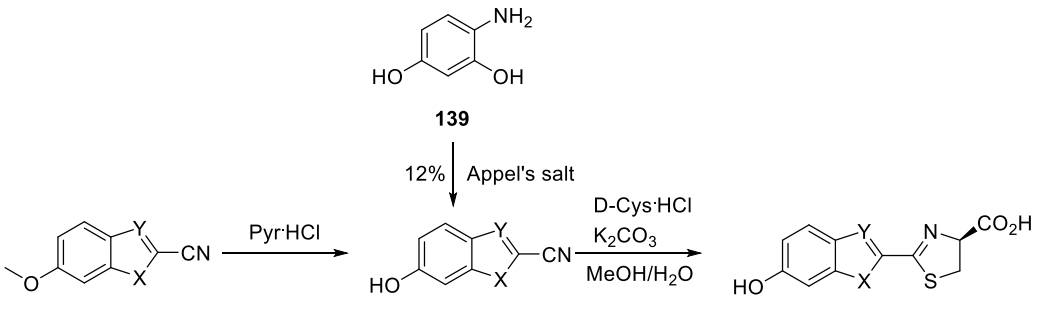

132a-d

133a, X = NH ; Y = CH, 63%
133b, X = O ; Y = CH, 76%
133c, X = S ; Y = CH, 68.%
133d, X = N ; Y = NH, n.r.%
133e, X = N ; Y = O

140a, **InLH$_2$**, X = NH ; Y = CH, n.r.% (λ_{max} = no emission)
140b, BfLH$_2$, X = O ; Y = CH, 52% (λ_{max} = 527 nm)
140c, BtLH$_2$, X = S ; Y = CH, 84% (λ_{max} = 522 nm)
140d, BiLH$_2$, X = N ; Y = NH, n.r.% (λ_{max} = 600 nm)
140e, BoLH$_2$, X = N ; Y = O, 63% (λ_{max} = 580 nm)

Scheme 31 The Synthesis of Heterocyclic Luciferins **140a-e**

The use of naphthalene and quinoline as core structures was reported by Branchini and co-workers in 1989. [63] Protodemethylation of compounds **141a-b** followed by condensation with D-cysteine gave the desired products **143a**, **NPLH$_2$** and **143b**, **QLH$_2$** in overall 50% and 28% yields respectively (Scheme 32). The **143b**, **QLH$_2$** gave a longer wavelength bioluminescent emission at 608 nm compared to D-luciferin. However, the emission of **143a**, **NPLH$_2$** was only 524 nm. These results demonstrate a single atom change could lead to significant wavelength difference.

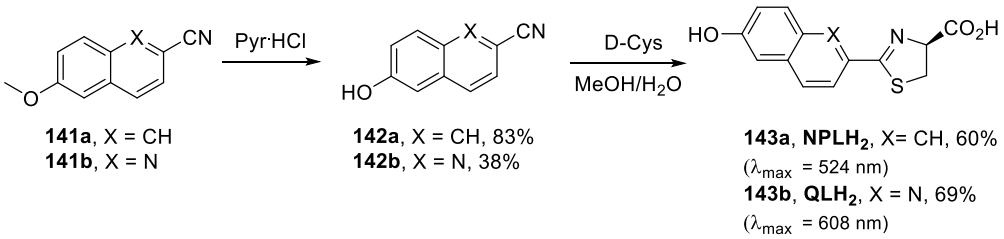

Scheme 32 The Synthesis of **$NPLH_2$** and **QLH_2**

In 2010, Takakura and co-workers synthesized quinolylluciferin, naphthylluciferin, and coumarylluciferin derivatives bearing amino groups. [64] The synthesis of naphthylamino and quinolylamino analogues were delivered through the same synthetic route (Scheme 33). The intermediates **144c-f** were synthesized from **144a-b** *via* reductive alkylation by treatment with formaldehyde and $NaBH_4$. After condensation with D-cysteine hydrochloride under basic condition, the corresponding luciferin analogues **145a-e** were produced. Their bioluminescence emissions varied were from yellow to orange. The more *N*-methylated derivatives gave longer peak wavelengths.

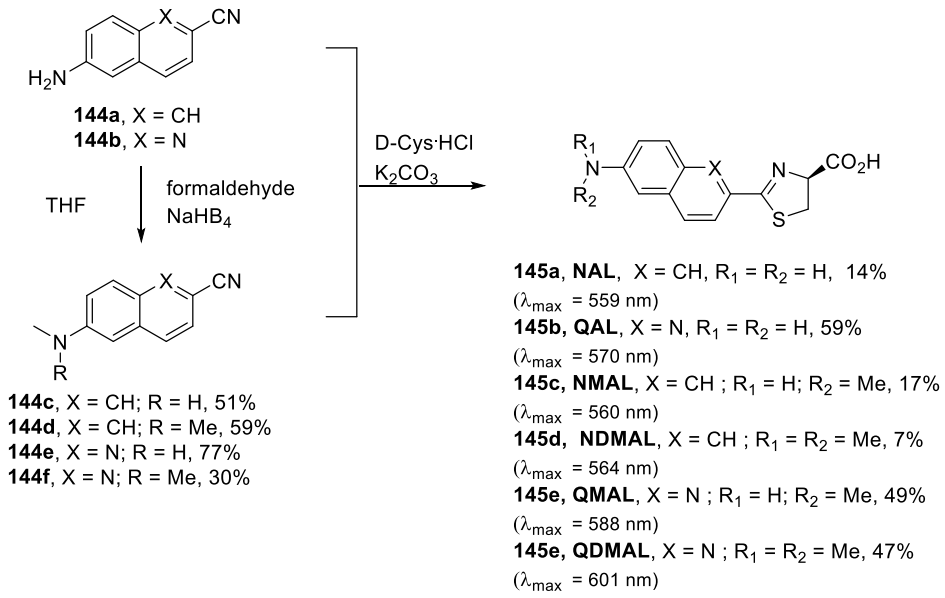

Scheme 33 The Synthesis of Quinoly and Naphthyl Luciferin Analogues

The coumarylluciferin derivatives were prepared by using 2-methoxy-4-nitrobenzaldehyde (**146**) as starting material (Scheme 34 (a)). Deprotection of the methyl ether group with BBr_3 was followed by Knoevenagel reaction of the aldehyde with malononitrile under basic conditions followed by intramolecular cyclization with concentrated HCl to provide 7-nitro-2-oxo-2H-chromene-3-carbonitrile (**148**). The nitro group of **148** was reduced with Pd/C under H_2 atmosphere to give the amino precursor **149** which was treated with D-

cysteine to give compound **CAL**, **145f**. Reductive alkylation of compound **149** provided mono *N*-methylated **150**, but the *N*,*N*-dimethylated product was not isolated under these conditions. An alternative synthetic route was attempted for the development of the *N*,*N*-dimethylated analogue (Scheme 34 (b)) starting from 3-(dimethylamino)phenol (**151**). Vilsmeier Haack reaction gave aldehyde **152** and the coumaryl intermediate was produced as before by Knoevenagel reaction and intramolecular ring closure. Standard condensation of compounds **149**, **150** and **153** with D-cysteine gave the expected luciferin analogues **145f-h** in very poor yields due to the electrophilicity of the coumarins causing complications. These coumarylluciferin derivatives **145f-h** gave bioluminescence emissions from 500 nm to 526 nm which were blue-shifted in comparison to the quinolylluciferin, and naphthylluciferin derivatives **145a-e**.

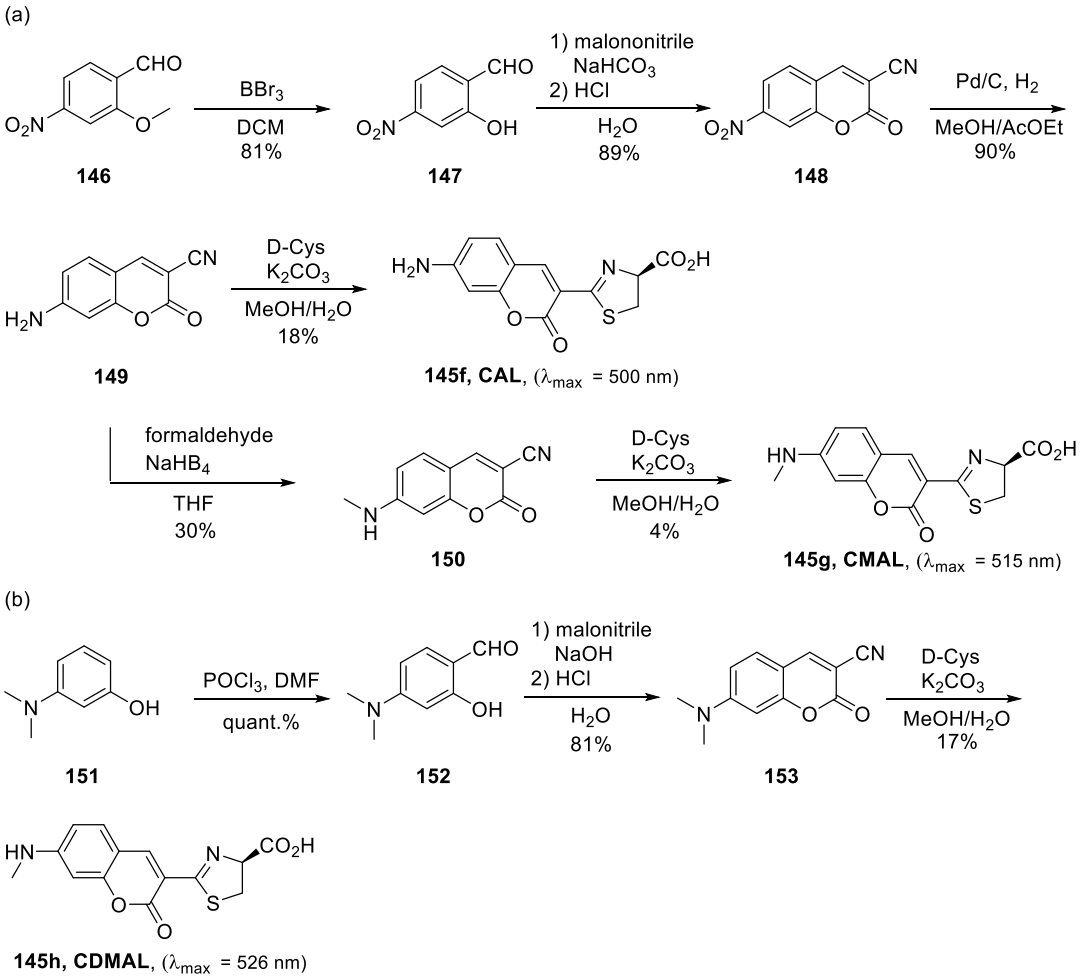

Scheme 34 The Synthesis of Coumarylluciferin analogues **145f-h**

In 2018, Zhang and co-worker reported pyridone-tautomer based luciferins. [65a] Many drugs such as ricinine and arthpyrone contains the pyridone skeleton, [65b] which suggests that the pyridone luciferins would be stable under physiological conditions. According to Appel's salt chemistry, cyanothioformamide **155** was synthesized by treatment of aniline **154** with Appel's salt in a one pot reaction (Scheme 35). The construction of thiazolopyridines **156a-b** was achieved under palladium/copper catalysed C-H functionalisation. Demethylation with pyridine hydrochloride followed by reprotection with acetic anhydride gave the nitrile intermediates **157a-b**. Reaction of the nitrile compounds with D-cysteine provided the corresponding pyridone luciferin analogues **158a-b**. With native firefly luciferase, these two regioisomeric pyridone luciferins gave only weak photon fluxes, around 1% of D-luciferin. The wavelengths of these new compounds had hypsochromic (blue-shifted) emission compared with D-luciferin. Luciferin **158a** gave an emission at 570 nm and compound **158b** at 530 nm. Computational studies were conducted to support the emission wavelengths of their corresponding oxyluciferins. The results gave the calculated emissions of **158a** and **158b** at 582 nm and 510 nm respectively, which is quite close to the experimental values.

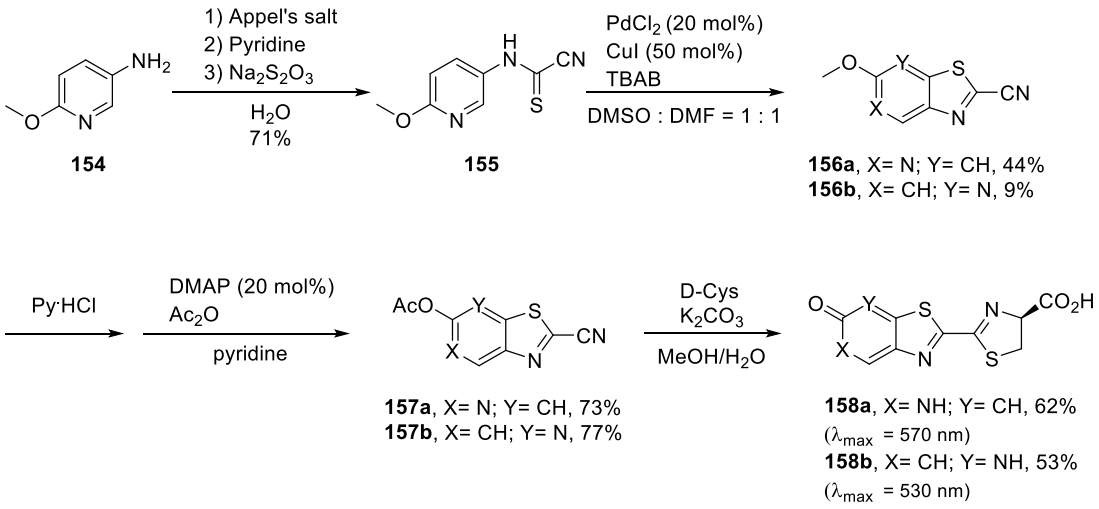

Scheme 35 The Synthesis of Pyridone Luciferins

In 2018, two naphthyl-based luciferin analogues, one bearing a hydroxyl group (**OH-NpLH$_2$**) and another an amino group (**NH$_2$-NpLH$_2$**), were synthesized by Hall and co-workers (Scheme 36). [66] The hypothesis was that introduction of an additional phenyl ring on the benzothiazole portion would extend the conjugation of the light emitting species

and result in red-shifted emission. Bromination of naphthalenes **159a-b** was achieved with NBS to give the bromonaphthalenes **160a-b**. In the reaction with Appel's salt followed by intramolecular copper-catalyzed cyclization, cyanobenzothiazoles **161a-b** were constructed. Deprotection of **161a** with TFA and demethylation of **161b** gave the amino compound **162a** and hydroxyl moiety **162b**, respectively. The deprotected compounds were condensed with D-cysteine to give the corresponding luciferin analogues **163a**, **NH_2-$NpLH_2$** and **163b**, **OH-$NpLH_2$**. With native luciferase, **163a**, **NH_2-$NpLH_2$** had two emissions at 678 nm (major peak) and 719 nm (minor peak) but **163b**, **OH-$NpLH_2$** did not give any light output. With mutant luciferase CBR, **163a**, **NH_2-$NpLH_2$** gave an emission at 664 nm and **163b**, **OH-$NpLH_2$** was particularly striking at 758 nm which is the longest wavelength in bioluminescence system to date. However, the intensities of these new analogues were much lower (~5000-500,000 fold) than D-luciferin. Moreover, bioluminescence tomography in mouse brain was investigated by using these two nIR compounds. The result showed that analogue **163a**, **NH_2-$NpLH_2$** has better cell membrane permeability than D-luciferin. **163a**, **NH_2-$NpLH_2$** gave emission wavelength at 730 nm in mice. As a result, it is a valuable alternative *in vivo* bioluminescent probe for the future. Moreover, chiral HPLC analysis of **163b**, **OH-NpLH2** showed high enantiopurity, but **163a**, **NH_2-$NpLH_2$** was racemic

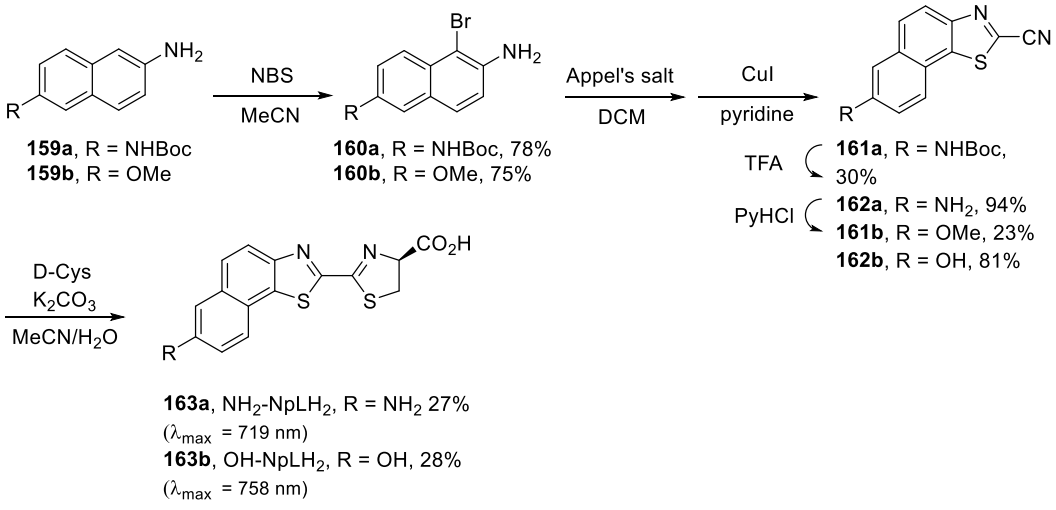

Scheme 36 The Synthesis of nIR Luciferin Analogues NH_2-$NpLH_2$ and OH-$NpLH_2$

In 2012, McCutcheon and co-workers synthesized luciferins **166**, **169** and **170**. [67] They suggested that bioavailability and metabolic stability would be changed by modification of the electronics of the heterocyclic rings. Compared to the preparation by Woodroofe, [62] imidazole **133d** was rapidly prepared and scaled up from the alternative synthesis by the

utility of Appel's salt (Scheme 37(a)) in this study. Reduction of 4-methoxy-2-nitroaniline with Pd/C under H_2 provided the bis-aniline **165**. The diamino groups of **165** were condensed with Appel's salt to give the cyclized imidazole **132d**. The key intermediate 2-cyano-6-hydroxybenzimidazole (**133d**) was obtained by removal of the methyl protecting group with Py·HCl. This precursor **133d** was reacted with $HCl_{(g)}$ to form the methoxy intermediate hydrochloride salt and then condensed with (*R*)-2,3-diaminopropanoic acid to yield the desired product **166**. Methylation of imidazole **132d** followed by the deprotection to give the *N*-methylated imidazole **168** (formed as part of a mixture). Condensation of nitrile group of **168** with D-cysteine provided the other final analogue **169**. These two imidazole-based compounds gave bioluminescent emissions around 460 nm with native luciferase. Moreover, benzothiazole-based derivative **170** was delivered by treatment of nitrile benzothiazole **34** with (*R*)-2,3-diaminopropanoic acid (Scheme 37(b)). However, this molecule lost its bio-activity and did not give any emission because of the poor binding to luciferase.

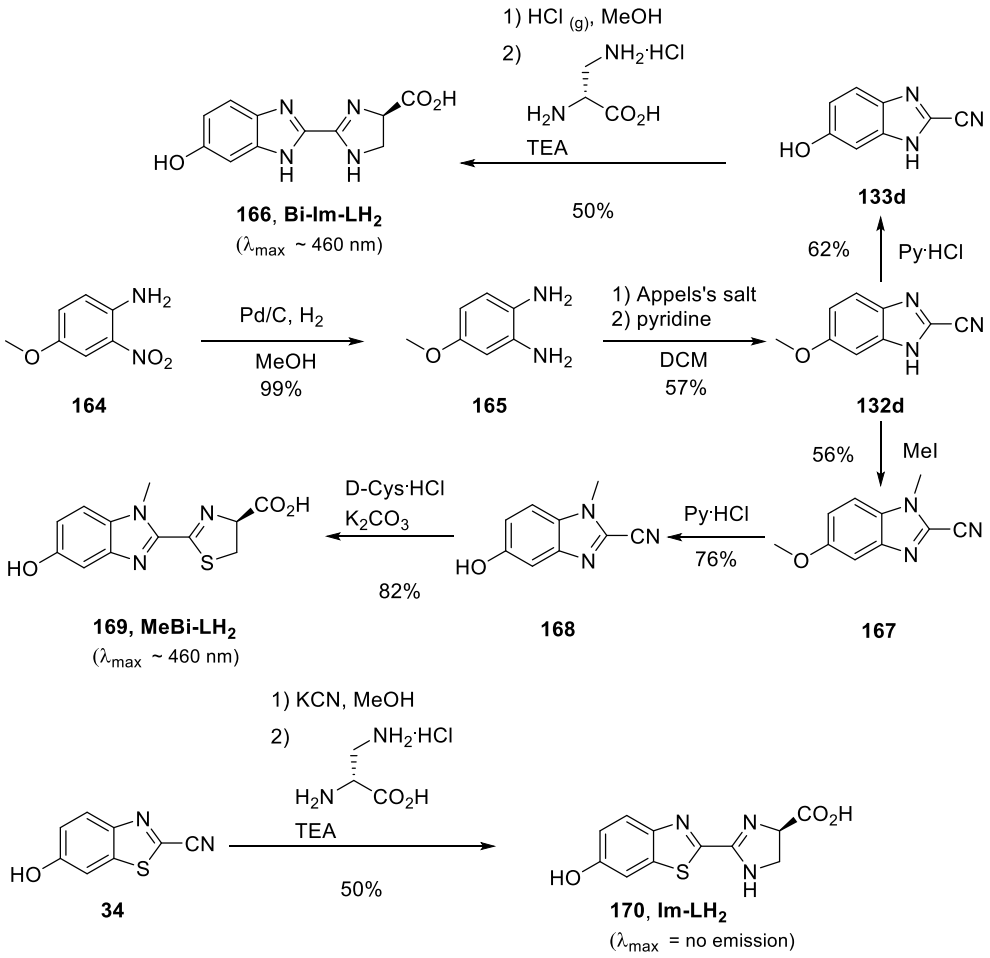

Scheme 37 The Synthesis of Electronic Modified Luciferins in 2012

In 2012, Conley and co-workers synthesized selenium D-luciferin analogue **171**. [68] The synthesis involved condensation between (S)-2-amino-3-hydroselenopropanoic acid with nitrile **53a** (Scheme 38). The selenium luciferin **171** gave red light emission at 600 nm *in vitro*. However, luciferin **171** had low quantum yield about 74% of amino luciferin **54a** due to the heavy atom effect. In contrast the time courses of bioluminescence emission intensity for **171** and **54a** were comparable. Nevertheless, the difference between *in vitro* and *in vivo* results cannot be explained theoretically. The authors also suggested a new application for the luciferase-expressing tumour model with **171**, because ^{77}Se (S = ½) has stable nuclei with a wide range of chemical shifts and narrow lines. In principle, this analogue could be detected by magnetic resonance imaging (MRI) if hyperpolarization was applied.

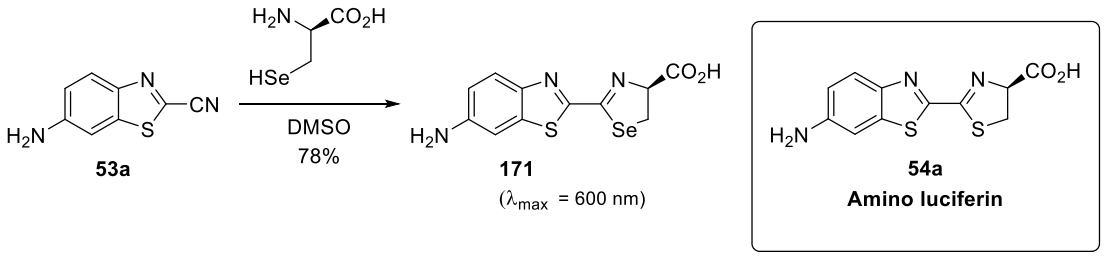

Scheme 38 The Synthesis of Selenium Luciferin **171**

In 2016, Ioka and co-workers synthesized two thiazoline modified luciferin derivatives based on oxazoline **177** and pyrroline rings **185**. [69] The first target synthesis consisted of 7 steps (Scheme 39). Hydrolysis of the nitrile group of 2-cyano-6-hydroxybenzothiazole (**34**) in the presence of methanol gave methyl ester **172**. Protection of the hydroxyl group with methoxymethyl chloride (MOMCl) produced MOM-protected **173**. A coupling reaction between compound **173** and D-serine, followed by cleavage of the MOM group by TFA, generated uncyclized intermediate **174**. Selective acetylation of **174** with acetic anhydride followed by treatment with diethylaminosulfur trifluoride (DAST) gave oxazoline methyl ester **176**. Hydrolysis of the methyl ester with Lipase PS IM Amano gave the expected luciferin **177**, **Oxa-LH$_2$**. However, this compound was unable to produce bioluminescence.

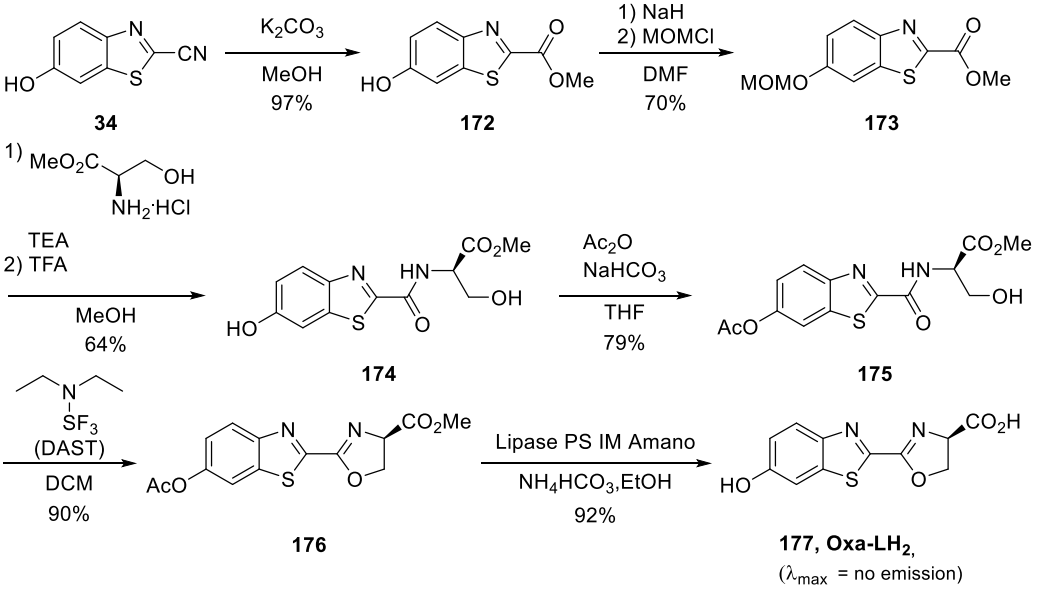

Scheme 39 The Synthesis of Oxazoline Luciferin **Oxa-LH$_2$**

The synthetic route (Scheme 40) for the development of pyrroline luciferin started with a Sandmeyer reaction of the amine **178** to give 2-bromo-6-methoxybenzothiazole (**179**). Demethylation of the methoxy group with BBr_3, followed by re-protection the hydroxyl group with *t*-butyl-dimethylsilyl chloride (TBDMSCl) gave **181**. Treatment with *n*-BuLi followed by addition of Boc-protected reagent **182** provided the glutamate-linked intermediate **183**. The desired product was delivered *via* two more steps involving desilylation with tetrabutylammonium fluoride (TBAF) and intramolecular cyclization by using DAST. This novel compound **185**, **Pyrr-LH$_2$** had an emission at 547 nm and its quantum yield was 0.5% of D-luciferin.

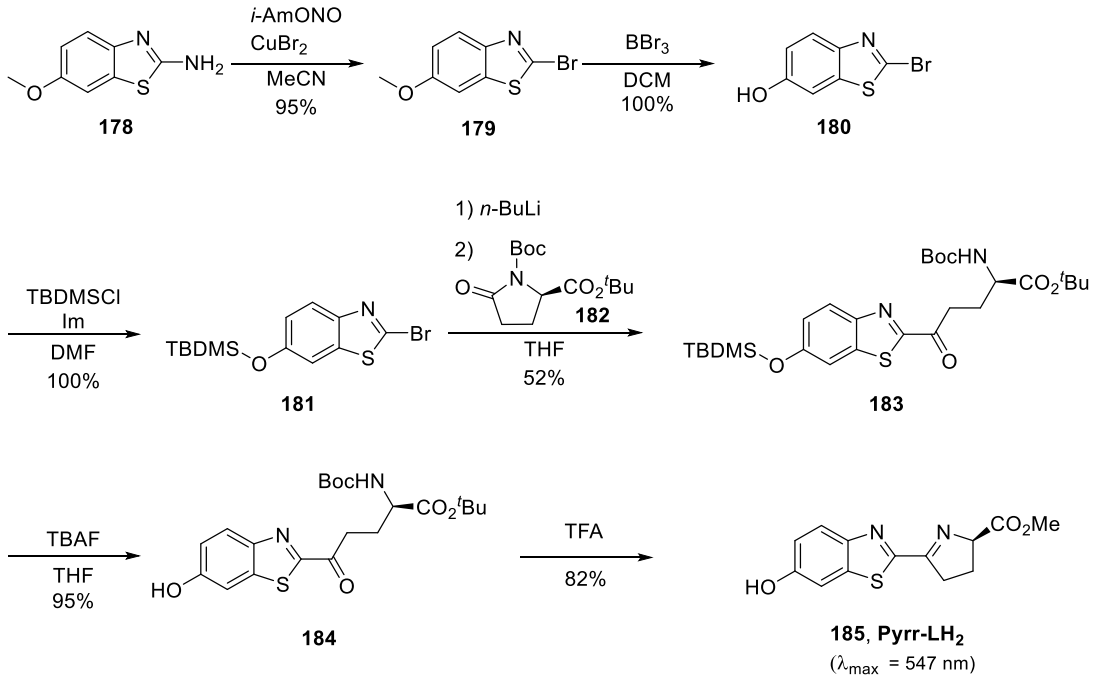

Scheme 40 The Synthesis of Pyrroline Luciferin **Pyrr-LH$_2$**

In 2013, Miura and co-workers reported the synthesis of biphenyl-type firefly luciferin analogues **192a-c** for bioluminescence. [70] From their study of emission and structure relationship, the insertion of more than three double bonds between the aromatic ring and the thiazoline reduced the stability of these analogues. [71] They expected that replacement of three doubles with a biphenyl system would increase the photo and air stabilities. Moreover, their docking studies suggested that the linear biphenyl might be able to fit the active site in *Photinus pyralis* luciferase. The biphenyl compounds **187a-b** were synthesized by treating ethyl 4-iodobenzoate with suitable boronic moieties **186a-b** *via* Suzuki-type reaction (Scheme 41). Subsequent hydrolysis of ethyl esters **187a-b** provided their carboxylic products **188a-b**. The preparation of hydroxyl precursor **188c** was not reported. Amide coupling reaction of carboxylic acid compounds **188a-c** with D-Cys(S-Trt)-OMe mediated by 4-(4,6-dimethoxy-1,3,5-triazin-2-yl)-4-methyl-morpholinium chloride (**189**) (DMTMM) gave the corresponding amide products **190a-c**. Intramolecular cyclization of amides **190a-c** was conducted with the Hendrickson reagent. The nitro group of **191b** was reduced by iron in acidic conditions to give amino biphenyl methyl luciferin **191d**. The final step was hydrolysis of the methyl ester of **191a, c, d** with LiOH to give the expected biphenyl luciferin analogues **192a-c**. Among these novel derivatives, only **162a**, **Me$_2$NBiPh-LH$_2$** showed bioluminescence at 675 nm, but the light intensity of it was far less than 1% of D-luciferin.

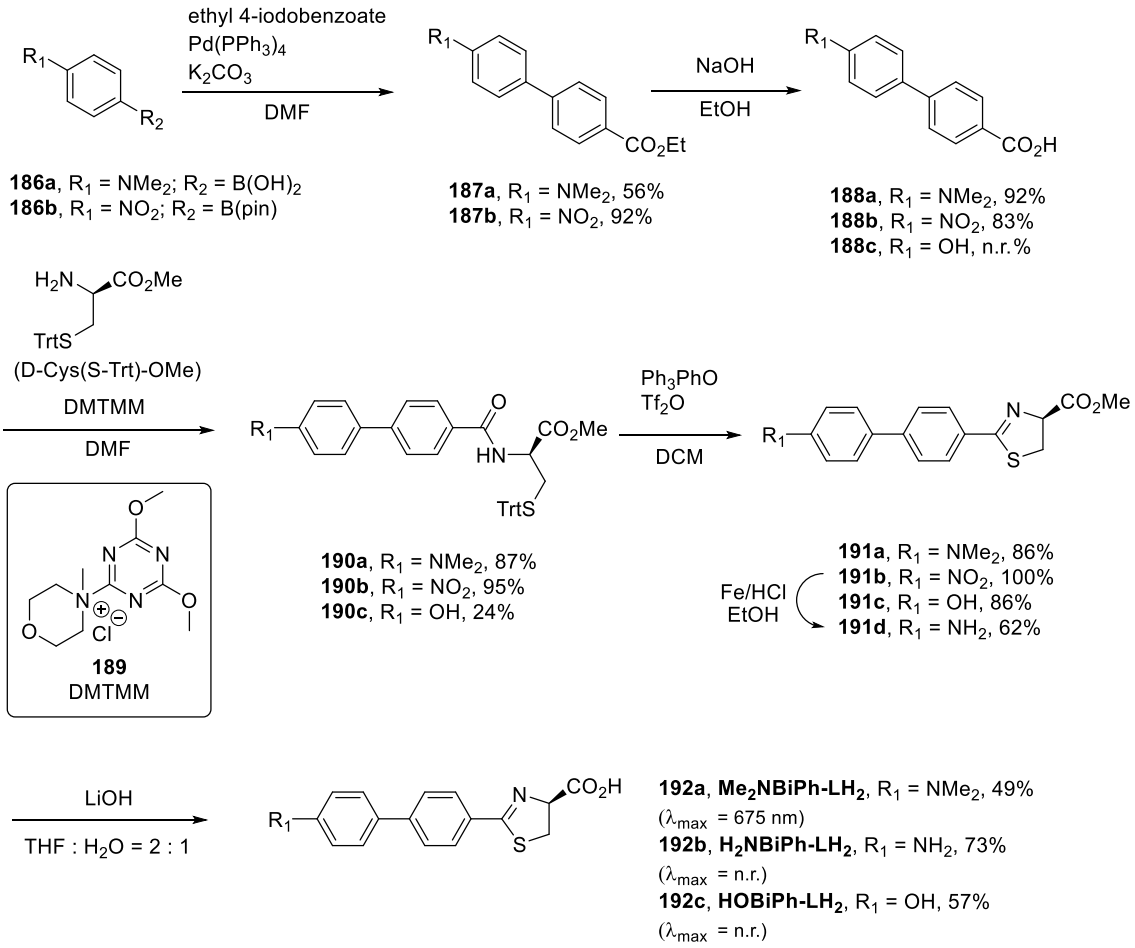

Scheme 41 The Synthesis of Biphenyl Luciferin Analogues **192a-c**

1.7.3.3 Third Modification: The Synthesis of pi-Conjugated Analogues

The development of novel luciferin analogues with nIR emission by the introduction of additional pi-conjugated bond between two heterocyclic rings has been proposed.

In 2013, Iwano and co-workers developed five non-benzothiazole based firefly luciferin analogues emitting blue, green and red light. [71] In this study, the first luciferin **195a** was synthesized through two steps. Heck-reaction of 4-iodophenol with acrylonitrile gave **194** which was treated with D-cysteine to deliver the desired phenol **195a** with one alkene separating the phenol from the thiazoline (Scheme 42(a)). This compound gave a bioluminescent emission at 530 nm.

The formation of the thiazoline in **195a** using the classic method was low yielding, possibly because the nitrile condensation with D-cysteine suffers from side reactions such as conjugate addition. In order to prepare other more extended derivatives an alternative synthesis of the thiazoline was developed. The synthesis of naphthyl-based luciferin **195b** required seven steps. Starting with 6-hydroxy-2-naphthonitrile (**142a**), the hydroxyl group was protected by TBDMS to give silyl ether **196** (Scheme 42(b)). Reduction of the nitrile group of **196** with DIBAL followed by Wittig reaction gave the naphthyl-alkenyl-ester intermediate **197**. The ester group was saponified with NaOH an amide intermediate **200** formed with (S)-trityl-D-cysteine methyl ester using 1-Ethyl-3-(3-dimethylaminopropyl) carbodiimide (EDC). The TBDMS group was removed in the Wittig reaction so an additional step for deprotection was not required. The formation of the thiazoline ring was by treatment of amide **200** with Ph_3PO and Tf_2O (Hendrickson reagent) to yield methyl ester luciferin **201**. The methyl ester could be hydrolysed enzymatically to generate a luciferin derivative **195b**. This novel luciferin **195b** gave an emission at 609 nm. In the same manner, the dimethylamine analogue **195c** was produced with emission wavelength at 560 nm.

The third group of luciferin analogues were composed of phenol or *N*,*N*-dimethylaniline with two double bonds linking the thiazoline (Scheme 42(c)). Following the same reaction conditions for the development of **195b**, appropriate aldehydes **201a-b** were converted into their corresponding luciferin derivatives in five steps. The free phenol luciferin **195d** showed the emission at 640 nm and dimethylamine **195e** (AkaLumine) had a nIR emission

at 675 nm. The same group, recently, has improved the light output *in vivo* by using the nIR analogue **195e** as precursor to give the hydrochloride salt **195f**.[72] This salt form is much brighter than other nIR D-luciferin analogues when administered at low concentration due to the optimal solubility. It has a good balance between cell-permeability, product inhibition, and enzyme saturation.[73]

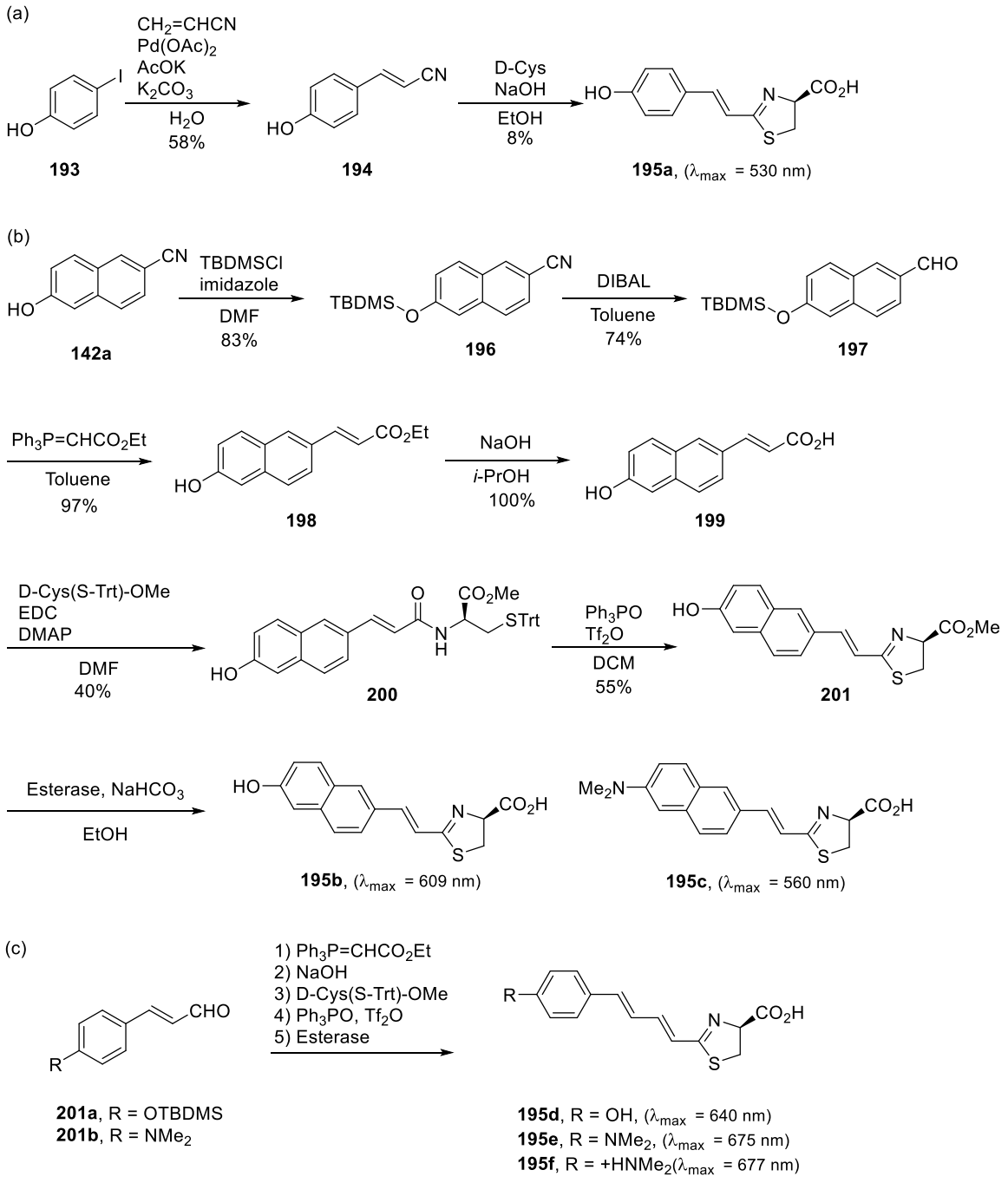

Scheme 42 The Synthesis of non-Benzothiazole Luciferin 195a-f with pi-Bond(s)

In 2018, Kitada and co-workers synthesized non-benzothiazole allyl substituted firefly luciferins with double bond linkers. [74] The allyl modification was hypothesized to be able to occupy the hydrophobic microenvironment in the active pocket. In this research, the reaction conditions and yields of each compound were not fully reported. The synthesis of allylated **202a** began with formation of the allyl ether followed by a Claisen rearrangement and condensation with D-cysteine to provide luciferin **202a** (Scheme 43(a)). This new compound, without a double bond linking the aromatic ring and thiazoline ring, gave emission at 570 nm which is similar to the wavelength of D-luciferin (**1**).

The second group based on a naphthyl structure with a pi-bond between and at the end of the structure (Scheme 43(b)). Allylation of the of hydroxyl group of **203** followed by the Claisen rearrangement gave the double allylated compound **204**. After protection of the phenol as its TBDMS ether, followed by exhaustive reduction of the allyl ester with DIBAL, the resulting alcohol was oxidized with MnO_2 to generate aldehyde **205**. After five steps included installation of the pi-bond *via* Wittig reaction, hydrolysis of the ethyl ester, amide condensation, cyclization by Hendrickson reagent, and hydrolysis of the methyl ester with HCl (4M), the desired compound **202b** was delivered. Allylated **202b** gave a nIR emission at 690 nm.

The third group of allylated luciferin derivatives in this series have a dimethylamine substituent in place of the phenol, with one or two pi-bond(s) between the aromatic ring and thiazoline (Scheme 43(b)). The synthesis of the luciferins **202c-d** started with the bromination of 4-dimethylaminobenzaldehyde (**206**), followed by a palladium-mediated Stille reaction with allyltributyltin to give the allylated intermediate **207**. In the same manner as for the synthesis of analogue **202b**, the aldehyde was reacted with suitable ylides *via* a Wittig reaction and Horner-Wadsworth-Emmons reaction (HWE reaction) followed by hydrolysis, amide condensation with (S)-trityl-D-cysteine methyl ester, cyclization by using Hendrickson reagent, and acidic hydrolysis to provide the products **202c** and **202d**, respectively. Luciferin **202c** with one double bond gave an emission at 670 nm and **202d** gave light output at 685 nm. The emission wavelength of these two compounds was in the nIR window. However, all these novel analogues with nIR emission gave far weaker light intensities than D-luciferin. This was probably because the allyl group dramatically suppresses the binding strength with luciferase. Moreover, the replacement of the benzothiazole ring by other aromatic moieties could also reduce the enzymatic recognition.

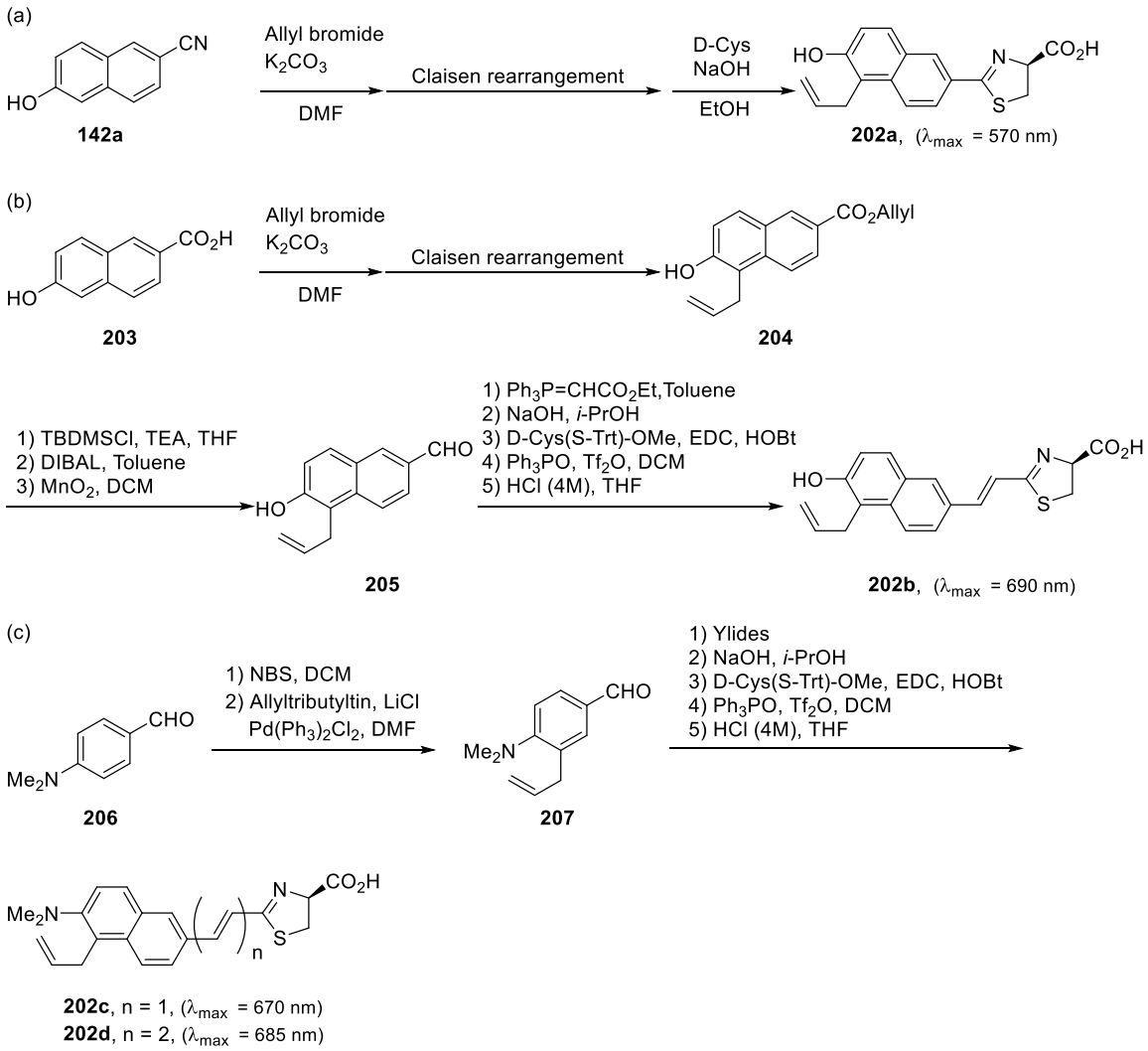

Scheme 43 The Synthesis of Allylated non-Benzothiazole Luciferins

In 2018, Kiyama and co-workers synthesized four new luciferin analogues with cyclic amino groups appended to the structure of AkaLumine luciferin **195e**. [75] Installation of various amino groups was achieved *via* S_NAr reaction on 4-fluorobenzaldehyde (**208**) to provide amino-benzaldehydes **209a-d** (Scheme 44). Conversion of the aldehydes into diene ethyl esters **210a-d** was achieved by the HWE reaction with triethyl-4-phosponocrotonate. Carboxylic acids **211a-d** were prepared by the hydrolysis of the ethyl ester of **210a-d** with NaOH. The thiazoline rings of each compound **213a-d** were constructed by treatment of the amides **212a-d** with Tf_2O (without Ph_3PO). The final step was the removal of the methyl ester by using HCl (4M) to provide the expected AkaLumine based luciferins with cyclic amino groups. With *Photinus pyralis* luciferase, all compounds showed major emissions over 650 nm. In addition, the *ee* values of **209a-209d** were measured as 77%, 75%, 77%, and 62% respectively by chiral HPLC.

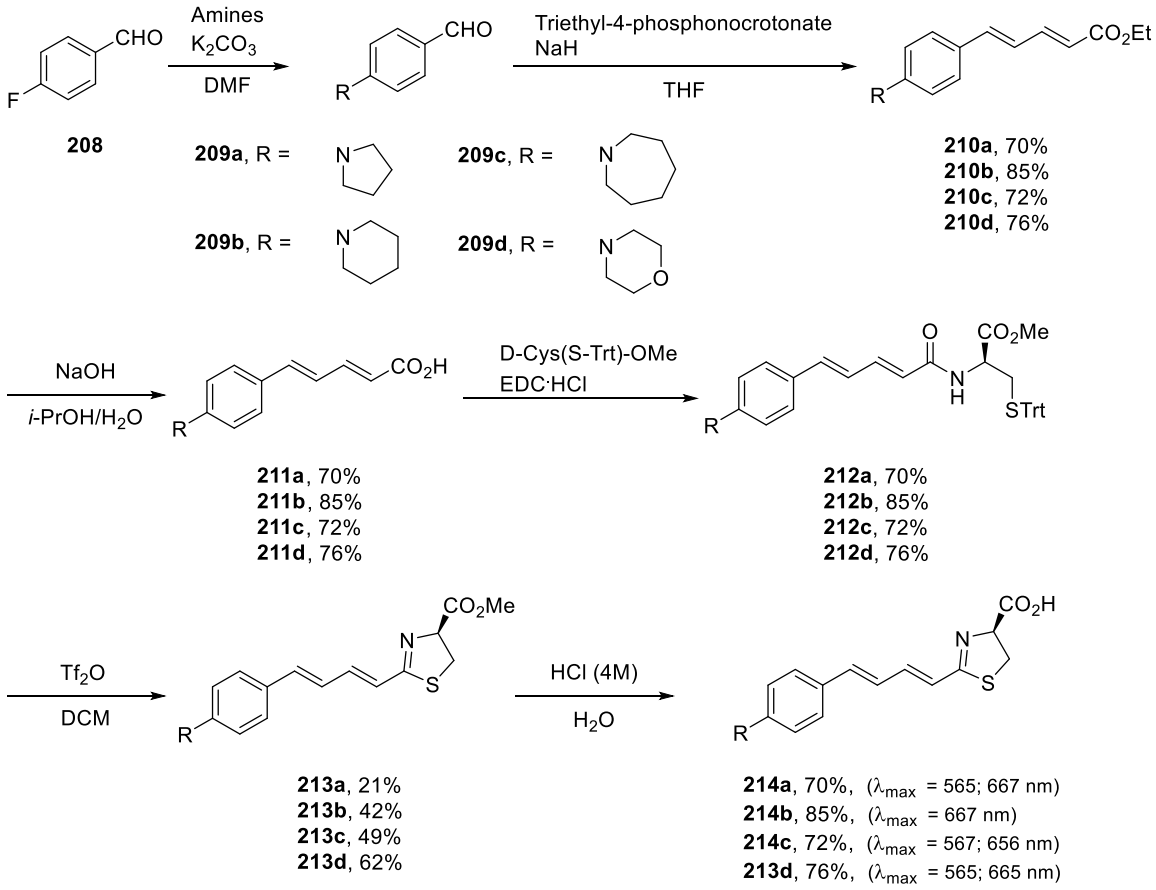

Scheme 44 The Synthesis AkaLumine Luciferin Analogues with Various Cyclic Amino Groups

In 2014, the Anderson group synthesised a pi-extended version of luciferin, infra-luciferin. [76] Taking inspiration from the work of Iwano and co-workers (Scheme 42) [71] an alkene linkage was introduced between the benzothiazole and thiazoline to extend conjugation (Scheme 45). The synthetic route consisted of 10 steps and utilised the Hendrickson method of forming the thiazoline. Protection of 2-bromo-6-hydroxylbenzothiazole (**108**) with benzyl bromide (BnBr) followed by formylation by using *n*-BuLi and DMF to provide the formylated benzothiazole **216**. The alkenyl ester was introduced *via* an HWE reaction and then the ester was hydrolysed with NaOH to provide the carboxylic acid intermediate **216**. Amide condensation with D-Cys(S-trt)-OMe mediated by BOP to yield amide **220**. The thiazoline cyclization was formed by the Hendrickson reagent method, and the benzyl group was removed by BCl_3 to give the methyl ester infra-luciferin **222**. This methyl ester **222** could be hydrolysed by pig liver esterase (PLE) to give the expected infra-luciferin **iLH2**. With a mutant enzyme x5S294T Fluc/6, this novel luciferin gave a nIR emission at 706 nm. This is the first firefly luciferin analogue with emission wavelength over 700 nm without BRET. However, this route suffered from some difficulties which resulted in poor

isolated yields of intermediates and the final product. For example, the two steps of cyclisation and deprotection were temperamental on scale-up and only a small scale (~ 10 mg) of final product could be obtained. Therefore, an alternative non-linear route was sought to improve the yield.

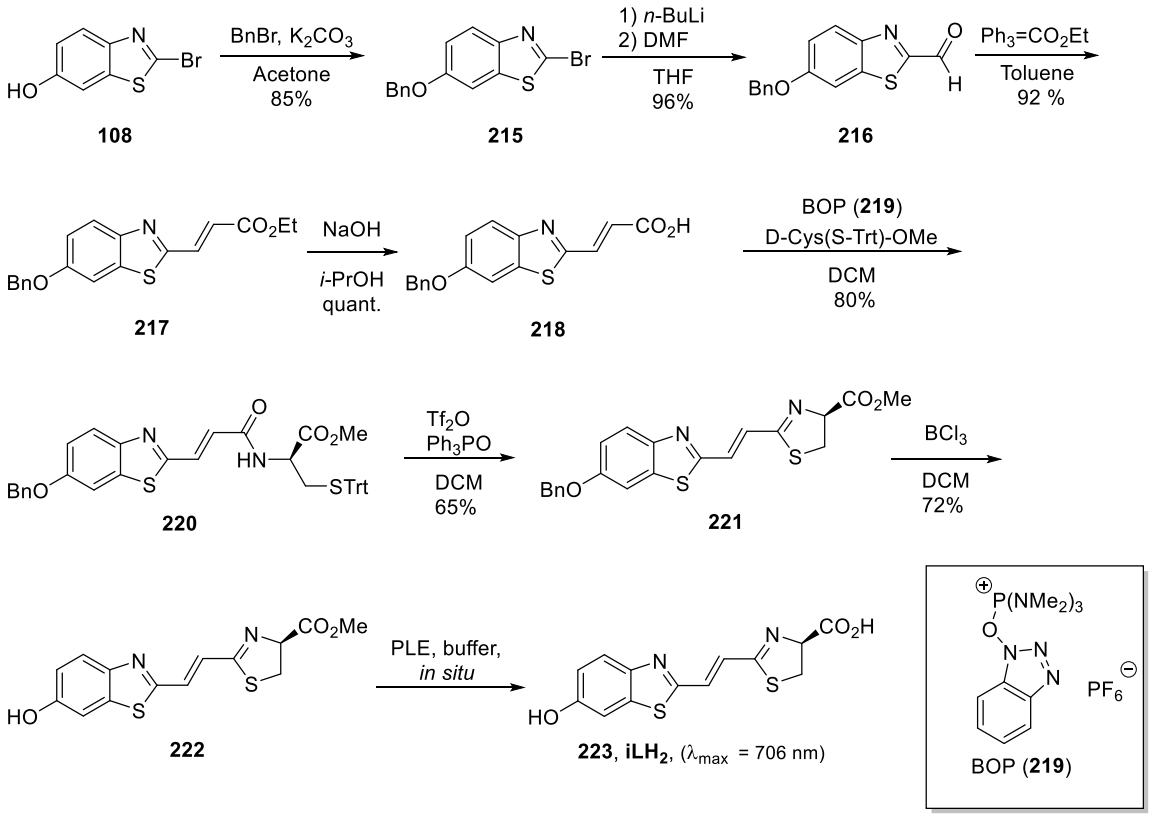

Scheme 45 The First Synthesis of **iLH$_2$**

In 2017, the Anderson group reported a new convergent synthetic route towards racemic infra-luciferin **233**, **iLH$_2$** in high yield. [77] In this synthesis, the MEM protected formyl benzothiazole **226** was prepared by following the similar route depicted in Scheme 45. Olefination of phosphonate **227** with aldehyde benzothiazole **226** provided the precursor **228** which was subjected to ring closing cyclization by DAST (Scheme 46(a)). The final compound **233**, **iLH$_2$** could be obtained after the removal of MEM with TFA and hydrolysis of the methyl ester with LiOH in high overall yield. Moreover, the luciferin analogue **226** with a diene between the two aromatic rings was delivered in the same manner (Scheme 46(b)). This diene luciferin **226** emitted bioluminescence at 675 nm with wild-type *Photinus pyralis* luciferase.

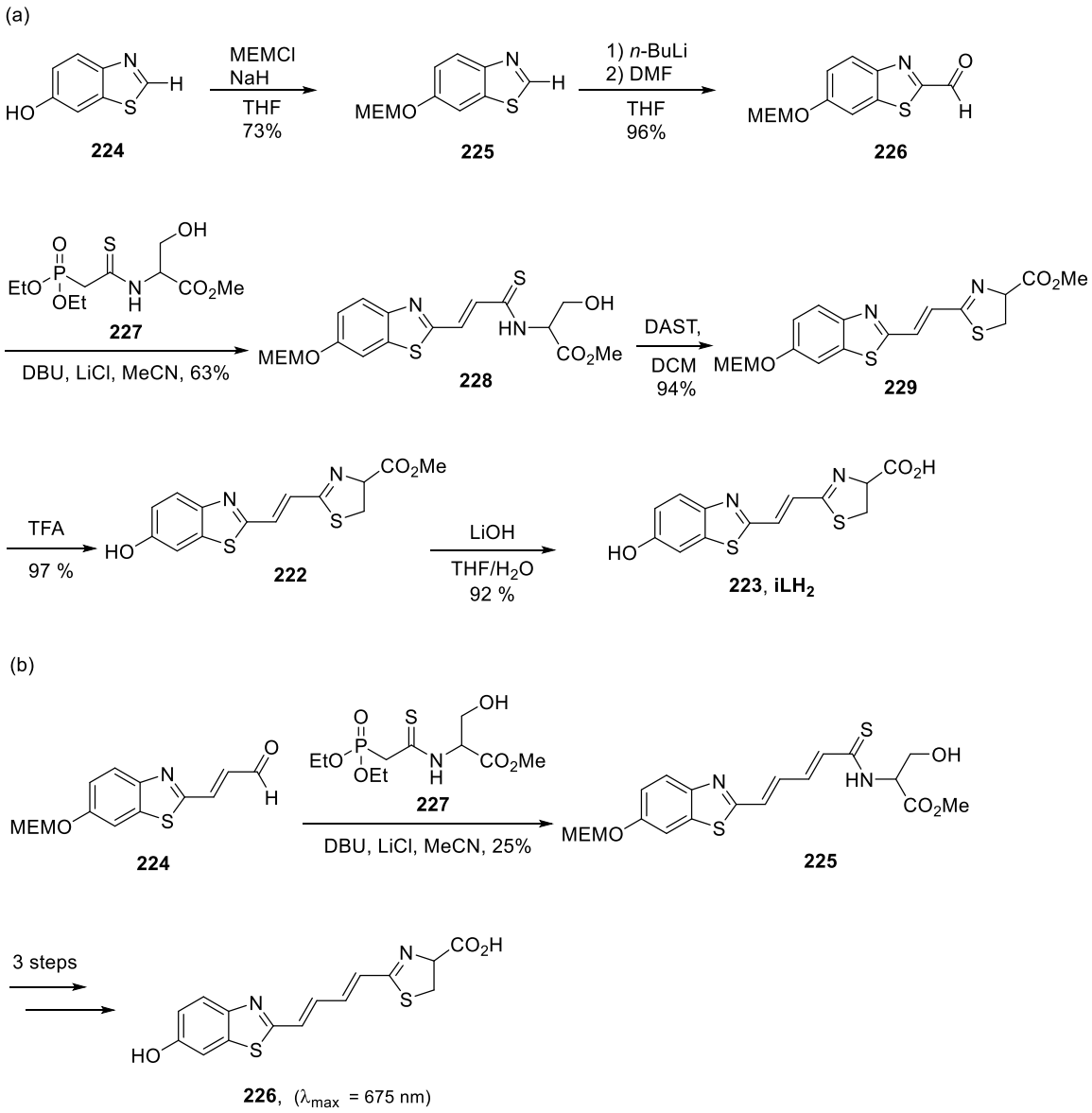

Scheme 46 The Convergent Synthesis of iLH_2 and Diene Luciferin

In this study, the important key reactant, phosphonate **227,** opened up new possibilities for the development of infra-luciferin analogues. According to the literature, [78] ethyl 2-(diethoxyphosphoryl)ethane- dithioate (**232**) was prepared in two consecutive steps *via* temperature sensitive intermediate **231** (kept below -20 °C). Treatment of compound **232** with serine methyl ester gave the phosphonate thioamide **227** in 92% (Scheme 47).

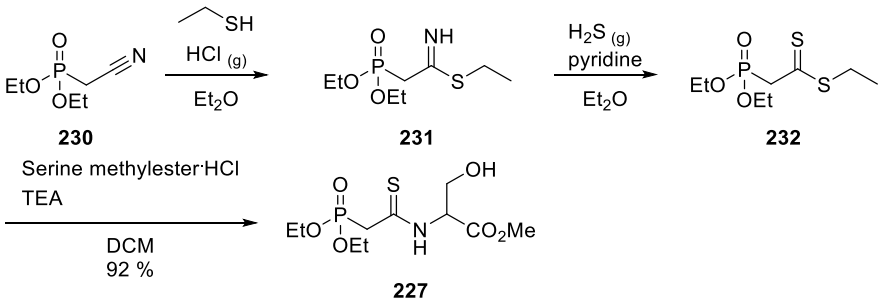

Scheme 47 The Synthesis of Key Intermediate Phosphonate

In 2019, Anderson group reported the synthesis of rotationally restricted infra-luciferin **245** for bioluminescence. Rigidification was investigated to increase light production by reducing the degrees of freedom and minimise radiation less decay. [79] For comparison purposes the benzimidazole infra luciferin was also synthesized from phenol **233**. Protection with TIPSCl under standard conditions gave silyl ether **234** (Scheme 48(a)). In a one pot reaction, imidazole **235** was obtained *via* reduction of the nitro group of **243** and intermolecular cyclisation with triethyl orthoformate in a mixture of Pd/C in acetic acid under H_2. Further protection of the amine group with 2-(trimethylsilyl)ethoxymethyl chloride (SEMCl) followed by oxidation with SeO_2 gave the corresponding formyl isomeric products **237a-b** that were separated. The alkenyl linker was introduced by reacting the aldehyde group of each isomer with the key phosphonate **227** to generate the corresponding amide products **238a-b**. Protodesilylation with TBAF followed by cyclization with DAST gave isomers **240a-b**. These two precursors could be turned into a single form after the SEM was removed by $SnCl_4$. Hydrolysis of methyl ester with PLE provided the desired benzimidazole luciferin **241**, **BiLH$_2$**. The rotationally restricted infra-luciferin **245** was synthesized from another synthetic route in two steps (Scheme 48(b)). Condensation of 2-aminopyridine with 1,4-benzoquinone under acidic conditions gave the nitrile **244** which was reacted with racemic cysteine to provide the desired rigid luciferin **245**, **PBliLH$_2$**. Further investigation of their bioluminescence, with the CBR mutant enzyme, gave an emission at 561 nm for **241**, **BiLH$_2$** and **245**, **PBliLH$_2$** had two peaks which were located at 608 nm (major) and 714 nm (minor). The minor emission of **245**, **PBliLH$_2$** is in the nIR window.

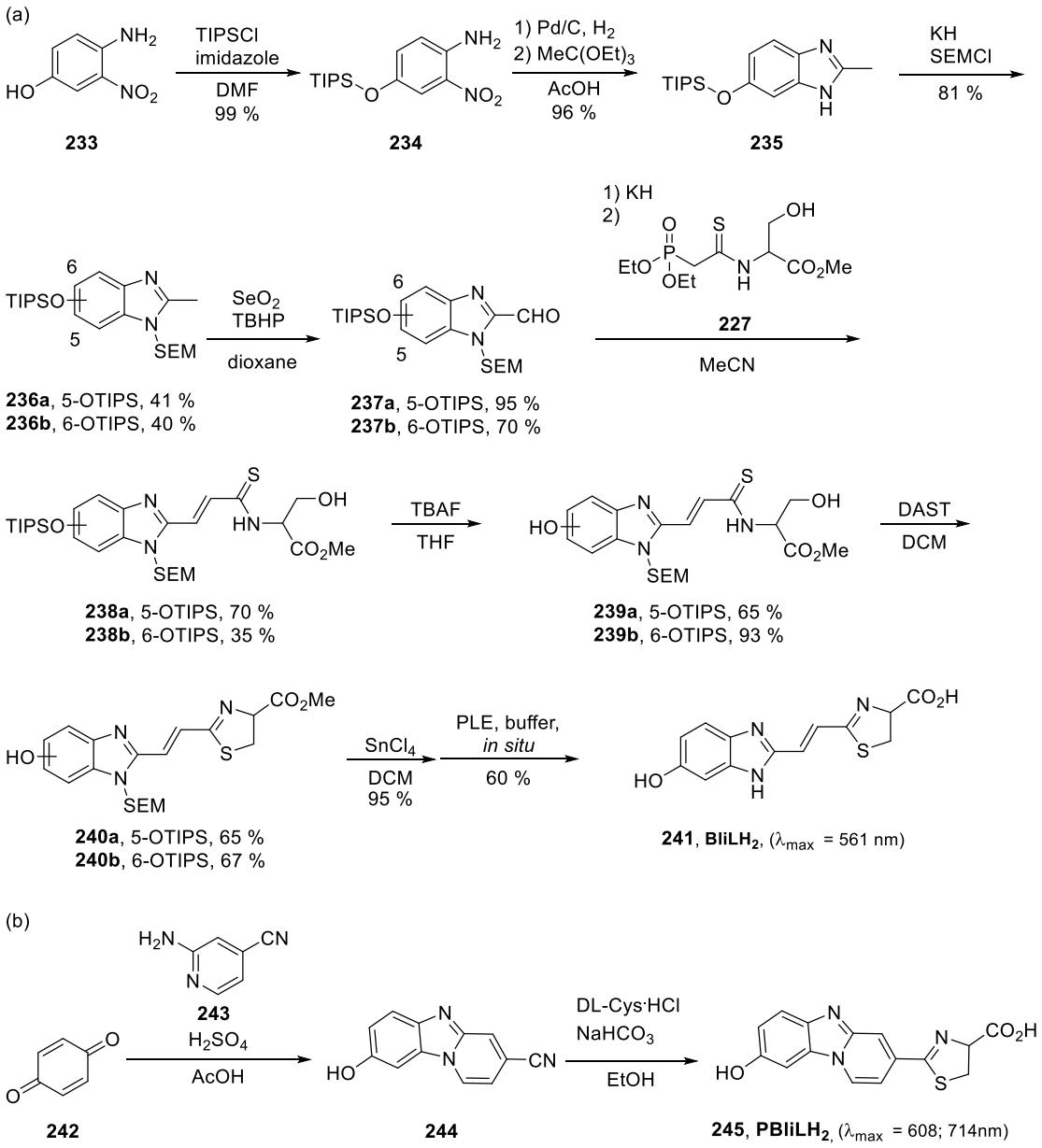

Scheme 48 The Synthesis of $BiLH_2$ and $PBliLH_2$

In 2020, Ikeda and co-workers synthesized six nIR luciferin analogues based on AkaLumine luciferin derivative **195e**. [80] In the same manner for the synthesis of AkaLumine luciferin **195e** (Scheme 42), the different ring-fused amino analogues **252a-f** were prepared (Scheme 49). These amino luciferins gave pH-independent bioluminescence with native firefly luciferase in the nIR region. Moreover, these compounds had excellent blood retention and showed brighter photon flux than D-luciferin (7-fold overall, 16-fold in the nIR window) in an *in vivo* study.

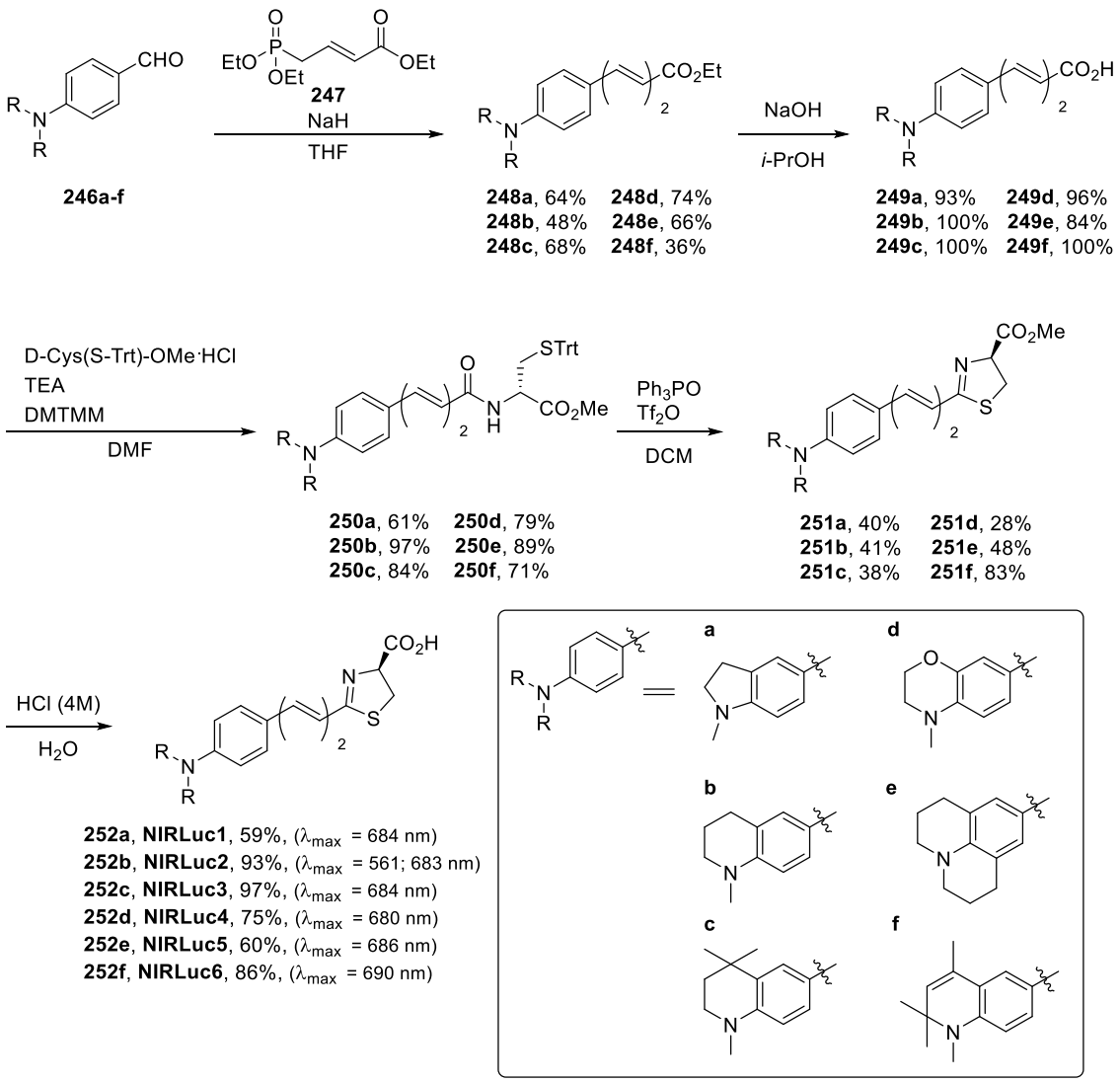

Scheme 49 The Synthesis of Ring-Fused NIRLuc

A vast array of firefly luciferin analogues has been synthesized by different synthetic approaches. Most analogues showed more red-shifted emissions than D-luciferin, some in the near-infrared window. However, these novel analogues are characterized by very much reduced quantum yields (QYs), some of around 10%, but normally 0.001-1% as bright as luciferin. How to synthesize firefly luciferin analogues with a high QY is still a challenge and the reasons behind it are discussed in the next chapter.

2. Basic Photophysical Principles

2.1 Bioluminescence Quantum Yield

The bioluminescence quantum yield ($\emptyset_B$) of firefly luciferin has been carefully measured at 0.42 by using luminol as reference. [81] Chapter 1 showed that the firefly luciferin analogues have a range of wavelengths from blue to nIR, but that the light intensities of the emissions are still far weaker than D-luciferin at between 0.01-5%. Therefore, the measurement of bioluminescence quantum efficiency or quantum yield ($\emptyset$) is important to investigate the fundamental mechanisms of photochemical and photophysical chemistry.

In the early 19th Century, the first law in photochemistry was developed. The Grotthus-Draper Law states that "only light absorbed in a chemical system is effective for a photochemical reaction to occur". A century later the Stark-Einstein Law was developed which stated that "for each photon absorbed only one molecule is activated for a chemical reaction" which is known as the Law of Photochemical Equivalence. [1] Photons participate in chemical reactions involving absorption or emission and the number of photons must be accounted for in the reactants or products in the overall stoichiometry. The equivalence is measured by the quantum yield, which is determined as the ratio of the moles of photons absorbed to those emitted.

The photochemical quantum yield is defined as Equation 1. In a pure photochemical reaction, if $\emptyset_p$ = 1.0, it indicates that a mole of reactant A absorbs one einstein and a mole of compound C is generated. When $\emptyset_p$ is less than unity, it means that other competing pathways are occurring and may lead to other unexpected products. In photo-induced or radiation-induced radical chain reactions, $\emptyset_p$ can be greater than unity.

$$A + photon \rightarrow A^* \rightarrow B \rightarrow C$$

$$\emptyset_p = \frac{(moles\ A\ coumsumed\ or\ C\ produced)}{einsteins\ absorbed} = \frac{moleculars\ of\ A\ or\ C}{photons\ absored}$$

Equation 1 The Definition of Photochemical Quantum Yield

In the event of bioluminescence, the bioluminescence quantum yield ($\emptyset_B$) is determined inversely from the photochemical reaction (Equation 2). The photons are released after

luciferins are consumed in the enzyme. The overall quantum yield of bioluminescence consists of 3 dominant factors. Chemical yield ($\emptyset_Y$) represents how many excited molecules can be generated during the chemical reaction. In the case of oxyluciferin* a highly reactive excited state intermediate is produced. In general, the chemical yield ($\emptyset_Y$) is less than unity, because the high energy intermediate can undergo side reaction(s) to give undesired product(s). Second, the excitation efficiency ($\emptyset_E$) indicates that the fraction of product produced in its excited state. Third, the fluorescence quantum yield ($\emptyset_f$) of the oxyluciferin shows the natural luminescent property. It can be the dominant part of $\emptyset_B$. For few fluorophores such as BODIPY, [82] the fluorescence quantum yield reaches unity because non-radiative decay is minimal for this structure. To summarise, the overall bioluminescence quantum yield is always less than unity.

$$Luciferin \rightarrow Adenyl-luciferin \rightarrow Oxyluciferin^* \rightarrow Oxyluciferin + photons$$
$$\emptyset_B = \emptyset_Y \emptyset_E \emptyset_f < 1.0$$

Equation 2 Equation of Bioluminescence

Fluorescence is a related photophysical property of certain molecules and the quantum yield can be interpreted in a slightly different expression (Equation 3). In this equation the quantum yield is equal to the ratio of the number of photons emitted to the number of photons absorbed. If $\emptyset_f$ = 1.0, it indicates that a mole of fluorophores can emit all the photons which are absorbed during excitation. By contrast when $\emptyset_f$ = 0.0, a mole of chromophores can absorb all the photons without any light output after excitation. The energy of excited electrons can be transferred to heat, molecular vibrations/rotations or be used for other chemical reactions. The term k_f is the rate of fluorescence and $\sum_i k_{nri}$ is the sum of the rates of different non-radiative decays in the photophysical process such as the rate of photochemistry (k_{chem}), energy transfer (k_{ET}), electron transfer (k_{eT}), internal conversion (k_{ic}) and intersystem crossing (k_{isc}). As a result, reducing the rates of all the non-radiative decay mechanisms $\sum_i k_{nri}$ leads to a higher $\emptyset_f$.

$$\emptyset_f = \frac{photons\ emitted}{photons\ absored} = \frac{k_f}{k_f + \sum_i k_{nri}} = \frac{k_f}{k_f + k_{chem} + k_{ET} + k_{eT} + k_{ic} + k_{isc} \ldots}$$

Equation 3 The Fundamental Definition of Photochemistry Quantum Yield in Fluorescence

2.2 Energy Gap Law

The energy gap law (EGL) dictates that a small band gap material usually gives low fluorescence quantum yield due to strong vibronic coupling between the ground and excited state. [83] In this case the electron prefers to undergo nonadiabatic coupling leading to non-radiative decay. It is unlike classical mechanics where the electron transitions are through simple harmonic motion. According to quantum mechanics, the energy gaps are quantized into discrete energy levels. This implies that the energy release or loss is also quantized. For a small band gap material, the rate of electron transition within different vibrational states is greater than that for larger band gap materials because the wavefunctions are similar and overlap significantly (Figure 13). As a result, an electron in a narrow band gap system can undergo non-radiative transitions multiple times resulting in greater energy loss. By contrast, the rate of non-radiative decay (k_{nr}) for large band gap material is smaller, which gives rise to an opportunity for conversion of the energy to photons instead of heat. Therefore, it remains a challenge to develop a narrow band gap material with high fluorescence quantum yield.

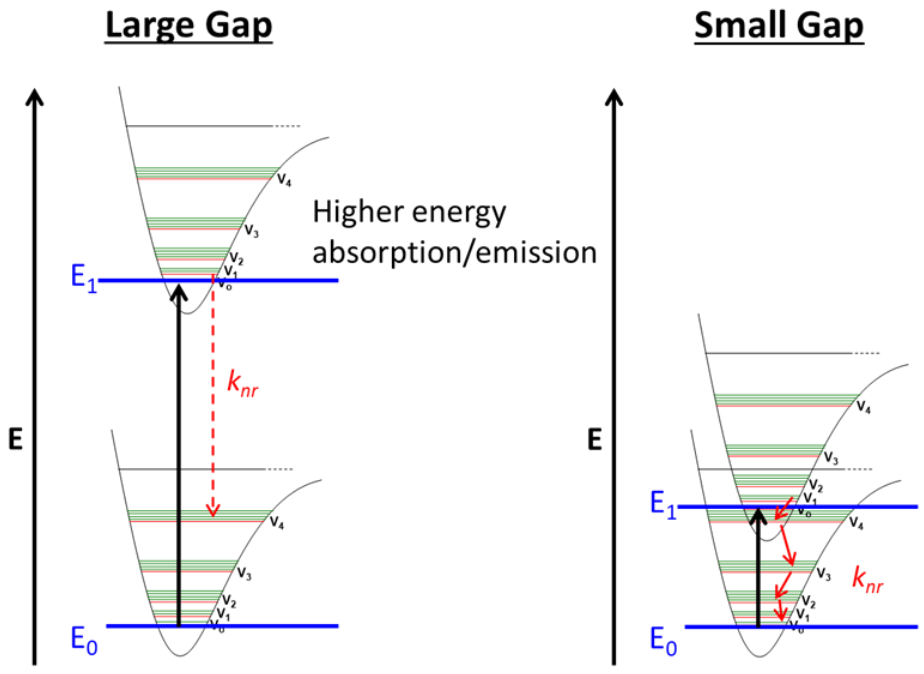

Figure 13 The Rate of Electron Transition between Large and Small Band Gap [83d]

2.3 Jablonski Diagram

The Polish physicist Aleksander Jablonski depicted a diagram (Figure 14) to illustrate the electronic states of a molecule and electron transition within a molecular system. [84] In this diagram, the number of interactions such as energy transfer (ET), molecular collisions, and solvent effect… etc. are excluded. According to Kasha's rule and the Franck-Condon Transition (10^{-15} sec), the electrons at ground state (S_0) can be excited to higher energy levels (S_1, S_2…etc.) and then the singlet excited state electrons rapidly relax to the lowest vibrational level (v = 0) of S_1 after internal conversion (IC) within 10^{-12} sec. Theoretically, 25% of singlet excited state electrons at v = 0 go back to S_0 with fluorescence in 10^{-8} sec. In general, a rigid molecule gives higher $\emptyset_f$ because the intramolecular motion of a molecule is supressed to give a smaller k_{ic}. The other 75% of singlet excited state electrons go to their triplet state (T_1) *via* intersystem crossing (ISC) and then return to S_0 with phosphorescence (sec-min). Molecules containing heavy atoms such as bromine or iodine increases the rate of ISC and reduce $\emptyset_f$. This diagram gives us a basic idea of how the suppression of the rate of the non-radiative decays including k_{ic} and k_{isc} can reduce non-radiative decay and thus enhance $\emptyset_f$. Because $\emptyset_f$ plays an important role in $\emptyset_B$ and it can reach 1.0, increasing $\emptyset_f$ is a possible approach to enhance the overall $\emptyset_B$.

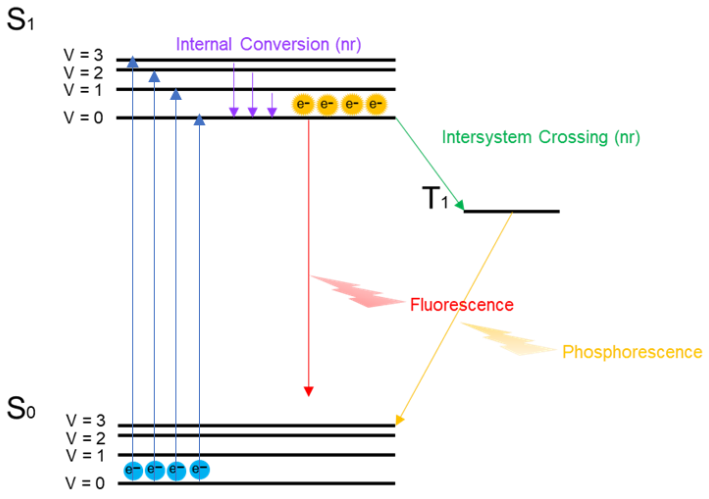

Figure 14 One form of a Jablonski Diagram

2.4 Fluorescence Quenching

As discussed above, internal conversion (IC) and intersystem crossing (ISC) can naturally reduce $\emptyset_f$ naturally. This phenomenon that suppresses the emission intensity of a fluorophore is called fluorescence quenching. Most of the time, fluorescence quenching is notorious, and scientists are always trying to avoid it. However, it is very difficult to predict $\emptyset_f$ beforehand, because the quenching process of a new compound is based on experimental results instead of calculations. A variety of mechanisms and molecular interactions can lead to fluorescence quenching. A knowledge of these mechanisms can enable scientists to design new efficient fluorophores for luminescence research. Some of common factors that lead to fluorescence quenching are detailed below.

Collisional quenching takes place when a fluorophore comes into contact with a quencher. For example, oxygen is a well-known quencher which can deactivate any fluorophore. [85] When measuring the $\emptyset_f$ and its lifetime it is necessary to remove dissolved oxygen by purging the sample with nitrogen. However, the quenching mechanism by oxygen is still unclear. The widely accepted hypothesis is that the paramagnetic oxygen induces the singlet state fluorophore to exist in its triplet state through ISC. Indole, carbazole and their derivatives are also easy to quench by H^+, Cu^{2+}, Pb^{2+}, Cd^{2+}, and Mn^{2+}. This is because the excited state electron of these fluorophores can be trapped by these electron scavengers through collisions. Additionally, indole, tryptophan and their derivatives can be quenched by acrylamide, succinimide, dichloroacetamide, dimethylformamide, pyridinium hydrochloride, imidazolium hydrochloride, methionine, Eu^{3+}, Ag^+, and Cs^+. [86]

Static quenching takes place when a complex is formed between the fluorophore and the quencher. For example, a mixture of anthracene and diethylaniline in nonpolar solvents generates a fluorescent exciplex, but fluorescence quenching occurs in highly polar solvent systems.

If the distance between the two counterparts is less than 2 Å it can lead to aggregation caused quenching (ACQ). [87] The ACQ can result from the strong electrostatic interactions based on strong π-π stacking. [83b] The fluorescence emission of aromatic compounds bearing -NO_2 are usually weak because the strong electron withdrawing group leads to larger non-radiative decay values (k_{nr}) caused by fast charge recombination. [88]

Aromatic compounds with azo groups are regarded as dark quenchers and photoswitch with no native fluorescence. [89] The suppression of the radiative decay process can be attributed to the fact that the energy is used for the formation of a photo-isomer and the vibration of the azo bond.

Energy transfer (ET) is another reason for fluorescence quenching and it is different from electronic relaxation where the energy is converted into heat *via* non-radiative decay such as IC and ISC. [90] Förster resonance energy transfer (FRET) is the most well-known of the ET processes and has been applied to materials and the life sciences for more red-shifted emission. This type of energy transfer can be intra- or intermolecular and happens whenever the emission spectrum of a fluorophore (donor) partially overlaps with the absorption of another fluorophore (acceptor). This mechanism can be simply illustrated by a Jablonski diagram of FRET (Figure 15). The relaxation energy from the donor is allowed to excite the acceptor *via* FRET and the acceptor gives a longer wavelength fluorescence with lower intensity than the initial excitation energy. Moreover, resonance energy transfer processes reduce the emission intensity of the donor leading to weak or no fluorescence.

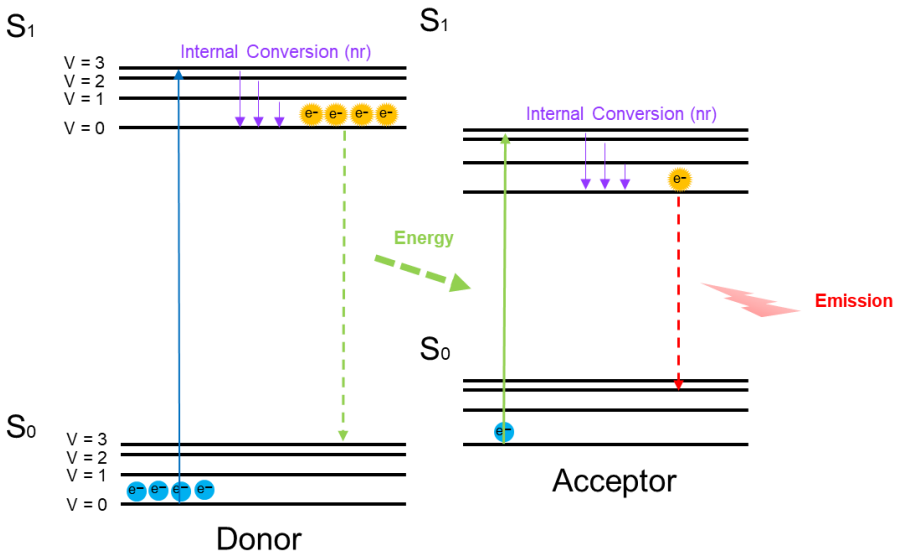

Figure 15 Jablonski Diagram of FRET

FRET is distance dependent and the rate $k_T(r)$ can be defined by the distance between the donor and the acceptor (Equation 4). The Förster distance (R_0) refers to the separation distance between the donor and the acceptor when the ET efficiency reaches 50%; r is the

distant between the centre of the donor and the acceptor; τ_D is the lifetime of the donor in the absence of ET.

$$k_T(r) = \frac{1}{\tau_D}(\frac{R_0}{r})^6$$

Equation 4 The Rate of Energy Transfer

The efficiency E can be given by the Equation 5. The R_0 can range from 10 Å to 100 Å, which is shorter than the radiation wavelength.

$$E = \frac{R_0^6}{R_0^6 + r^6}$$

Equation 5 The Energy Transfer Efficiency E

Intra- and intermolecular electron transfer (eT) could lead to non-radiative decay. This process is known as Dexter electron transfer (DeT). [84] The electron transfer can be stepwise or concerted. The mechanism is depicted in Figure 16. The electron in the LUMO of the excited donor transfers to the LUMO of the acceptor and then the electron in the HOMO of the acceptor transfers back to the HOMO of the donor. As a result, the excited electron is allocated in the acceptor part. The distance between the donor-acceptor pair is less than 10 Å and this process requires wavefunction and electron orbital overlap. Moreover, high concentration (1 M) is generally required for intermolecular Dexter interactions. For intramolecular electron transfer systems, the mechanism is the same as intermolecular DeT. The distant (~10 Å) is important to allow electrons to jump from the donor to the acceptor even through a non-conjugated space.

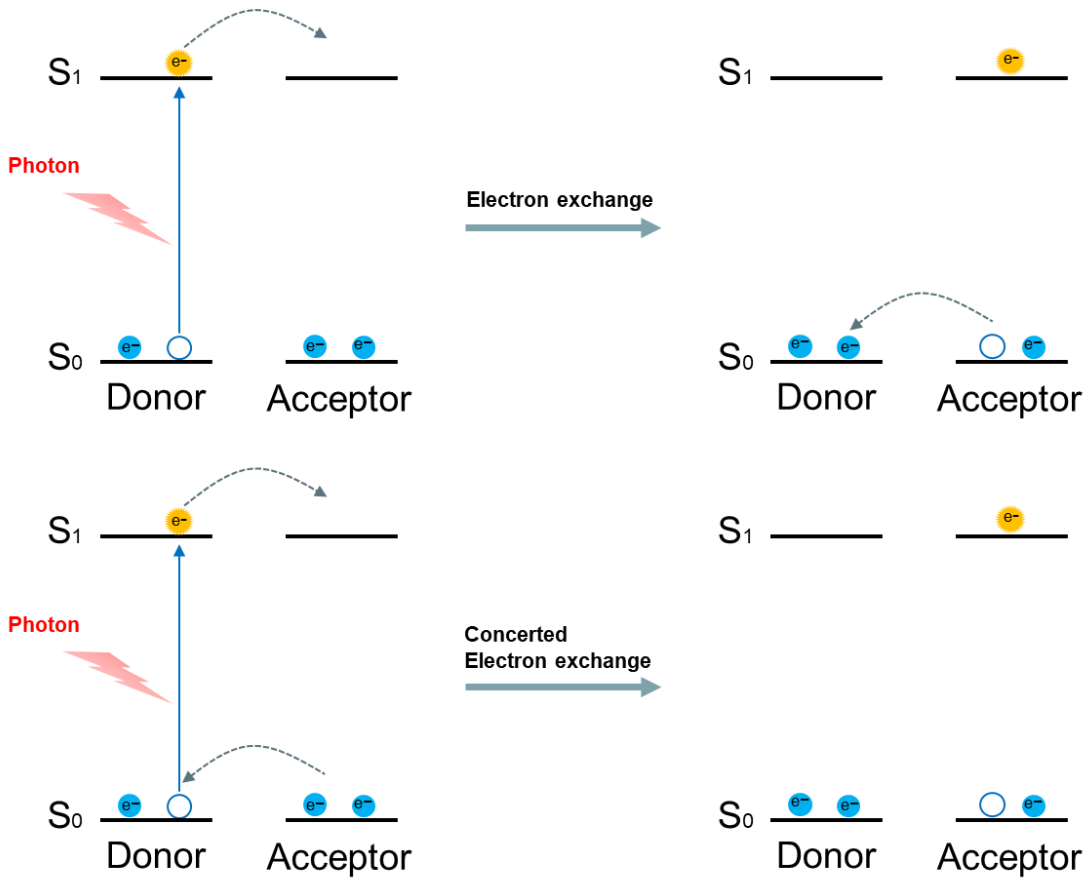

Figure 16 The Diagram of Electron Transfer (et)

2.5 Photophysical and Photochemical Study of D-Luciferin and its Derivatives

2.5.1 Quantum Yield Suppression *via* Photophysical Process

Bioluminescent enzyme-induced electron transfer (BioLeT) is a non-radiative decay leading to excited state luminescence quenching. According to the concept of electron transfer (eT), in 2015, Takakura and co-workers proposed a new strategy for the detection of nitic oxide (NO) *in vivo* by synthesising a series of bioluminogenic probes based on the skeleton of amino-luciferin. [91] In this study, the luminescence signal (on/off) could be tuned by installation of various phenyl groups onto the amino-luciferin moiety. They hypothesized that the rate of electron transfer (k_{eT}) was dependent on the HOMO energy of the electron donor part. Treatment of *Photinus pyralis* luciferase with **Substrate 2** bearing a bulky and less electron-donating anilide gave 70-fold stronger bioluminescence intensity at 600 nm than **Substrate 1** bearing a strong electron-donating aniline (Figure 17). This was attributed to fact that the rate of electron transfer (k_{eT}) between suitably similar donor and acceptor orbitals can take place much faster than the usual light emitting

process. The higher HOMO energy of **Substrate 1** facilitates k_{eT} and the electron rapidly jumps to the HOMO of the excited luminophore. The original excited electron of the luminophore cannot return to the ground state *via* radiative decay because the electron orbital has been occupied by the electron from the donor part.

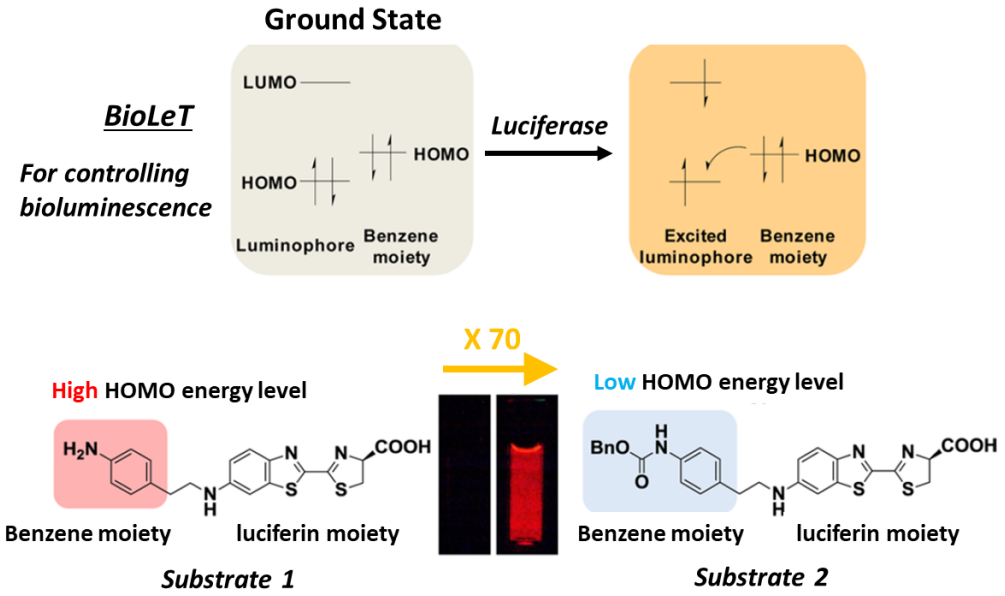

Figure 17 Mechanism of BioLet quenching and Chemical Structure of **Substrate 1** and **2** [91]

In addition, to investigate whether the concept of BioLet was a suitable method to modulate bioluminescence intensity, a group of urethane amino-luciferin analogues were rationally designed and synthesized (Figure 18 (A)). Novel amino-luciferin analogues were prepared by installation of a range of benzene moieties with HOMO energy levels within -7.0 and -4.5 eV. The correlation (Figure 18 (B)) between HOMO energy and luminescence intensity was recorded. The bioluminescence intensities of new analogues were suppressed as the HOMO energy of benzene moieties increased. It is worth noting that when the HOMO energy was above -5.0 eV, the amino-luciferins were non-luminescent due to BioLet quenching. The HOMO energy level of benzene moieties can be predicted by computational calculation or measured by using cyclic voltammetry before synthesis.

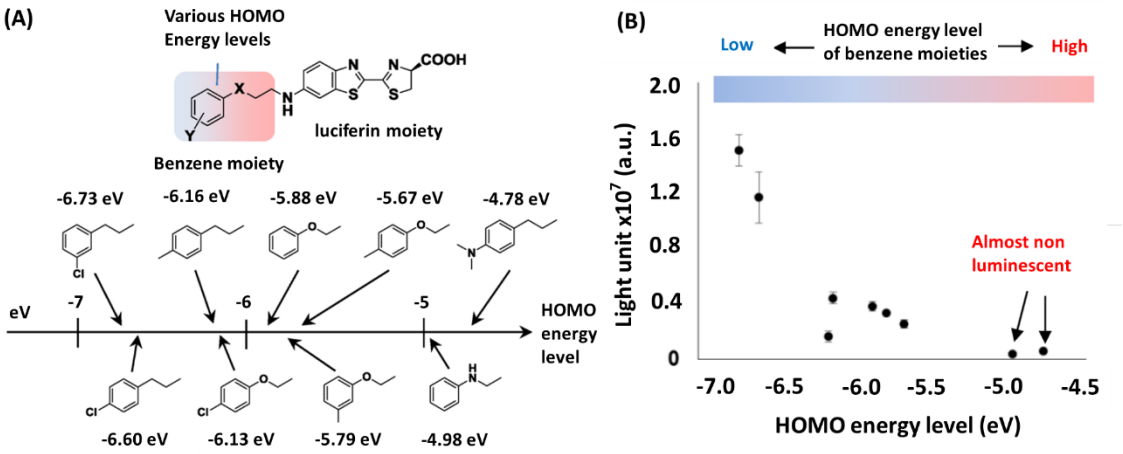

Figure 18 (A) The Benzene Moieties (B) The Correlation Between Light Intensity and HOMO [91]

Finally, a new nitric probe DAL with a diamino group was prepared according to the concept of BioLet (Figure 19). In the presence of NO and O_2, the strong electron-donating diamino-phenyl group of DAL was converted into an electron-withdrawing triazole to give a lower HOMO level product DAL-T which gave luminescence *in vivo* and *in vitro*.

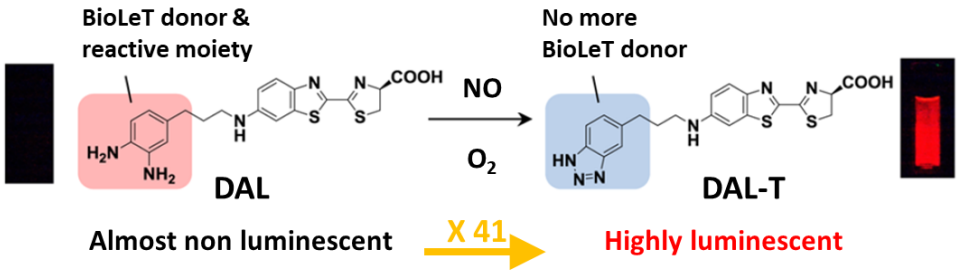

Figure 19 Development of the highly luminescent NO probe **DAL** [91]

2.5.2 Factors Affecting the Quantum Yield *via* Photochemical Process

The reason why the $\emptyset_B$ of D-luciferin (0.42) is less than unity is not fully understood. One of the reasons might be the suppression by photochemical (keto-phenolate tautomerization etc. Figure 4) process.

In 2017, Pirrung and co-worker prepared β-deuterium luciferin to investigate the tautomerism effect and isotope effects on bioluminescence (Scheme 50). [92] Theoretically, compound **16a** would show slower tautomerization than oxyluciferin **16** and give stronger light intensity due to less non-radiative decay. However, the result showed an insignificant

tautomerism effect on bioluminescence. The hypothesis also proposed that by reducing the formation of the two powerful inhibitors **17** and **17a** would be possible to enhance $\emptyset_B$. Di-deuterated luciferin **1a** was expected to impede the rate to form inhibitor **17a** and further impact bioluminescent efficiency. However, the bioluminescence intensity did not change significantly. The tautomerization process might not be a dominant factor in the suppression of the $\emptyset_B$ of D-luciferin.

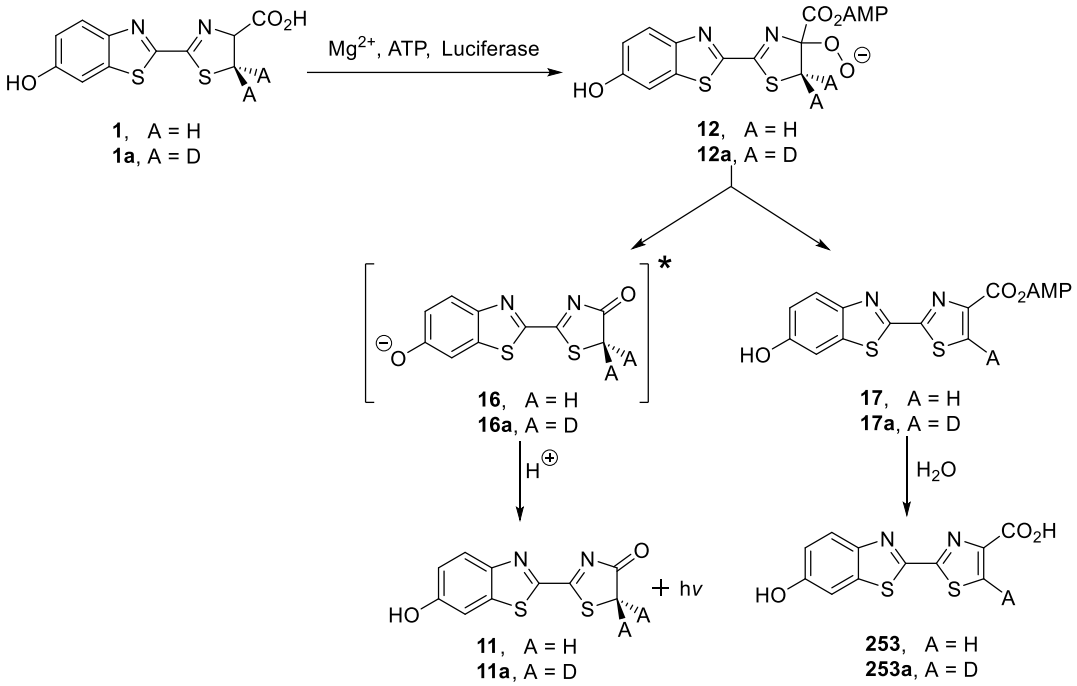

Scheme 50 Structural investigation of factors affecting $\emptyset_B$

3. Boron-based Luciferin Analogues

Synthesis of New Boron-Based Luciferin Analogues

3.1 Introduction of Boron Dyes

Boron aromatic complexes (Figure 20) are typical fluorescent dyes that have versatile applications in organic optical materials, electronic devices, and chemosensors. [93] These types of fluorescent materials usually give long wavelength emissions and high fluorescence quantum yields due to their planar and rigid structures. Different synthetic approaches have been applied to the synthesis of N-heteroaromatic ring-fused moieties bridged with a boron atom. The electrophilic boron atom possessing an empty electron orbital allows the generation of stable four-coordinate boron complexes by formation of intramolecular N-B-N or N-B-O chelated bonds. The addition of a strong electron accepting unit, most commonly enhanced by fluoride substitution, or bulky substituents such as mesityl groups to these π-conjugated frameworks have been employed to modulate HOMO and LUMO energy levels for different colour emissions. The bulkier groups prevent unnecessary nucleophilic attack to the boron and increase the stability of these complexes.

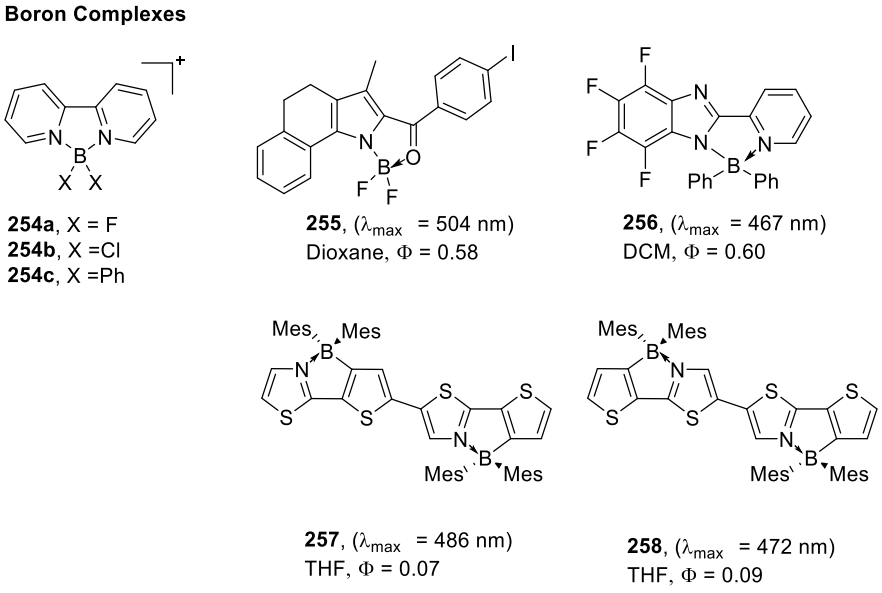

Figure 20 The Structures of Boron Complexes and Boron Dyes

3.2 Aim of Project and Research Proposal

The aim of this project was to develop bright nIR bioluminescent molecules for deep tissue imaging. This would be achieved through the synthesis of luciferin analogues with improved quantum yields and nIR emissions.

Stronger vibration and rotation in luciferin analogues may be the largest component of radiation-less decay. This could be exacerbated in infra-luciferin **223** compared to D-luciferin due to there being two sigma bonds that allow additional intramolecular motions.

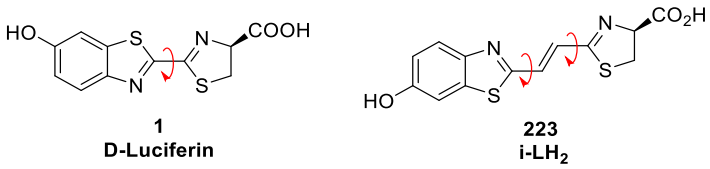

Figure 21 nIR Luciferin **223** with 2 Flexible Bonds

In this project, we investigated whether the rigidification of luciferin derivatives will increase the quantum yield of their bioluminescence. We proposed to do this by introducing a coordinated boron species to certain positions which enables linkage of adjacent hetrocyclic rings.

Studies in the literature with fluorescent molecules have shown the beneficial effect of boron coordination. Boron complexes (Figure 20) are considered as rigid structures and have been applied to many optical materials. Quantum yields and red-shifted emissions have been increased due to a reduction in the degrees of freedom and rigidification which enhances conjugation. We proposed to apply these concepts to luciferin structures and investigate the bioluminescence characteristics of the new analogues.

3.3 Design and Synthesis of Boron-Based D-Luciferin

Based on the concept that boron can coordinate between donor atoms we envisaged that boron could possibly link the two nitrogen atoms of the benzothiazole and thiazoline units of D-luciferin (**260**, Scheme 51). We decided to investigate and characterize the coordination complex between D-luciferin and $BF_3{\cdot}OEt_2$. The effect that boron coordination may have on the light output and its wavelength would be investigated by

fluorescence, chemiluminescence and bioluminescence measurements on the isolated compound.

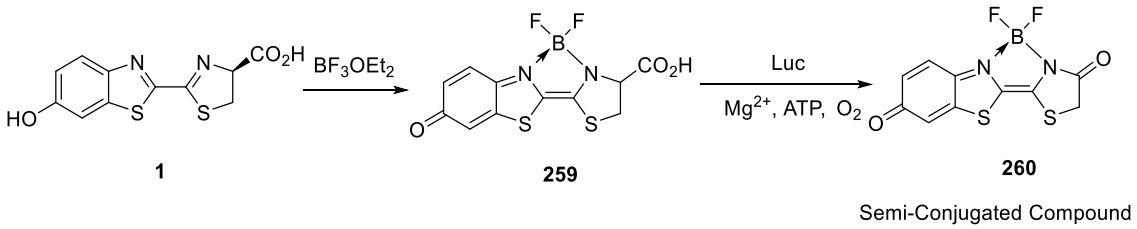

Scheme 51 Boron-Based D-Luciferin Analogues

In 1973, the crystal structure of D-luciferin (Figure 22 (a)) was analysed by Dennis and co-workers. [94a] From the X-ray crystal structure, it showed that the two sulfur atoms were *trans* to one another. The crystal of luciferin-luciferase substrate 5'-*O*-[N-(dehydroluciferyl)- sulfamoyl]adenosine (DLSA) was investigated by Nakatsu in 2006. [94b] The two sulfur atoms were also in a *trans* position to each other. In the proposed boron complexes **260**, the two sulfur atoms are *cis* and the two *cis* nitrogen atoms provide their lone pairs for coordination to the boron. The effect of this on the emission properties of the molecule could be very interesting.

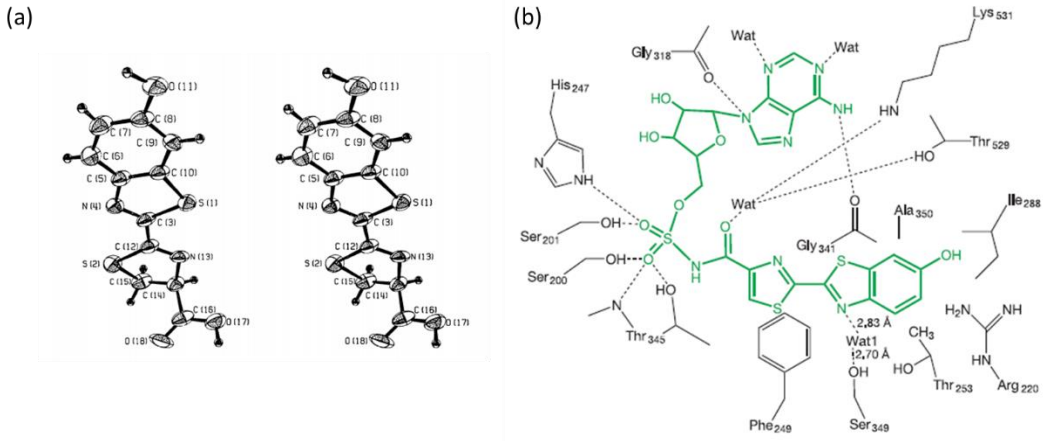

Figure 22 (a) X-Ray Crystal of D-Luciferin in Solid State [94a] (b) X-Ray of DLSA [94b]

The bonds between the boron and the two nitrogen atoms determine the chemical and physical properties of the products. The coordination of boron could occur in a variety of ways and we will characterize the mode of bonding on these novel complexes by NMR spectroscopy and X-ray diffraction where applicable. We were aware before our studies that the carboxylic acid group could interfere with the desired chelation.

3.3.1 Work Plan I

We first attempted to prepare a boron-based D-luciferin **260** (Scheme 51) based on the similar structure of the group of complexes **254** (Figure 20). To enable this, we synthesized racemic luciferin by following the synthetic routes published by White in 1961, [6a] and Prescher in 2012. [39]

Appel's Salt (**36**) is a well-known chemical devoted to reactions with phenol, arylamines and active methylene compounds. This was prepared by treating chloroacetonitrile (**261**) with sulfur monochloride (Scheme 52) to give **36** in a high yield of 95%.

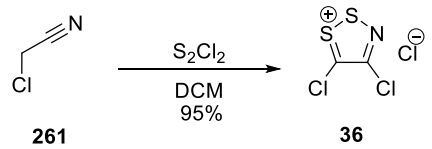

Scheme 52 The Preparation of Appel's Salt

Various mechanisms have been investigated for Appel's salt formation from chloroacetonitrile (**261**), but there is no concrete evidence available. [95] The reaction is believed to be initiated by the nucleophilic attack of chloroacetonitrile (**261**) to sulfur monochloride followed by re-chlorination to give the imine intermediate **262** (Scheme 53). The cyclised product was produced after imine-enamine tautomerism, the nucleophilic addition to S_2Cl_2, followed by the release of protons and disulfur to give Appel's salt (**36**).

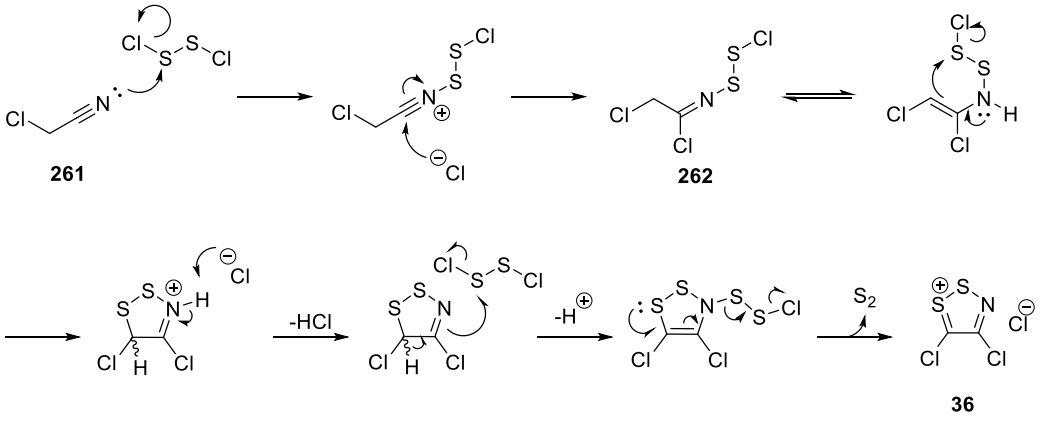

Scheme 53 A Possible Mechanism of Appel's Salt Formation

According to the published procedures, [40] *p*-anisidine (**27**) was treated with Appel's salt (**36)** to provide the desired dithiazole product which was purified by chromatography on

silica gel to give **39** in an excellent yield of 95% (lit.[39] yield 99%). (Scheme 54). The dithiazole product **39** was dissolved in sulfolane and heated to 180 °C for 20 min to give 2-cyano-6-methoxybenzothiazole (**33)**, which was used in the next step without any purification. Nitrile **33** was mixed with pyridine hydrochloride (10 eq) and heated to 180 °C for 1 hour to give phenol compound **34** in isolated yields of 58-65% (lit.[39] yield 61%). To investigate whether the reaction procedure could be shortened for the transformation **39** to **34**, a one pot reaction where compound **39** and pyridine hydrochloride (10 eq) were heated in sulfolane at 180 °C for 1 hour was attempted. However, both benzothiazole products **33** and phenol **34** could not be obtained due to degradation. Nitrile **34** was then condensed with racemic cysteine hydrochloride monohydrate under mild conditions to provide racemic luciferin (**1)** in a good yield of 90% (lit.[39] yield 86%).

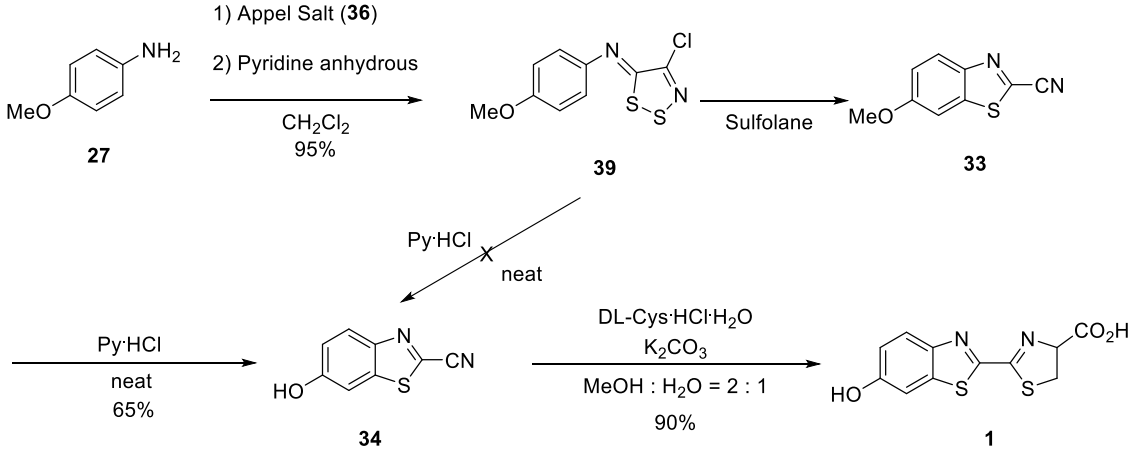

Scheme 54 The Synthetic route of Boron-Based D-Luciferin

The coordination of racemic luciferin (**1**) with $BF_3{\cdot}OEt_2$ was studied by ^1H NMR spectroscopy. Racemic luciferin (5.0 mg) and $BF_3{\cdot}OEt_2$ (1 eq) were dissolved in methanol-d_4 in an NMR tube (Scheme 55).

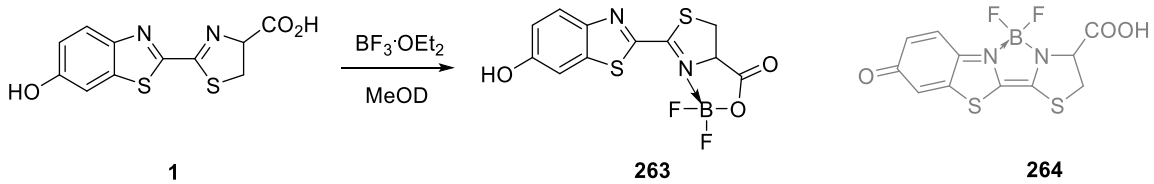

Scheme 55 Treatment of Luciferin with $BF_3{\cdot}OEt_2$

Clear shifts in proton signals indicated some coordination complex formation (Figure 23(a)) and the chemical shift of these protons are detailed in Table 2. From the time zero

spectrum (Figure 23(b)) to the spectrum of 3 h at rt, new peaks (H_a', H_b', and H_c') were observed. The strong electron withdrawing ability of the BF_2 group could explain the down field shift of the signals. After 24 hours, all the starting material had been consumed, and the conversion of desired product was achieved quantitatively and in high chemical purity in the NMR spectrum.

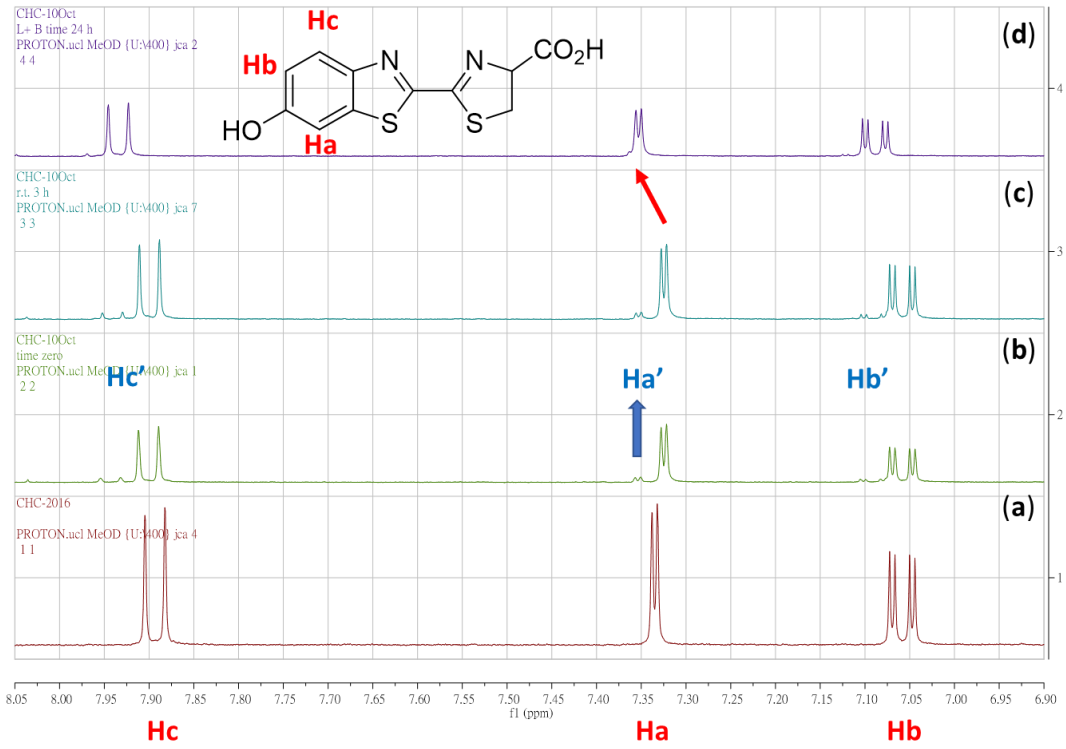

Figure 23 (a) The peaks of Racemic Luciferin within Aromatic Range (b) Time Zero Spectrum of DL-Luciferin mixed with BF_3·OEt_2 (c) Reaction at r.t. for 3 h (d) Reaction at r.t. for 24 h. *Solvent (methanol-d_4).

	Time Zero (T = 0)		After 24 h
H_a	7.32 ppm (2.0 Hz)	H_a'	7.35 ppm (2.0 Hz)
H_b	7.01 ppm (8.0 Hz)	H_b'	7.05 ppm (8.0 Hz)
H_c	7.90 ppm (8.0 Hz)	H_c'	7.93 ppm (8.0 Hz)

Table 2 The Chemical Shift of Protons (H_a, H_b and H_c at Time Zero and H_a' H_b' and H_c' After 24 h)

In order to confirm the structure of the new product, the isolation of a single crystal was attempted from different solvent systems in the sample vials for X-ray diffraction analysis. At the beginning, there were four solvent systems and two conditions attempted to grow a single crystal (Table 3). However, after a week, there were no suitable crystal formed in all

attempts. In addition, the colour of the solutions changed from yellow to colourless. This phenomenon could be attributed to the degradation of the boron-based complex.

Solvent Systems	Conditions
MeOH/Hexane	8 °C (in the Fridge), Darkness, Under air
MeOH/Ether	8 °C (in the Fridge), Darkness, Under air
MeOH/DCM	8 °C (in the Fridge), Darkness, Under air
MeOH (Vaporized)	rt, Darkness, Under air

Table 3 The Solvent Systems and conditions for Growing Single Crystal

Due to the unsuccessful growth of a single crystal, we explored alternative techniques to determine the structure. We investigated X-ray photoelectron spectroscopy (XPS) to detect the binding energy for this complex. Coordination of boron is a determinative factor in the structural identification of this complex. The XPS spectra provided the optimized fitted binding energy of boron, and nitrogen atoms (Figure 24). Figure 24 (A) shows that the binding energy of boron was：B-F (195.2 eV), B-O (192.9 eV), and B-N (190.9 eV) respectively. The intense binding energy indicative of the B-O bond suggests that this product is not the expected structure **264**. However, a weak signal that can be attributed to a B-N bond could also be seen in the boron XPS spectrum, but the low signal to noise ratio is insufficient to prove whether the B-N bond really existed or nots in this structure. The binding energy of nitrogen was also investigated. Figure 24 (B) demonstrates that the corresponding peak N-B (398.3 eV) could also be observed and together with the weak signal in (Figure 24 (A)) provides some support for a N-B bond. In conclusion, the XPS data suggested that the structure of this boron complex was more likely to be **263** instead of **264**.

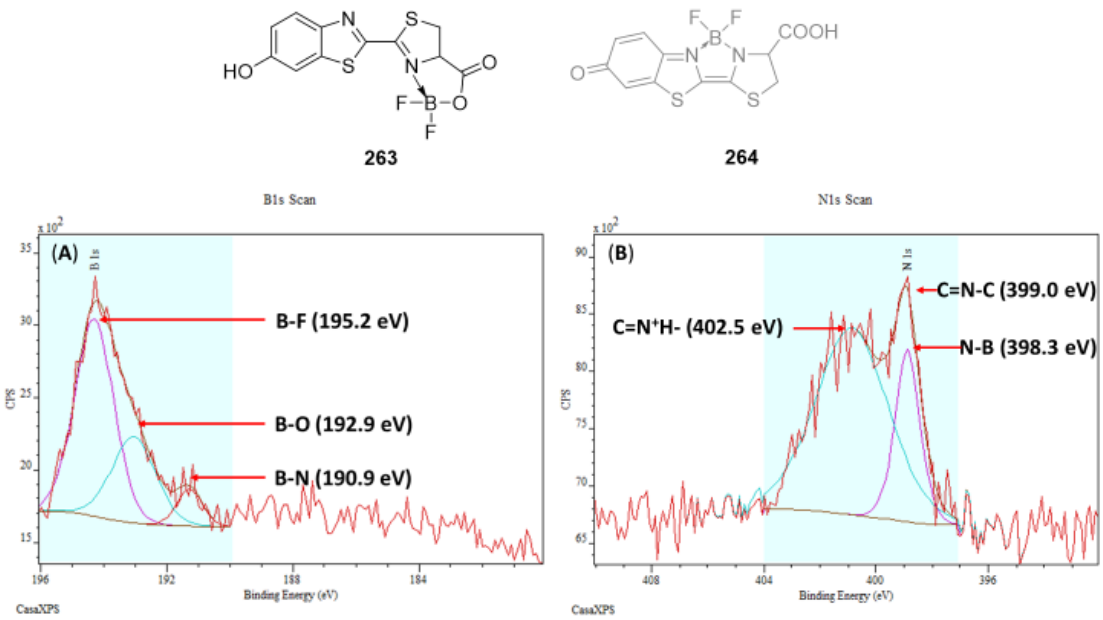

Figure 24 XPS Analysis (A) Binding Energy of Boron (B) Binding Energy of Nitrogen

This structure is also supported by the fact that boron is oxyphilic. It has been noted in the literature that, in the presence of a compound with a carboxyl group and a nearby donor atom (O or N), chelation can produce a stable five- or six-membered ring complex (Figure 25). [96] Therefore, the complex **263** is a likely structure.

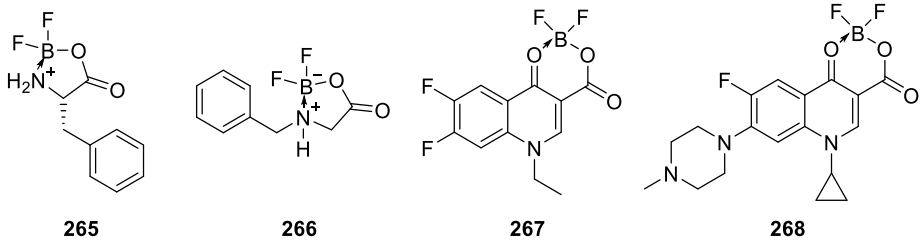

Figure 25 The Five- and Six- Membered Ring Boron Complexes

In order to fully confirm the accurate structure of complex **263**, the growth of a single crystal was attempted. Seven solvent systems were surveyed to obtain the crystals (Table 4). All the samples were kept in the sealed sample vials in the dark at 8 °C. After a week, single crystals were obtained in the bi-layer system (MeOH/Hexane). The single-crystal x-ray data showed that complex **263** had undergone esterification to form luciferin methyl ester **43** (Figure 26).

Solvent Systems	Conditions
MeOH/Hexane	8 °C (in the Fridge), Darkness, Not under inert gas
MeOH/THF	8 °C (in the Fridge), Darkness, Not under inert gas
MeOH/EtOAc	8 °C (in the Fridge), Darkness, Not under inert gas
MeOH/Ether	8 °C (in the Fridge), Darkness, Not under inert gas
MeOH/DCM	8 °C (in the Fridge), Prevent Light, Not under inert gas
MeOH	8 °C (in the Fridge), Prevent Light, Not under inert gas
MeOH (Vaporized)	8 °C (in the Fridge), Prevent Light, Not under inert gas

Table 4 The Solvent Systems and conditions for Growing Single Crystal **263**

The molecular structure is planar in the single crystal state (Figure 26). The torsion angle calculated between benzothiazole and thiazoline rings (S1-C3-C4-S2) is -178.9°, and the two nitrogen atoms are in the *anti*-position. The bond lengths of each carbon-carbon bond are appropriate for an aromatic ring (~1.4 Å) and there is π-electron delocalization through whole molecule except the carboxylic acid group.

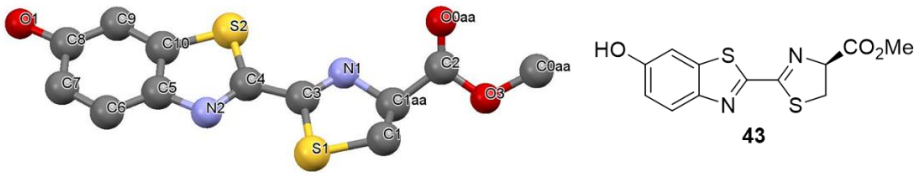

Figure 26 Single Crystal Structure of D-Luciferin Methyl Ester
Molecular structure of D-Luciferin Methyl Ester. Selected Bond Lengths [Å]: Selected Bond Angle [°]:

In the presence of MeOH, the complex **263** suggested from the XPS data (Figure 24) could be converted to its methyl ester under boron promoted Lewis acid esterification (Scheme 56).[97]

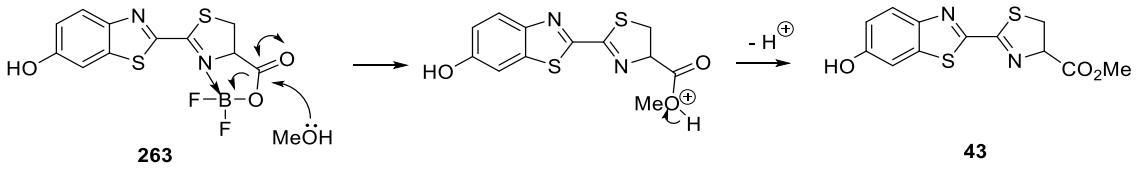

Scheme 56 The Possible Mechanism of Esterification of D-Luciferin

In summary, the treatment of DL-luciferin with BF_3·OEt in methanol gave DL-luciferin methyl ester *via* esterification. The boron reagent preferred to form a chelate between the carboxylic acid group and the thiazoline nitrogen, in preference to a *N*,*N*'-chelated structure. This suggested that protection of the carboxylic group is required.

3.4 Designed and Synthesis of Boron-based Benzimidazole-Luciferin

The benzimidazole luciferin analogue **140a** has two potential modes of chelation with boron species, **269** and **270** (Scheme 57). We hypothesized that these two isomers, when oxidised to their respective oxyluciferins **271** and **272** if recognised by the luciferase enzyme, will have different electronic interactions, which will lead to different wavelengths of emission.

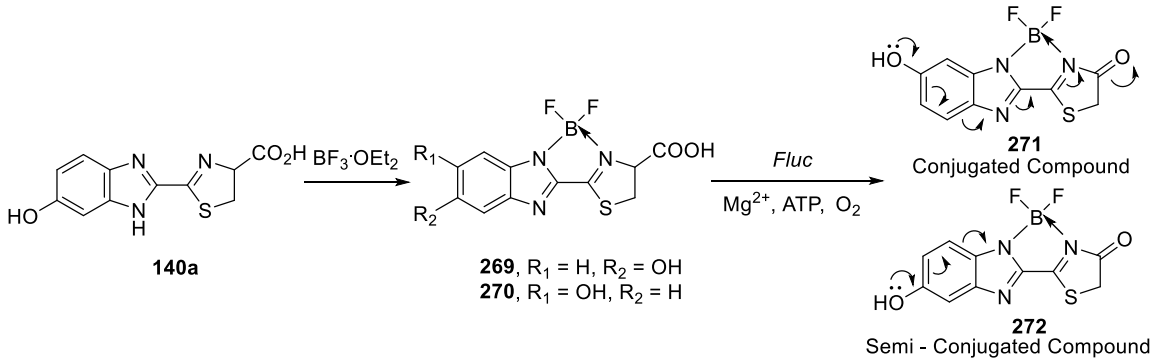

Scheme 57 Boron-based Benzimidazole-Luciferin

To enable the integrity of the phenol group to be maintained while encouraging *N*,*N*-chelation, we decided to investigate the benzimidazole-based luciferin **140a** with $BF_3{\cdot}OEt_2$. In order to prevent covalent attachment of boron to the carboxylic acid, we proposed to protect the carboxylic acid as its methyl ester (Scheme 58). We would hope that the methyl ester would be hydrolysed by lipase under mild conditions [76] if its bioluminescence was investigated.

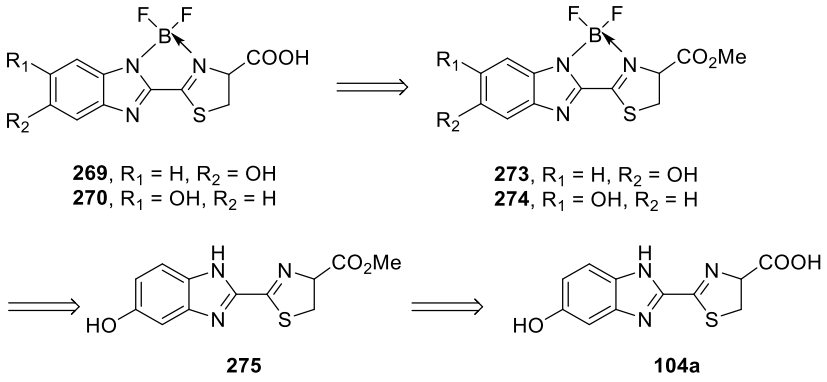

Scheme 58 Retrosynthesis of Boron-Based Benzimidazole Luciferin Analogues

The precursor **140a** of compounds **269**, **270** was synthesized by following the procedures published by Prescher in 2012 (Scheme 59). [39] Commercially available 4-methoxy-2-nitroaniline (**164**) was reduced with hydrogen and palladium on charcoal at rt for 72 hours. The unstable diamine product **165** was used without further purification. Treatment of compound **165** with Appel's salt (**36**) in anhydrous pyridine gave 2-cyano-6-methoxybenzimidazole (**132d**) in 60% isolated yield (lit.[39] yield 56%). However, attempted synthesis of intermediate product **133d** by protodemethylation was inefficient, presumably because the harsh reaction conditions (over 180 °C) led to the decomposition of 2-cyano-6-methoxybenzimidazole (**132d**). We obtained the corresponding 2-cyano-6-hydoxybenzimidazole (**133d**) in poor yield, 3-28% (lit.[39] yield 62%). The amount of product isolated was insufficient for further study. Strategies to increase the amount of compound **133d** were therefore investigated.

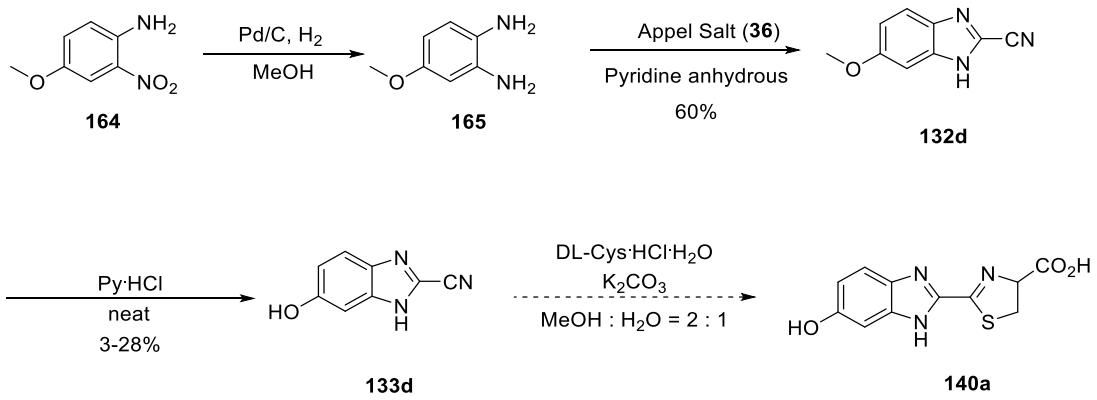

Scheme 59 The Synthetic Route Towards Compound 133d

3.4.2 Work Plan II

In plan II, we attempted a synthetic route (Scheme 60) to afford 2-cyano-6-hydoxybenzimidazole (**133d**) that started with phenol **133** in an attempt to avoid the high temperature (180 °C) required for protodemethylation. Following similar reaction conditions to that used for the methyl protected analogue (Scheme 59), [39] 4-amino-3-nitrophenol (**233**) was reduced with hydrogen and palladium on charcoal at rt until the starting material **233** had been consumed by thin layer chromatography (TLC). The corresponding diamine compound **276** was used in next step immediately because of the poor stability. Originally, we expected compound **133d** could be obtained through nucleophilic substitution by treating compound **276** with Appel's salt, but no desired

product was formed. We assume that protection of the 6-hydroxygroup plays a vital role in this synthesis.

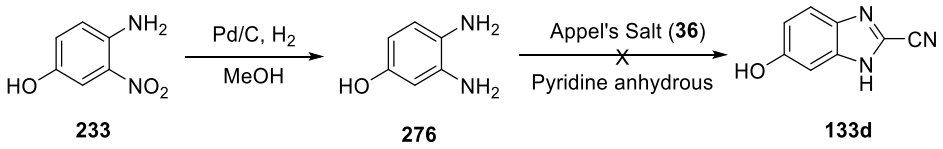

233 276 133d

Scheme 60 First modified route to 2-cyano-6-hydoxybenzimidazole

3.4.3 Work Plan III

In view of unsuccessful work plan I and II, an alternative synthetic route was attempted. The silyl protecting group TBDMS was chosen as the protecting group, which can be removed by TBAF under mild conditions. Protected product **277** was obtained in a high yield of 95% without any chromatographic purification. The TBDMS protected benzimidazole **279** was provided in a yield of 50% over two steps by the reduction of compound **277** with palladium on charcoal under hydrogen for 7 h, followed by the nucleophilic substitution reaction of the crude diamine product **278** and Appels' salt (**36**). The key intermediate **133d** could be supplied in high yield (90%) after deprotection with TBAF under standard conditions. This new synthetic route gave a higher overall yield of 45% in the formation of 2-cyano-6-hydoxybenzimidazole than the original method which gave only 1.8-15% yield (lit.[39] yield 35%) (Scheme 59). Based on this new synthetic route, the benzimidazole-based luciferin synthesis could be scaled up for the following reactions.

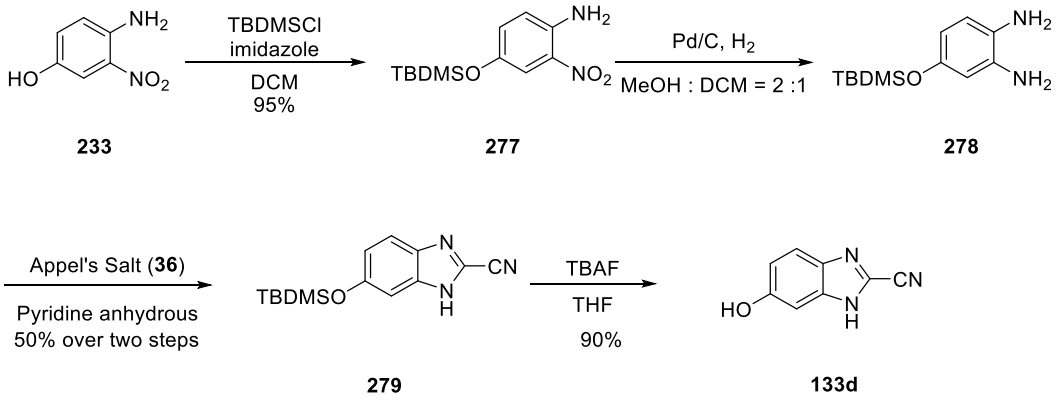

233 277 278 279 133d

Scheme 61 The Second Attempt to Afford 2-cyano-6-hydoxybenzimidazole

A model reaction to prepare the benzimidazole luciferin methyl ester was attempted by using the cheaper L-cysteine methyl ester instead of the enantiomeric D-cysteine methyl ester. Unfortunately, the cyclization of 2-cyano-6-hydroxybenzimidazle (**133d**) with commercially available L-cysteine methyl ester hydrochloride failed under a variety of reaction conditions (Scheme 62). Extending the reaction time or increasing of the reaction temperature gave no desired product (Table 5). In addition, extending the reaction time at 80 °C caused decomposition. A solution to this problem was to esterify the known benzimidazole luciferin **140a**.

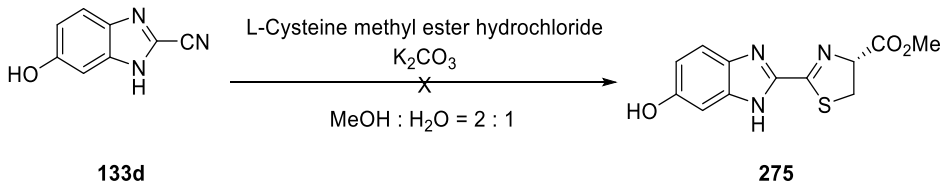

133d **275**

Scheme 62 The First Try to Synthesize Compound **275**

Attempt	Temperature	Reaction Time
1	rt	30 min
2	rt	24 h
3	80 °C	30 min
4	80 °C	24 h

Table 5 Attempted Reaction Conditions for The Synthesis of Compound **271**

Benzimidazole luciferin **140a** could be prepared by the cyclisation of compound **133d** with DL-cysteine in a yield of 52% (lit.[39] yield 82%) (Scheme 63). The carboxyl group of benzimidazole-based luciferin analogue **140a** was esterified *via* methylation using thionyl chloride in MeOH at rt for 2 h. Monitoring by NMR in methanol-d_4 showed that the conversion reached 99% after 2 h. Treatment of compound **275** with triethylamine (1.1 eq) followed by $BF_3{\cdot}OEt_2$ (1.0 eq) was expected to produce the two chelated isomers **273** and **274**.[98]

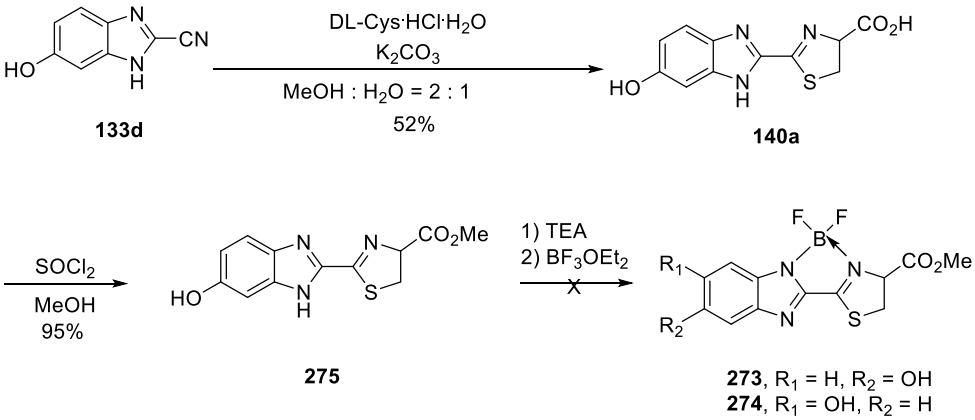

Scheme 63 An Alternative Synthetic Route for The Synthesis of **273** and **274**

This co-ordination experiment was investigated by ^{1}H NMR spectroscopy in methanol-d_4 after 24 h. From the crude ^{1}H NMR spectrum (Figure 27), two new signals for the proton alpha to the carboxyl group (Ha' and Ha'') were observed with an integration ratio of 1 to 1. Compared to the proton signal (Ha) from compound **275**, the Ha' and Ha'' proton signals were shifted upfield. It was unlikely that the lower chemical shifts of these protons were from the desired products. As the desired compound **274** possesses an electron-withdrawing group (BF_2), we would have expected that the corresponding proton signals should shift downfield.

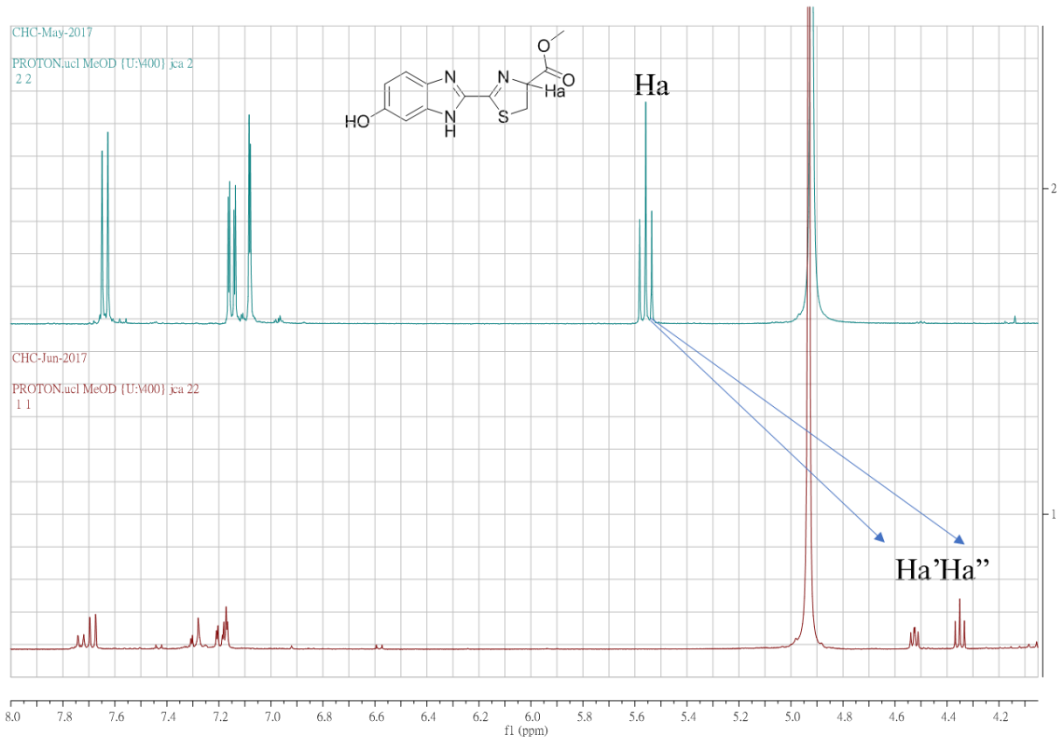

Figure 27 The Possible Product of **273** and **274** in methanol-d_4

A mechanism and possible structure were suggested to explain this phenomenon (Scheme 64). Deprotonating the phenol by TEA would lead to a covalent neutral N-BF_2 bond with the nitrogen atom still retaining its lone pair. This would be less electron withdrawing than was anticipated. Potential tautomerization could account for two compounds **281** and **281a** in the ^{1}H NMR spectrum.

It is noteworthy that three plausible atoms labelled in red and bold (nitrogen and oxygen) can coordinate to boron to form 5-membered rings. In order to confirm the actual coordination sites, isolation of these compounds was attempted by extraction with EtOAc. Drying ($MgSO_4$) of these extracts and then evaporation of the solvent gave the starting material **275** (confirmed by ^{1}H NMR). We assume that the compounds were unstable and easily underwent hydrolysis. The instability of boron complexes has been noticed in many BF_3-complexations. [99] In addition, boron-based D-luciferin **263** also appeared to have these similar properties. In view of this, the reaction mixtures were applied directly to the silica gel chromatography without any extraction. However, no product showing the same chemical shift as that observed in (Figure 27**)** was isolated.

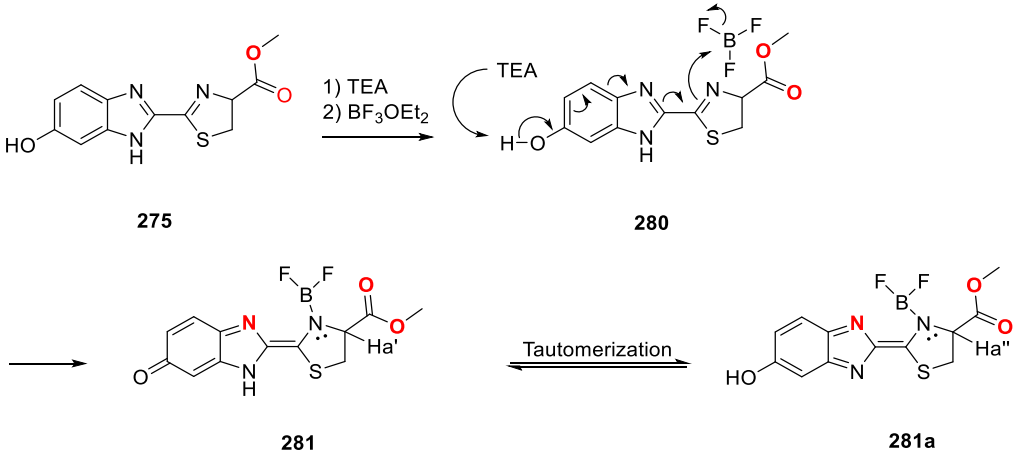

Scheme 64 A Supposed Mechanism for The New Boron-Based Benzimidazole Luciferin

For further study, triphenylborane (BPh_3) was chosen as the boron species instead of $BF_3{\cdot}OEt_2$ due to its less electron-withdrawing ability and steric hinderance which may impede water hydrolysis. The reaction was performed as before with triethylamine as base and then triphenylborane added in anhydrous THF (Scheme 65).

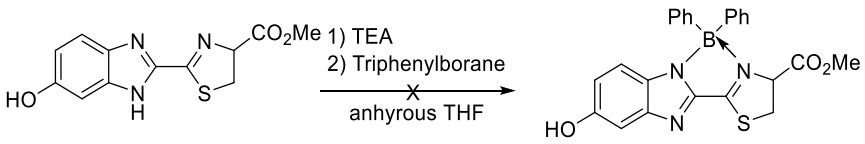

275 **282**

Scheme 65 Attempted Use of Triphenylborane

In the literature, [100] there were four conditions which had been used for borylation with triphenylborane (Table 6). In condition one, no base was added. Presumably a phenyl anion would disassociate and sequester any proton from the donor molecule to make a neutral complex. However, the reaction showed no reaction by ^1H NMR. The second and third attempts were carried out with triethylamine (1.1 eq) and BPh_3 (1.0 eq) at 14 ˚C and 80 ˚C in anhydrous THF for 24 h respectively. These reactions also did not work. In a final attempt, the amount of base and BPh_3 were doubled. After 24 h, no reaction was detected.

Entry	Eq of Base	Eq of BPh_3	Temperature	Time	Results
1	0	1.0	14 ˚C	24 h	No reaction
2	1.1	1.0	14 ˚C	24 h	No reaction
3	1.1	1.0	80 ˚C	24 h	No reaction
4	2.0	2.0	80 ˚C	24 h	No reaction

Table 6 Screening the Borylation Using Triphenylborane
Reagents: Benzimidazole Luciferin Methyl Ester **275** (20.0 mg, 0.9 mmol), anhydrous THF (0.5 mL), Triphenylborane, and TEA

Based on these studies of boron-based luciferin analogues, we believe that the proposed structures **269** and **270** were unstable. The strong electron-withdrawing group of boron difluoride encourages ready hydrolysis by water. In addition, the desired chelates may suffer from ring strain because of the formation of three fused 5-membered rings (Figure 28). Inspection of molecular models suggested that the orientation of the heterocyclic N lone pairs were not conducive to being able to chelate a central boron atom. When a boron atom forms a sigma bond with a heterocyclic nitrogen, it may be unfavourable for the other heterocyclic donor atom to form a dative bond due to ring strain. Examples of the most stable boron-complexes in the literature (Figure 20) shows that for instance complex **255** is composed of two 5-membered rings and compound **256** is composed of 5-, 5-, 6-membered rings. The common stable BODIPY **283** consists of fused 5-, 6-, 5-membered rings, the central 6-membered ring allowing the correct geometry required for co-ordination. [82]

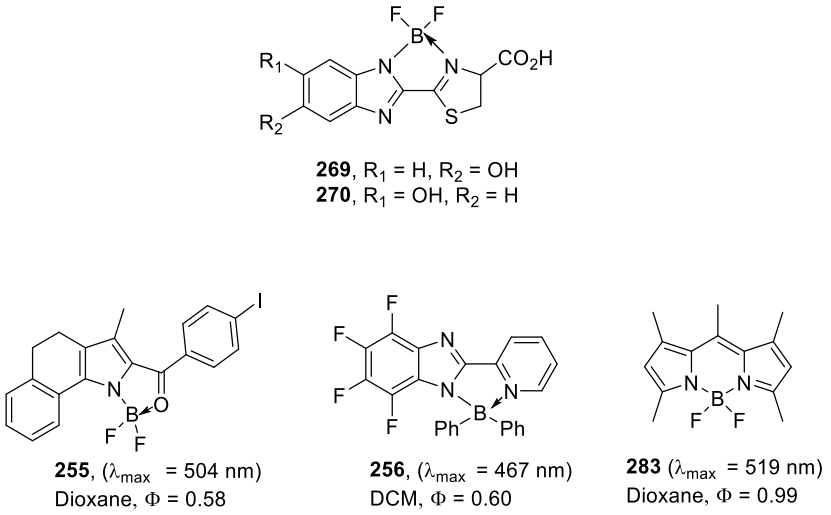

Figure 28 Estimated Bond Angles of Compound **265**, **266** and Stable Boron-Complexes

In conclusion, we found that the complexes **269** and **270**, or something like them, were moisture sensitive. We hypothesized that the ring strain plays an important role in coordination. If the ring strain could be accommodated, more stable boron complexes could be produced.

3.5 Designed and Synthesis of Boron-based Infra-Luciferin

Based on the previous study, we concluded that ring strain might be an important factor in the construction of stable boron chelate complexes. In this study, the novel boron coordination complex **284** was investigated in Figure 29. The chelate ligand is based on infra-luciferin **233**. The desired chelation would form a 5-5 system reminiscent of the literature complex **255** (Figure 28). Boron-based infra-luciferin analogues may be possible candidates to increase brightness *via* rigidification of infra-luciferin, thus reducing radiation less decay.

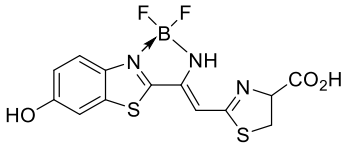

284

Figure 29 The Boron-Based Infra-Luciferin

3.5.1 Work Plan I

Previous work in the group has shown that potential intermediate **285** can be synthesised *via* a Thorpe reaction (Scheme 66).[101] Intermediate **285** could be used towards the synthesis of boron-based infra-luciferin analogues containing a C-C double bond between the benzothiazole and thiazoline moieties.

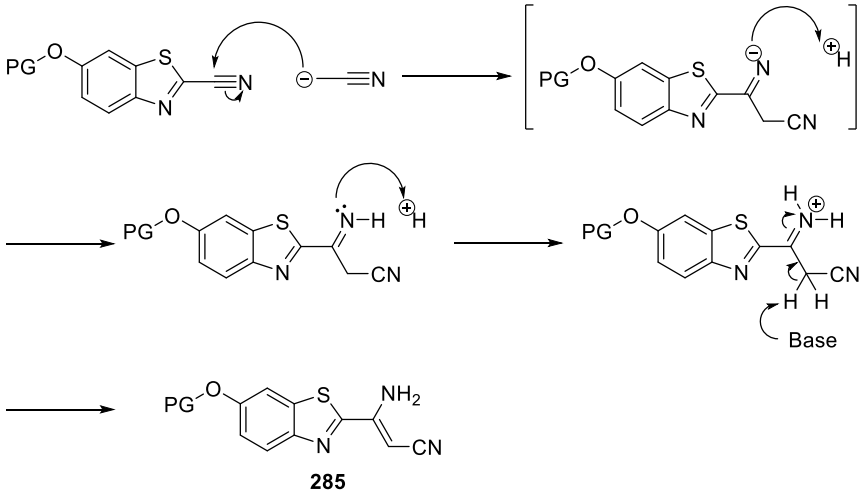

285

Scheme 66 Mechanism of Thorpe Reaction and Formation of **285**

In order to use this intermediate, a retrosynthetic route for the synthesis of infra luciferin analogue **284** was developed (Scheme 67). The target product **284** could be delivered by condensation of nitrile **286** with cysteine. We expected that the key boron complex **286** could be produced by treating intermediate **285** with boron reagents such as $BF_3 \cdot OEt_2$. The enamine product **285** comes from 2-cyano-6-hydroxybenzothiazole (**34**) *via* protection of the phenol group and Thorpe Reaction.

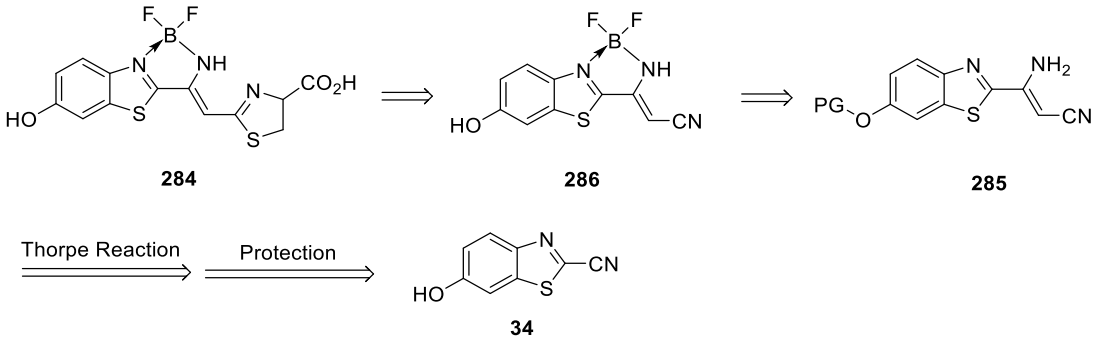

Scheme 67 Retrosynthesis of Boron-Based Infra-Luciferin **284**

A TIPS protecting group was chosen as we speculated that the synthetic approaches we could devise to **286** might involve the use of strong bases. A TIPS protecting phenol ether is more tolerant of basic condition than the TBDMS protected group. The phenol group was protected by using TIPSCl in the presence of imidazole to give **287** in 99% isolated yield (Scheme 68). Compound **287** in THF was then injected into a solution of deprotonated acetonitrile. The reaction was then quenched with $BF_3 \cdot OEt_2$, extracted with EtOAc, dried ($MgSO_4$), and purified by silica gel chromatography. However, no desired product **288** or **289** was isolated.

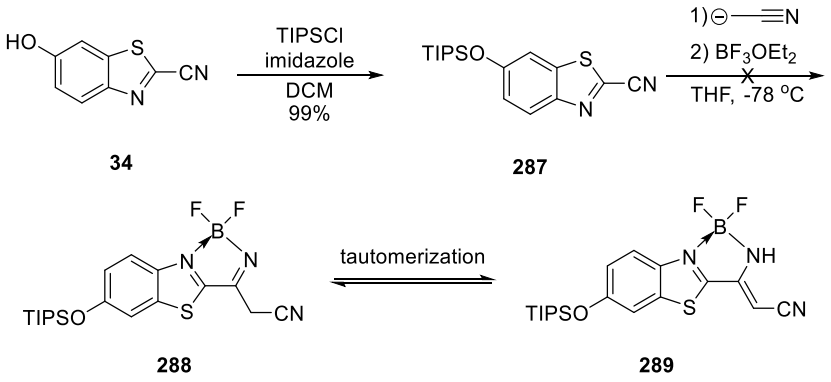

Scheme 68 Synthesis of Boron-Based Infra-Luciferin **284** Precursor **289**

3.5.2 Work Plan II

An alternative synthetic route was proposed from compound **290** (Scheme 69). One of the methods to synthesize boron-complexes could be based on **Mechanism I**, the electron lone pair of the enamine nitrogen first attacks BF_3, followed by deprotonation with a less nucleophilic base, may then provide compound **289**. Alternatively, the desired product **289** could be provided *via* the **Mechanism II**. Irreversible deprotonation by a strong base such as *n*-BuLi or LDA followed by addition of $BF_3{\cdot}OEt_2$. The metallo-enamine anion could capture BF_3 to give compound **289**.

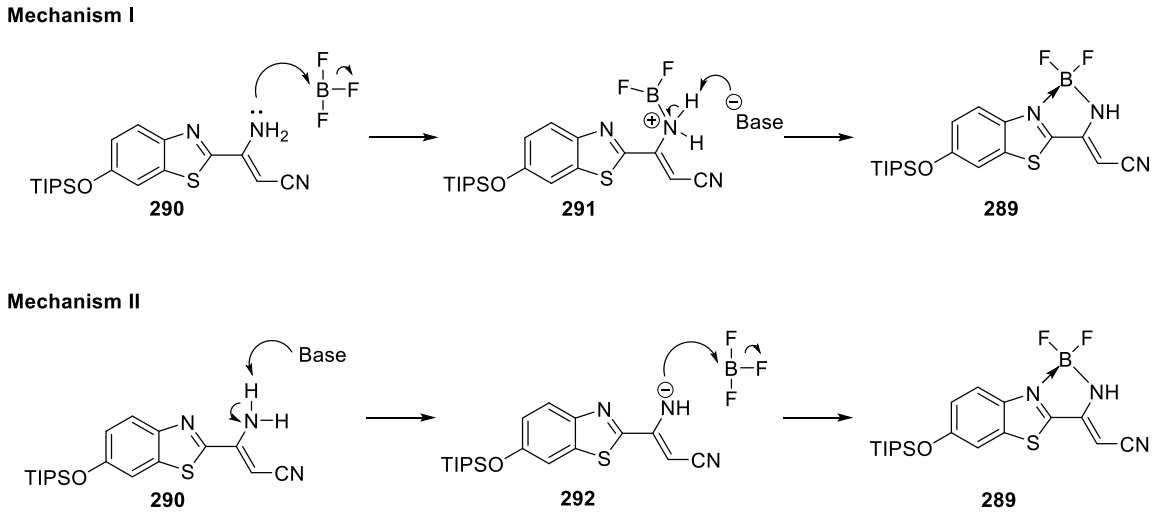

Scheme 69 The Proposed Mechanism for The Synthesis the Intermediate **289**

In order to investigate both pathways, the precursor **290** (Scheme 70) was prepared by treatment of **287** with acetonitrile anion in a good yield of 83%. In this reaction, not only was the desired product **290** isolated, but also the by-products **34** and **293** without protecting group in the ~3% and ~10% isolated yields respectively. Despite using the hindered TIPS silyl ether as protecting group, the basic conditions were strong enough to induce some minor deprotection. Compound **293** could potentially be one of the candidates for the synthesis of infra-luciferin analogue **284**.

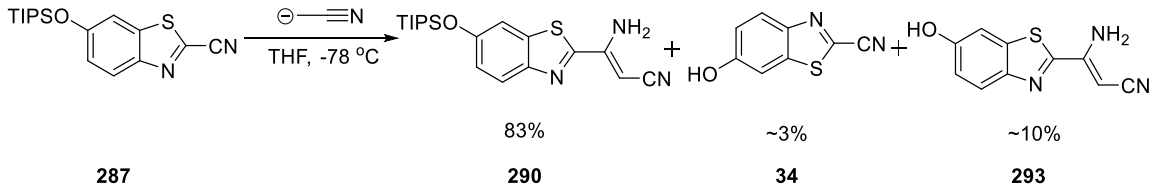

Scheme 70 The synthesis of Compound **290**

To investigate **Mechanism I**, compound **290** was treated with $BF_3 \cdot OEt_2$ in the presence of TEA at rt for 24 h. From TLC analysis, only starting material was observed (Scheme 71). The reaction temperature was increased to 40 °C for 24 h. However, the starting material **290** then decomposed.

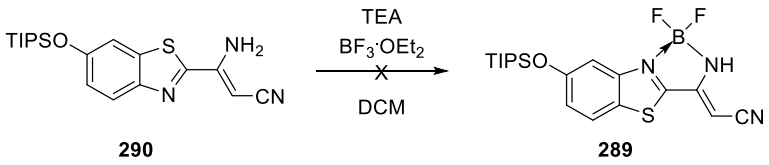

Scheme 71 The synthesis of Compound **289** *via* The **Mechanism I**

To Investigate **Mechanism II**, compound **290** was fully deprotonated by *n*-BuLi at -78 °C and then $BF_3 \cdot OEt_2$ was injected into the solution (Scheme 72). The temperature was allowed to rise to rt and stirred for an additional 2 h. During this process, the colour of solution changed from brown-yellow to red, which could be attributable to a new coordination complex. This reaction was then quenched with water. At this stage, the colour of solution turned to dark-brown. After purification by silica gel chromatography, the starting material **290** was recovered about 80%, along with some decomposed products.

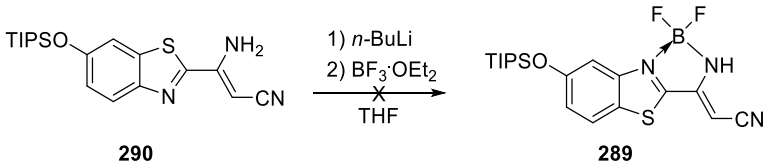

Scheme 72 The synthesis of Compound **289** *via* The **Mechanism II**

We have attempted many synthetic routes to synthesize boron-based luciferin analogues, but no stable boron complexes have yet been obtained. The coordinating compounds could be extremely water sensitive so attempting their synthesis under N_2 in a glove box might be a possible method. In addition, the two key compounds **290** and **293** were isolated successfully *via* the Thorpe reaction. They could be potential candidates for the development of rigid infra luciferin *via* intramolecular H-bonds (*vide infra*).

4. Rigid Infra-luciferin *via* H-bonds

4.1 Concept of ESIPT

Excited state intramolecular proton transfer (ESIPT) is a fully reversible photochemical process including 4 energy levels (Figure 30) where isomers are generated with different electronic structures. [102] The electron in the ground state of the enol tautomer E(S_0) is excited to E*(S_1) and then can relax to the excited state of keto tautomer K*(S_1) *via* ESIPT. The electron when in both excited states E*(S_1) and K*(S_1) could return to their ground state E(S_0) and K(S_0) with different wavelength emissions. The enol form could be re-generated from the keto form ground state K(S_0) through ground state intramolecular proton transfer (GSIPT). The pre-requisite of proton transfer is the formation of strong intramolecular H-bond(s) between the proton donor and the proton acceptor in 5, 6, or 7 member rings. The common H-bond(s) donors are hydroxyl or amino groups and the H-bond(s) acceptors can be carbonyl oxygen or imine nitrogen in a molecule. Upon electronic excitation, the electron density is redistributed dramatically. The movement of electronic density from the H-bond donor to the H-bond acceptor provides the driving force for ESIPT within a femtosecond time domain. This charge redistribution is fast and significantly affects photophysical events.

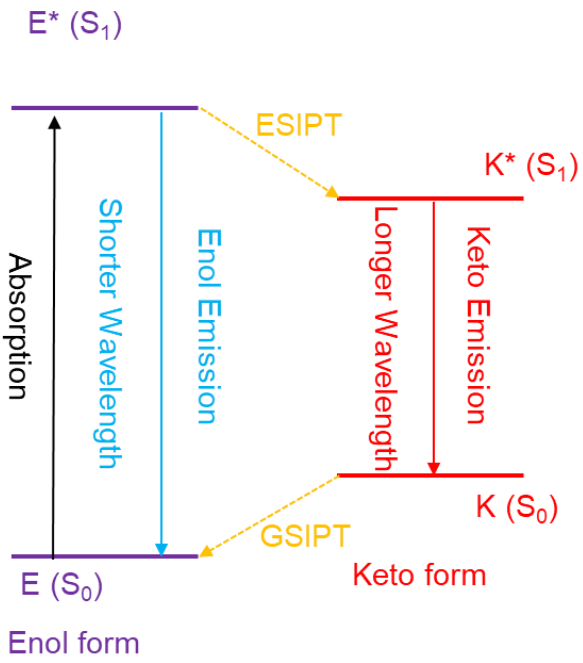

Figure 30 A Basic ESIPT Process

ESIPT type molecular emitters have a wide range of applications such as optoelectronics, [103] and cellular fluorescent probes. [104] Most research of ESIPT fluorophores has been on derivatives of benzimidazole **294**, **295** and benzothiazole **296**, **297** (Scheme 73). [105] The ESIPT fluorophores have common photophysical properties like large Stokes shift (~200 nm), duel emissions (enol form and keto form), or a broad emission band which is capable of covering all visible light to generate white emission.

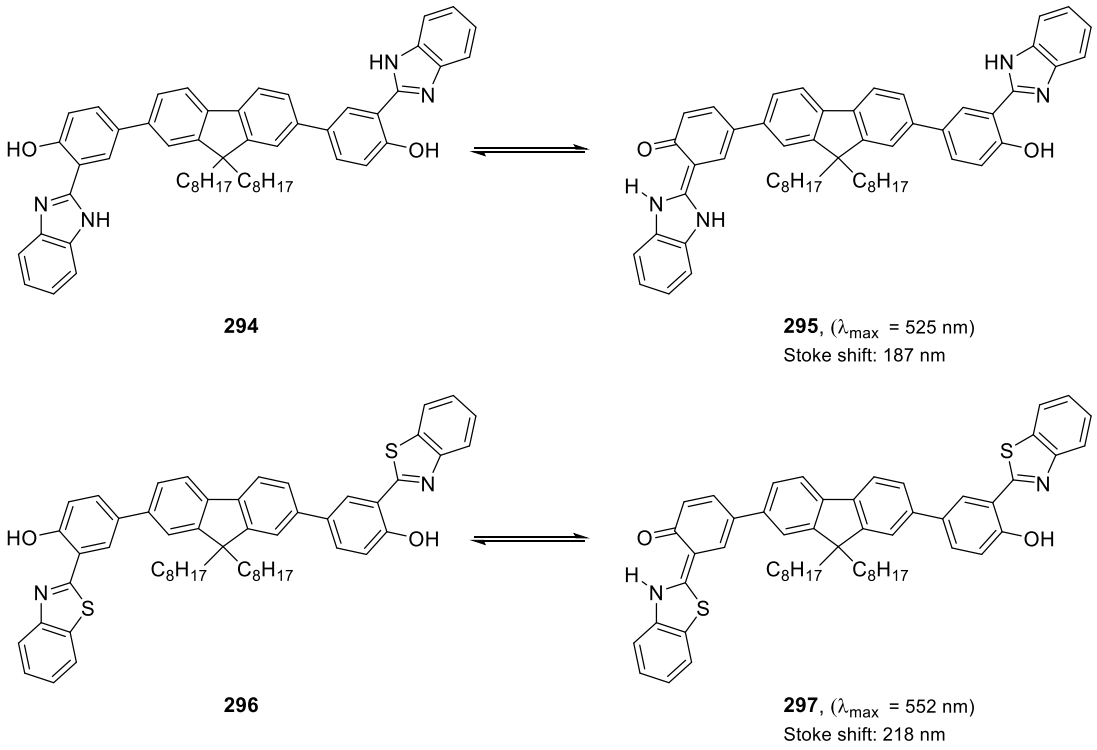

Scheme 73 The Benzothiazole and Benzimidazole Based ESIPT Fluorophores

4.2 Aim of Project and Research Proposal

Based on the concept of ESIPT, we have designed a new luciferin analogue **298** where an amine group was introduced on to the alkenyl linker group of infra-luciferin (Figure 31). We expect that compound **298** can give two emissions based on the enamine form **299** (shorter wavelength) and the imine form **300** (longer wavelength). The excitation source in this bioluminescent system is chemical energy rather than common photoexcitation. The chemical energy would be generated when compound **298** in the presence of Mg^{2+}, O_2, ATP and luciferase is converted to excited state oxyluciferin. This energy may not only excite the electron but also provide the driving force leading to tautomerization. In addition, a rigid structure could be achieved *via* intermolecular hydrogen bonds to enhance the $\emptyset_f$.

It would be interesting to investigate whether this type of luciferin can undergo different tautomerizations and give various bioluminescence emissions or not.

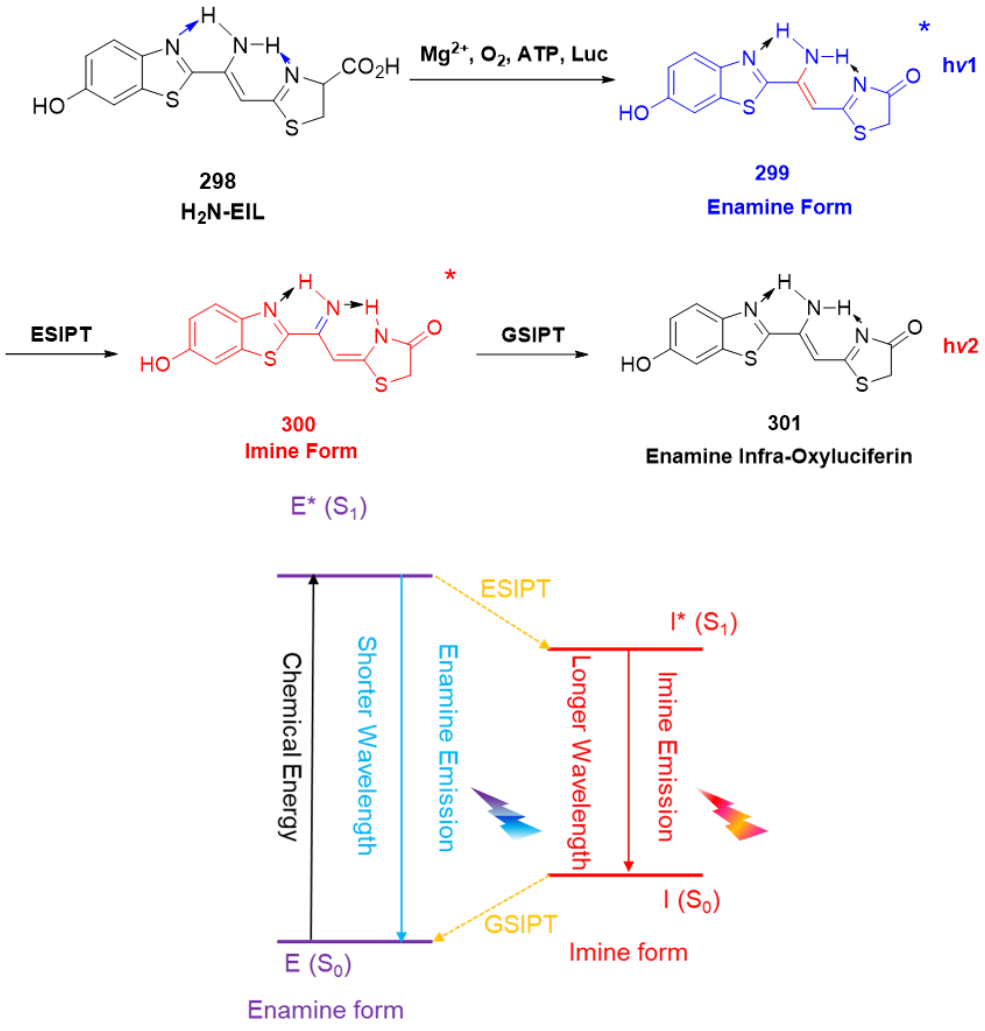

Figure 31 The Potential ESIPT Cycle of Rigid Luciferin **298**

4.3 Synthesis of ESIPT luciferin

A retrosynthetic route (Scheme 74) was designed for the development of H_2N-Enamine Infra-Luciferin **298 (H_2N-EIL)**. The desired compound **298** could be delivered over two steps from nitrile **290** by deprotection and condensation with cysteine.

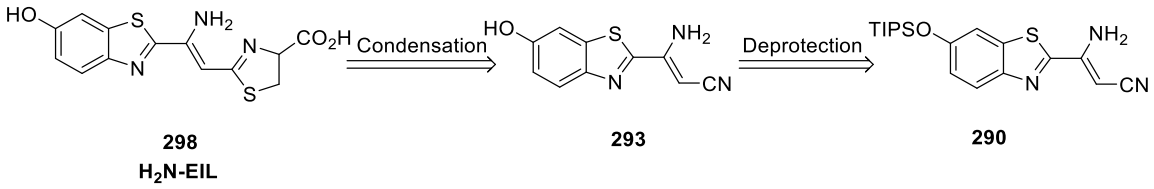

298
H_2N-EIL

293

290

Scheme 74 Retrosynthesis of H_2N-Enamine Infra-Luciferin **298**

In previous work (Scheme 70), the intermediate **293** had been synthesized but only as low yield by-product. A higher yielding synthetic route was required.

The silyl group (TBDMS) had been successfully removed by TBAF from a similar compound **278** (Scheme 61). The same reaction conditions were applied to the deprotection of **290 (**Scheme 75**)**. Treatment with TBAF (3 eq) in THF for 2 h gave the deprotected phenol **293** in 99% isolated yield.

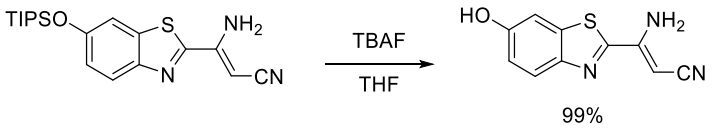

290

293

Scheme 75 Synthesis of Compound **293** *via* Deprotection by TBAF

The condensation between compound **293** and cysteine is a challenging step due to potential problems with conjugate addition to the unsaturated nitrile. Following the standard literature procedure [39] to synthesize the thiazoline ring of luciferins, reaction of nitrile **293**, racemic cysteine hydrochloride (1.1 eq), and K_2CO_3 (1.1 eq) in MeOH for 30 min (Scheme 76) did not give any thiazoline ring signals in the crude ^{1}H NMR spectrum. More forcing conditions at 80 ˚C gave the same result. Unidentifiable by-products were produced from the complete consumption of the starting material. In addition, due to the carboxylic acid group being introduced, these compounds could not be separated easily by normal phase silica gel chromatography.

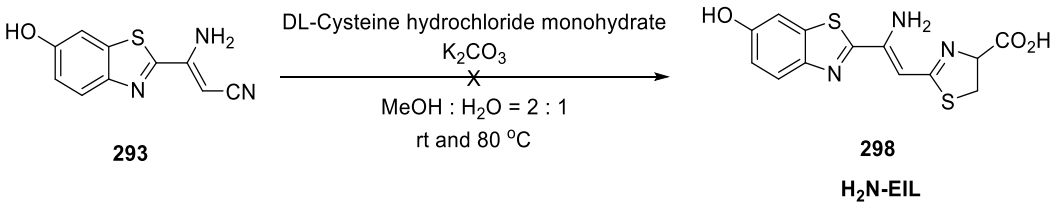

Scheme 76 The Synthesis of **H_2N-EIL 298**

In order to find suitable conditions, anhydrous methanol was investigated in further optimisation studies (Scheme 77) along with temperature, equivalents of base and other solvents. The common literature reaction conditions [106] were performed on compound **293** (5.0 mg, 0.23 mmol) with K_2CO_3 (4.0 eq) and cysteine (1.05 eq) in anhydrous MeOH (0.5 mL) at different temperatures 50, 60 ,70 and 80 ˚C for 24 h. The crude NMR spectrum showed no formation of thiazoline and much degradation.

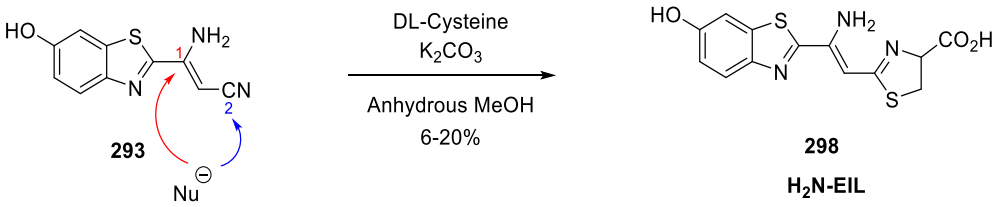

Scheme 77 The Synthesis of **H_2N-EIL 298** in anhydrous condition

The equivalents of base were decreased to 1.05 eq and the experiments repeated at 50, 60, 70, and 80 ˚C. Fortunately, in the final attempt at 80 ˚C, the thiazoline ring and relevant peaks appeared in the crude ^{1}H NMR spectrum (Figure 32). The signals at δ 5.45 (1H, s) and δ 4.99 (1H, td, 8 Hz) ppm were tentatively assigned to the vinyl and thiazoline protons respectively. The compound was purified by reversed phase high performance liquid chromatography (HPLC) eluting with a gradient solvent system composed of H_2O and MeOH (2% MeOH：98% H_2O to 98% MeOH：2% H_2O in 28 min) without additives such as acid in a low yield of 10-20%. The retention time was 14.7 min in this purification. In this reaction, the carbon 1may be a better Michael accepter than the carbon 2, which would account for the low yield of final product (Scheme 77).

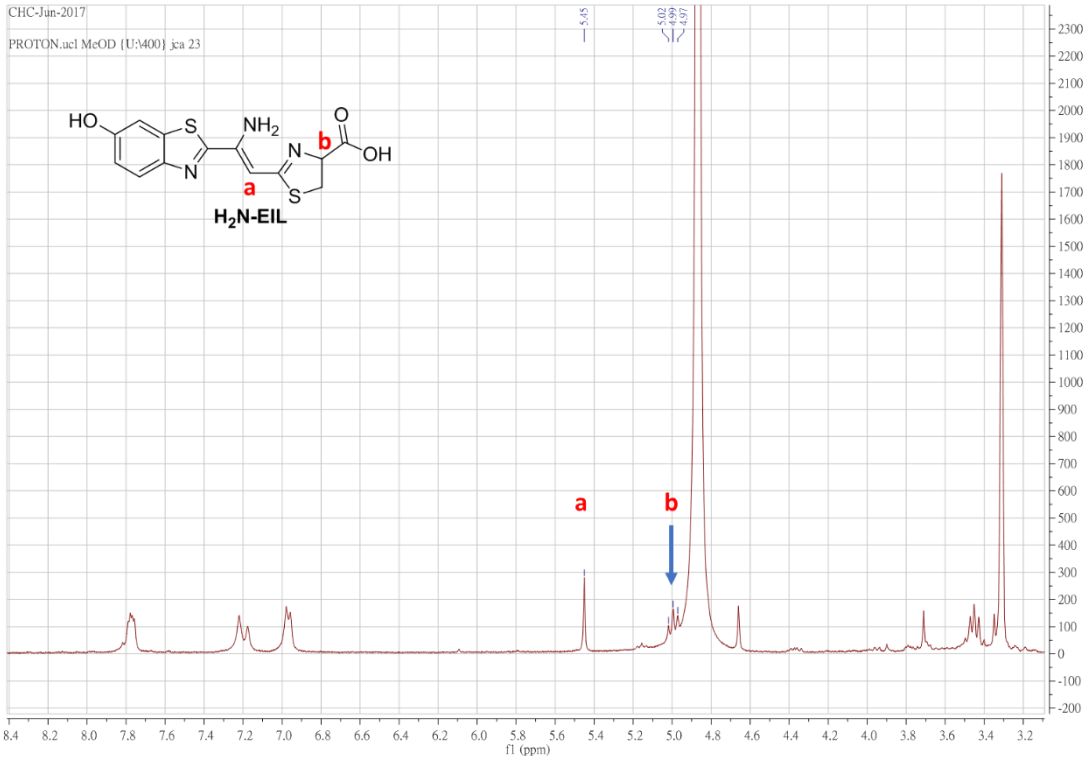

Figure 32 The Crude NMR of **H_2N-EIL 298**

A control reaction in MeOH rather than anhydrous MeOH was performed to verify whether the hypothesis that water was also responsible for the unsuccessful condensation. Under the same reaction conditions using undried MeOH, no cyclization product was observed, suggesting that this reaction was water sensitive. The novel compound **298** will be subjected to bioluminescence measurements.

5. The First BODIPY Firefly Luciferin

5.1 Introduction to BODIPY

Boron dipyrromethene (BODIPY or 4,4-difluoro-4-bora-3a,4a-diaza-s-indacene) derivatives with a planar and rigid structure were first synthesized in 1968 by Treibs and Kreuzer. [107] In general, the stable BODIPY compounds (Figure 33) were fully or partially substituted at the (α, β or *meso*) positions with alkyl or aryl groups and showed various fluorescence emissions. The unstable non-substituted structure was not isolated and fully characterized until 2009, because the pyrrole-carbons without substituents are prone to electrophilic addition. [108] The synthesis of BODIPYs can be performed under mild conditions, and a number of flexible synthetic routes gives the opportunity to install a wide range of functional groups to the core structure. The α, β and *meso* positions of BODIPY scaffold are easily modified to introduce different functional groups and longer conjugated systems to give a wide range of fluorescence emissions.

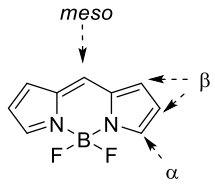

Figure 33 The BODIPY Skeleton

In the past few decades, a large number of BODIPY-based fluorophores have been synthesized for a variety of applications ranging from molecular probes, [109a] electronic devices [109b] to bio-imaging. [109c] Among the diverse types of small molecule organic fluorophores, BODIPY molecules usually exhibit small stoke shifts, sharp excitation, good thermal- and photo- stabilities, insensitivity to the pH of environment and high fluorescence quantum yields. Due to these specific physical properties, they have attracted much attention in optical studies. For example, BODIPY **302** has been used as a fluorescent probe with an emission of 525 nm and BODIPY **303** was a photo sensitizer in solar cell studies (Figure 34).

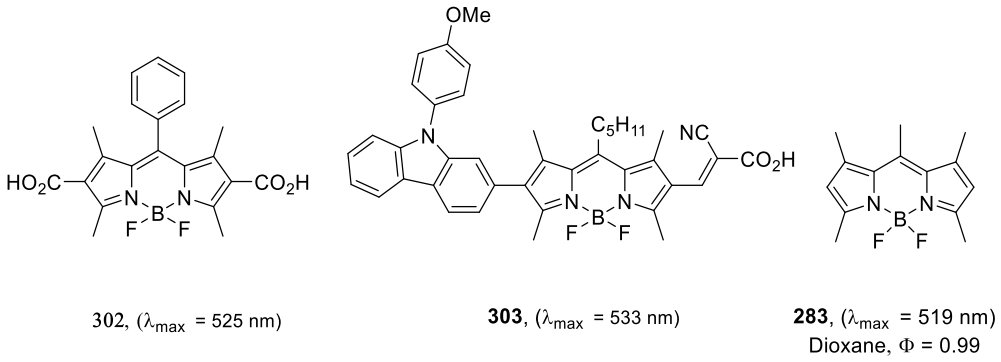

Figure 34 BODIPY Derivatives

5.2 Aim of Project and Research Proposal

As mentioned in Chapter 1, the more red-shifted luciferin analogues suffer a common drawback of low bioluminescence quantum yield ($\emptyset_B$). According to the equation $\emptyset_B = \emptyset_y\emptyset_E\emptyset_f$, fluorescence efficiency ($\emptyset_f$) has a large impact on $\emptyset_B$. In order to increase the $\emptyset_{Blu}$ of new novel compounds, choosing a core structure with high fluorescence quantum yield may be a viable approach.

The aim of this part of the project was to synthesize a new type of firefly luciferin analogue **304** (Figure 35) based on the BODIPY scaffold and investigate whether this novel molecule can give bioluminescence with high $\emptyset_f$ or not. From a literature review, [110] we found that BODIPY is a great candidate for our research because BODIPY dyes are stable boron complexes with low-band gap and they have shown versatile applications in scientific studies. One of the BODIPY structures bearing five methyl substitutions (**283**, Figure 34) showed $\emptyset_f = 0.99$ in Dioxane solution. [82] In addition, BODIPY fluorescent probes have enjoyed unprecedented success in bio-imaging, but there has been no research about BODIPY as a core structure for the development of firefly luciferin analogues. It would be interesting if BODIPY's attributes could be imported into a novel luciferin analogue to enable us to explore a brand-new area in which the central core of firefly luciferin is BODIPY instead of benzothiazole or benzimidazole.

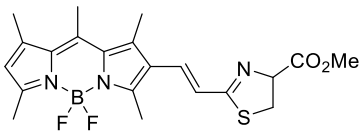

304
BODIPY Luciferin Methyl Ester

Figure 35 The Structure of New BODIPY Luciferin Methyl Ester

5.3 Design and Synthesis of BODIPY Luciferin

5.3.1 Work Plan I

The design and retrosynthesis of new BODIPY luciferin methyl ester **304** (Scheme 78) was based on the strategy for the development of the infra luciferin (iLH_2). [77] The ester was chosen as it should be easier to isolate and can be saponified either directly before use or *in vivo* by esterases. We also chose to synthesise racemic material as work in the group has previously shown that extended conjugation makes epimerisation of the carboxylic acid centre more facile. Other work in the group is devising an assay to monitor this epimerisation process and devise a single enantiomer synthesis. We would like to introduce an alkenyl linker between BODIPY and thiazoline moieties. By following the precedented synthetic route of iLH_2, the cyclization of thiazoline ring in BODIPY **304** could be achieved from thioamide **305** with DAST. Thioamide **305** could be formed by reacting formyl BODIPY **306** with the phosphonate **227** *via* a Horner-Wadsworth-Emmons reaction (HWE) that was developed for the synthesis of iLH_2. [77] The corresponding formyl BODIPY **306** is a literature complex which could be generated from compound **283** through Vilsmeier-Haack formylation. [111]

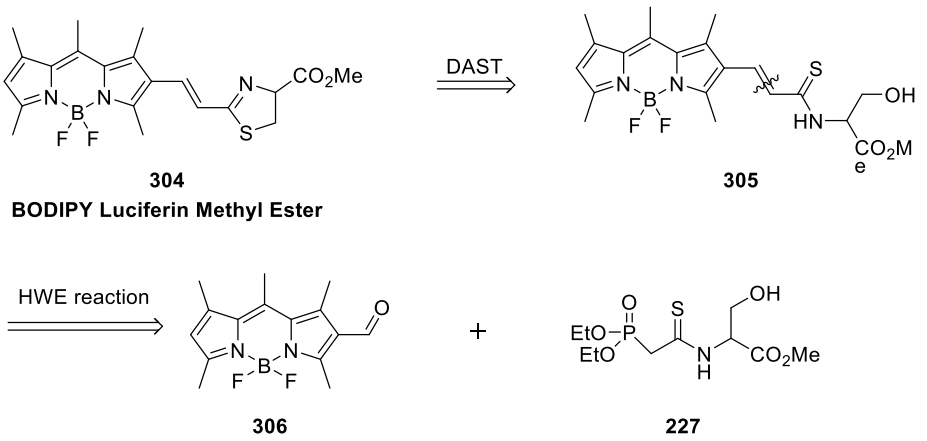

Scheme 78 First Retrosynthesis of BODIPY Luciferin Methyl Ester

The construction of the core structure of BODIPY was delivered by following the reported procedures (Scheme 79). [82] Commercially available 2,4-dimethylpyrrole (**307**) in anhydrous DCM was treated sequentially with acetylchloride, *N*,*N*-diisopropylethyl amine (DIPEA), and $BF_3{\cdot}OEt_2$ under N_2 and the reaction was stirred for 5 h. The desired product **283** was isolated as an orange solid in excellent yield of 69% (lit. [82a] yield 42%). Next, the formylation was performed by treatment of BODIPY **283** with $POCl_3$ and DMF in anhydrous DCM at rt for 30 min *via* the Vilsmeier-Haack mechanism. The formyl BODIPY **306** could be obtained as a reddish solid in yield of 67% (lit. [82b] yield 89%).

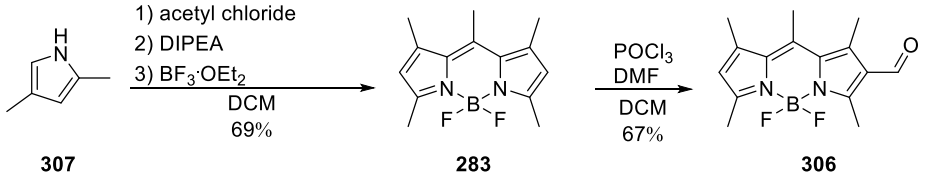

Scheme 79 The Synthesis of Formyl BODIPY **306**

The Vilsmeier-Haack reaction [112] is a common method to convert an electron rich aromatic ring to an aryl aldehyde by combining DMF and $POCl_3$ followed by aqueous work up. The mechanism of the formation of Vilsmeier reagent is depicted in Scheme 80. The DMF reacts with $POCl_3$ and then the oxygen on the amide is replaced by chloride with the loss of PO_2Cl_2. The highly reactive iminium salt also known as Vilsmeier reagent is produced.

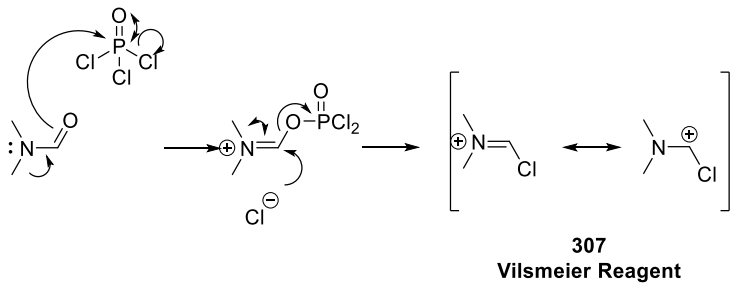

Scheme 80 The Formation of Vilsmeier Reagent

The Vilsmeier reagent **307** is a highly reactive iminium cation. The de-aromatization of electron rich aromatic rings with the Vilsmeier reagent **307** followed by re-aromatization gives a more stable iminium salt **309** (Scheme 81). After aqueous work up, the iminium is hydrolysed by water to give the corresponding aldehyde **310**.

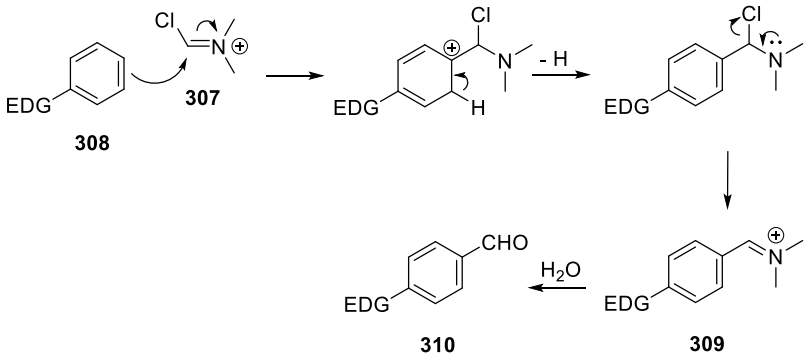

Scheme 81 The Vilsmeier-Haack Reaction Mechanism

With formyl BODIPY **306** in hand, we expected that the HWE reaction could proceed as normal by mixing LiCl, DBU, and the phosphonate reagent **227** at rt for 2 h (Scheme 82). However, this reaction did not work, and the starting material **306** was fully recovered (over 99 %) after column purification. Harsher conditions at higher temperatures were attempted. Heating the reaction at reflux overnight gave the same result. No desired compound **306** was observed from the crude ^{1}H NMR spectrum. This might be attributed to the fact the electron rich pyrrole moieties donate electron density to the carbonyl group and reduces it's electrophilicity. The shielded carbon was difficult to attack by the phosphonate reagent **227** even at high temperature. Therefore, an alternative synthetic route was considered.

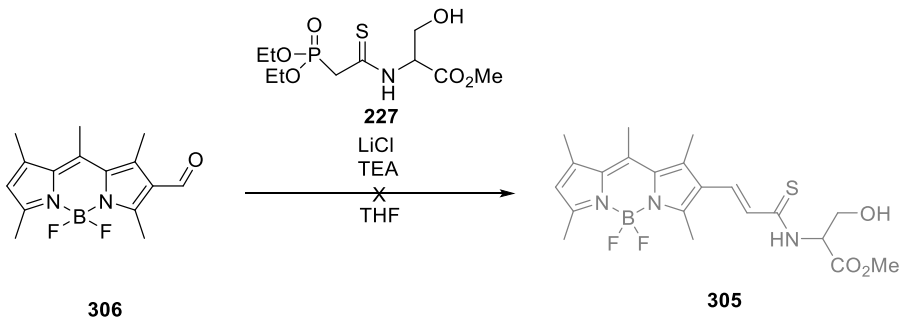

Scheme 82 The Synthesis of Compound **297** *via* HWE Reaction

5.3.2 Work Plan II

A new retrosynthetic route was designed (Scheme 83) that referred to the original iLH_2 synthesis by the Anderson group in 2014. [76] The thiazoline ring can be formed by cyclisation of a suitably substituted cysteine amide derivative **311** by Hendrickson reagent (also called "POP reagent"). The amide BODIPY **311** could be assembled through amide condensation of cysteine derivative **312** with compound **313**. The BODIPY derivatives **314** with different esters (-CO_2Et **314a** and -$CO_2{}^t$Bu **314b**) could be produced from formyl **306** *via* the Wittig reaction. Wittig reagents are normally more reactive than unsaturated phopshonate reagents due to less resonance stabilisation of the carbanion. The ethyl ester could by hydrolysed to give the corresponding carboxylic acid BODIPY **313** with base such as NaOH, and the *t*-butyl ester could be removed easily under acidic conditions by using TFA. The synthesis of **306** was previously prepared, and its synthetic route has been shown in Scheme 79.

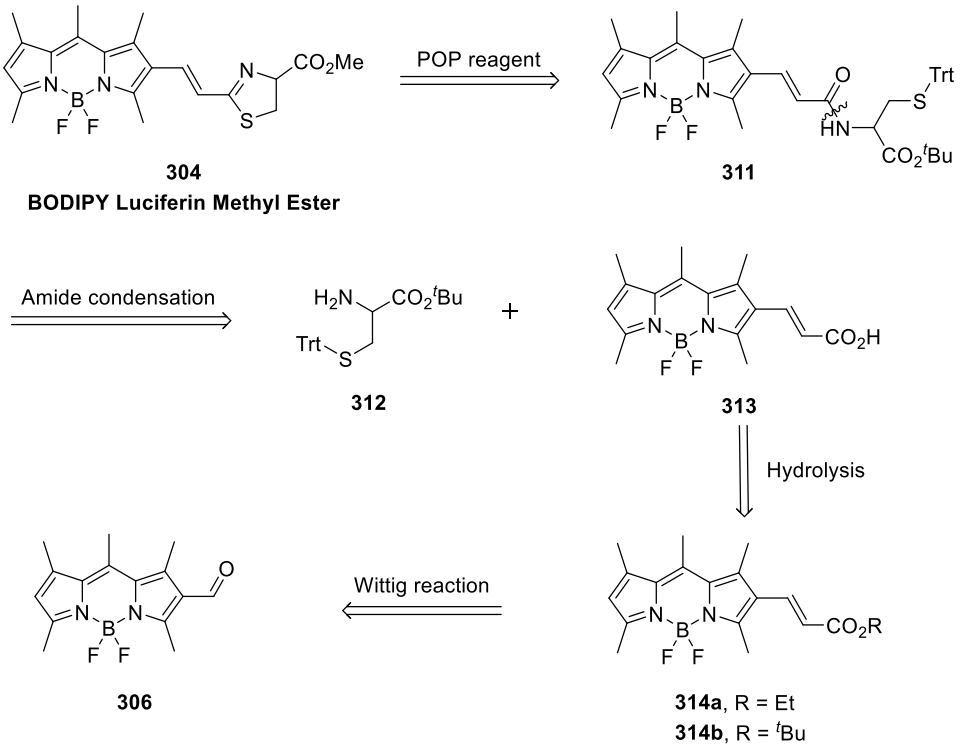

Scheme 83 The Second Retrosynthesis of BODIPY Luciferin Methyl Ester

Treatment of formyl BODIPY **306** with the ethyl ester and *t*-butyl ylides gave the alkenyl products **314a** and **314b** in 78% (lit. [111] 50%) and 78% yield respectively (Scheme 84).

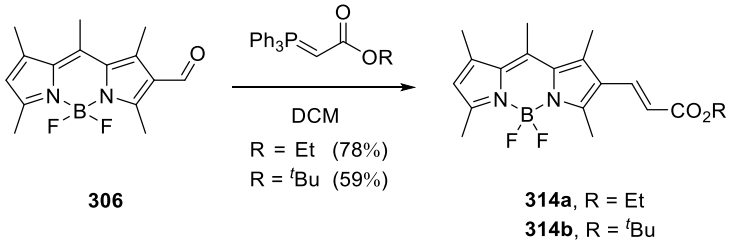

Scheme 84 The Synthesis of BODIPY Esters *via* the Wittig Reactions

The two ester BODIPY compounds **314a** and **314b** were hydrolysed under different conditions (Scheme 85). First, deprotection of ethyl ester BODIPY **314a** was conducted with an aqueous solution of NaOH (4N) in DCM at rt and monitored by TLC. From the TLC analysis it was observed that compound **314a** decomposed under these reaction conditions giving many components with short wavelength emissions. It indicated that the conjugated system was breaking down. Deprotection of ethyl ester BODIPY **314a** was also attempted under acidic conditions with HCl (6N) in DCM at 50 ˚C overnight. However, the ethyl ester group was not cleaved under these acidic conditions and **314a** was recovered in quantitative yield. Although we did not isolate the desired product **313**, we knew that BODIPY derivatives might be more stable to acidic conditions rather than basic condition from these attempted saponification experiments.

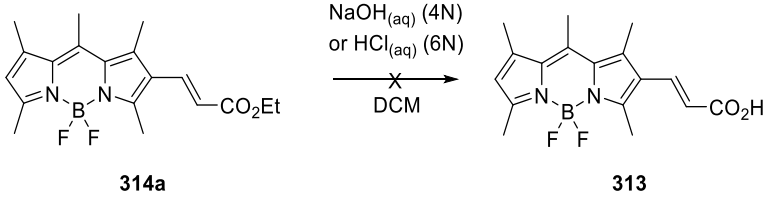

Scheme 85 Hydrolysis of BODIPY Ethyl Ester

Simultaneously, deprotection of *t*-butyl ester **314b** proceeded by treatment with TFA at rt overnight (Scheme 86).

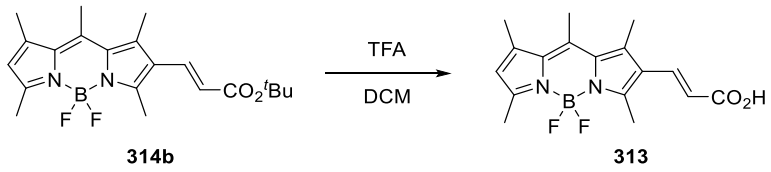

Scheme 86 The Deprotection BODIPY tert-Butyl Ester **313**

In comparison to the ^{1}H NMR spectrum of *t*-butyl ester BODIPY **314b** in $CDCl_3$, the crude ^{1}H NMR spectrum (Figure 36) showed that the *t*-butyl group was missing, and all peaks were shifted downfield after the deprotection. The ^{1}H NMR results indicated that a stronger electron withdrawing group (COOH) was generated.

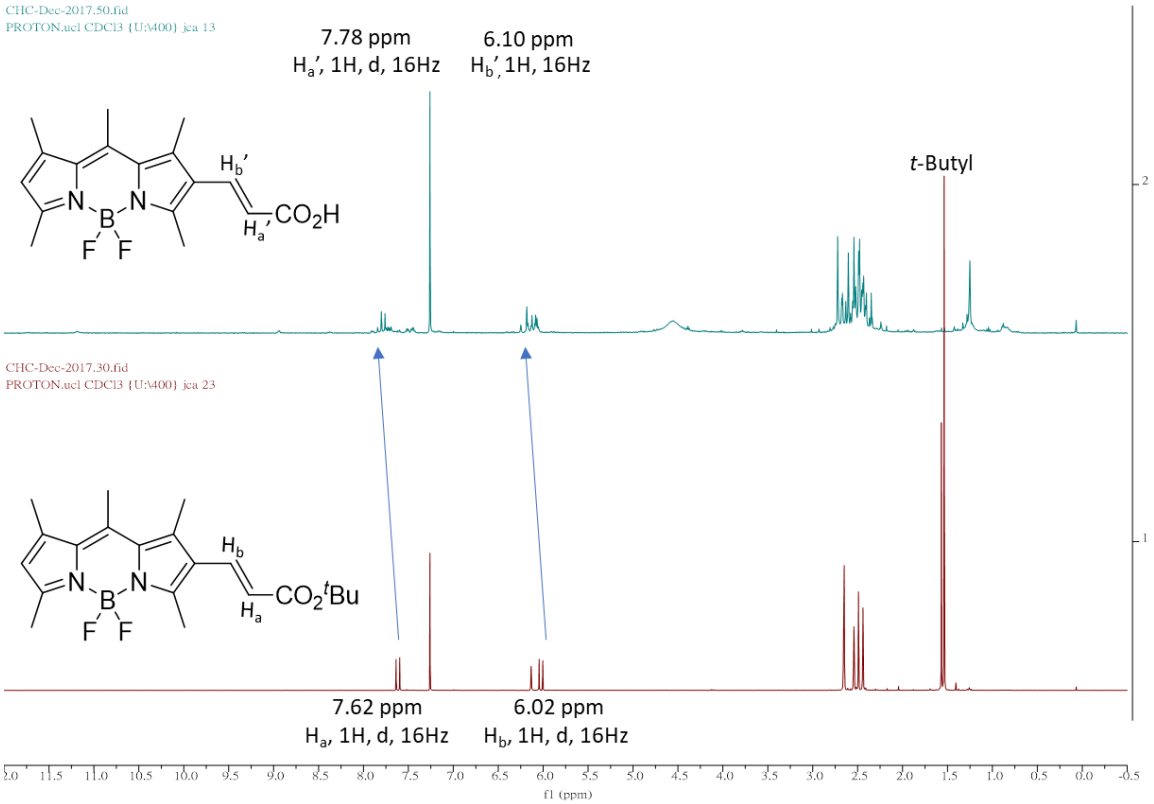

Figure 36 The Stacked ^{1}H NMR of BODIPY Carboxylic acid and BODIPY *t*-Butyl Ester

Additionally, BODIPY **313** $[C_{17}H_{18}BF_2N_2O_2+H]^+$ = 331.1539 was detected by the HRMS (Figure 37). The result also supported that carboxyl BODIPY **313** was the major product in the reaction mixture. The crude product **313** was sonicated in DCM, the filtrate removed and the remaining solid BODIPY **313** was used without further purification.

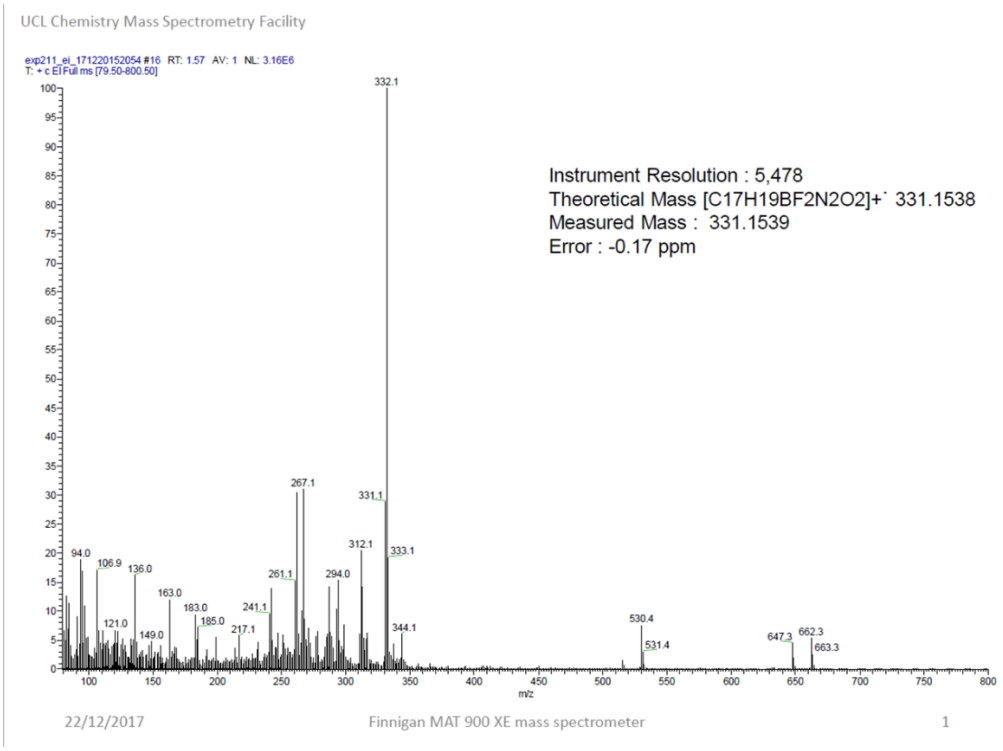

Figure 37 The HRMS of BODIPY Carboxylic acid

Carboxyl BODIPY **313**, commercially available DL-cys(S-trt)-O^{t}Bu **312**, TEA, and BOP were stirred in a co-solvent system of DCM and DMF at 0 ˚C for 2 h (Scheme 87). From the crude ^{1}H NMR in $CDCl_3$, plenty of unidentified compounds were produced and the core structure of BODIPY was not observed. It seemed that the carboxylic acid BODIPY **313** was degraded in these reaction condition. In order to confirm whether the product **311** was formed or not, the crude mixture was further investigated by HRMS. However, the result was negative and target compound **311** was not produced in this reaction. This frustrating result demonstrated that known procedures have their limitations for the development of new luciferin analogues. A new synthetic strategy needed to be taken into consideration.

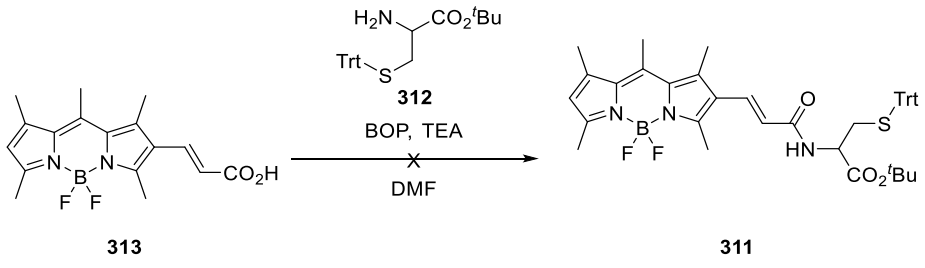

Scheme 87 The Synthesis of Amide BODIPY *via* Amide Condensation

The general mechanism of the amide condensation was depicted in Scheme 88. Benzotriazol-1-yloxytris(dimethylamino)phosphonium hexafluorophosphate (**219**) (BOP) called Castro's reagent is a common reagent for general amide formation. The deprotonated R_1COO^- attacks the electrophilic phosphonium centre to give the R_1 containing phosphonium species. The addition of anion BtO to the carbonyl group produces the corresponding benzotriazole ester which is further attacked by R_2-NH_2 to give the amide product by releasing the benzotriazole species and a proton. [113]

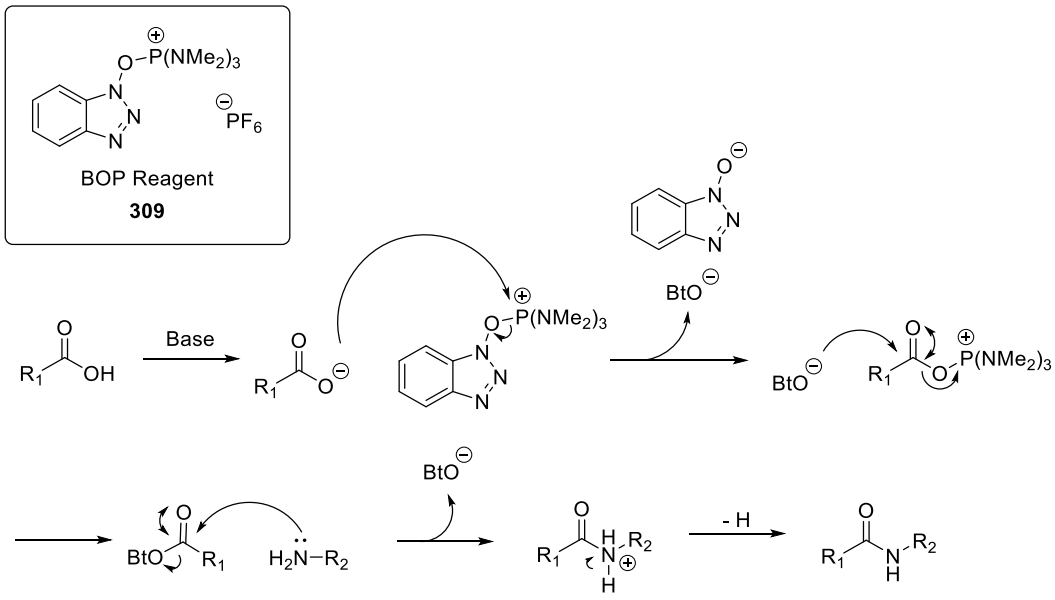

Scheme 88 Mechanism of BOP-mediated coupling reagent

5.3.3 Work Plan III

The formation of the intermediate **311** was a challenge in this synthesis. A new retrosynthesis was devised (Scheme 89). We decided to construct intermediate **315** bearing methyl ester by joining the two vinyl compounds **316** and **317** *via* cross olefin metathesis. The vinyl cysteine could be obtained by following literature procedures [114] and the vinyl BODIPY **317** could be prepared by a C-C cross-coupling reaction under Pd catalysis. The Stille reaction is a base free coupling reaction and it has been used in the synthesis of other BODIPY-based compounds. [115] We speculated that the installation of the vinyl group to BODIPY could be achieved *via* the Stille reaction. Finally, the halogen BODIPY **318** could be built from BODIPY **283** by the use of *N*-iodosuccinimide (NIS). [116]

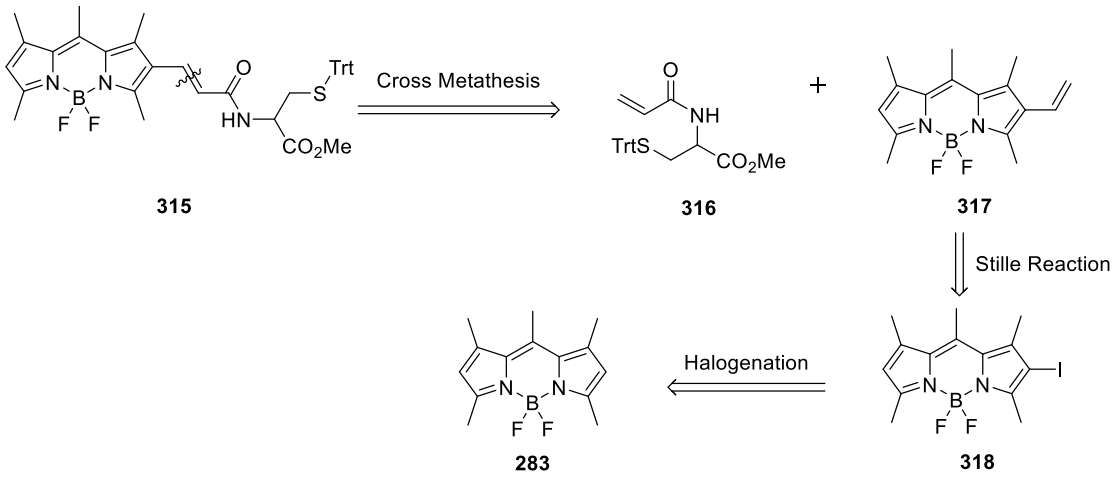

Scheme 89 The Retro Synthesis of Key Intermediate Amide BODIPY **315**

This convergent synthesis (Scheme 90) began with the iodination of BODIPY **283** by the addition of a solution of NIS in DCM into a solution of BODIPY **283** protected from light and gave BODIPY **318** in quantitative yield (lit.[116] yield 77%). The introduction of vinyl group proceeded by treatment of iodo-BODIPY **318** with tri-*n*-butyl(vinyl)tin and 10 mol% of $Pd(PPh_3)_4$ in refluxing toluene overnight gave the corresponding vinyl product **317** in 63% yield.

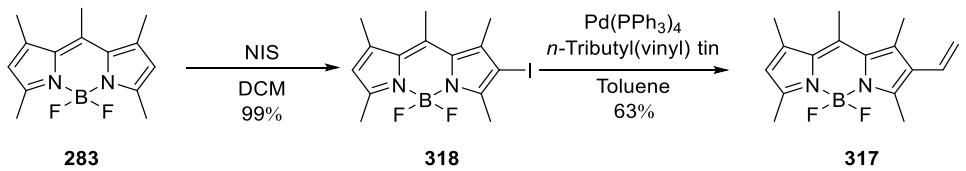

Scheme 90 The Synthesis of Vinyl BODIPY

The Stille coupling was first reported in the late 1970s, [117] and it has been widely applied for the formation of C-C bond between stannanes and aromatic halides under palladium catalysis. The mechanism (Scheme 91) starts from the oxidative addition of a halo-arene to give a $L_2Pd(II)ArX$ intermediate, which then undergoes transmetallation with an organostannane. Isomerization to provide the *cis*-Pd(Ar)(R') complex is followed by reductive elimination, releasing the product and re-generating the Pd(0) species for further catalytic cycles.

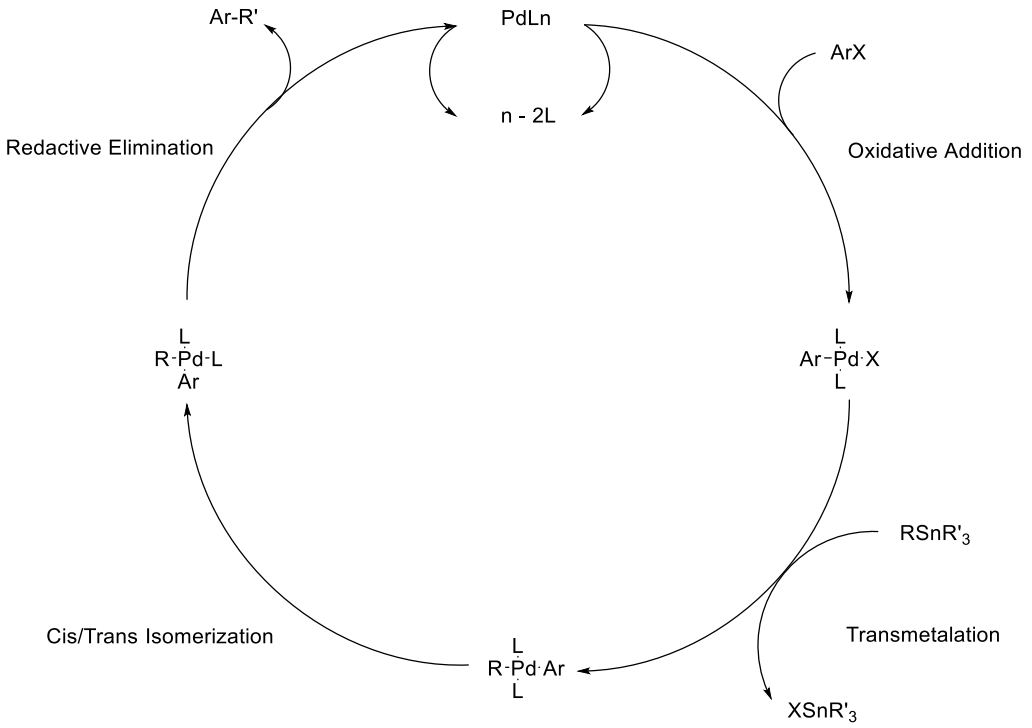

Scheme 91 Mechanism of Stille Reaction

The synthesis of amide cysteine **316** was based on reported procedures (Scheme 92). [114] Treatment of cysteine with excess acetyl chloride in MeOH at reflux gave the cysteine methyl ester in quantitative yield. Treatment of the cysteine methyl ester with triphenylmethanol (Trt-OH) in TFA at rt for 2 h provided the thiol protected DL-Cys(S-Trt)-OMe. The production of vinyl cysteine **316** was achieved by subjecting the DL-Cys(S-Trt)-OMe to acryloyl chloride and TEA in DCM at rt overnight. The desired vinyl cysteine **316** was obtained in an excellent 95% yield over 3 steps (lit. [114] yield 90%).

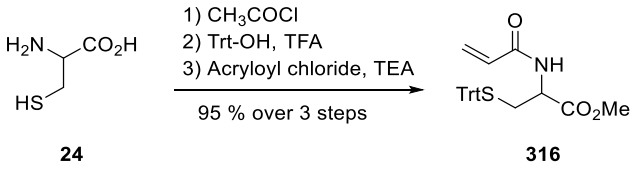

24 316

Scheme 92 The Synthesis of Vinyl Cysteine **316**

The olefin metathesis (Scheme 93) was attempted by mixing amide **316** and vinyl-BODIPY **317** in DCM in the presence of Hoveyda-Grubbs II (20 mol%) catalyst at rt overnight. The key intermediate amide BODIPY **315** was produced successfully in good 83% yield. The formation of amide BODIPY **315** was confirmed by ^{1}H and ^{13}C NMR spectroscopy, but satisfactory HRMS could not be obtained.

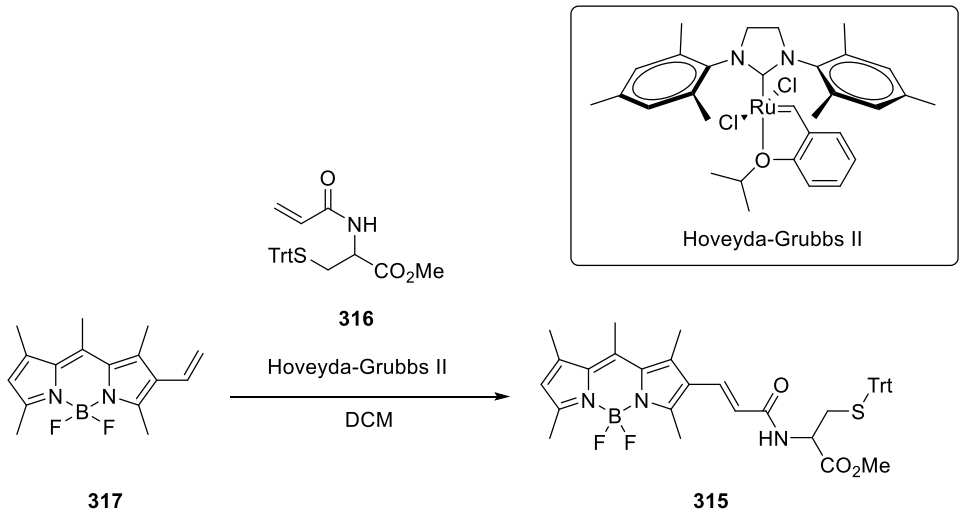

Scheme 93 Synthesis of Amide BODIPY **315** *via* Grubbs Metathesis

The Heck reaction [118] was also attempted for the development of the key intermediate **315** (Scheme 94). The reaction was performed by refluxing the mixture of iodo-BODIPY **318**, cysteine **316**, K_2CO_3, and $Pd(PPh_3)_4$ (10 mol%) in toluene under N_2 overnight. However, we found that the starting material BODIPY **318** was decomposed under these conditions according to TLC analysis.

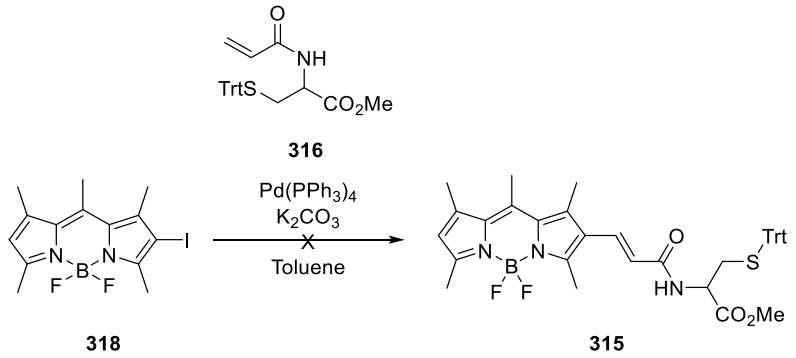

Scheme 94 Attempted Synthesis of Amide BODIPY

Scheme 95 shows a general Heck reaction starting from $L_nPd^{(0)}$. The first step involves the oxidative addition to R_1X to give the halide $L_nPd^{(II)}R_1X$ complex. Then migratory insertion of alkene $R_2HC=CR_3R_4$ generates the *syn*-isomer of R_1 and $Pd^{(II)}$ species. After C-C bond rotation, the *cis*-H-C-C-$Pd^{(II)}$ complex undergoes β-elimination to form the desired compound $R_1R_2C=CR_3R_4$, usually the *trans*-alkene. In the final step, the $L_nPd^{(0)}$ catalyst is re-generated by base in the system *via* reductive elimination.

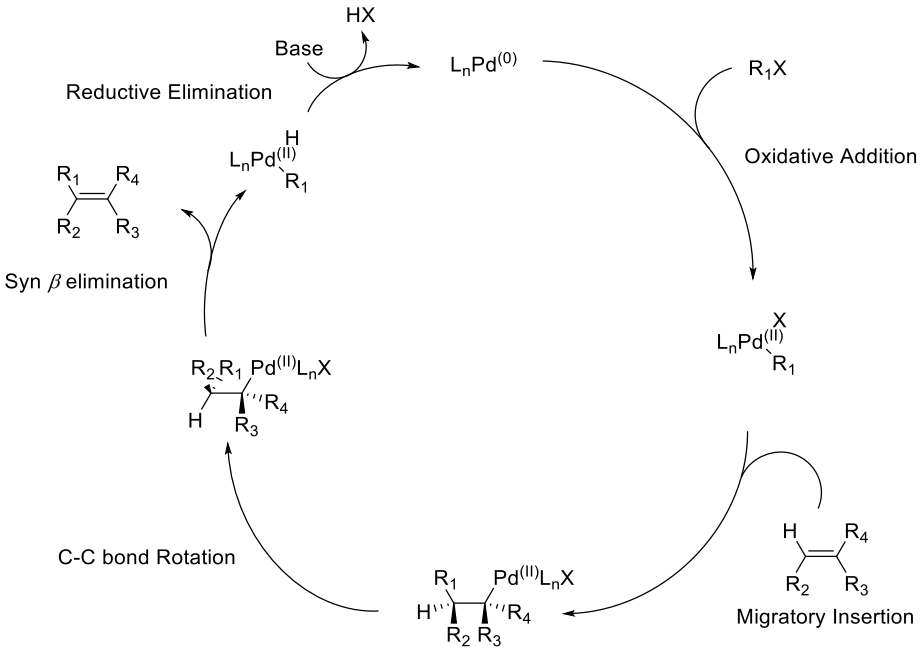

Scheme 95 The Mechanism of Heck Reaction

The final step was the intramolecular cyclization where amide BODIPY **315** was treated with POP reagent at 0 ˚C for 10 min to give the first BODIPY luciferin methyl ester **304** in 78% yield (Scheme 96).

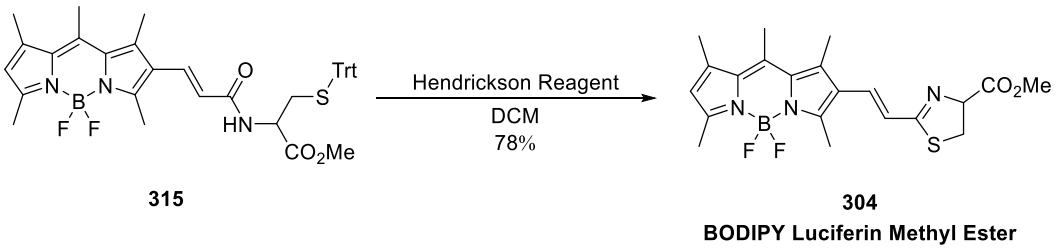

Scheme 96 The Synthesis of BODIPY Luciferin Methyl ester

The reaction mechanism of the intramolecular cyclisation by using POP reagent is depicted in Scheme 97. The Hendrickson reagent (triphenylphosphonium anhydride trifluoromethane sulfonate) is formed in situ as a solution in DCM by combining trifluromethanesulfonic anhydride and 2 equivalents of triphenylphosphine oxide at 0 ˚C. [119] The reagent is very reactive and has versatile applications such as ester formation and thiazoline construction. The first step of this reaction is the formation of the strong P-O bond between amide and POP reagent to give the corresponding phosphonium species. The trityl group might be removed when CF_3SO_3H is generated by traces of moisture. The lone pair on the sulphur undergoes nucleophilic addition to the imine carbon, releasing another molecule of Ph_3PO and a proton to give a thiazoline ring.

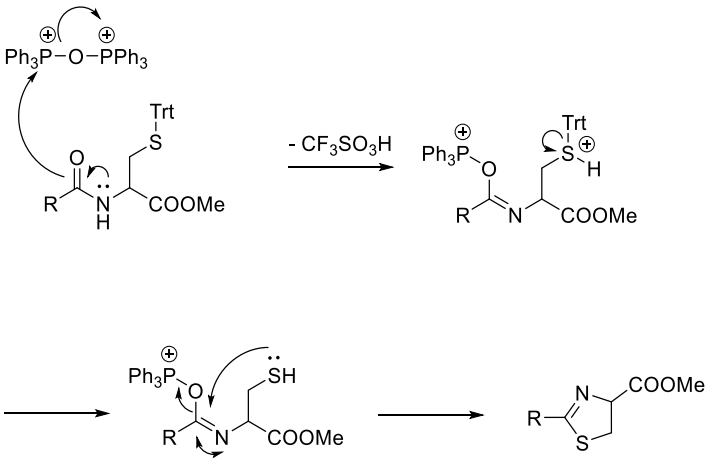

Scheme 97 The Mechanism of Thiazoline Formation by POP Reagent

The hydrolysis of the BODIPY methyl ester **304** was performed by PLE to give BODIPY carboxylic acid **319** (Scheme 98) that was used directly in a bioluminescence assay with firefly luciferase. The hydrolysis and bioluminescence assay were conducted by our collaborator Dr. Amit P. Jathoul at Cardiff University.

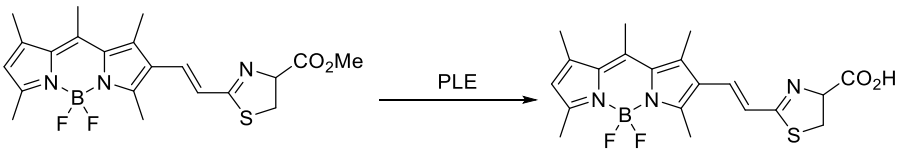

304
BODIPY Luciferin Methyl Ester

319

Scheme 98 Hydrolysis of BODIPY Methyl Ester by PLE

5.4 Bioluminescence Result

The bioluminescence properties of BODIPY **319** were measured in a combination with six luciferases (WT, WT E354R, x11, iluc1, Eluc, and CBR) and in three concentrations (200 µM, 20 µM, and 2 µM) by our collaborator Dr. Amit P. Jathoul at Cardiff University.

In the presence of Mg^{2+}, O_2, ATP and luciferases, this novel BODIPY-based luciferin exhibited bioluminescence emissions (Figure 38). In general, with luciferase WT, WT E354R, x11, iluc1 and Eluc, BODIPY gave a similar level of intensity at ~1000 times less than DL-luciferin no matter what the concentrations were. However, with mutant enzyme CBR, the brightness of BODIPY luciferin was similar to some amino D-luciferin analogues which give only 10-fold weaker light output than D-luciferin. Moreover, we also found that the light intensity had reached a maximum even with the lowest concentration as the intensities showed no difference between concentrations of 200 µM and 20 µM. This could be due to the system reaching a steady state, but the dynamic study has not been performed. At the present time we do not understand this phenomenon and further investigation by Dr Pule is ongoing.

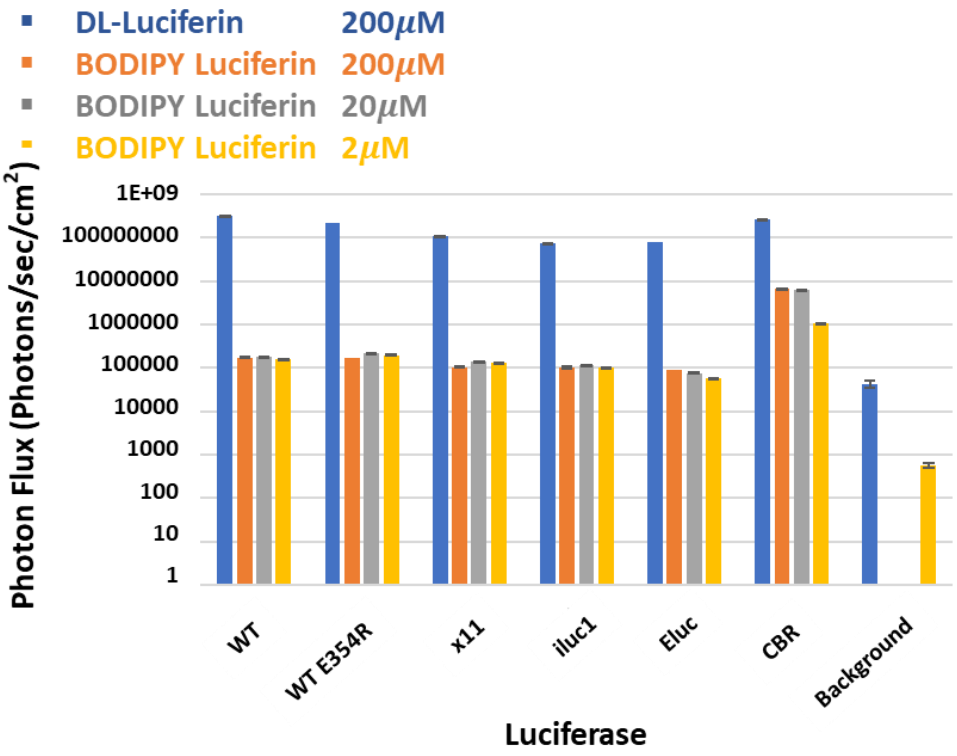

Figure 38 The light Intensity of BODIPY Luciferin with Various Luciferases

The emission spectra of DL-luciferin and BODIPY-luciferin with each enzyme were recorded in Figure 39 and Table 7. With enzymes WT, x11, iluc1 and Eluc, DL-luciferin gave expected emissions λ_{max} around 555 nm. With mutant WT E354R, DL-luciferin displayed duel emissions including a major peak at 572 and a minor at 612 nm. The most red-shifted emission with a maximum at 614 nm was observed with CBR. Compared to DL-luciferin, BODIPY luciferin performed slightly red-shifted emissions λ_{max} at 572 nm with luciferases, except CBR which remained at 572 nm compared to DL-luciferin at 614 nm. With mutant enzymes WT E354R and iluc1, BODIPY luciferin emitted λ_{max} at 572 nm with broad shoulders in a range from 670 nm to 697 nm which are located in the nIR window. The lower intensity broad shoulder emissions could be light emission from a different isomer/tautomer of the light giving species or a light giving degradation product.

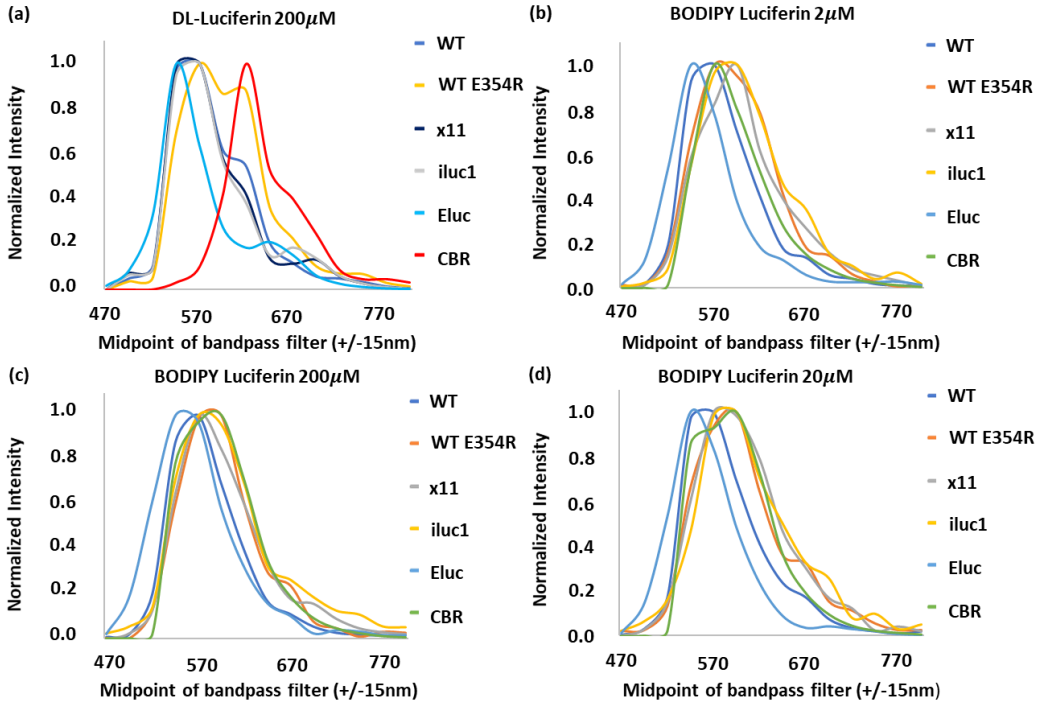

Figure 39 Bioluminescence of DL-Luciferin and BODIPY Luciferin

	DL-luciferin	BODIPY Luciferin
WT	555	572
WT E354R	572, 612[a]	572, 672[a]
x11	555	572
iluc1	555	572, 697[a]
Eluc	547	547

CBR	614	572

Table 7 Bioluminescence Peak Wavelengths of Enzymes; [a] minor shoulder peak

We were interested in the fluorescence properties of iLH_2 methyl ester **222** and BODIPY luciferin methyl ester **304** because they share the same skeleton with a pi-bond between the two rings. The free acid compounds were difficult to obtain and usually gave poor yields after basic hydrolysis, so we used their methyl ester **222**, and **304** instead. The fluorescence properties (Figure 40) of these methyl ester derivatives were measured in DMSO ($5.0x10^{-5}$ M) at rt. Compound **222** possessing a hydroxyl group gave a blue emission at 477 nm. Upon addtion of *t*-BuOK (1 eq) into the solution of iLH_2 methyl ester **222**, to make the phenolate species **320**, the emission peak rapidly shifted by 126 nm to 603 nm because the stronger electron donating group (EDG) oxygen anion **320** was generated. Due to the absence of EDG on BODIPY luciferin ester **304**, an orange emission was observed at 560 nm which is 43 nm blue-shifted than phenolate iLH_2 methyl ester **222**. In the future, installation of an EDG, particulary a phenol group, to the BODIPY core might give more red-shifted emission in fluorescence and bioluminescence. The complete emission spectra of BODIPY was missing below ~525 nm and can be attributed to the overlap between the emission band and the excitation wavelength. As a result, the $\emptyset_f$ could not be calculated in this study.

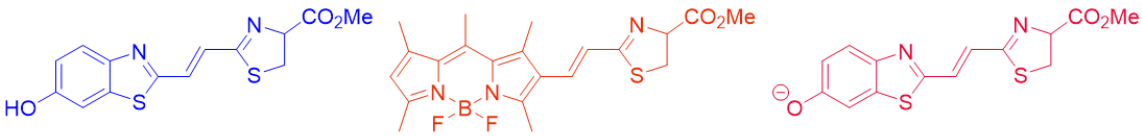

222
iLH_2 Methyl Ester
(λ_{max} = 477 nm)

304
BODIPY Luciferin Methyl Ester
(λ_{max} = 560 nm)

320
phenolate-iLH_2 Methyl Ester
(λ_{max} = 603 nm)

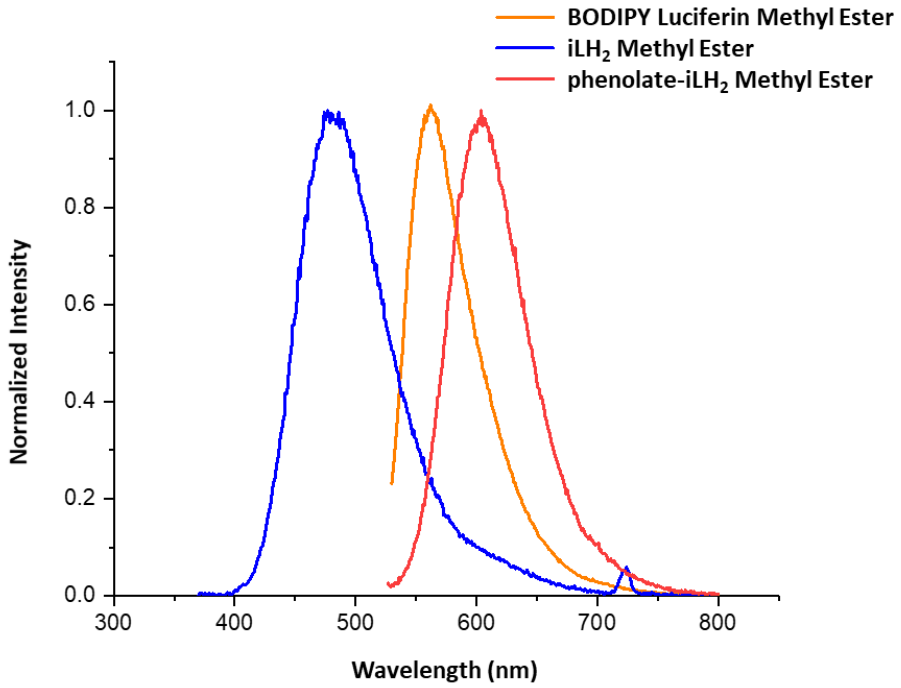

Figure 40 The Fluorescence Study of BODIPY Analogue and iLH_2

6. ICT Enhanced Infra-Luciferin

6.1 Concept of Intramolecular Charge Transfer (ICT)

The creation of organic materials for use in solar cells, [120] organic thin film transistors, [121] and fluorescent probes [122] with intramolecular charge transfer (ICT) properties has attracted significant attention in the past few decades. The photophysical properties of these organic compounds can be controlled by donor and acceptor strengths which changes the charge distribution in a molecule between ground state and excited state (Figure 41). Upon absorption of energy, an electron is excited from the HOMO of an electron-rich moiety to a LUMO of electron-deficiency within a molecule. The initial excited electron rests at the local excited state (LE) before an intramolecular relaxation process from the local excited state (LE) to its ICT state *via* ICT. This charge separation or re-distribution phenomenon is termed ICT. Relaxation from the ICT state results in a longer wavelength emission (γ^{max} (ICT)). In fluorescence studies, a strong ICT molecule could help to decrease band gap and give red-shifted emission. [123]

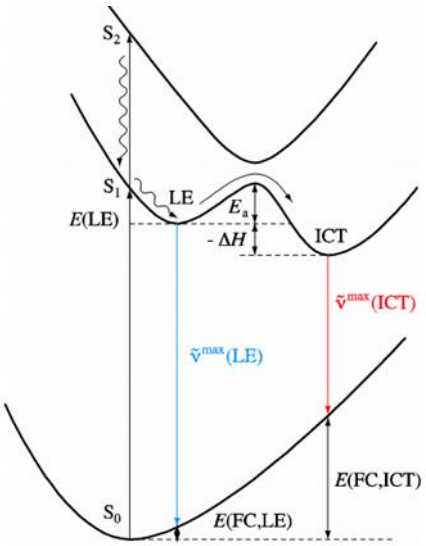

Figure 41 Diagram of ICT Process [123b]

6.2 Aim of Project and Research Proposal

The aim of this project was to develop a novel infra-luciferin methyl ester **321** (Figure 42) with two hydroxyl groups to achieve longer bioluminescent emission than iLH_2. In general, adding an electron donating group (EDG) can promote ICT. The additional EDG at the 4-position (this position is ultimately in conjugation with the oxy-light giving species) should make intramolecular charge transfer (ICT) more favourable and give nIR emission.

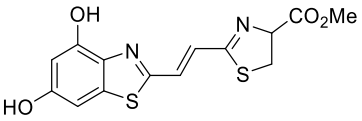

321

Figure 42 Structure of 4,6-Dihydroxy Infra-luciferin Methyl Ester **321**

6.3 Computational data analysis

In order to gain a deeper understanding of the effects of the hydroxyl groups on oxy infra-luciferins oxy-iLH$_2$ **322** and **oxy-323**, density functional theory calculations (DFT) at the B3LYP/6-311++G(3df,3pd) level were performed the results summarized in Figure 43 and Table 8. The electron densities are delocalized on the backbones of each compound within the HOMO and LUMO, which indicates that these oxyluciferins are highly conjugated. The HOMOs of the luciferins are located on the benzothiazole portions and the LUMOs are mainly located on the thiazolone parts. The electron transfer could thus initiate from phenolate part to the ketone. For **oxy-323** the hydroxyl group at 4'-position can contribute to the electron transfer process. Their dipole moment values were also investigated because dipole moment (μ) has a large impact on ICT process, [124] The calculations show that **oxy-323** has a larger dipole moment (μ = 7.43 Debye) than oxy-iLH$_2$ **322** (μ = 6.03 Debye) indicating that **oxy-323** has stronger ICT characteristics which should lead to more red-shifted emission. Consequently **oxy-323** has higher HOMO/LUMO energy levels (HOMO: -6.27 eV/ LUMO: -3.13 eV) and a smaller band gap (ΔE_{gap} = 3.14 eV) than oxy-iLH$_2$ **322** (HOMO: -6.49 eV/LUMO: -3.19 eV, ΔE_{gap} = 3.30 eV) due to one more electron donating group (-OH) at the 4'-position. The calculations suggest that **oxy-323** would be able to give longer emission wavelength than oxy-iLH$_2$ **322**.

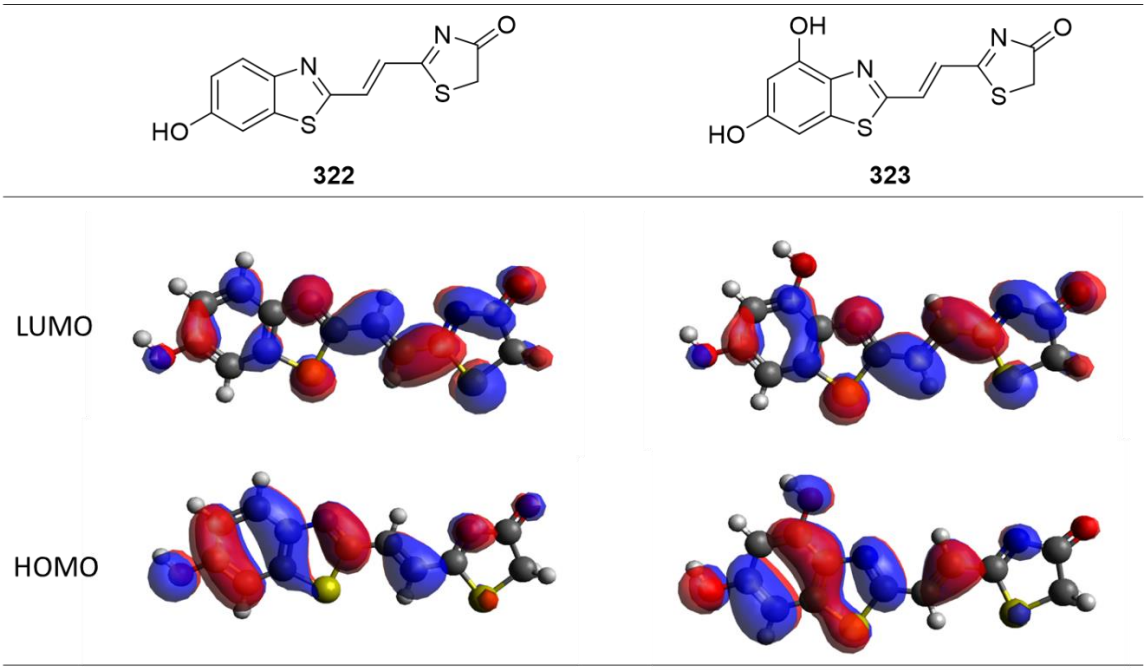

Figure 43 Frontier Orbitals of Oxy-iLH$_2$ **322** and **Oxy-323** (Isovalue = 0.02)

	μ (Debye)	HOMO/LUMO (eV)	ΔE_{gap} (eV)
Oxy-iLH$_2$ **322**	6.03	-6.49/-3.19	3.30
Oxy-323	7.43	-6.27/-3.13	3.14

Table 8 Summary of Computational Results of Oxy-iLH$_2$ **322** and **Oxy-323**

6.4 Designed and Synthesis of ICT Enhanced Infra-luciferin

6.4.1 Work Plan I

A previous Masters project in our laboratory, [125] found that formylation of **324** by using *n*-BuLi followed by anhydrous DMF was low yielding. It was observed that temperature control was important in this reaction. Deprotonation of compound **324** was inefficient at -78 ˚C and most of the starting material was recovered. Therefore, to facilitate deprotonation, the temperature was increased to -50 ˚C. Unfortunately, the higher temperature decomposed compound **324**. In addition, the synthesis of compound **326** *via* the HWE reaction did not work (Scheme 99). Therefore, we re-designed a new convergent synthetic route for the synthesis of our target compound **321**.

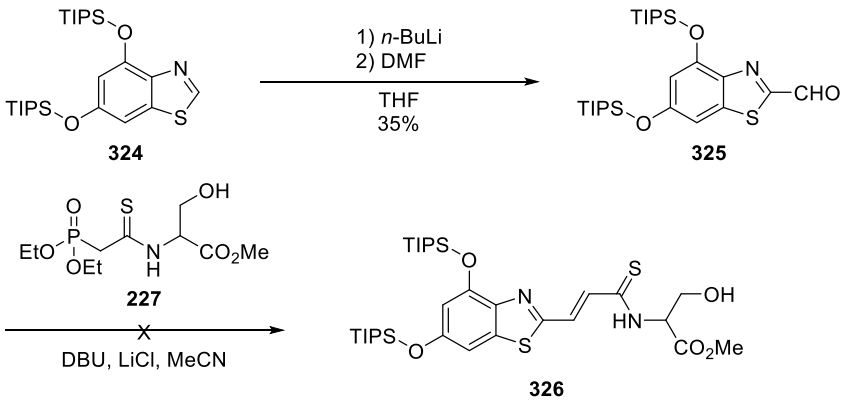

Scheme 99 The Synthesis of Product **326** *via* HWE Reaction

The retrosynthetic route (Scheme 100) of 4,6-dihydroxy infra-luciferin methyl ester **321** was based on our BODIPY-based luciferin work (Scheme 89). Compound **321** could be delivered by deprotection of the phenol groups, followed by intramolecular cyclisation to form the thiazoline with Hendrickson reagent from **328**. Product **328** could come from treatment of vinyl cysteine **316** with vinyl benzothiazole **329** *via* olefin metathesis. The Stille cross-coupling could be used to generate compound **329**. The brominated benzothiazole **330** could be derived from **331** *via* a Sandmeyer reaction. The 2-amino-4,6-dimethoxybezothizole **331** is known and can be synthesised from commercially available 2,4-dimethoxyaniline (**332**). [126]

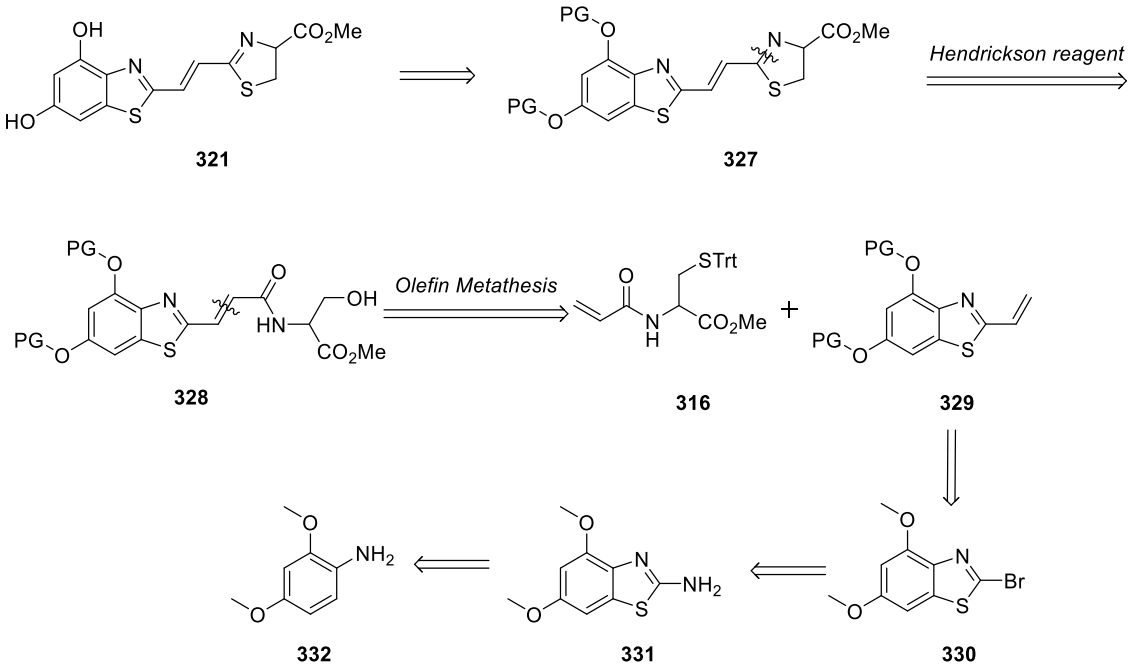

Scheme 100 The Retrosynthesis of Compound **321** *via* Olefin Metathesis

The synthesis of 2-amino-4,6-dimethoxybenzothiazole **331** (Scheme 101) had been prepared previously in the group by a Masters student.[125] Their modified procedure, improved the yield of compound **331** from 28%[126] to 38%. Generated the highly reactive Br-SCN species first by injecting Br_2 into a solution of KSCN in AcOH at 0 °C for 30 min. This turned out to be more efficient than the literature one-pot synthesis where all the reagents were mixed together at 0 °C.

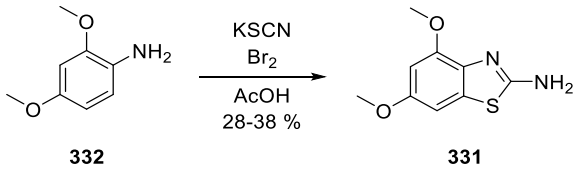

Scheme 101 Modified Synthesis of Compound **329**

The mechanism (Scheme 102) occurs by *ortho* substitution next to the electron-rich amine group, followed by re-aromatization to provide 2,4-dimethoxy-6-thiocyanatoaniline (**333**). The cyclisation to the thiazole ring takes place by nucleophilic addition of the amine group to the cyano carbon under acidic conditions. Subsequent tautomerization gives the desired compound **331**.

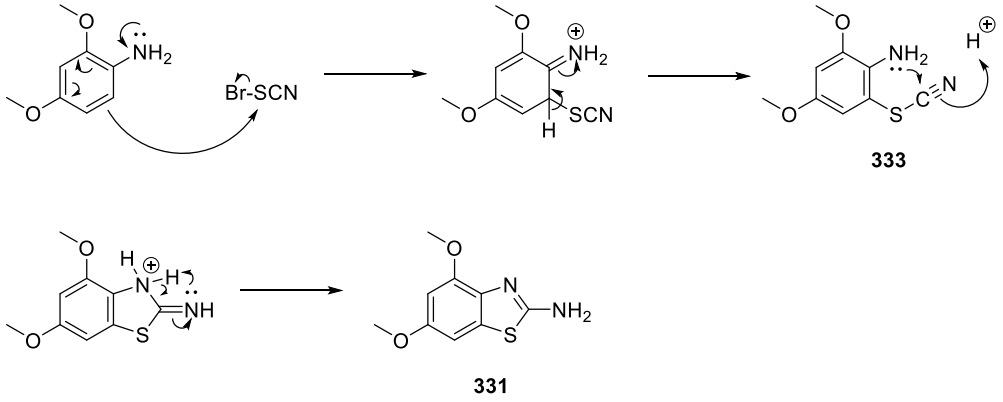

Scheme 102 Mechanism of Formation of Benzothiazole **331**

Unfortunately, an attempt to synthesise **330** using standard Sandmeyer conditions (Scheme 103) was unsuccessful. From the ^1H NMR in $CDCl_3$ starting material was consumed and a range of unidentified compounds were produced.

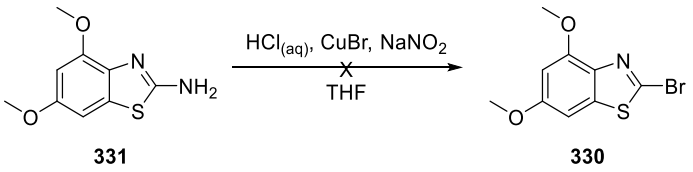

Scheme 103 Attempted Synthesis of Bromo Benzothiazole **330** *via* Standard Sandmeyer reaction

We decided to investigate introducing bromine substituent in two steps by reductive deamination [127] followed by bromo substitution [128] (Scheme 104). The deamination was carried out by refluxing starting material **331** with isopentyl nitrite in THF. The benzothiazole **334** product was obtained in 42% yield. Bromination took place by using *t*-BuOLi and CBr_4 in DMF at 110 °C to produce bromo compound **330** in 26% yield.

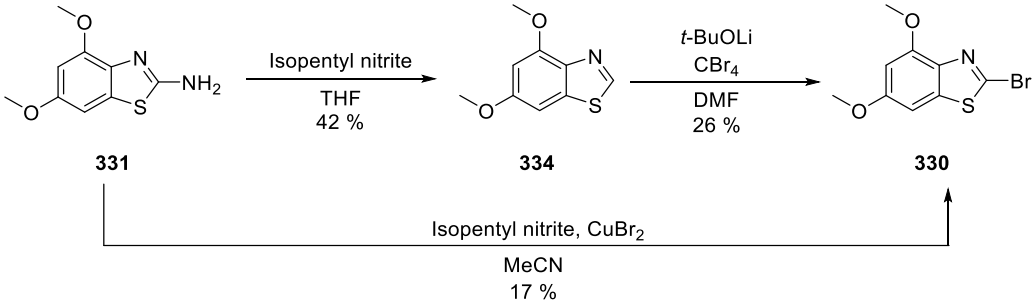

Scheme 104 The Synthesis of Compound **330**

Modified Sandmeyer reaction conditions were attempted with $CuBr_2$ and isopentyl nitrile in MeCN at 50 °C for 2 h. This one pot reaction gave the bromide **330** in 17% yield. While still a low yield, it was superior to the 11% overall yield for the two-step process.

The mechanism of reductive deamination (Scheme 105) using isopentyl nitrile is an interesting Sandmeyer reaction example because no formal hydride donor is added to the reaction mixture. After reaction of the amine with isopentyl nitrile, the diazene intermediate is produced. After loss of N_2, the aryl radical abstracts a hydrogen atom from THF to give the reduced product.

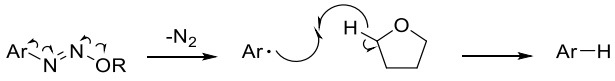

Scheme 105 Mechanism of Modified Sandmeyer reaction

Treatment of compound **330** with BBr_3 (1M) in DCM gave the corresponding dihydroxy benzothiazole **335** in good 95% yield (Scheme 106). Boron trifluoride is a strong Lewis acid and commonly used to cleave methyl ethers *via* a Lewis acid mediated S_N2 type reaction.

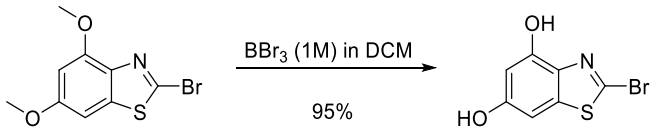

330 **335**

Scheme 106 The Synthesis of Compound **335**

The vinyl group was installed *via* the Stille reaction using similar conditions used for the vinyl BODIPY synthesis (Scheme 90) to give the corresponding vinyl benzothiazole **336** in 50% yield (Scheme 107). Due to solubility issues of the bis-phenol the solvent was changed to DMF.

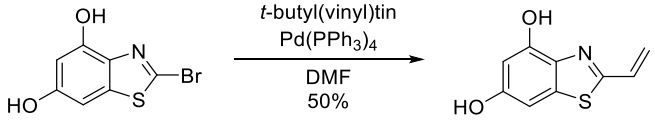

335 **336**

Scheme 107 Formation of Vinyl Group **336**

In order to avoid potential problems to do with solubility of future compounds, the two phenolate groups of vinyl benzothiazole **336** were protected as their TBDMS ethers (Scheme 108). The silyl protected compound **337** was isolated in a quantitative yield. The silyl protecting groups significantly increased solubility in DCM, which is the common solvent for olefin metathesis.

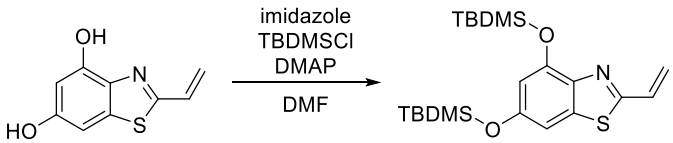

336 **337**

Scheme 108 The Synthesis of Silyl Protected **337**

However, the protected vinyl product **337** seemed to be unstable because even when the sample was stored under nitrogen, in the dark, at low temperature, its colour changed from colourless to brown-yellow after a day. The stability of compound **337** was monitored by ^1H NMR spectroscopy in $CDCl_3$. Although we did not identify any significant change in

the ^{1}H NMR spectrum over a week, a brown oily layer was clearly observed in the NMR tube. This unidentified oil showed poor solubilities in common solvents such as EtOAc, acetone and DCM and is most probably some insoluble polymeric material. As a precaution freshly prepared **337** was used in further reactions.

Olefin metathesis was attempted by treating a solution of vinyl compound **337**, cysteine **316** with Hoveyda-Grubbs II catalyst (20 mol%) in DCM at rt (Scheme 109). The amide compound **338** was tentatively assigned, but could not be purified properly by silica gel chromatography due to co-running impurities. The yield of compound **338** was estimated to be below 30%.

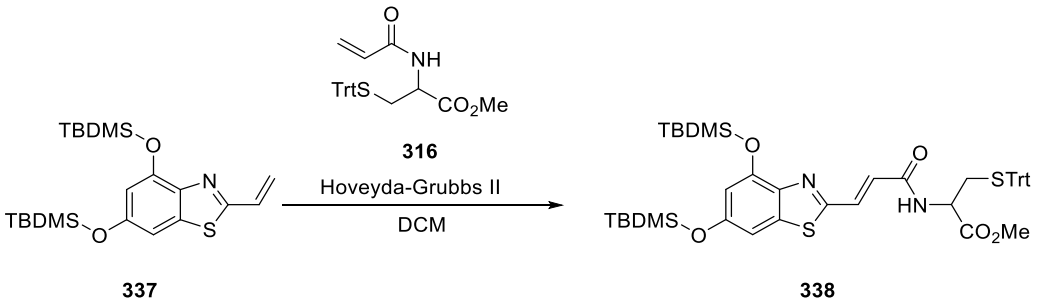

Scheme 109 The Synthesis of Intermediate **338** *via* Olefin Metathesis

From a clear ^{1}H NMR spectrum (400 MHz, $CDCl_3$) the protons of the *trans*-alkene were observed at δ 7.73 ppm (1H, d, 16 Hz, H_a) and δ 6.54 ppm (1H, d, 16 Hz, H_b) (Figure 44). Other peaks have also been labelled in Figure 44. The impurities could not be removed by standard purifications. We decided to see whether the impurities could be separated after cyclisation by POP reagent.

Note: Large amount of impurities were from commercial EtOAc which was contaminated in the factory.

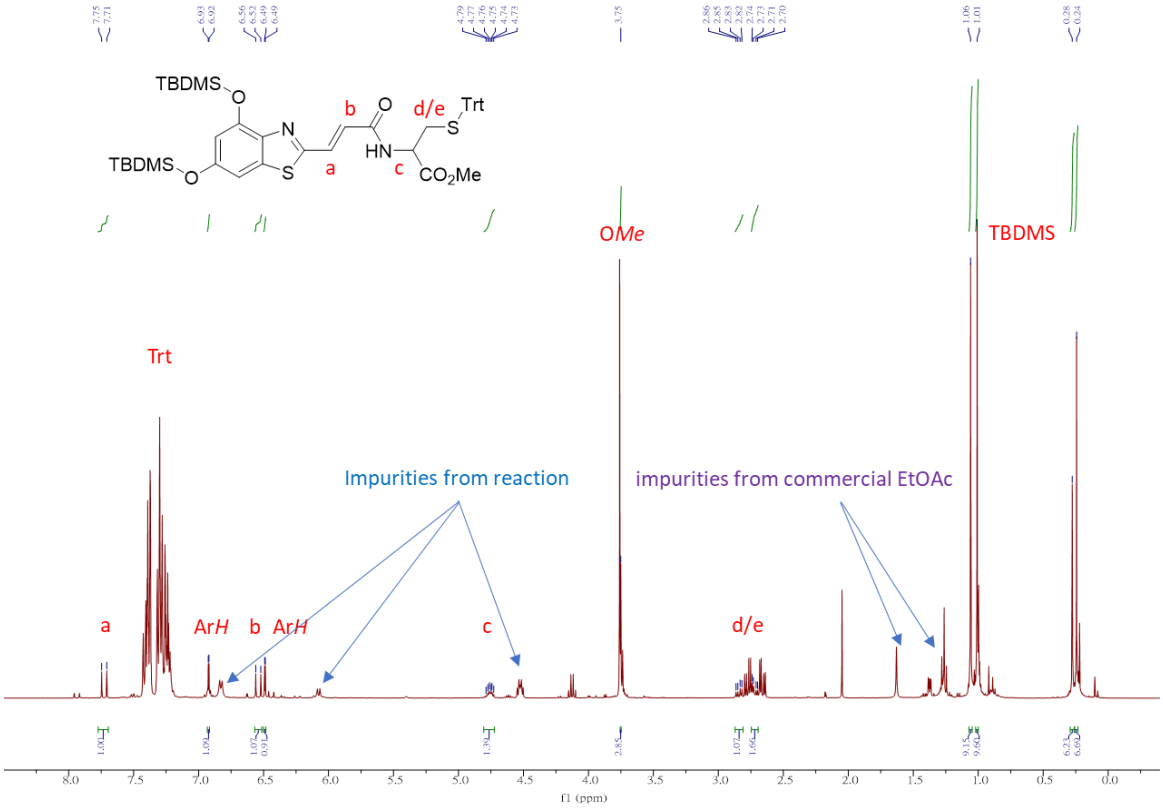

Figure 44 ^{1}H NMR of Compound **338**

Due to the low yield (around 30%) in the key olefin metathesis step, we attempted to optimise reaction conditions by investigating different temperatures (rt and 40 ˚C) and quantities of Hoveyda-Grubbs II (20 and 40 mol%) respectively (Table 9). We found that the yields of compound **338** were strongly dependent on the catalyst loadings. The results demonstrated that this reaction might be stoichiometric, rather than catalytic, in Hoveyda-Grubbs II. This suggests that Hoveyda-Grubbs II catalyst might be poisoned during the reaction. This should be further investigated in future synthetic studies.

Entry	Temperature	Catalyst loading	NMR Yields
1	rt	20 mol%	~30%
2	rt	40 mol%	~ 50%
3	40 °C	20 mol%	~30%
4	40 °C	40 mol%	~50%

Table 9 Screening of the Metathesis Reactions to Prepare **336**

A small-scale reaction was attempted to construct the thiazoline ring. Treatment of precursor **338** (30.0 mg) with POP reagent in DCM at 0 ˚C provided the silyl protected infra-luciferin **339** (Scheme 110). However, the isolated yield of **339** could not be calculated accurately because the impurities were still present in the product.

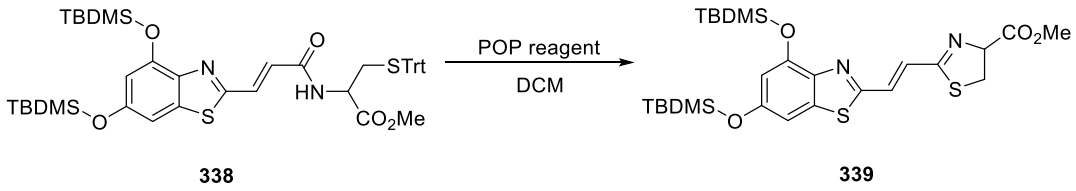

338 **339**

Scheme 110 Synthesis of Silyl Protected Compound **339**

After standard workup and purification, the proton (H_c) of thiazoline was observed in the ^{1}H NMR spectrum (400 MHz, $CDCl_3$) at δ 5.24 ppm (1H, dt, 8Hz, H_c) (Figure 45) and the HRMS result (ESI-TOF, m/z) (calcd. for $C_{26}H_{41}N_2O_4S_2Si_2$ $[M+H]^+$ 565.2024, found 565.2022) also confirmed the formation of **339** We utilized this impure compound **339** in the next step because some impurities were still impossible to remove.

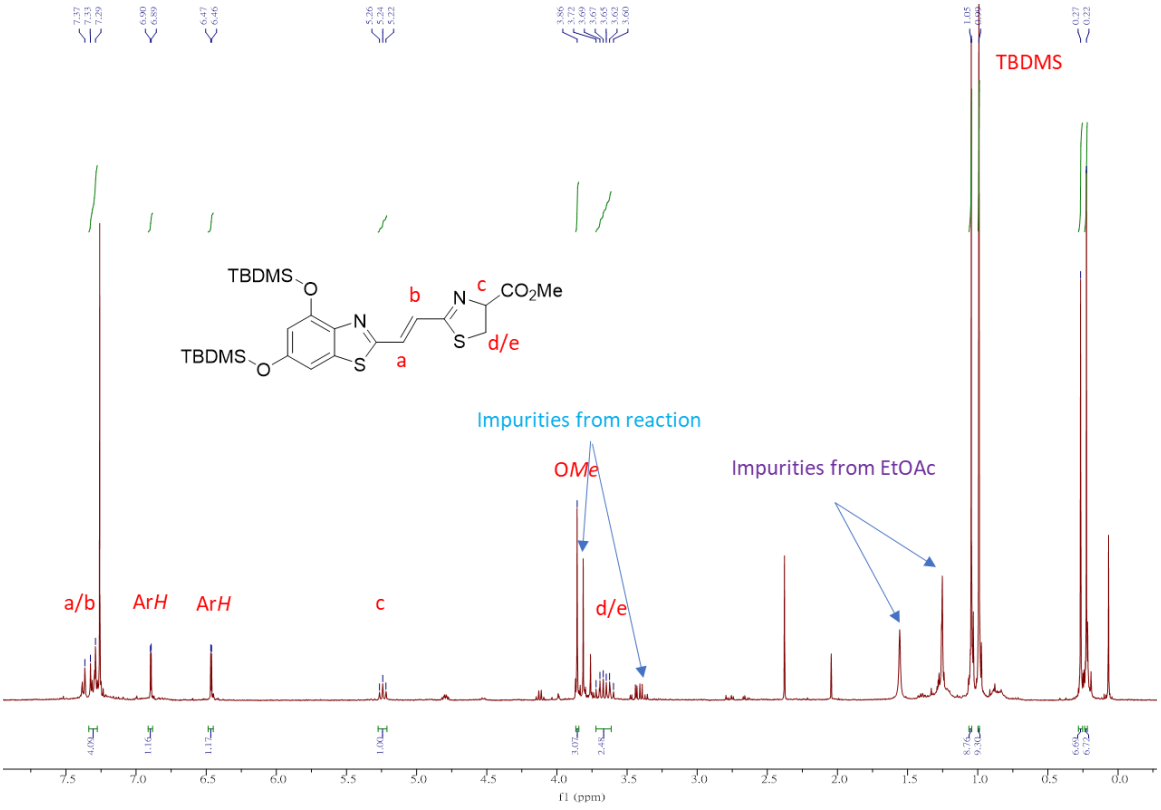

Figure 45 ^{1}H NMR of Compound **339**

The TBDMS phenol ethers could be cleaved by LiCl under mild conditions. [129] Mixing the impure precursor **339** and LiCl in MeCN at rt under N_2 overnight gave the final dihydroxyl infra-luciferin methyl ester **321** (Scheme 111), but in less than 6% isolated yield over 3 steps. The purification of target compound **321** was attempted by two methods in sequence. The highly polar impurities were removed by silica gel chromatography and the low polar impurities could be removed by sonication in chloroform and filtering off the remaining solid.

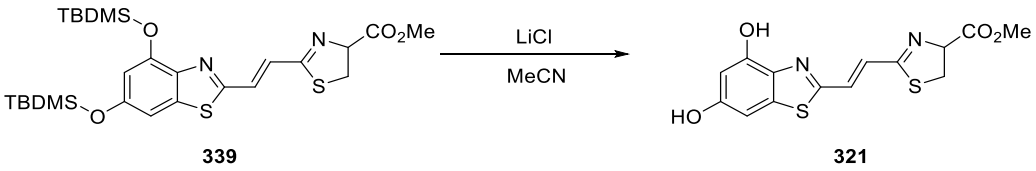

339 **321**

Scheme 111 The Synthesis of Final Compound **321**

However, from the ^{1}H NMR spectrum (600 MHz, MeOD), around 10% of reaction impurities could still be observed (Figure 46). Attempts to remove them by HPLC were unsuccessful.

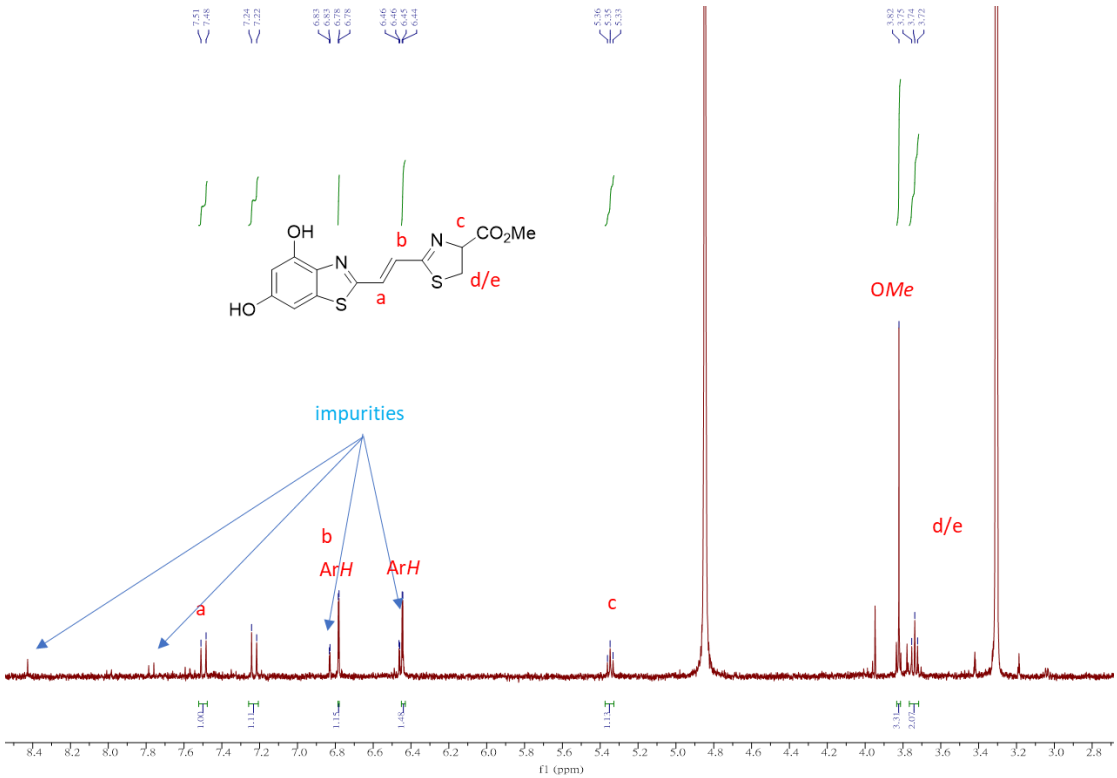

Figure 46 ^{1}H NMR of Dihydroxyl Infra-Luciferin Methyl Ester **321**

In this study, we have synthesized the target product **321** *via* olefin metathesis followed by POP reagent. However, the metathesis was inefficient, and the Hoveyda-Grubbs II catalyst was expensive. We therefore decided to return to the route originally attempted by the Masters student in our laboratory [125] and modify some of the steps to produce the target **321**.

6.4.2 Work Plan II

The formations of compounds **340** and **341** had been found to be challenging. [125] A new retrosynthesis was devised in Scheme 112. We expected that key intermediate **340** could be formed by disconnecting the C=C bond to give the aldehyde **341** and phosphonate ester **227** as before. Formylation of compound **341** could be delivered by halogen exchange with *n*-BuLi followed by reaction with DMF. From other syntheses in the laboratory we know that bromo benzothiazoles undergo rapid halogen-metal exchange at low temperature (-78 °C). This proposed step is different from the original synthetic route (Scheme 99) where the deprotonation by *n*-BuLi was found to be inefficient between -78 and -50 °C (at -78 °C, the starting material **324** was recovered but the benzothiazole **324** degraded at -50 °C).

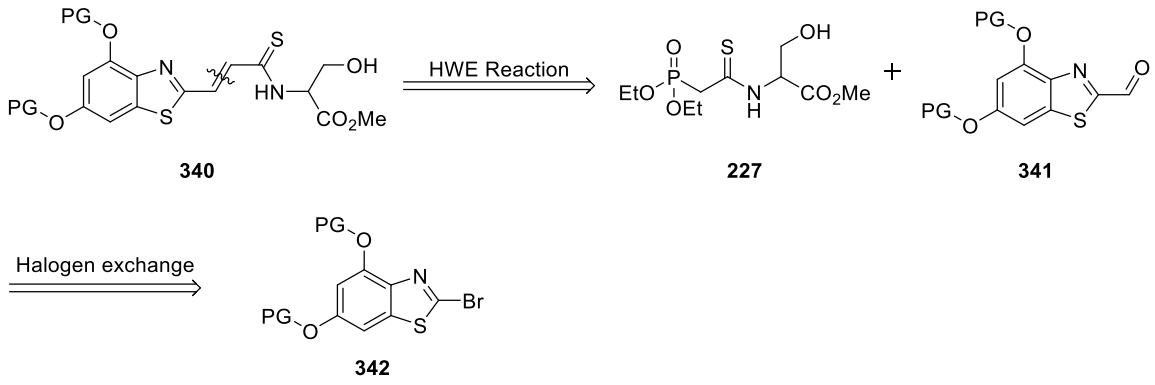

Scheme 112 The Retrosynthesis of Intermediate **340**

We decided to use the TBDMS protecting group as it seemed to withstand the conditions of the previous route well. The silyl protected bromo benzothiazole **343** was synthesized by treating dihydroxyl **335** with imidazole (5 eq), TBDMSCl (4 eq), and DMAP (5 mol%) in quantitative yield (Scheme 113).

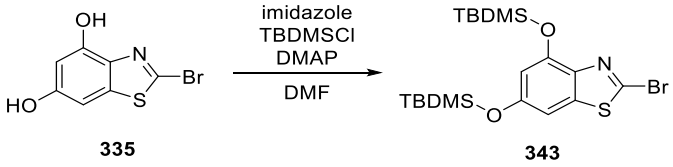

Scheme 113 The Synthesis of Silyl Protected **343**

Formylation by lithium halogen exchange was performed by treatment of compound **343** with *n*-BuLi at -78 °C for 30 min (Scheme 114). Anhydrous DMF was injected into the solution of lithium benzothiazole at -78 °C and after work up gave aldehyde benzothiazole **344** in a much improved 62% yield.

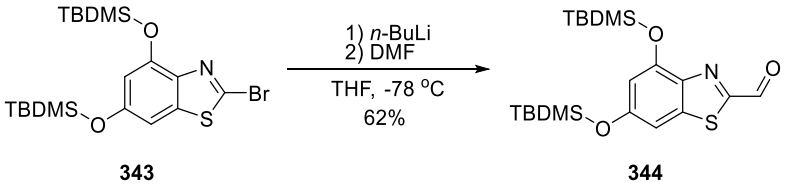

Scheme 114 The Synthesis of Aldehyde **344**

The HWE olefination proceeded by mixing phosphonate **227**, DBU and LiCl in MeCN, followed by the addition of a solution of aldehyde **344** in MeCN (Scheme 115). After standard purification, the deprotected product **345** was isolated rather than the expected TBDMS protected **346**. Olefination and deprotection were completed in one step. Deprotection could be attributed to the silyl groups which became labile in the presence of LiCl. Compound **345** was found to be quite polar and difficult to purify. After simple purification by a short silica gel plug, compound **345** was used directly in the next step.

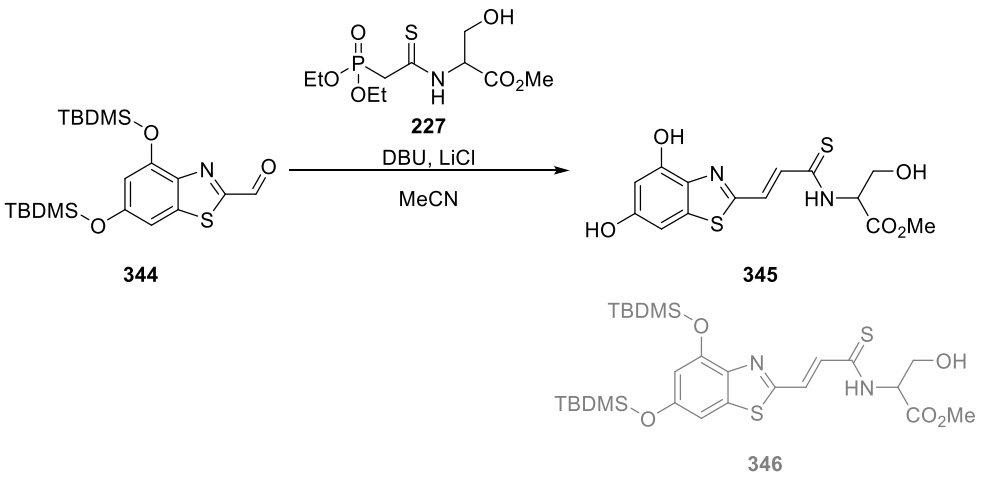

Scheme 115 The Synthesis of Compound **345** *via* HWE Reaction

Treatment of thioamide **345** with DAST reagent (3 eq) at -78 ˚C led to the final compound **321** in 3% yield over two steps.

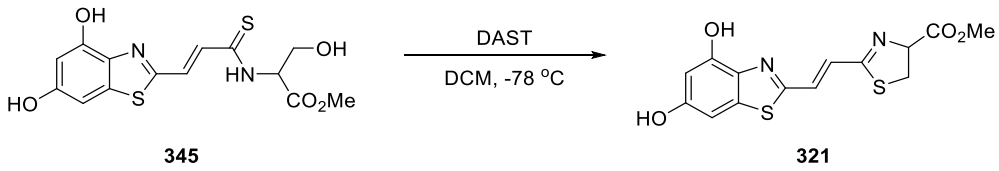

Scheme 116 The Synthesis of Dihydroxyl Infra-Luciferin Methyl Ester **321** by DAST

The mechanism of the ring construction involves (Scheme 117) the primary alcohol being activated by the DAST reagent. Intramolecular nucleophilic attack by the thioamide provides the thiazoline compound.

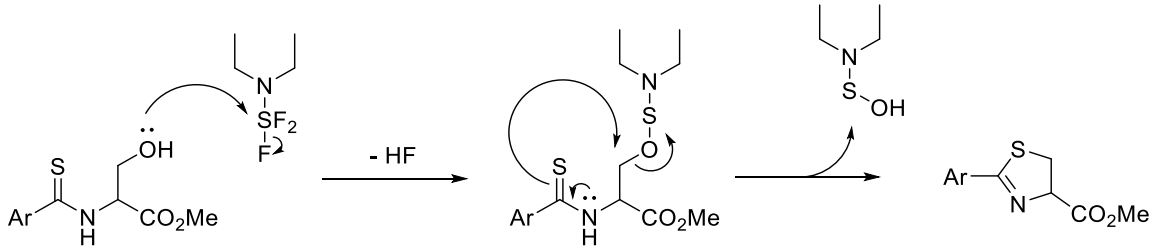

Scheme 117 Mechanism of Cyclisation by DAST Reagent

Although luciferin methyl ester **321** was **s**ynthesized, the small amount of compound was insufficient for bioluminescence analysis. The low yield over the last two steps was due to the TBDMS protecting groups being easily cleaved in the HWE reaction. Using a more stable protecting group, such as TIPS, might be a practical method to overcome this in future.

7. Novel V-shaped Luciferins

7.1 Introduction of Thiazole-Annulated Scaffolds

Thiazole-annulated scaffolds are the prominent core structures in chromophores and fluorophores with multiple applications [130] such as organic field-effect transistors (OFETs), [131] and two-photon absorbing fluorophores. [132] Compound **346**, **Q3Me** containing the V-shaped benzobisthiazole core is a two-photon material that is a diagnostic agent in 3D fluorescence imaging with nIR emission (Figure 47). This novel compound has fluorescence emission around 500 nm and two-photon emission above 800 nm.

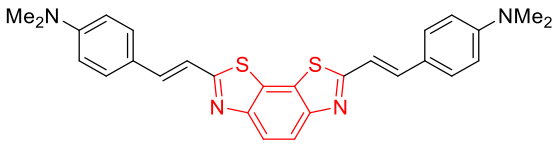

346
Q3Me

Figure 47 An example of a Thiazole-annulated fluorophore

In addition, the benzobisthiazole core structure can also be found in medicinal chemistry as kinase inhibitors (Figure 48). Protein Kinases are important regulators linked to a variety of diseases such as viral infections, neurodegenerative disorders and metabolic regulation. In 2016 Prak and co-workers reported a series of cdc2-like kinases (CLKs) inhibitors. Among the different CLKs inhibitors investigated, a novel skeleton benzobisthiazole (in red) had greater inhibitions in their screens. [133]

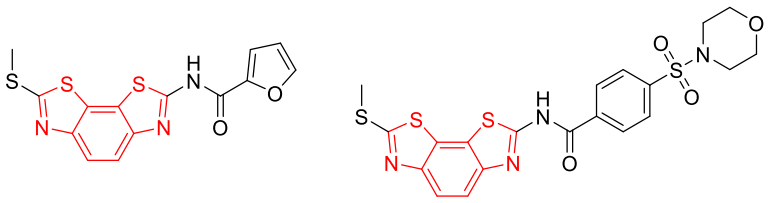

347
SE4

348
5F4

Figure 48 CLKs Inhibitors Based on Thiazole-annulated scaffold

These two studies demonstrated that the benzobisthiazole core was fluorescent. This suggested to us that the benzobisthiazole core has a potential application as a chromophore in bioluminescence. Even though this core structure has been applied to many fields, there

are no reports of luciferin analogues based on this structure. It would be interesting to use this core for the development of a new type of luciferin and investigate their bioluminescence properties.

7.2 Aim of Project and Research Proposal

According to the bioluminescence emission results from previous luciferin analogues, we hypothesized that a V-shaped core might fit well into the active site of luciferase and give efficient light emission. From the reported luciferin analogues, we found that luciferins **65b** [47] and **73b** [48] have a similar conjugation length from the pendant amines, as the electron donating groups (EDGs), to the position of the light giving ketone group upon oxidation (the corresponding oxy-luciferin). However, luciferin **73b** demonstrated a more red-shifted emission than luciferin **65b** by 35 nm (Figure 49). This difference might have something to do with the shape of each compound. Compound **65b** is a linear skeleton and luciferin **73b** has a V-shaped (in purple). Different shapes might have different fits with luciferase and could give rise to different colour emissions due to subtle differences between interactions with amino acid residues in the active site. Additionally, luciferin analogue **163b**, **OH-NpLH2**, which also has a V-shaped core, has the longest bioluminescence emission (768 nm) so far. [66]

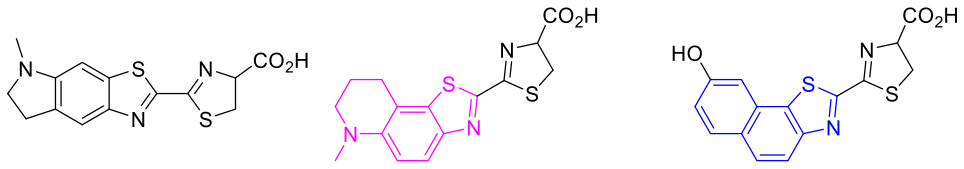

65b, **CycLuc2**
λ_{max} = 607 nm

73b, **CycLuc10**
λ_{max} = 642 nm

163b, **OH–NpLH2**
λ_{max} = 768 nm

Figure 49 Reported Luciferins **65b**, **73b** and **163b** and Their Emissions

In this study, we would like to develop a series of luciferin analogues based on V-shaped benzobisthiazole scaffolds bearing different amines as electron donating groups (EDGs) for bioluminescence research (Figure 50).

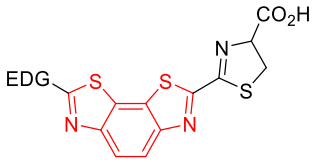

EDG= -NMe_2, Piperidine, Pyrrolidine, Morpholine

349

Figure 50 Proposed Benzobisthiazole Luciferins with Different Amine Donating Groups

7.3 Computational study

Because the luminescence data for benzobisthiazole **350** and naphtho[2,1-*d*]thiazole **351** were incomplete, a computer-aided calculation was employed to estimate their basic luminescence properties. The singlet transition of core structures **350** and **351** were conducted by time-dependent density functional theory (TD-DFT) at the level td B3LYP/6-311++G(d).

From their energy levels (Table 10), core **350** has a deeper HOMO/LUMO energy levels (-6.55 eV/-2.07 eV) than **351** (-6.0 eV/-1.95 eV), because of the additional thiazole ring present in the structure. The band gaps of naphtho[2,1-*d*]thiazole **351** (4.05 eV) and proposed core **350** (4.48 eV) were obtained from the difference between their HOMO/LUMO values. It suggested that core structure **351** has a smaller band gap and might have longer wavelength emission. However, dipole moment (μ) and oscillator strength (f) ascribed to predominately charge transfer transitions also contribute to emission wavelength. Compared to naphtho[2,1-*d*]thiazole **351** (μ = 1.5086, f = 0.0434), benzobisthiazole **350** has a larger dipole moment (μ = 1.6983 Debye) and smaller oscillator strength (f = 0.0393). The magnitude of these values suggests that core structure **350** might give more red-shifted emission than **351**, because of its stronger ICT characteristic. The data conflict each other and we cannot simply conclude which core structure has a more red-shifted emission from these calculations alone. As a result, the excitation energy (E_{s1}) was calculated and investigated. According to the excitation energies (E_{s1}) of **350** (3.88 eV) and **351** (3.62 eV), these two structures might have similar emissions, but **350** might be a little more blue-shifted than **351** (*a more accurate computational study will be conducted through a collaboration with theoretical chemists in the near future*). From these data, we expect that core structure **350** is a comparable candidate for bioluminescence study.

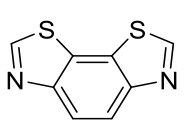

350

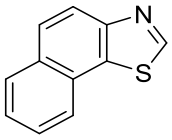

351

	HOMO/LUMO (eV)	ΔE_{gap} (eV)	μ (Debye)	f	E_{s1} (eV)
350	-6.55/-2.07	4.48	1.6983	0.0393	3.88
351	-6.0/-1.95	4.05	1.5086	0.0434	3.62

Table 10 Summary of Computational Studies of **350** and **351**

7.4 Synthesis of V-shaped Luciferins

7.4.1 Work I

As depicted in the retrosynthesis (Scheme 118) the formation of the thiazoline ring was proposed from the standard condensation of nitrile fragment **352** with cysteine which has been used in many luciferin analogue syntheses. The benzobisthiazole **352** could be built up by heating the imine product **353** at high temperature. Treatment of amino benzothiazole **354** with Appel's salt would give the imine benzothiazole **353** as used by previous syntheses of luciferin analogues. Reduction of **355** could provide amino benzothiazole **354**. Furthermore, installation of different electron donating group (EDG) from **355** could be incorporated by S_NAr reaction. Finally, the halogen benzothiazole leads back to the commercially available 2-amino-6-nitro-benzothiazole **357**.

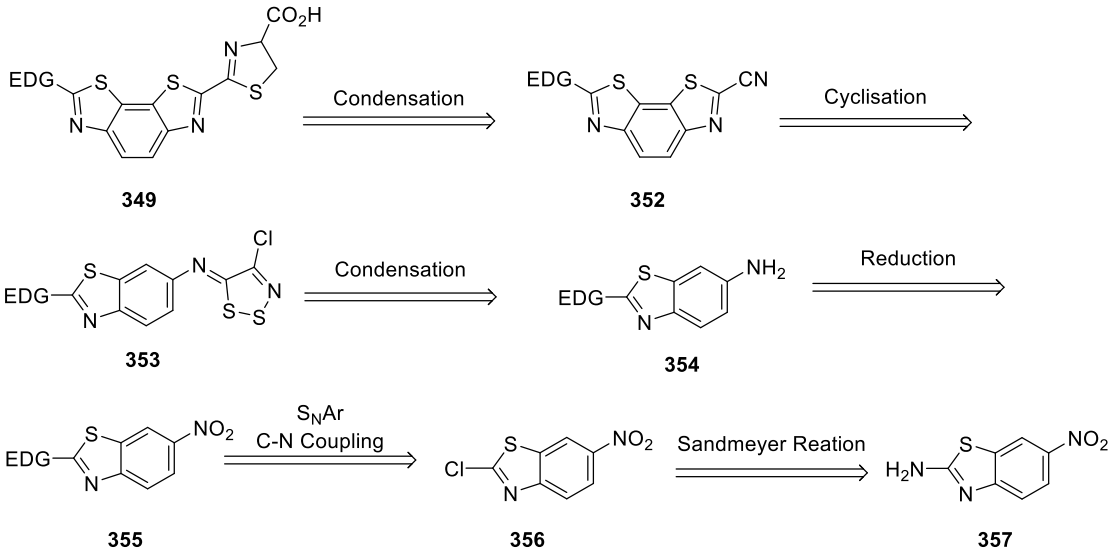

Scheme 118 Retrosynthetic analysis of Benzobisthiazole Luciferins

Our synthesis started with a Sandmeyer reaction of commercially available 2-amino-4-nitrobenzothiazole with CuCl, $NaNO_2$, and $HCl_{(aq)}$ in THF from 0 °C to reflux, which gave chlorinated compound **356** in quantitative yield (lit. [134] yield 65%) (Scheme 119).

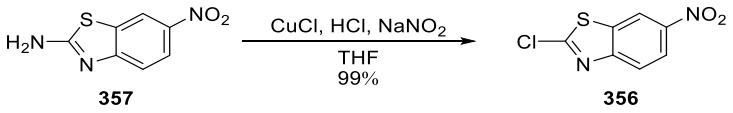

Scheme 119 The Synthesis of **355** *via* Sandmeyer reaction

Exposure of chloro-benzothiazole **356** to dimethylamine (2M) THF solution at rt gave the desired product **358** *via* an S_NAr reaction in quantitative yield (lit. [134] yield 87%) (Scheme 120).

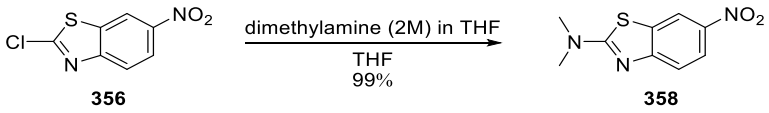

Scheme 120 The Synthesis of Compound **358**

However, reduction of nitro compound **358** to the corresponding amine failed under several conditions (Scheme 121) such as Fe/HCl in EtOH; $SnCl_2$ in EtOH at 78 °C. All starting material degraded under these conditions. Catalytic hydrogenation using Pd/C was also attempted. Although the desired compound **359** was detected by HRMS, isolation of **358** was unsuccessful by column chromatography. These frustrating results might be attributed to the two strong electron donating groups (-NMe_2 and -NH_2) present in the desired product. They could have a combined effect of increasing the HOMO energy making the product sensitive to forcing reaction conditions and further oxidation reactions during isolation. We decided to change our initial work plan.

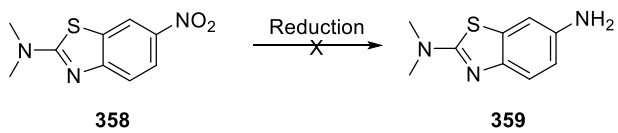

Scheme 121 Attempted to Reduce Nitro Group of Compound **358**

7.4.2 Work II

The new proposed synthetic route reordered the sequence of the previous suggested steps (Scheme 122). The final step was the synthesis of our target product **349** by reacting nitrile compound **352** to cysteine, which is the same as our initial work plan. However, in work plan II, we proposed to construct the core structure first and then introduce the amine EDGs in order to avoid the hypothetical over oxidation problem. Another advantage of this new route is that a variety of amine precursors **352** could be delivered and screened quickly by using the same V-shaped core structure **360** *via* C-N crossing coupling or S_NAr reaction. The possible synthetic method to provide the V-shaped core structure could be created by heating imine compound **361** at high temperature. The formation of product **361** was suggested by condensation of Appel's salt with known 2-chlorobenzo[d]thiazol-6-amine (**52a**) which could be obtained by chemo selective reduction of 2-chloro-6-nitrobenzo[d]thiazole (**356**). [47]

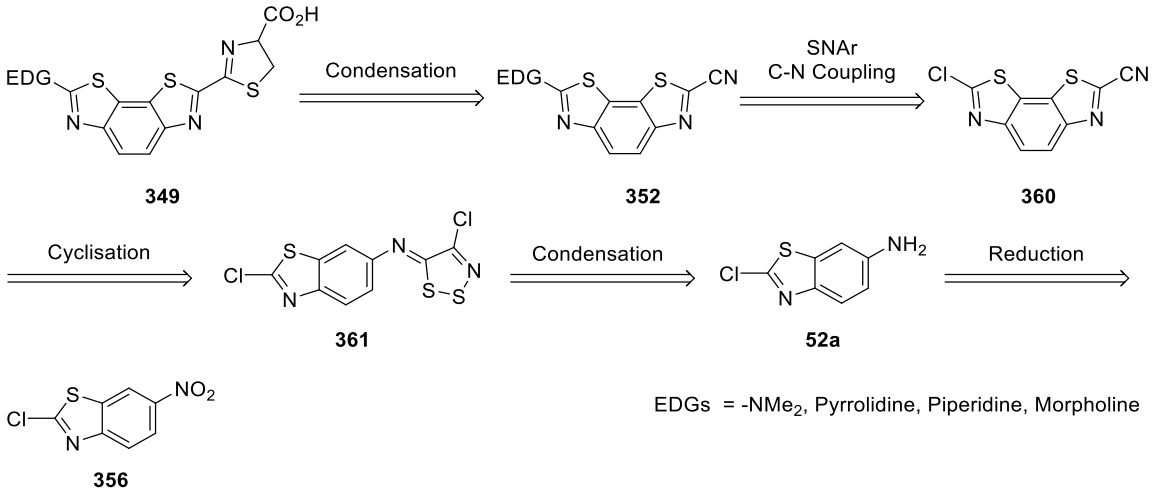

Scheme 122 Alternative Retrosynthesis of Target **349**

With nitrobenzothiazole **356** in hand, the reduction could proceed according to the literature conditions by mixing tin (II) chloride in EtOH at 78 °C until the suspension turned to a clear brown solution. After standard work up, the desired product **361** was obtained in 80% yield (lit. [47] yield 77%) (Scheme 123).

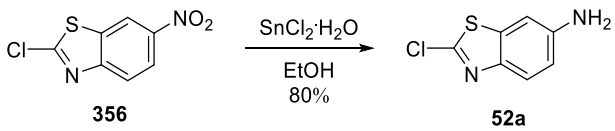

Scheme 123 Reduction of Compound **356**

Condensation of aminobenzothiazole **52a** with Appel's salt followed by pyridine gave the desired imine product **361** in 69% yield as a yellow solid (Scheme 124).

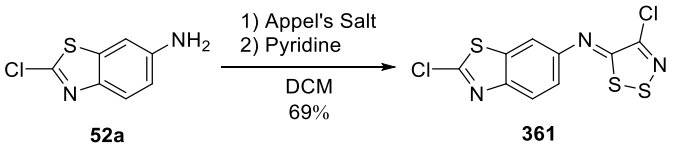

Scheme 124 The Synthesis of Compound **361**

Heating compound **361** in sulfolane at 180 ˚C for 30 min gave V-shaped benzobisthiazole **360** in 20% yield with uncyclized compounds (Scheme 125). The reaction time could be further extended to 2 h, and the yield was increased to 53%. Surprisingly, no linear benzobisthiazole **362** was observed in this condition. The formation of V-shaped product **360** rather than linear **362** might be attributed to the C^7 position being more reactive than C^5. A similar selectivity was also be found with compound **114c** which preferred to undergo substitution at the 7 position rather than 5 position (Scheme 26).

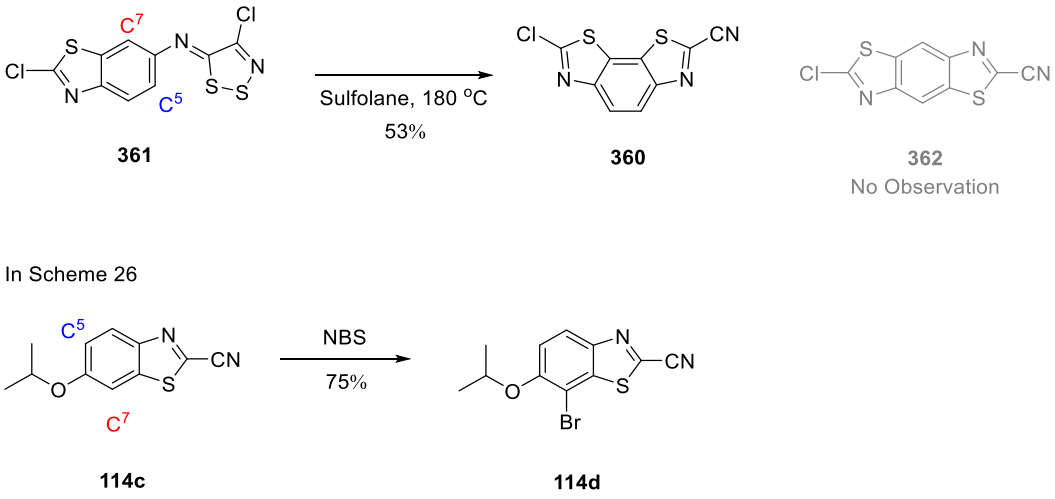

Scheme 125 The Synthesis of V-Shaped Core **359**

With the desired core **360** in hand, a series of amine groups were installed *via* S_NAr reactions (Scheme 126). In the presence of morpholine, dimethylamine, pyrrolidine, or piperidine, the nitrile V-shaped compounds **360** gave the corresponding amine V-shaped precursors **352a-d** in 23-58% yields.

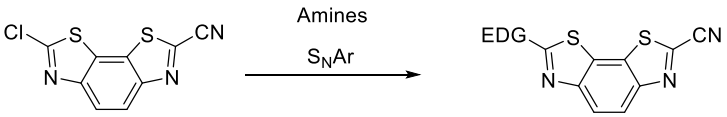

360

352a, EDG = morpholine, 58%
352b, EDG = dimethylamine, 58%
352c, EDG = piperidine, 23%
352d, EDG = pyrrolidine, 26%

Scheme 126 The Synthesis of Intermediates **352a-d**

Final, condensation of amine benzobisthiazole **352a-d** with cysteine in a co-solvent system of DCM and MeOH gave our target V-shaped luciferin analogues in the 69 to 90% yields (Scheme 127). These analogues will be subjected to bioluminescence investigation in due course.

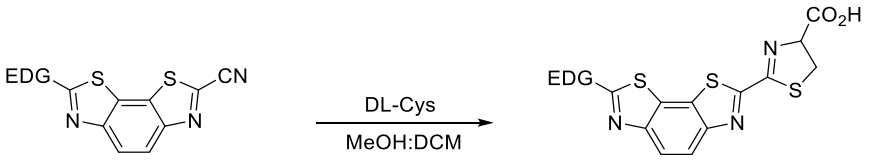

352a, EDG = morpholine
352b, EDG = dimethylamine
352c, EDG = piperidine
352d, EDG = pyrrolidine

349a, EDG = morpholine, 90%
349b, EDG = dimethylamine, 69%
349c, EDG = piperidine, 75%
349d, EDG = pyrrolidine, 90%

Scheme 127 Synthesis of V-Shaped Luciferins **349a-d**

8. Conclusion and Future Work

8.1 Conclusion

In our research, we have synthesized diverse luciferin analogues including a potential ESIPT type infra luciferin **298**, BODIPY based luciferin methyl ester **304**, ICT enhanced luciferin methyl ester **321** and V-shaped luciferins **349a-d** (Figure 51).

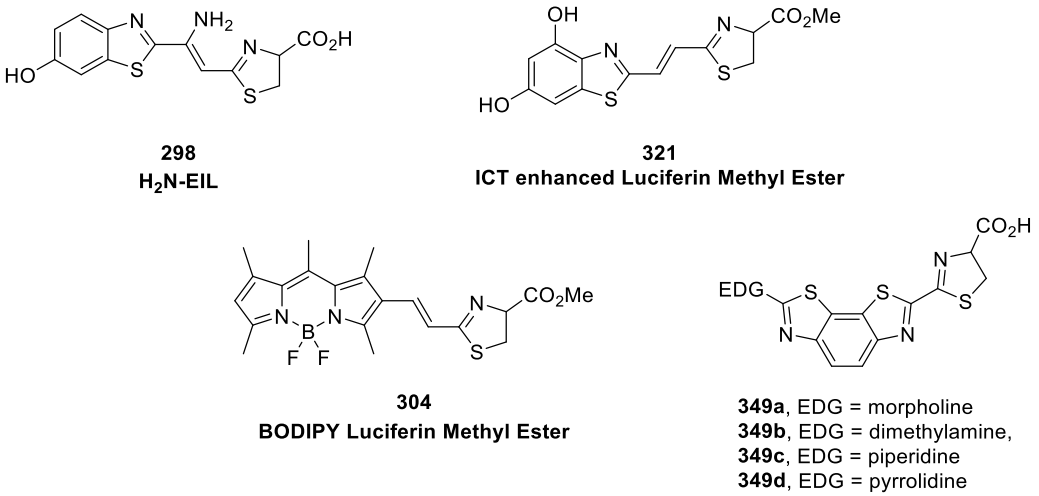

Figure 51 The Structures of Different Luciferins

The ESIPT type of luciferin **298** is rigidified by the intramolecular H-bonds which is used to suppress the non-radiative decay. We expect this compound **298** could have nIR emission and give stronger $\emptyset_{Blu}$ than iLH$_2$.

To enable the first synthesis of a luciferin analogue based on a BODIPY core structure a novel convergent synthetic route to introduce the central C=C bond *via* alkene cross metathesis was developed. This method is different from the previous routes developed by our group and others for alkene linked luciferin analogues that have involved HWE type approaches. the alkene cross metathesis approach may be applicable to new luciferin analogues in the future.

It was shown by computational methods that the additional hydroxyl group at the 4 position of dihydroxyl luciferin **321** can facilitate ICT and give longer wavelength emission. Using Appel's salt chemistry, nitrile V-shaped core structure **359** were synthesized in pure form. Diverse amines groups could be installed to this novel core structure easily *via* S$_N$Ar reactions. From the commercially available 6-nitrobenzo[d]thiazol-2-amine (**357**), a group

of V-shaped luciferins can be synthesized in 5 steps. These new analogues are good candidates for bioluminescence SAR study.

The bioluminescence properties of BODIPY luciferin **319** was measured. With iLuc1 mutant luciferase, BODIPY luciferin gave longest emission wavelength at 697 nm but the $\emptyset_B$ was 0.1% of D-luciferin. With CBR luciferase, BODIPY luciferin **319** gave the strongest $\emptyset_B$ which is 10% of D-luciferin. According to this encouraging result, we expected that BODIPY can become a new core structure in bioluminescence research. The other synthesised luciferin analogues will be submitted for bioluminescence study in the very near future.

8.2 Future Work

Based on the strategy for the synthesis of BODIPY luciferin methyl ester **304**, new analogues **363-365** can be proposed (Figure 52). The conjugation of BODIPY **363** can be extended by introducing an additional phenyl ring which may provide longer wavelength emission. Compounds **364** have different EDGs such as (-OH) or (-NMe_2) to enhance their ICT properties. Compared to **364**, luciferins **365** are anticipated to have reduced intramolecular motion due to the 4 proximal methyl groups and give higher $\emptyset_B$.

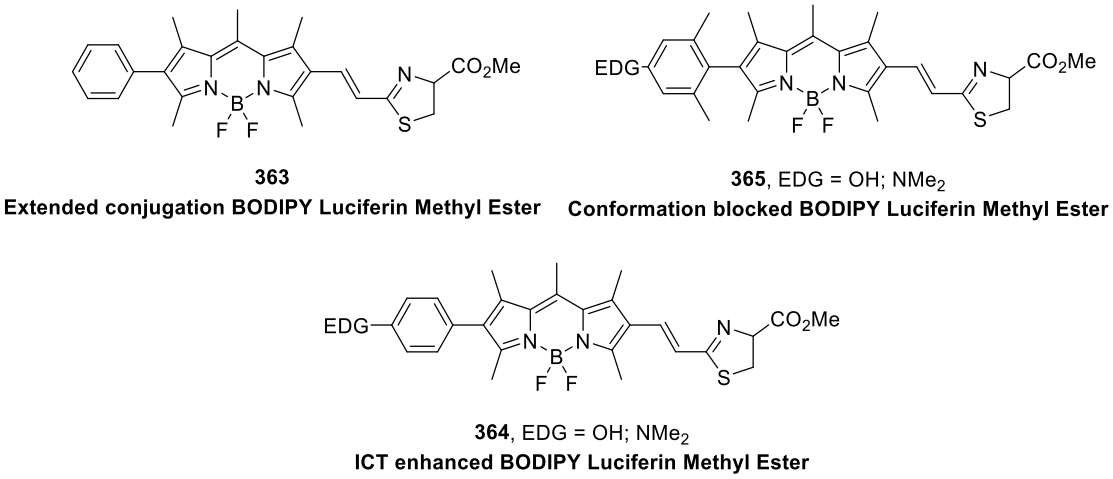

Figure 52 Proposed Novel BODIPY Luciferins

Their synthesis could make use of known diiodo BODIPY **366** [116] (Scheme 128). A selective C-C cross coupling reaction could introduce a series of arenes and the unsaturated thiazole portion could be appended following the synthetic devised in this work (Scheme 89).

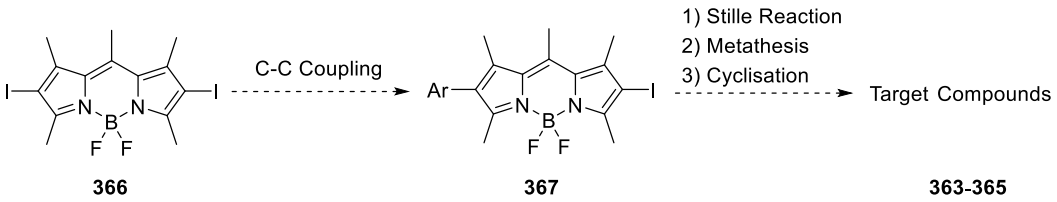

Scheme 128 Attempted Synthesis to targets **363-365**

Target **368** with an extra C=C bond between benzobisthiazole and thiazoline can also be proposed (Figure 53). The additional double bond can elongate the conjugation for more red-shifted emission as we have shown between luciferin **1** and infra luciferin **223**.

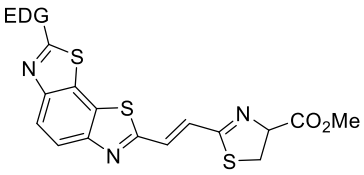

368

Figure 53 Proposed V-Shaped Luciferins **368** with a C=C bond

These could be prepared from nitrile benzobisthiazole **352** by controlled reduction to give aldehyde **369** (Scheme 129). Follow our literature procedure (Route I), the target compounds can be achieved by reacting aldehyde **369** with phosphonate **227** followed by treatment with DAST. The alternative synthetic route *via* cross-metathesis can also be proposed (Route II). The final products can be synthesized *via* the Wittig reaction, cross-metathesis and cyclisation with Hendrickson reagent.

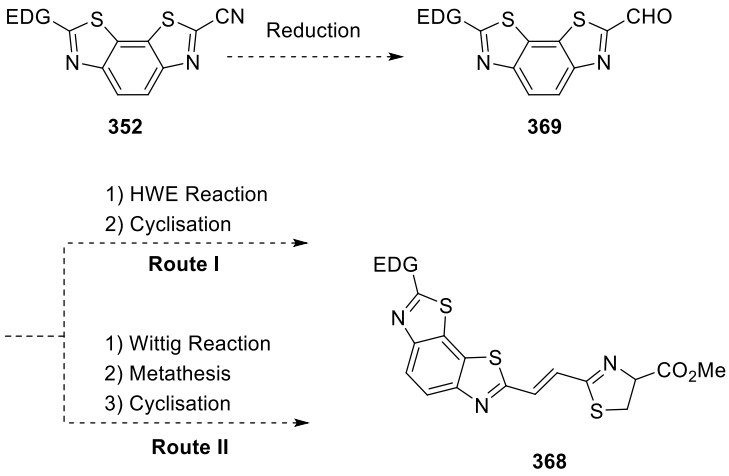

Scheme 129 Forward Synthesis of Targets **367**

Experimental techniques

General Experiment Details

Anhydrous reactions were performed in flame dried glassware under a positive flow of nitrogen gas. Rection temperatures of 0 °C was achieved by the use of an ice-water bath and of -78 °C by using a dry ice in acetone bath. All commercially available solvents and chemicals were used without further purification. The anhydrous solvents tetrahydrofuran (THF), dichloromethane (DCM) and toluene were obtained from the in house drying solvent system. Thin layer chromatography (TLC) was carried out on Merck aluminum backed DC 60 F254 0.2 mm pre-coated plates. Visualization of the TLC was under ultraviolet light (254 nm or 364 nm). Flash column chromatography was prepared on Gedran silca gel 60, 40-63 μm.

The ^{1}H and ^{13}C NMR spectra were recorded on the following machines: Bruker Acance 300 spectrometer, Bruker Avance III 400, Bruker Avance III 600, and Bruker Acance Neo 700 spectrometer. All the NMR spectra were manipulated using MestReNova (Version 11.0). The chemical shife (δ) was reported in parts per million (ppm) and coupling constants are quoted in Hertz (Hz). Two dimensional NMR (COSY, HSQC, HMBC and NOESY) were used to assist full assignment where required. A Perkin Elmer Spectrum 100 FT/IR with 100 μATR machine was used to collect IR spectra under thin film conditions or as a fine solid. Mass spectra were obtained on a ThermoMAT900 and an Accela LC-Finnigan LTQ instruments. X-ray diffraction (XRD) data were collected from a single crystal using SuperNova A (Dual) Diffractometer System. X-ray photoelectron spectroscopy (XPS) measurements were carried out on a Thermo Scientific K-Alpha XPS machine with a monochromated AI K_{α} (E= 1486.6 eV), a double focusing 180° hemisphere analyser of ~125 mm radius and detected with an 18 channel position-sensitive detector. Reverse phase HPLC was carried out with ZoRBAX 300SB-C18, 5 μm, 9.4*250 mm column with ASI-100 Automated Sample Injector. Computational study was conducted by Gaussian 09, Revision D.01 [135] and visualized by Avogadro.

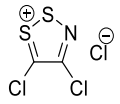

36

4,5-Dichloro-1,2,3-dithiazolium chloride (Appel's salt) (36) [37]

A solution of chloroacetonitrile (20.0 mL, 0.31 mol) in anhydrous DCM (50 mL) was injected sulfur monochloride (101 mL, 1.24 mol) at rt under N_2. The solution was left without agitation for 48 h. The colour of this mixture turned to black from orange within 3 h and lots of gas was produced. After 48 h, a dark green solid precipitated. This dark solid was collected and washed with anhydrous DCM (3 X 100 mL). Appel's salt (62.9 g, 95%) (lit. [37] 90%) could be used without further purification and was stored in a desiccator.

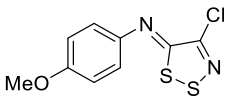

39

4-Chloro-5-((4-methoxyphenyl)imino)-5*H*-1,2,3-dithiazole (39) [39]

To a solution of *p*-Anisidine (4.92 g, 40.0 mmol), and anhydrous DCM (96 mL) was added Appel's salt (**36**) (8.32 g, 40.0 mmol) at rt under N_2. The mixture was stirred for 1 h and then anhydrous pyridine (6.4 mL, 80 mmol) was injected into the mixture and stirred for an additional 2 h. After the volatile materials were removed by reduced-pressure, the sticky crude product was purified by column chromatography (silica hexane followed by DCM.) The product was obtained as a yellow solid (9.84 g, 95%) (lit. 99%). m.p. = 91 (dec.) °C (lit. [136] 89 ºC); R_f = 0.5 (100% DCM); ^{1}H NMR (400 MHz, $CDCl_3$) δ 7.28 (2H, d, *J* = 8.0, Ar*H*), 6.99 (2H, d, *J* = 8.0 Hz, Ar*H*), 3.85 (3H, s, OCH_3). The the data agreed with the literature. [39]

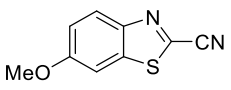

33

2-Cyano-6-methoxybenzothiazole (33) [39]

A solution of compound **39** (2.00 g, 7.75 mmol) in sulfolane (5 mL) was heated to 180 ˚C for 30 min. The solution was then cooled to rt, extracted with MTBE (3 x 30 mL), the combined organic layers washed with saturated aqueous NH_4Cl (30 mL), and dried

($MgSO_4$). After filtration, the volatile materials were removed *in vacuo*, the crude product was purified by column chromatography (silica 75% hexane：EtOAc 25% EtOAc). The product was obtained as a white solid (0.93 g, 63%). m.p. 131 °C (lit. [137] 131-132 °C); R_f = 0.5 (75% hexane：EtOAc 25% EtOAc); ^{1}H NMR (400 MHz, $CDCl_3$) δ 8.09 (1H, d, *J* = 9.2, Ar*H*), 7.36 (1H, d, *J* = 2.4, Ar*H*), 7.25 (1H, dd, *J*= 9.2, 2.4, Ar*H*), 3.92 (3H, s, OCH_3). All the data agreed with the literature. [39]

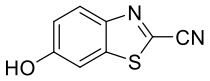

34

2-Cyano-6-hydroxybenzothiazole (34) [39]

To a mixture of compound **33** (0.30 g, 1.58 mmol) and pyridine hydrochloride (1.83 g, 15.8 mmol) was heated to 180 °C for 1 h under N_2. The mixture was then cooled to rt, and diluted with water (5 mL) and ethyl acetate (20 mL). The mixture was separated and further extracted with EtOAc several times until no fluorescence was visible in the aqueous layer. The organic layers were combined, dried ($MgSO_4$), and filtered. After the volatile materials were evaporated *in vacuo*, the crude product was purified by column chromatography (silica 50% hexane：50% EtOAc). The product was obtained as pale a yellow solid (0.18 g, 65%) (lit. [14] 61%). m.p. 183 °C (lit. [6a] 212-215 °C); R_f = 0.25 (20% hexane：80% EtOAc); ^{1}H NMR (400 MHz, Methanol-d_4) δ 7.97 (1H, d, *J* = 8.0, Ar*H*), 7.37 (1H, d, *J* = 4.0, Ar*H*), 7.13 (1H, dd, *J* = 8.0, 4.0, Ar*H*). The data agreed with the literature. [39]

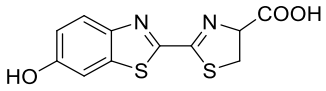

1

DL-Luciferin (1) [39]

To a solution of compound **34** (20.0 mg, 0.11 mmol), DL-cysteine hydrochloride monohydrate (18.8 mg, 0.12 mmol), K_2CO_3 (15.7 mg, 0.11 mmol), and MeOH (2 mL in 1 mL H_2O) at rt under N_2. The suspension was stirred for 30 min. The mixture was acidified with 3 M HCl to pH = 3 with pH paper. The MeOH was removed *in vacuo*, and the remaining solution was extracted with EtOAc for several times until no colour was observed in the aqueous layer. The organic layers were combined, dried ($MgSO_4$), and filtered. After the volatile materials were removed *in vacuo*, the crude product was purified

by column chromatography (silica gel 100% EtOAc followed by 1% AcOH：99% EtOAc). The product was obtained as a white solid (28 mg, 90%) (lit. [138] 86%). m.p. 196 °C (lit. 202 ºC (dec.)); ^{1}H NMR (400 MHz, Methanol-d_4) δ 7.89 (1H, d, J = 8.9, Ar*H*), 7.33 (1H, d, J = 2.3, Ar*H*), 7.06 (1H, dd, J = 8.9, 2.3, Ar*H*), 5.35 (1H, app t, J = 9.0, C*H*(COOH)CH_2), 3.71-3.79 (2H, m, CH_2S). The data agreed with the literature. [39]

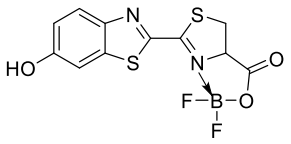

263

Boron-Based DL-luciferin 263

To a suspension of DL-Luciferin (**1**) (50.0 mg, 0.18 mmol) and MeOH (0.5 mL) was added BF_3OEt_2 (26.0 µL, 0.21 mmol) at rt, and the reaction was stirred for 24 h. The reaction was monitored by ^{1}H NMR until starting material had been consumed (24 h.) After all the volatiles were removed *in vacuo*, the product was obtained as a yellow solid (59.2 mg, 99%). m.p. 177 ˚C (dec.); R_f = 0.95 (10% MeOH：90% EtOAc); IR υ_{max} (solution in MeOH): 3329 (O-H), 2943 (C-H), 2832 (C-H), 1646 (C=C) cm^{-1}; XPS (eV) B 1S region: 195.2 eV (B-F), 192.9 eV (B-O), 190.9 eV (B-N), N 1S region: 402.5 eV ($C=N^+$), 339.0 eV (C=N-C), 398.3 eV (N-B); ^{1}H NMR (400 MHz, Methanol-d_4) δ 7.97 (1H, d, J = 8.0, Ar*H*), 7.33 (1H, s, Ar*H*), 7.13 (1H, d, J = 8.0, Ar*H*), 5.53 (1H, app t, J = 9.0, C*H*(COOB)), 3.89-3.93 (2H, m, CH_2S). ^{13}C NMR (150 MHz, Methanol-d_4) δ 172.8 ((*C*=O)), 171.1 (Ar*C*OH), 159.9 (Ar*C*), 148.3 (Ar*C*), 140.2 (Ar*C*), 138.6 (Ar*C*), 126.7 (Ar*C*H), 119.4 (Ar*C*H), 107.3 (Ar*C*H), 75.9 (*C*H(COOBF_2)), 35.5 (*C*H_2S).

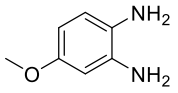

165

4-Methoxybenzene-1,2-diamine (165) [39]

To a suspension of 4-methoxy-2-nitroaniline **(164)** (2.69 g, 16.0 mmol) in MeOH (50 mL) was added 10% Pd/C (270 mg) as a slurry in MeOH at rt. The dark solution was purged with H_2 for 3 times, and then the reaction was stirred at rt for 72 h under H_2. The mixture was filtered through celite, and the filtrate was concentrated *in vacuo*. The crude product was obtained as purple oil and was used without further purification.

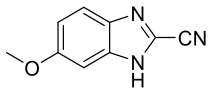

132d

2-Cyano-6-methoxybenzimidazole (132d) [39]

To a solution of 4-methoxybenzene-1,2-diamine (**165**) (4.92 g, 40.0 mmol), and anhydrous pyridine (20 mL) was added Appel's salt (**36**) (8.32 g, 40.0 mmol) at 0 ˚C under N_2, and the mixture was stirred for 24 h. After the volatile materials were removed by reduced-pressure, the sticky crude product was directly filtered by a pad of silica gel gradually eluting with 100% hexane followed by 100% EtOAc. The product was obtained as a brown solid (1.66 g, 60%) (lit. [14] 56%). m.p. 173.5 ˚C; R_f = 0.5 (50% hexane：50% EtOAc); ^{1}H NMR (400 MHz, DMSO-d_4, 393 K) δ 7.63 (1H, d, *J* = 9.0, Ar*H*), 7.13 (1H, s, *J* = 8.0, Ar*H*), 7.02 (d, *J* = 9.0, 1H), 3.83 (3H, s, OCH_3). The data agreed with the literature [39]

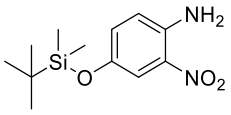

277

4-(*tert*-butyldimethylsilyloxy)-2-nitroaniline (277) [139]

To a solution of 4-amino-3-nitrophenol (**233**) (3.00 g, 19.6 mmol), imidazole (2.66 g, 39.2 mmol), and DMF (20 mL) was added TBDMSCl (4.00 g, 26.5 mmol) at rt, and the solution was stirred for 24 h. The solution was extracted with Et_2O (3 x 20 mL), the organic layers were combined, dried ($MgSO_4$), and filtered. After the volatile materials were removed *in vacuo*, the crude product was used without further purification. The product was obtained as a red solid (5.0 g, 95%). m.p. 100 ºC (Lit. not Reported); R_f = 0.8 (20% hexane：80% EtOAc); ^{1}H NMR (400 MHz, $CDCl_3$) δ 7.56 (1H, d, *J* = 8.0, Ar*H*), 6.97 (1H, d, *J* = 4.0, Ar*H*), 6.71 (1H, dd, *J* = 8.0, 4.0, Ar*H*), 0.98 (9H, s, SiC(CH_3)$_3$), 0.19 (6H, s, OSi(CH_3)$_2$). The data agreed with the literature. [139]

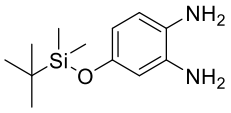

278

4-(*tert*-butyldimethylsilyloxy)benzene-1,2-diamine (278)

To a suspension of 4-(*tert*-butyldimethylsilyloxy)-2-nitroaniline (**277**) (1.75 g, 6.52 mmol) in MeOH (10 mL) was added 10% Pd/C (550 mg) as a slurry in MeOH. The dark solution

was purged with H_2 for 3 times, and then the reaction was stirred at rt for 7 h under H_2. The mixture was filtered through celite, and then the filtrate was concentrated *in vacuo*. The crude product was obtained as a purple oil and was used without further purification.

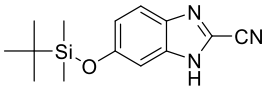

279

6-(*tert*-Butyldimethylsilyloxy)-1H-benzo[d]imidazole-2-carbonitrile (279)

To a solution of diamine **278** (1.55 g, 6.51 mmol), and anhydrous pyridine (20 mL) was added Appel's salt (**36**) (1.22 g, 5.85 mmol) at 0 °C under N_2, and the mixture was stirred for 24 h. After the volatile materials were removed *in vacuo*, the crude product was purified by column chromatography (80% hexane：20% EtOAc) to give **279** (1.66 g, 60%) as a pale-yellow solid. m.p. 178 °C; R_f = 0.6 (80% hexane：20% EtOAc); IR υ_{max} (solution in $CDCl_3$): 2953 (C-H), 2930 (C-H), 2892 (C-H), 2239 (CN), 1626 (C=C) cm^{-1}; ^{1}H NMR (400 MHz, $CDCl_3$) δ 7.59 (1H, d, *J* = 8.0, Ar*H*), 7.05 (1H, s, Ar*H*), 7.02 (1H, d, *J* = 8.0, Ar*H*), 1.03 (9H, s, SiC(C*H*$_3$)$_3$), 0.25 (6H, s, OSi(C*H*$_3$)$_2$). ^{13}C NMR (150 MHz, $CDCl_3$) δ 155.8 (Ar*C*OSi), 125.2 (Ar*C*), 121.7 (Ar*C*N), 112.7 (Ar*C*H). 25.1 (SiC(*C*H$_3$)$_3$), 19.0 (Si(*C*H$_3$)$_2$). HRMS (ESI$^+$) Calcd. for $C_{14}H_{20}N_3OSi$ $[M + H]^+$ 274.1376, found 274.1375.

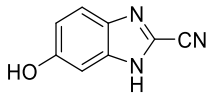

133d

2-Cyano-6-hydroxybenzimidazole (133d) [39]

Method 1：To a solution of compound **132d** (300 mg, 1.73 mmol) and pyridine hydrochloride (2.00 g, 18.0 mmol) was heated to 180 °C for 1 h under N_2. The crude product was directly purified by column chromatography (silica 20% hexane：80% EtOAc). The product was obtained as a yellow solid (8.6 mg, 3%) (lit. [14] 62%). R_f = 0.25 (20% hexane：80% EtOAc); ^{1}H NMR (400 MHz, Methanol-d_4) δ 7.51 (1H, d, *J* = 8.0, Ar*H*), 6.96 (1H, dd, *J* = 8.0, 4.0, Ar*H*), 6.92 (1H, d, *J* = 4.0 Hz, Ar*H*). The data agreed with the literature. [39]

Method 2：To a solution of compound **279** (0.2 g, 0.7 mmol) in THF (10 mL) was added a solution of (1.0 M in THF) TBAF (0.16 mL, 1.4 mmol) at 0 ˚C. The reaction was stirred for 2 h. After the volatile materials were removed *in vacuo*, the crude product was purified by column chromatography (silica 20% hexane：80% EtOAc) to give **133d** (0.13 g, 90%) as a yellow solid. R_f = 0.25 (20% hexane：80% EtOAc); ^{1}H NMR (400 MHz, Methanol-d_4) δ 7.51 (1H, d, *J* = 8.0, Ar*H*), 6.96 (1H, dd, *J* = 8.0, 4.0, Ar*H*), 6.92 (1H, d, *J* = 4.0 Hz, Ar*H*).

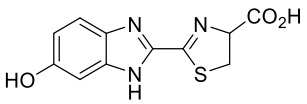

140a

Benzimidazole-based Lucifeirn (140a) [39]

To a solution of compound **133d** (60.0 mg, 0.37 mmol), DL-cysteine hydrochloride monohydrate (70.1 mg, 0.39 mmol), K_2CO_3 (54.0 mg, 0.39 mmol), and MeOH (2 mL and H_2O (1 mL) at rt under N_2. The suspension was stirred for 30 min. The mixture was acidified with 3 M HCl to pH = 3 (pH paper.) The MeOH was removed *in vacuo*, and the remaining solution was extracted with EtOAc for several times until no colour was observed in the aqueous layer. The organic layers were combined, dried ($MgSO_4$), and filtered. After the volatile materials were removed *in vacuo*, the crude product was purified by column chromatography (silica gel 100% EtOAc followed by 1% AcOH：99% EtOAc). The product was obtained as a yellow solid (98 mg, 93%) (lit. [39] 82%). m.p. 203 ˚C (lit. not Reported); ^{1}H NMR (400 MHz, Methanol-d_4) δ 7.48 (1H, d, *J* = 8.9, Ar*H*), 6.94 (1H, d, *J* = 2.3, Ar*H*), 6.85 (1H, dd, *J* = 8.9, 2.3, Ar*H*), 5.27 (1H, app t, *J* = 9.0, C*H*(COOH)), 3.71 (2H, d, *J* = 9.0, CH_2S). The data agreed with the literature. [39]

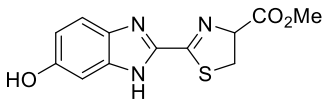

275

Benzimidazole-based luciferin methyl ester 275

To a solution of compound **140a** (0.10 g, 0.38 mmol) in MeOH (2 mL) was added thionyl chloride (0.14 mL, 1.9 mmol) at 0 ˚C. The solution was stirred for 3 h. After the volatile materials were removed *in vacuo*, the crude product was purified by column

chromatography (silica gel 100% EtOAc). Compound **275** was obtained as a yellow solid (0.11g, 99%). m.p. 107.2 °C; R_f = 0.4 (50% hexane：50% EtOAc); IR υ_{max} (solution in MeOH): 3311 (O-H), 2940 (C-H), 2829 (C-H), 1742 (C=O), cm^{-1}; ^{1}H NMR (400 MHz, Methanol-d_4) δ 7.66 (1H, d, *J* = 8.0, Ar*H*), 7.15 (1H, d, *J* = 8.0, Ar*H*), 7.08 (1H, s, Ar*H*), 5.56 (1H, app t, *J* = 8.0, C*H*(COOH)), 3.98 (2H, d, *J* = 9.0, CH_2S), 3.84 (3H, s, COOCH_3). ^{13}C NMR (150 MHz, Methanol-d_4) δ 171.4 (*C*OOCH$_3$), 159.3 (N*C*S), 158.3 (Ar*C*OH), 141.5 (N*C*N), 135.1 (Ar*C*), 128.0 (Ar*C*), 119.4 (Ar*C*H), 116.9 (Ar*C*H), 99.0 (Ar*C*H), 79.6 (N*C*H), 53.4 ((COO*C*H$_3$)), 37.5 (*C*H$_2$); HRMS (ESI$^-$) Calcd. for $C_{12}H_{10}N_3O_3S$ $[M - H]^-$ 276.0443, found 276.0435.

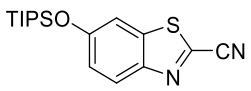

287

6-(triisopropylsilyloxy)benzo[*d*]thiazole-2-carbonitrile (287)

To a solution of 2-cyano-6-hydroxybenzothiazole **(34)** (0.20 g, 1.13 mmol), imidazole (0.12 g, 1.80 mmol), and DMF (20 mL) was added TIPSCl (0.32 mL, 1.46 mmol) at rt, and the solution was stirred for 24 h. The solution was extracted with EtOAc (3 x 20 mL), the organic layers were combined, dried ($MgSO_4$), and filtered. After the volatile materials were removed *in vacuo*, the crude product was purified by column chromatography (silica 80% hexane：20% EtOAc) to give compound **287**. The product was obtained as a brown oil (0.38 g, 99%). R_f = 0.63 (80% hexane：20% EtOAc); IR υ_{max} (solution in $CDCl_3$): 2940 (C-H), 2863 (C-H), 2225 (CN), 1594 (C=C), cm^{-1}; ^{1}H NMR (400 MHz, $CDCl_3$) δ 8.05 (1H, d, *J* = 8.0, Ar*H*), 7.36 (1H, d, *J* = 4.0, Ar*H*), 7.19 (1H, dd, *J* = 8.0, 4.0, Ar*H*), 1.31 (3H, sept, *J* = 8.0, OSiC*H*(CH$_3$)$_2$, 1.12 (18H, d, *J* = 8.0, OSiCH(CH_3)$_2$). ^{13}C NMR (150 MHz, Methanol-d_4) δ 157.3 (Ar*C*), 147.17 (Ar*C*), 137.2 (Ar*C*H), 133.8 (Ar*C*H), 125.9 (Ar*C*), 122.5 (Ar*C*), 113.4 (Ar*C*), 110.8 (Ar*C*H), 18.0 (OSi*C*H), 12.8 (OSiCH(*C*H$_3$)$_2$); HRMS (ESI$^+$) Calcd. for $C_{17}H_{25}N_2OSSi$ $[M + H]^+$ 333.1457, found 333.1443.

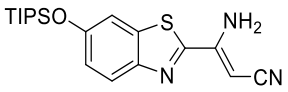

290

(Z)-3-amino-3-(6-(triisopropylsilyloxy)benzo[d]thiazol-2-yl)acrylonitrile (290)

To a solution of compound **287** (0.25 g, 0.75 mmol), in an anhydrous THF (2 mL) was injected acetonitrile anion solution in THF (1 mL, 1.2 M, 1.2 mmol) -78 °C under N_2. The mixture was stirred for 1 h and quenched with water. The mixture was extracted with EtOAc (3 x 20 mL), the organic layers were combined, dried ($MgSO_4$), and filtered. After the volatile materials were removed *in vacuo*, the crude product was purified by column chromatography (silica 80% hexane：20% EtOAc) to give compound **290**. (0.25 g, 83%) as a pale-yellow solid. m.p. 177 °C; R_f = 0.45 (80% hexane：20% EtOAc); IR υ_{max} (solution in $CDCl_3$): 3458.7 (NH_2), 3321 (NH_2), 2939 (C-H), 2930 (C-H), 2887 (C-H), 2194 (CN), 1618 (C=C) cm^{-1}; ^1H NMR (400 MHz, $CDCl_3$) δ 7.87 (1H, d, *J* = 8.0, Ar*H*), 7.31 (1H, d, *J* = 4.0, Ar*H*), 7.08 (1H, dd, *J* = 8.0, 4.0, Ar*H*), 4.68 (1H, s, C=C*H*-CN), 1.30 (3H, sept, *J* = 8.0, OSiC*H*$(CH_3)_2$, 1.12 (18H, d, *J* = 8.0, OSiCH(C*H*$_3)_2$). ^{13}C NMR (150 MHz, $CDCl_3$) δ 158.6 (Ar*C*OSi), 155.8 (*C*NH_2), 152.6 (Ar*C*), 147.7 (Ar*C*), 136.6 (Ar*C*), 124.7 (Ar*C*H), 121.2 (Ar*C*H), 118.3 (Ar*C*N), 111.4 (Ar*C*H), 66.3 (C=*C*-CN), 12.8 (OSiCH(*C*$H_3)_2$); HRMS (ESI^+) Calcd. for $C_{19}H_{28}N_3OSSi$ $[M + H]^+$ 374.1722, found 374.1731.

Preparation of Acetonitrile Anion Solution in THF (1.2 M)

To a solution of acetonitrile (0.07 mL, 1.22 mmol) in an anhydrous THF (1 mL) was injected *n*-BuLi (0.76 mL, 1.6 M) at -78 °C for 1 h. The prepared reagent could be used without purification.

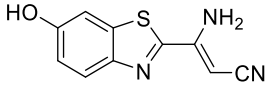

293

(Z)-3-amino-3-(6-hydroxybenzo[d]thiazol-2-yl)acrylonitrile (293)

To a solution of compound **290** (0.20 g, 0.70 mmol), and anhydrous pyridine (20 mL) was added TBAF (2.5 mL, 1M, 2.10 mmol) at 0 °C, and the reaction was stirred for 2 h. After the volatile materials were removed *in vacuo*, the crude product was purified by column chromatography (silica 50% hexane：50% EtOAc) to give **293** (0.15 g, 95%) as a pale-yellow solid. m.p. 169 °C (dec.); R_f = 0.2 (80% hexane：20% EtOAc); IR υ_{max} (solution in MeOH): 3448.9 (NH_2), 3369.9 (OH), 2202.7 (CN), 1635.2 (C=C), 1592.9 (N-H) cm^{-1}; ^1H NMR (400 MHz, Methanol-d_4) δ 7.87 (1H, d, *J* = 8.0, Ar*H*), 7.31 (1H, s, Ar*H*), 7.05 (1H, d, *J* = 8.0, Ar*H*), 4.71 (1H, s, C=C*H*-CN). ^{13}C NMR (150 MHz, Methanol-d_4) δ 159.7

(Ar*C*OH), 158.6 (*C*NH$_2$), 155.0 (Ar*C*), 148.0 (Ar*C*), 138.2 (Ar*C*), 125.6 (Ar*C*H) 119.6 (Ar*C*N), 118.0 (Ar*C*H), 107.3 (Ar*C*H), 63.8 (C=*C*-CN), 18.0 (OSi*C*H(*C*H$_3$)$_2$), 12.8 (OSiCH(*C*H$_3$)$_2$); HRMS (ESI$^+$) Calcd. for $C_{10}H_8N_3OS$ [M + H] $^+$ 218.0413, found 218.0388.

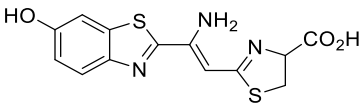

298
H$_2$N-EIL

H$_2$N-Enamine Linked Infra-Luciferin (H$_2$N-EIL) 298

To a solution of compound **293** (10.0 mg, 0.05 mmol), DL-cysteine (6.0 mg, 0.05 mmol), and anhydrous K_2CO_3 (6.2 mg, 0.05mmol) in anhydrous MeOH (1 mL) under N_2, and the mixture was stirred for 24 h at 80 °C. After the volatile materials were removed *in vacuo*, the crude product was purified by reversed phase C18 HPLC with gradient eluent (5% Methanol：95% H_2O followed by 95% Methanol：5% H_2O) to give **H$_2$N-EIL** (0.90 g, 6%) as a pale yellow solid. m.p. 141.6 °C (dec.); IR υ_{max} (solution in $CDCl_3$): 3413 (COOH), 2953 (C-H), 2863 (C-H), 1618 (C=O, C=N, C=C) cm^{-1}; ^{1}H NMR (400 MHz, Methanol-d_4) δ 7.79 (1H, d, *J* = 8.0, Ar*H*), 7.25 (1H, s, Ar*H*), 6.97 (1H, d, *J* = 8.0, Ar*H*), 5.45 (1H, s, NH$_2$-C=C*H*), 4.98 (1H, app t, *J* = 8.0, C*H*(COOH)), 3.44 (2H, dd, *J* = 8.0, 4.0, C*H*$_2$S). ^{13}C NMR (150 MHz, Methanol-d_4) δ 179.4 (*C*OOH), 166.8 (C=CH-N*C*S), 161.9 (N*C*S), 159.1 (Ar*C*OH), 147.7 (Ar*C*), 146.2 (NH$_2$-*C*=CH), 137.7 (Ar*C*), 124.8 (Ar*C*H). 117.9 (Ar*C*H), 107.4 (Ar*C*H), 91.1 (NH$_2$-C=*C*H), 83.5 (*C*HCOOH), 36.5 (*C*H$_2$); HRMS (ESI$^+$) Calcd. for $C_{13}H_{12}N_3O3S$ [M + H] $^+$ 322.0333, found 322.0320.

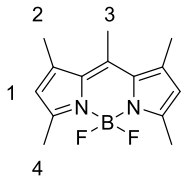

283

BODIPY 283

To a solution of 2,4-dimethylpyrrole (0.50 mL, 4.80 mmol) in anhydrous DCM (20 mL) was added acetyl chloride (0.69 g, 9.60 mmol) dropwise at rt under N_2, and the mixture was stirred for 1 h, and then heated to reflux for an additional 30 min. The solution was treated with TEA (2.0 mL, 14.4 mmol) and stirred for 15 min followed by $BF_3{\cdot}OEt_2$ (2.3 mL, 20.0

mmol) and then stirred overnight. After the volatiles were removed *in vacuo*, the crude product was purified by column chromatography (silica 50% hexane：50% EtOAc) to give BODIPY **283** (0.43 g, 69%) (lit.[82a] yield 42%) as an orange solid. m.p. 183 ˚C (dec.) (lit. not reported); R_f = 0.8 (50% hexane：50% EtOAc); ^{1}H NMR (600 MHz, $CDCl_3$) δ 6.06 (2H, s, H_1), 2.59 (3H, s, H_3), 2.52 (6H, s, H_4), 2.42 (6H, s, H_2). The data agreed with the literature.[82a]

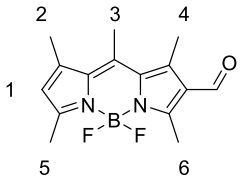

306

BODIPY 306

To a solution of BODIPY **283** (0.10 g, 0.38 mmol) in anhydrous DCM (25 mL) was added anhydrous DMF (0.9 mL, 11.5 mmol) and $POCl_3$ (3.50 g, 38.0 mmol) dropwise at 0 ˚C under N_2. This solution was stirred for 5 h, and then heated to reflux for an additional 30 min. The solution was quenched with $K_2CO_{3(aq)}$ at 0 ºC until effervescence ceased. The solution was extracted several times, first with DCM and then Et_2O until no colour in the aqueous layer. The organic layers were combined, dried ($MgSO_4$), and filtered. After the volatile materials were removed *in vacuo*, the crude product was purified by column chromatography (silica 50% hexane：50% EtOAc) to give BODIPY **306** (0.07 g, 67%) (lit.[82b] yield 89%) as an orange solid. m.p.190 ˚C (lit. not reported); R_f = 0.55 (50% hexane：50% EtOAc); ^{1}H NMR (600 MHz, $CDCl_3$) δ 10.09 (1H, s, C*H*O), 6.23 (1H, s, H_1), 2.77 (3H, s, H_3), 2.72 (3H, s, H_6), 2.67 (3H, s, H_5), 2.57 (3H, s, H_4), 2.46 (s, 3H_2). The data agreed with the literature.[82b]

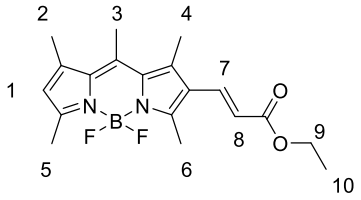

314a

BODIPY 314a

A solution of BODIPY **306** (50.0 mg, 0.17 mmol), and (carbethoxymethylene)triphenylphosphine (0.18 mg, 0.51 mmol) in DCM (2 mL) was stirred overnight at rt. After the volatiles were removed *in vacuo*, the crude product was purified by column chromatography (silica 75% hexane：25% EtOAc) to give BODIPY **314a** (48.0 mg, 78%) (lit. [111] 50%) as an orange solid. m.p. 195 °C (lit. not reported); R_f = 0.4 (25% hexane：75% EtOAc); ^{1}H NMR (400 MHz, $CDCl_3$) δ 7.69 (1H, d, *J* = 16.2, H_7), 6.13 (1H, s, H_1), 6.08 (1H, d, *J* = 16.2, H_8), 4.26 (2H, q, *J* = 7.1, H_9), 2.65 (3H, s, H_3), 2.62 (3H, s, H_6), 2.54 (3H, s, H_5), 2.48 (3H, s, H_4), 2.42 (3H, s, H_2), 1.34 (3H, t, *J* = 7.1, H_{10}). The data agreed with the literature. [111]

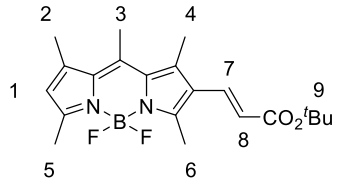

314b

BODIPY 314b

The BODIPY **306** (0.10 g, 0.35 mmol) and was subjected to the Wittig reactions as for the preparation of BODIPY **314a** with (*tert*-butoxycarbonylmethylene)triphenylphosphine (0.29 mg, 0.70 mmol). The desire product **314b** was obtained as an orange solid (0.08 g, 58%). m.p. 190 °C; R_f = 0.6 (50% hexane：50% EtOAc); IR υ_{max} (solution in $CDCl_3$): 2975 (C-H), 2929 (C-H), 1697 (C=O), 1625 (C=C) cm^{-1}; ^{1}H NMR (600 MHz, $CDCl_3$) δ 7.62 (1H, d, *J* = 16.2, H_7), 6.14 (1H, s , H_1), 6.03 (1H, d, *J* = 16.2, H_8), 2.66 (6H, app s, H_3 and H_6), 2.55 (3H, s, H_5), 2.50 (3H, s, H_4), 2.45 (3H, s, H_2), 1.54 (9H, s, H_9). ^{13}C NMR (150 MHz, $CDCl_3$) δ 167.1 (*C*OO^{t}Bu), 156.4 (BODIPY-*C*), 152.8 (BODIPY-*C*), 143.0 (BODIPY-*C*), 142.2 (BODIPY-*C*), 138.2 (BODIPY-*C*), 135.0 (C_7), 133.4 (BODIPY-*C*), 131.7 (BODIPY-*C*), 125.0 (BODIPY-*C*), 122.7 (C_1), 120.0 (C_8), 80.5 (O*C*$(CH_3)_3$), 28.4 (C_9), 17.8 (C_4), 17.2 (C_3), 15.1(C_2), 14.8 (C_5), 14.7 (C_6). HRMS (ESI^+) Calcd. for $C_{21}H_{28}BF_2N_2O_2$ $[M + H]^+$ 387.2164, found 387.2165.

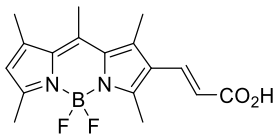

313

A solution of BODIPY **314b** (0.08 g, 0.2 mmol) and TFA (0.1 mL) in DCM (1 mL) was stirred overnight at rt. After the volatiles were removed *in vacuo*, the product **313** was obtained and used without column purification.

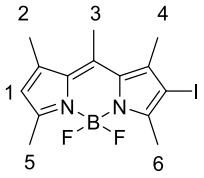

318

BODIPY 318

To a solution of BODIPY **283** (0.10 g, 0.38 mmol) in DCM (25 mL) was added a solution of NIS (0.09g, 0.38 mmol) in DCM (20 mL), and the reaction was stirred overnight protected from light. After the volatiles were removed under reduced pressure. The product **318** was obtained as a reddish solid with quantitative yield (lit.[116] yield 77%) and it could be used without further purification. m.p. 186 °C (lit. not reported); R_f = 0.8 (50% hexane：50% EtOAc); ^{1}H NMR (400 MHz, $CDCl_3$) δ = 6.10 (1H, s, H_1), 2.57 (3H, s , H_6), 2.56 (3H, s, H_3), 2.51 (3H, s , H_5), 2.41 (s, 3H, H_4), 2.40 (3H, s, H_2). The data agreed with the literature. [116]

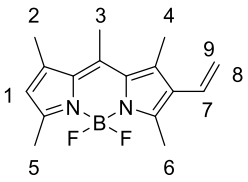

317

BODIPY 317

A solution of **BODIPY 318** (0.09 g, 0.23 mmol), $Pd(PPh_3)_4$ (0.08 mg, 5 mol%), tert-butyl(vinyl)tin (0.14 mg, 0.46 mmol) in toluene (5 mL) was heated to reflux for 5 h. After cooling, the reaction was quenched with sat. aq. $KF_{(aq)}$, extracted with DCM (3 X 10 mL), dried ($MgSO_4$), and purified by chromatography (silica 25% hexane：75% EtOAc) to give BODIPY **317** as a reddish solid (0.04g, 63%). m.p. 165 °C; R_f = 0.6 (25% hexane：75% EtOAc); IR υ_{max} (solution in $CDCl_3$): 3092 (C=C-H), 3009 (C=C-H), 2959 (C-H), 2920 (C-

H), 2867(C-H), 1625 (C=C)cm^{-1}; ^{1}H NMR (700 MHz, $CDCl_3$) δ 6.55 (1H, dd, *J* = 17.8, 11.6, H_7), 6.06 (1H, s, H_1), 5.39 (1H, d, *J* = 11.5 Hz, H_8), 5.32 (1H, dd, *J* = 17.8, 2.0 Hz, H_9), 2.62 (3H, s, H_3), 2.59 (3H, s, H_6), 2.52 (3H, s, H_5), 2.42 (3H, s, H_4), (3H, s, H_2). ^{13}C NMR (175 MHz, $CDCl_3$) δ 141.5 (BODIPY-*C*), 141.2 (BODIPY-*C*), 137.0 (BODIPY-*C*), 131.9 (BODIPY-*C*), 129.1 (BODIPY-*C*), 128.1 (C7), 121.6 (C_1), 117.6 (C8), 17.6 (C4), 17.0 (C3), 15.2 (C2), 14.6 (C5), 13.7 (C6). HRMS (ESI^+) Calcd. for $C_{16}H_{20}BF_2N_2$ $[M + H]^+$ 288.1718, found 288.1724.

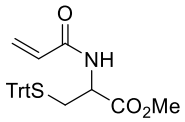

316

DL-cysteine-N-acryl-S-(triphenylmethyl)methyl ester 316

To a solution of DL-cysteine (0.10 g, 0.83 mmol) in MeOH (5 mL) was added $SOCl_2$ (0.60 mL, 8.30 mmol) and then this solution was heated to reflux overnight. After cooling to rt, the volatiles were removed *in-vacco*. To the resulting mixture was added TrtOH (0.24 g, 0.91 mmol) in TFA (5 mL). The solution went orange and was stirred at rt for 2 h and then the TFA was removed *in-vacuo* to form methyl S-tritylcysteinate which was used without any purification. A solution of methyl S-tritylcysteinate (0.30 g, 0.83 mmol), triethylamine (0.23 mL, 1.66 mmol), and excess acryloyl chloride in anhydrous DCM (5 mL) was stirred overnight at rt. After the volatiles were removed *in-vacco*, the crude compound was purified directly by column chromatography (silica 75% hexane：25% EtOAc) to give the desired product (0.35 g, 95% over 3 steps) (lit. [114] yield 90%) as a milky oil. R_f = 0.4 (75% hexane：25% EtOAc); ^{1}H NMR (700 MHz, Methanol-d_4) δ 7.38 – 7.36 (6H, m, S-*Trt*), 7.30 – 7.27 (6H, m, S-*Trt*), 7.25 – 7.20 (3H, m, S-*Trt*), 6.29 (1H , dd, *J* = 17.1, 10.1, C*H*=CH_2), 6.22 (1H, dd, *J* = 17.1, 1.8, CH=CH_2), 5.69 (1H, dd, *J* = 10.1, 1.8, CH=CH_2), 4.57 (1H, s, N*H*), 4.29 (1H, dd, *J* = 8.3, 5.2, C*H*(COOMe)), 3.63 (3H, s, O*Me*), 2.65 (1H, dd, *J* = 12.8, 8.3, SCH_2), 2.58 (1H, dd, *J* = 12.8, 5.2, SCH_2). The data agreed with the literature. [114]

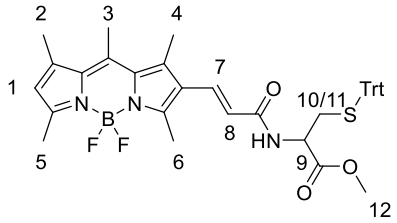

315

BODIPY 315

To a solution of BODIPY **317** (5.0 mg, 0.017 mmol), cysteine ester **316** (11.2 mg, 0.026 mmol) and Hoveyda-Grubbs II (20 mol%) in DCM (1 mL) was heated to reflux for 4 hours. After cooling to rt, the crude mixture was directly purified by column chromatography (silica 70% hexane：30% EtOAc) to give BODIPY **315** as a red solid (9.3mg, 82%). mp. 163 °C; R_f = 0.4 (70% hexane：30% EtOAc); IR υ_{max} (solution in DCM): 3268 (N-H), 3052 (C-H), 3026 (C-H), 2949 (C-H), 2921 (C-H), 2849 (C-H), 1742 (C=O), 1654 (C=C), 1616 (C=C) cm^{-1}; ^{1}H NMR (700 MHz, $CDCl_3$) δ 7.65 (1H, d, *J* = 15.8, H_7), 7.40 (6H, dd, *J* = 7.0, 1.2, Trt-*H*), 7.28 (6H, t, *J* = 7.0, Trt-*H*), 7.22 (3H, t, *J* = 7.0, Trt-*H*), 6.14 (1H, s, H_1), 6.02 (1H, d, *J* = 15.8, H_8), 6.01 (1H, d, *J* = 7.7, N*H*), 4.83 – 4.72 (1H, m, H_9), 3.74 (3H, s, H_{12}), 2.74 (1H, d, *J* = 12.5, H_{10}), 2.74 (1H, d, *J* = 5.2, H_{11}), 2.67 (3H, s, H_3), 2.65 (3H, s, H_6), 2.55 (3H, s, H_5), 2.49 (3H, s, H_4), 2.44 (3H, s, H_2).; ^{13}C NMR (175 MHz, $CDCl_3$) δ 171.2 (*C*OOMe), 165.9 (*C*ONH), 156.5 (BODIPY-*C*), 152.7 (BODIPY-*C*), 144.5 (Trt-*C*), 143.1 (BODIPY-*C*), 143.3 (BODIPY-*C*), 138.3 ((BODIPY-*C*), 133.6 (C_7), 131.7 (BODIPY-*C*), 129.7 (Trt-*C*-H), 128.2 (Trt-*C*-H), 127.1 (Trt-*C*-H), 125.1 (BODIPY-*C*), 122.8 (C_1), 119.6 (C_8), 67.1 (Trt-*C*-S), 52.8 (C_{12}), 51.5 (C_9), 34.1 (C_{10}), 17.8 (C_4), 17.3 (C_3), 15.2 (C_2), 14.8 (C_5), 14.3 (C_6).

Note: The HRMS for this compound could not be determined.

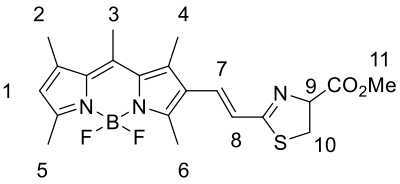

304

BODIPY Luciferin Methyl Ester

BODIPY Luciferin Methyl Ester 304

A solution of Ph_3PO (36.1 mg, 0.13 mmol) in anhydrous DCM (0.5 mL) was cooled to 0 °C and treated with a drop of Tf_2O (14 μL, 0.08 mmol). The resultant solution was stirred at 0 °C for 30 min and a solution of BODIPY **315** (20.0 mg, 0.03 mmol) in anhydrous DCM

(0.5 mL) was then injected dropwise. The reaction was stirred at 0 °C for 10 min and then quenched with water. The mixture was extracted with DCM (3 X 10 mL), dried ($MgSO_4$), and purified by column chromatography (silica 50% hexane：50% EtOAc) to provide BODIPY luciferin methyl ester **304** as isolated as a reddish solid (10,1 mg, 78%). mp. 182 °C (dec.); R_f = 0.25 (50% hexane：50% EtOAc); IR υ_{max} (solution in $CDCl_3$): 2954 (C-H), 2920 (C-H), 2851 (C-H), 1740 (C=O), 1626 (C=C) cm^{-1}; 1H NMR (700 MHz, $CDCl_3$) δ 7.09 (1H, d, *J* = 16.4 Hz, H_7), 6.75 (1H, d, *J* = 16.4 Hz, H_8), 6.13 (1H, s, H_1), 5.20 (1H, dt, *J* = 9.2 Hz, H_9), 3.84 (3H, s, H_{11}), 3.60 – 3.53 (2H, m, H_{10}), 2.64 (6H, s, H_3 and H_6), 2.54 (s, 3H, H_5), 2.48 (3H, s, H_4), 2.44 (3H, s, H_2). ^{13}C NMR (175 MHz, $CDCl_3$) δ 171.4 (*C*OOMe), 170.7 (N*C*S), 156.6 (BODIPY-*C*), 152.4 (BODIPY-*C*), 143.1 (BODIPY-*C*), 142.2 (BODIPY-*C*), 137.3 (BODIPY-*C*), 134.1 (C_7), 133.5 (BODIPY-*C*), 133.1 (BODIPY-*C*), 125.4 (BODIPY-*C*), 123.1 (C_8), 122.8 (C_1), 78.1 (C_9), 53.0 (C_{11}), 34.5 (C_{10}), 17.8 (C_4), 17.3 (C_3), 15.3 (C_2), 14.8 (C_5), 14.0 (C_6). Calcd. for $C_{21}H_{24}BF_2N_3O_2S$ $[M + H]^+$ 432.1729, found 432.1727.

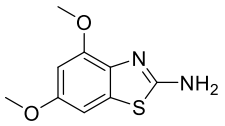

331

4,6-dimethoxybenzo[*d*]thiazol-2-amine (**331**)

To a solution of KSCN (3.55 g, 36.6 mmol) in AcOH (50 mL) at 10 °C was added dropwise bromine (1.25 mL, 24.40 mmol). The solution turned an orange colour and was left to stir at 10 °C for 30 min. This suspension was then added to a solution of 2,4-dimethoxyaniline (3.55 g, 23.18 mmol) in AcOH (50 mL) at 10 °C. The resultant solution was stirred at rt overnight. After cooling to 0 °C, the black and sticky mixture was neutralized by saturated $NaOH_{(aq)}$ to pH = 14. The black precipitate formed, and it was collected as a dark purple solid (1.85 g, 38%). mp. 143 °C (lit. not reported); R_f = 0.4 (98% DCM：2% MeOH). ^1H NMR (600 MHz, $CDCl_3$) δ 6.68 (1 H, d, J = 2.1, Ar*H*), 6.44 (1 H, d, *J* = 2.1, Ar*H*), 3.91 (3 H, s, O*Me*), 3.80 (3 H, s, O*Me*). The data agreed with the literature. [126]

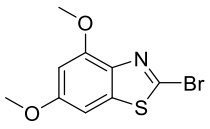

330

2-bromo-4,6-dimethoxybenzo[*d*]thiazole (**330**)

A solution of 4,6-dimethoxybenzo[*d*]thiazol-2-amine (**331**) (0.10 g, 0.48 mmol), CuBr (0.10 g, 0.72 mmol), and isopentyl nitrile (0.13 mL, 0.96 mmol) in MeCN (5 mL) was heated to reflux under N_2 for 5 h. After cooling to rt, the crude product was purified by column chromatography (silica 70% hexane：30% EtOAc) to give the desired product **330** (0.02 mg, 17%) as a white solid. mp. 84 ^{o}C; R_f = 0.5 (70% hexane：30% EtOAc); IR υ_{max} (solution in $CDCl_3$): 3002 (C-H), 2958 (C-H), 2937 (C-H), 2849 (C-H), 2832 (C-H) cm^{-1}. ^{1}H NMR (700 MHz, $CDCl_3$) δ 6.81 (d, J = 2.2 Hz, 1H), 6.51 (d, J = 2.2 Hz, 1H), 3.99 (s, 3H), 3.85 (s, 3H). ^{13}C NMR (175 MHz, $CDCl_3$) δ 159.5 (Ar*C*), 153.3 (Ar*C*), 139.8 (Ar*C*), 137.6 (Ar*C*), 133.7 (Ar*C*), 98.2 (Ar*C*H), 94.7 (Ar*C*H), 56.2 (ArO*C*H$_3$), 56.0 (ArO*C*H$_3$). HRMS (ESI$^+$) Calcd. for $C_9H_9BrNO_2S$ [M + H]$^+$ 273.9537, found 273.9532.

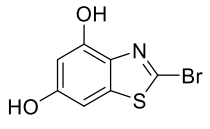

335

2-bromobenzo[*d*]thiazole-4,6-diol (**335**)

A solution of 2-bromo-4,6-dimethoxybenzo[d]thiazole (**330**) (0.20 g, 0.73 mmol) in anhydrous DCM (1 mL) was injected a solution of BBr_3 (1M) in DCM (2.2 mL, 2.2 mmol) and stirred for 5 h. This reaction was quenched with MeOH at 0 ˚C. After the volatiles were removed, the crude product was directly purified by column chromatography (silica 50% hexane：50% EtOAc) to give desired product **335** (0.17 g, 93%) as a white solid. mp. 186 ˚C; R_f = 0.5 (50% hexane：50% EtOAc); IR υ_{max} (solid): 3224 (O-H), 2957 (C-H), 2925 (C-H), 2854 (C-H) cm^{-1}. ^{1}H NMR (700 MHz, Methanol-d_4) δ 6.72 (s, 1H, Ar*H*), 6.42 (s, 1H, Ar*H*), 4.59 (s, 2H, O*H*). ^{13}C NMR (175 MHz, Methanol-d_4) δ 158.7 (Ar*C*), 152.2 (Ar*C*), 140.6 (Ar*C*), 136.9 (Ar*C*), 132.9 (Ar*C*), 102.2 (Ar*C*), 98.13 (Ar*C*). HRMS (ESI$^+$) Calcd. for $C_9H_{10}BrNO_2S$ [M + H]$^+$ 245.9219, found 245.9211.

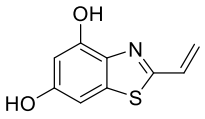

336

2-vinylbenzo[*d*]thiazole-4,6-diol (**336**)

A solution of 2-bromobenzo[*d*]thiazole-4,6-diol (**335**) (0.05 g, 0.18 mmol), $Pd(PPh_3)_4$ (0.01g, 20 mol%) and tert-butyl(vinyl)tin (0.12 g, 0.36 mmol) in anhydrous 1,4-dioxane (1 mL) was heated to 110 °C overnight under N_2. After the reaction was cooled down to rt, the mixture was directly purified by column chromatography (silica 50% hexane：50% EtOAc). The desired product **336** was obtained as a yellow oil (0.02 g, 50%). R_f = 0.5 (50% hexane：50% EtOAc); IR υ_{max} (solution in $CDCl_3$): 2953 (C-H), 2848 (C-H), 2229(CN) cm^{-1}. ^1H NMR (700 MHz, Methanol-d_4) δ 6.98 (1H, dd, *J* = 17.5, 10.9, C*H*=HCH), 6.73 (1H, d, *J* = 2.2, Ar*H*), 6.41 (1H, d, *J* = 2.2, Ar*H*), 6.02 (1H, d, *J* = 17.5, CH=*H*CH), 5.67 (1H, d, *J* = 10.9, CH=HC*H*). ^{13}C NMR (176 MHz, MeOD) δ 163.1 (Ar*C*), 158.7 (Ar*C*), 153.0 (Ar*C*), 138.1(Ar*C*), 137.6 (Ar*C*), 132.2 (*C*H=HCH), 121.7 (CH=H*C*H), 101.9 (Ar*C*H), 98.4 (Ar*C*H). HRMS (ESI^+) Calcd. for $C_9H_8NO_2S$ $[M + H]^+$ 194.0270, found 194.0267.

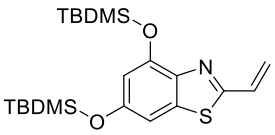

337

4,6-bis((*tert*-butyldimethylsilyl)oxy)-2-vinylbenzo[d]thiazole (**337**)

A solution of 2-vinylbenzo[*d*]thiazole-4,6-diol (**336**) (28.0 mg, 0.15 mmol), TBDMSCl (88.0 mg, 0.6 mmol), imidazole (50.0 mg, 0.75 mmol), and DMAP (1.0 mg, 5 mol%) in DMF (0.5 mL) was stirred at rt overnight. The crude compound was directly purified by column chromatography (silica 90% hexane：10% EtOAc) to give the desired product as a yellow oil (0.08 g, 61%). R_f = 0.8 (90% hexane：10% EtOAc); IR υ_{max} (solution in $CDCl_3$): 2955 (C-H), 2927 (C-H), 2895 (C-H), 28565 (C-H), 1683 (C=C) cm^{-1}. ^1H NMR (700 MHz, $CDCl_3$) δ 6.96 (1H, dd, *J* = 17.5, 10.8 Hz, C*H*=HCH), 6.88 (1H, d, *J* = 2.2 Hz, Ar*H*), 6.45 (1H, d, *J* = 2.2 Hz, Ar*H*), 6.03 (1H, d, *J* = 17.5 Hz, CH=*H*CH), 5.62 (1H, d, *J* = 10.9 Hz, CH=HC*H*), 1.05 (9H, s, C(CH_3)$_3$), 1.00 (9H, s, C(CH_3)$_3$), 0.26 (6H, s, Si(CH_3)$_2$), 0.22 (6H, s, Si(CH_3)$_2$). ^{13}C NMR (175 MHz, $CDCl_3$) δ 162.6 (N*C*S), 154.9 (Ar*C*), 150.4 (Ar*C*), 142.4 (Ar*C*), 136.8 (Ar*C*), 131.9 (*C*H=HCH), 121.3 (CH=H*C*H), 110.9 (Ar*C*H),

105.1 (Ar*C*H), 25.9 (C(*C*H$_3$)$_3$), 25.8 (C(*C*H$_3$)$_3$), 18.7 (*C*(CH$_3$)$_3$), 18.4 (*C*(CH$_3$)$_3$), -4.1 (Si(*C*H$_3$)$_2$), -4.3 (Si(*C*H$_3$)$_2$). HRMS (ESI$^+$) Calcd. for $C_{21}H_{36}NO_2SSi_2$ [M + H]$^+$ 422.2000, found 422.2008.

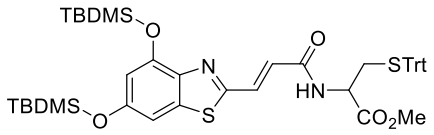

338

Methyl (*E*)-N-(3-(4,6-bis((*tert*-butyldimethylsilyl)oxy)benzo[*d*]thiazol-2-yl)acryloyl)-S-tritylcysteinate (**338**)

The vinyl benzothiazole **337** (35.0 mg, 0.08 mmol) was subjected to olefin metathesis as for the preparation of BODIPY **315**. The desire product was obtained as a brown oil after purification by column chromatography (silica 90% hexane : 10% EtOAc) (24.0 mg contained reaction impurities and was ~30% yield by ^{1}H NMR). ^{1}H NMR (400 MHz, $CDCl_3$) δ 7.73 (1H, d, *J* = 15.5 Hz, ArC*H*=CH), 7.20 – 7.43 (15H, m, Trt-*H*), 6.92 (1H, d, *J* = 2.2 Hz, Ar*H*), 6.54 (1H, d, *J* = 15.5 Hz, ArCH=C*H*), 6.49 (1H, d, *J* = 2.2 Hz, Ar*H*), 4.81 – 4.72 (1H, m, C*H*CO$_2$Me), 3.75 (3H, s, OMe), 2.84 (1H, dd, *J* = 12.7, 5.6 Hz, C*H*$_2$-STrt), 2.72 (1H, dd, *J* = 12.6, 4.5 Hz, C*H*$_2$-STrt), 1.06 (9H, s, C(C*H*$_3$)$_3$), 1.01 (9H, s, C(C*H*$_3$)$_3$), 0.28 (6H, s, Si(C*H*$_3$)$_2$), 0.24 (6H, s, Si(C*H*$_3$)$_2$).

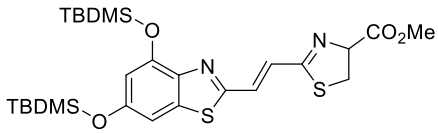

339

Methyl (*E*)-2-(2-(4,6-bis((*tert*-butyldimethylsilyl)oxy)benzo[*d*]thiazol-2-yl)vinyl)-4,5-dihydrothiazole-4-carboxylate (**339**)

Impure compound **338** (30.0 mg, 0.04 mmol) was subjected to ring cyclisation as for the preparation of **BODIPY 304**. After purification by column chromatography (silica 90% hexane : 10% EtOAc), the desired product **339** was obtained as a brown oil (22.6 mg contained reaction impurities and was ~50% yield by ^{1}H NMR). ^{1}H NMR (400 MHz, $CDCl_3$) δ 7.31 (1H, d, *J* = 14.3 Hz, ArC*H*=CH), 7.27 (1H, d, *J* = 14.3 Hz, ArCH=C*H*), 6.89 (1H, d, *J* = 2.2 Hz, Ar*H*), 6.46 (1H, d, *J* = 2.2 Hz, Ar*H*), 5.24 (1H, dt, *J* = 9.2 Hz, C*H*COOMe), 3.86 (3H, s, OMe), 3.72 – 3.61 (2H, m, SC*H*$_2$), 1.05 (9H, s, C(C*H*$_3$)$_3$), 0.99

(9H, s, C(CH_3)$_3$), 0.27 (6H, s, Si(CH_3)$_2$), 0.22 (6H, s, Si(CH_3)$_2$). HRMS (ESI$^+$) Calcd. for $C_{26}H_{41}N_2O_4S_2Si_2$ [M + H]$^+$ 565.2047, found 565.2022.

Note: The desired compound was isolated as a brown oil and the crude yield could not be calculated accurately because impurities presented.

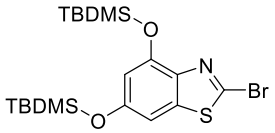

343

2-bromo-4,6-bis((*tert*-butyldimethylsilyl)oxy)benzo[*d*]thiazole (**343**)

A solution of 2-bromobenzo[*d*]thiazole-4,6-diol (**335**) (0.06 g, 0.24 mmol), DMAP (0.003 g, 10 mol%), imidazole (0.08 g, 1.2 mmol), and TBDMSCl (0.150 g, 0.96 mmol) in DMF (1 mL) was stirred overnight. The mixture was extracted with Et_2O (3 X 10 mL), dried ($MgSO_4$), and purified by column chromatography (silica 90% hexane：10% EtOAc) to give the desired product as a yellow oil (0.10 g, 92%). R_f = 0.8 (90% hexane：10% EtOAc); IR υ_{max} (solution in $CDCl_3$): 2953 (C-H), 2928 (C-H), 2895 (C-H), 2856 (C-H) cm^{-1}. ^{1}H NMR (700 MHz, Chloroform-*d*) δ 6.82 (1H, d, *J* = 2.2 Hz, Ar*H*), 6.44 (1H, d, *J* = 2.2 Hz, Ar*H*), 1.04 (9H, s, *t*Bu*H*), 0.99 (9H, s, *t*Bu*H*), 0.25 (6H, s, SiCH_3), 0.21 (6H, s, SiCH_3). ^{13}C NMR (175 MHz, Chloroform-*d*) δ 155.0 (*C*-Br), 149.7 (Ar*C*), 139.6 (Ar*C*), 133.1 (Ar*C*), 111.1 (Ar*C*H), 104.4 (Ar*C*H), 25.9, (*C*(CH$_3$)$_3$), 25.8 (*C*(CH$_3$)$_3$), 18. 7 (C(*C*H$_3$)$_3$), 18.4 (C(*C*H$_3$)$_3$), -4.2 (Si*C*H$_3$), -4.3 (Si*C*H$_3$). HRMS (ESI$^+$) Calcd. for $C_{19}H_{33}BrNO_2SSi_2$ [M + H]$^+$ 474.0594, found 474.0958.

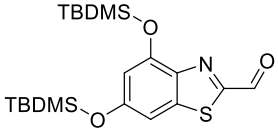

344

4,6-bis((*tert*-butyldimethylsilyl)oxy)benzo[*d*]thiazole-2-carbaldehyde (**344**)

To a solution of 2-bromo-4,6-bis((*tert*-butyldimethylsilyl)oxy)benzo[*d*]thiazole (**343**) (0.35 g, 0.70 mmol) in anhydrous THF (4 mL) was injected 1.6 M *n*-BuLi (0.48 mL, 0.77 mmol) dropwise at -78 °C under N_2. After 30 min, anhydrous DMF (0.1 mL) was added dropwise and stirred for an additional 2 h at -78 °C. The reaction was then quenched with $NH_4Cl_{(aq)}$ and extracted with Et_2O for several times, dried ($MgSO_4$), and purified by column chromatography (silica 75% Hexane：25% DCM) to give the desired compound (0.19 g,

65%) as a yellow brown oil. R_f = 0.5 (75% Hexane : 25% DCM); IR υ_{max} (solution in $CDCl_3$): 2951 (C-H), 2926 (C-H), 2893 (C-H), 2854 (C-H), 1752 (C=O) cm^{-1}. ^1H NMR (700 MHz, $CDCl_3$) δ 10.05 (1H, s, C*H*O), 6.97 (1H, s, Ar*H*), 6.54 (1H, s, Ar*H*), 1.07 (9H, s, SiC(CH_3)$_3$), 1.00 (9H , s, SiC(CH_3)$_3$), 0.29 (6H, s, Si(CH_3)$_2$), 0.25 (6H, s, Si(CH_3)$_2$). ^{13}C NMR (175 MHz, $CDCl_3$) δ 185.5 (*C*HO), 161 (S*C*N), 158.0 (Ar*C*), 152.9 (Ar*C*), 143.0 (Ar*C*), 139.5 (Ar*C*), 111.8 (Ar*C*H), 105.3 (Ar*C*H), 25.8 (SiC(*C*H_3)$_3$), 25.7 (SiC(*C*H_3)$_3$), 18.1 (Si*C*(CH$_3$)$_3$), 18.4 (Si*C*(CH$_3$)$_3$), -4.1 (Si(*C*H_3)$_2$), -4.2 Si(*C*H_3)$_2$. HRMS (ESI^+) Calcd. for $C_{20}H_{34}NO_3SSi_2$ $[M + H]^+$ 424.1798, found 424.1777.

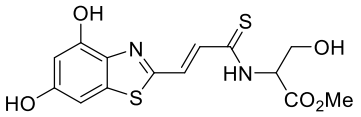

345

Methyl (*E*)-(3-(4,6-dihydroxybenzo[*d*]thiazol-2-yl)prop-2-enethioyl)serinate (**345**)

To a solution of phosphonate **227** (70.0 mg, 0.22 mmol) in MeCN (0.5 mL) was added LiCl (10.0 mg, 0.22 mmol) and DBU (30.0 µL, 0.22 mmol) and then stirred at rt for 15 min. After the solution turned clear, a solution of aldehyde **344** (85.0 mg, 0.20 mmol) in MeCN (0.5 mL) was added dropwise and stirred for additional 2.5 h. The reaction was purified by column chromatography (silica 90% EtOAc : 10% MeOH) to give a mixture of product **345** with some impurities as a brown oil. This crude mixture was used for next step.

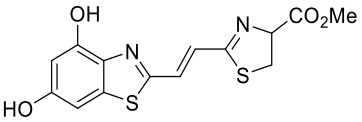

321

Methyl (*E*)-2-(2-(4,6-dihydroxybenzo[*d*]thiazol-2-yl)vinyl)-4,5-dihydrothiazole-4-carboxylate (**321**)

Method I

A solution of compound **339** (22.6 mg, 0.04 mmol) and LiCl (16.8 mg, 0.40 mmol) in MeCN (0.5 mL) was stirred at rt under N_2 overnight. After the volatiles were removed, the crude mixture was directly purified by column chromatography (silica 100% EtOAc) to give product **321** as a yellow solid (0.6 mg, 15%). mp. 85 °C (dec.); R_f = 0.5 (100% EtOAc); IR υ_{max} (solution in Methanol-*d*$_4$): 3143 (OH), 2954 (C-H), 2928 (C-H), 2855 (C-H), 1738

(C=O) cm^{-1}. ^{1}H NMR (700 MHz, Methanol-d_4) δ 7.42 (1H, d, *J* = 16.1, C*H*=CH), 7.20 (1H, d, *J* = 16.1, CH=C*H*), 6.77 (1H, d, *J* = 2.1, Ar*H*), 6.43 (1H, d, *J* = 2.1 Hz, Ar*H*), 5.31 (1H, app t, *J* = 9.0 Hz, C*H*(COOMe)), 3.81 (3H, s, OCH_3), 3.69 (2H, dd, *J* = 11.9, 8.1 Hz, SCH_2). ^{13}C NMR (175 MHz, Methanol-d_4) δ 172.1 (*C*OOMe), 167.4 (S*C*NCH), 159.4 (S*C*N), 153.8 (Ar*C*), 148.5 (Ar*C*), 139.0 (Ar*C*)136.0 (*C*H=CH), 128.0 (CH=*C*H), 127.0 (Ar*C*), 102.4 (Ar*C*H), 98.5 (Ar*C*H), 78.8 (*C*H(COOMe)), 53.1 (COO*Me*), 35.5 (S*C*H_2). HRMS (ESI^+) Calcd. for $C_{14}H_{13}N_2O_4S_2$ $[M + H]^+$ 337.0311, found 337.0311.

Method II

To a solution of impure methyl (*E*)-(3-(4,6-dihydroxybenzo[*d*]thiazol-2-yl)prop-2-enethioyl)serinate (**345**) (53 mg, 0.15 mmol) in anhydrous DCM (0.5 mL) at -78 °C was added DAST (30.1 µL, 0.19 mmol). After 1 h, the reaction was quenched with sat. aq. $NaHCO_3$, and extracted with DCM (3 X 10 mL), dried ($MgSO_4$), and purified by column chromatography (silica 100% EtOAc) followed by (90% EtOAc：10% MeOH) to give a mixture of compound **321** as a yellow oil. This yellow oil was added to $CHCl_3$ (1 mL) and sonicated to precipitate a yellow solid. The solvent was removed by pipette and the remaining solid was dried *in vacuo* and to give product **321** (3.0 mg, 3% over two steps) as a yellow solid.

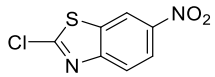

356

2-chloro-6-nitrobenzo[*d*]thiazole (**356**)

To a solution of 2-amino-6-nitrobenzothiazole **(357)** (1.0 g, 5.1 mmol), $CuCl_2$ (0.65 g, 4.8 mmol) in THF (5 mL) and $HCl_{(aq)}$ (16 mL) was added $NaNO_2$ (1.0 g, 15.3 mmol) slowly at 0 °C and the resulting suspension was stirred overnight at rt. To consume the starting material completely, the reaction was further heated to 55 °C for 30 min. The solution was then cooled to rt, extracted with $CHCl_3$ (2 x 100 mL), and dried ($MgSO_4$). After filtration, the volatile materials were removed *in vacuo*, to give the crude product that could be used without further purification. The product was obtained as a brown solid (1.1 g, 99%) (lit. [134] yield 65%). mp. 187 °C (lit. [140] 193-194 °C); R_f = 0.8 (100% CH_3Cl). ^{1}H NMR (400 MHz, $CDCl_3$) δ 8.75 (1H, s, SC*H*N), 8.38 (1H, d, *J* = 8.0, Ar*H*), 8.31 (1H, d, *J* = 8.07, Ar*H*). The data agreed with the literature. [134]

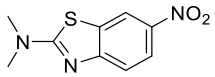

358

***N*,*N*-dimethyl-6-nitrobenzo[*d*]thiazol-2-amine** (**358**)

To a solution of 2-chloro-6-nitrobenzothiazole (0.5 g, 2.4 mmol) in THF (20 mL) was injected dimethylamine (2N in MeOH) (2.4 mL, 4.8 mmol) and the reaction was stirred at rt for 4 h. After the volatiles were removed under reduced-pressure, the desired product was obtained as a yellow solid in quantitative yield (lit. [134] yield 87%). mp. 202 °C (lit. [141] 209-211 °C); R_f = 0.4 (70 % hexane：30 % EtOAc). ^{1}H NMR (400 MHz, $CDCl_3$) δ 8.51 (1H, s, Ar*H*), 8.20 (1H, d, *J* = 8.0, Ar*H*), 7.51 (1H, d, *J* = 8.0, Ar*H*), 3.28 (6H, s, N(CH_3)$_2$). The data agreed with the literature. [134]

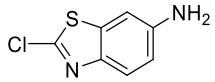

52a

2-chlorobenzo[*d*]thiazol-6-amine (**52a**)

A suspension of 2-chloro-6-nitrobenzo[*d*]thiazole (**356**) (1.0 g, 5.1 mmol) and tin(II) chloride dihydrate (5.2 g, 23.0 mmol) in EtOH (30 mL) and $HCl_{(aq)}$ (5 mL) was refluxed until it turned to a clear brown solution. The volatiles were removed *in-vacuo*, and the residue basified to pH = 14 with satd. aq. $NaOH_{(aq)}$, extracted with EtOAc (3 X 200 mL), and dried ($MgSO_4$). After filtration, the volatile materials were removed *in vacuo* again, the crude product was further purified column chromatography (silica 50% Hexane：50% EtOAc) to give the desired compound (0.69 g, 80%) (lit. [47] yield 77%) as a yellow solid. mp. 160 °C (lit. [142] 155-157 °C); R_f = 0.4 (50% Hexane：50% EtOAc). ^{1}H NMR (400 MHz, $CDCl_3$) δ 7.70 (1H, d, *J* = 8.7 Hz, Ar*H*), 6.99 (1H, d, *J* = 2.3 Hz, Ar*H*), 6.81 (1H, dd, *J* = 8.7, 2.3 Hz, Ar*H*), 3.85 (2H, s, NH_2). The data agreed with the literature. [47]

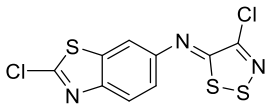

361

(*Z*)-4-chloro-*N*-(2-chlorobenzo[*d*]thiazol-6-yl)-5H-1,2,3-dithiazol-5-imine (**361**)

To a solution of 2-chlorobenzo[*d*]thiazol-6-amine (0.23 g, 1.25 mmol) in anhydrous DCM (7 mL) was added Appel's salt (0.29 g, 1.38 mmol), and the mixture stirred at rt under N_2 for 2 h. Then pyridine (0.20 mL, 2.50 mmol) was added to the yellow suspension and the reaction stirred for 1 h. The crude reaction mixture was directly purified by column

chromatography (silica 50% hexane：50% DCM) to give the desired product **361** as a yellow solid (0.25 g, 63%). mp. 108 °C (dec.); R_f = 0.4 (50% hexane：50% EtOAc); IR υ_{max} (solution in $CDCl_3$): 3085 (C-H), 3057 (C-H), 2959 (C-H), 2920 (C-H), 2850 (C-H) cm^{-1}. ^1H NMR (700 MHz, $CDCl_3$) δ 8.02 (1H, d, *J* = 8.7 Hz, Ar*H*), 7.62 (1H, d, *J* = 2.1 Hz, Ar*H*), 7.36 (dd, *J* = 8.7, 2.1 Hz, 1H, Ar*H*). ^{13}C NMR (175 MHz, $CDCl_3$) δ 159.9 (Ar*C*), 153.5 (N=*C*-S), 149.5 (Ar*C*), 149.1 (Ar*C*), 148.1 (S-N=*C*), 137.7 (Ar*C*), 124.4 (Ar*C*H), 119.5 (Ar*C*H), 111.8 (Ar*C*H). HRMS (ESI^+) Calcd. for $C_9H_4Cl_2N_3S_3$ $[M + H]^+$ 319.8944, found 319.8948.

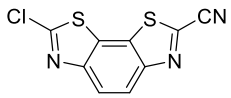

360

7-chlorobenzo[1,2-d:4,3-d']bis(thiazole)-2-carbonitrile (**360**)

A solution of (*Z*)-4-chloro-*N*-(2-chlorobenzo[*d*]thiazol-6-yl)-5H-1,2,3-dithiazol-5-imine (**361**) (0.50 g, 1.56 mmol) in sulfolane (3 mL) was heated to 180 °C for 2 h. After cooling to rt, the reaction mixture was purified directly by column chromatography (silica 75% hexane：25% EtOAc) to give product **360** as a yellow solid (0.17 g, 42%). mp. 212 °C (dec.); R_f = 0.4 (75% hexane：25% EtOAc); IR υ_{max} (solution in $CDCl_3$): 3086 (C-H), 3061 (C-H), 2925 (C-H), (C-H), 2855 (C-H), 2229 (CN) cm^{-1}. ^1H NMR (700 MHz, $CDCl_3$) δ 8.29 (1H, d, *J* = 8.9 Hz, Ar*H*), 8.18 (1H, d, *J* = 8.9 Hz, Ar*H*). ^{13}C NMR (175 MHz, $CDCl_3$) δ 154.38 (Ar*C*), 151.38 (Ar*C*), 150.86 (Ar*C*), 135.86 (Ar*C*), 128.46 (Ar*C*), 128.18 (Ar*C*), 123.88 (Ar*C*H), 123.30 (Ar*C*H), 112.57 (Ar*C*). HRMS (ESI^+) Calcd. for $C_9H_3ClN_3S_2$ $[M + H]^+$ 251.9451, found 251.9453.

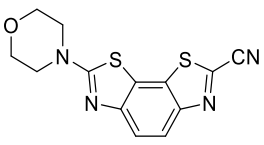

352a

7-morpholinobenzo[1,2-d:4,3-d']bis(thiazole)-2-carbonitrile (**352a**)

To a solution of 7-chlorobenzo[1,2-d:4,3-d']bis(thiazole)-2-carbonitrile (**360**) (0.05 g, 0.20 mmol) and Cs_2CO_3 (0.08 g, 0.24 mmol) in a co-solvent of DCM (0.5 mL) and water (0.5 mL) was added morpholine (0.02 mL, 0.24 mmol) at rt and then this reaction was stirred overnight. The crude product was purified directly by column chromatography (silica 50%

hexane：50% EtOAc). The desired product **352a** was obtained as a pale-yellow solid (0.04 g, 58%). mp. 179 °C (dec.); R_f = 0.8 (50% hexane：50% EtOAc); IR υ_{max} (solution in $CDCl_3$): 2957 (C-H), 2918 (C-H), 2848 (C-H), 2221 (CN) cm^{-1}. ^1H NMR (700 MHz, $CDCl_3$) δ 8.11 (1H, d, *J* = 8.9 Hz, Ar*H*), 7.80 (1H, d, *J* = 8.9 Hz, Ar*H*), 3.90 – 3.84 (4H, m, OCH_2), 3.73 – 3.67 (4H, m, NCH_2). ^{13}C NMR (175 MHz, $CDCl_3$) δ 169.8 (N-*C*=N), 148.4 (Ar*C*), 132.6 (*C*-CN), 128.7 (Ar*C*), 123.2 (Ar*C*H), 121.4, 120.5 (Ar*C*H), 113.3 (Ar-*C*N), 66.3 (O*C*H_2), 48.9 (N*C*H_2). HRMS (ESI^+) Calcd. for $C_{13}H_{11}N_4OS_2$ $[M + H]^+$ 303.0369, found 303.0369.

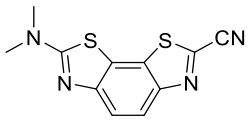

352b

7-(dimethylamino)benzo[1,2-d:4,3-d']bis(thiazole)-2-carbonitrile (**352b**)

Compound **360** (0.05 g, 0.20 mmol) was subjected to S_NAr reaction conditions with dimethylamine (2 M in THF) (0.18 mL, 0.36 mmol) as for the preparation of **352a**. After purification by column chromatography (silica 75% hexane：25% EtOAc), the desired product **352b** was obtained as a pale yellow solid (17.0 mg, 27%). mp. 209 °C (dec.); R_f = 0.25 (75% hexane：25% EtOAc); IR υ_{max} (solution in $CDCl_3$): 2923 (C-H), 2922 (C-H), 2223 (CN) cm^{-1}. ^1H NMR (700 MHz, $CDCl_3$) δ 8.08 (1H, d, *J* = 8.8 Hz, Ar*H*), 7.80 (1H, d, *J* = 8.8 Hz, Ar*H*), 3.28 (6H, s, N(CH_3)$_2$). ^{13}C NMR (175 MHz, $CDCl_3$) δ 169.7 (N-C=N), 154.3 (Ar*C*), 147.9 (Ar*C*), 132.1 (Ar*C*), 128.7 (Ar*C*), 123.1 (Ar*C*H), 121.7 (Ar*C*), 120.1 (Ar*C*H), 113.4 (Ar-*C*N), 40.6 (N(*C*H_3)$_2$). HRMS (ESI^+) Calcd. for $C_{11}H_9N_4S_2$ $[M + H]^+$ 261.0269, found 261.0271.

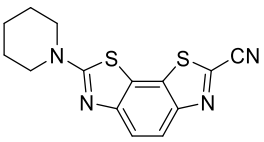

352c

7-(piperidin-1-yl)benzo[1,2-d:4,3-d']bis(thiazole)-2-carbonitrile (**352c**)

Compound **360** (0.05 g, 0.20 mmol) was subjected to S_NAr reaction conditions with piperidine (0.03 g, 0.36 mmol) as for the preparation of **352a**. After purification by column chromatography (silica 50% hexane：50% EtOAc), the desired product **352c** was obtained as a pale-yellow solid (18.0 mg, 26%). mp. 199 °C (dec.); R_f = 0.75 (50% hexane：50%

EtOAc); IR υ_{max} (solution in $CDCl_3$): 2940 (C-H), 2853 (C-H), 2223 (CN) cm^{-1}. ^1H NMR (700 MHz, $CDCl_3$) δ 8.06 (1H, d, *J* = 8.8 Hz, Ar*H*), 7.74 (1H, d, *J* = 8.8 Hz, Ar*H*), 3.71-3.63 (m, 4H, piperidinyl-*H*), 1.78-1.71 (6H, m, piperidinyl-*H*). ^{13}C NMR (175 MHz, $CDCl_3$) δ 169.6 (N-*C*=N), 154.2 (Ar*C*), 148.0 (Ar*C*), 132.0 (Ar*C*), 128.6 (Ar*C*), 123.0 (Ar*C*H), 121.3, 120.1 (Ar*C*H), 113.4 (Ar-*C*N), 50.2 (piperidinyl-*C*), 25.4 (piperidinyl-*C*), 24.2 (piperidinyl-*C*). HRMS (ESI^+) Calcd. for $C_{14}H_{13}N_4S_2$ $[M + H]^+$ 301.0582, found 301.0579.

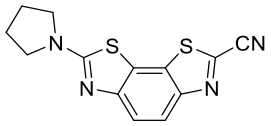

352d

7-(pyrrolidin-1-yl)benzo[1,2-d:4,3-d']bis(thiazole)-2-carbonitrile (**352d**)

Compound **360** (0.05 g, 0.20 mmol) was subjected to S_NAr reaction conditions with pyrrolidine (0.03 g, 0.36 mmol) as for the preparation of **352a**. After purification by column chromatography (silica 50% hexane ： 50% EtOAc). The desired product **352d** was obtained as a pale-yellow solid (18.0 mg, 26%). mp. 176 ˚C (dec.); R_f = 0.25 (50% hexane ： 50% EtOAc); IR υ_{max} (solution in $CDCl_3$): 2949 (C-H), 2922 (C-H), 2872 (C-H), 2852 (C-H), 2221 (CN) cm^{-1}. ^1H NMR (700 MHz, $CDCl_3$) δ 8.07 (1H, d, *J* = 8.8 Hz, Ar*H*), 7.80 (1H, d, *J* = 8.8 Hz, Ar*H*), 3.68-3.61(4H, m, pyrrolidinyl-*H*), 2.15-2.13 (4H, m, pyrrolidinyl-*H*). ^{13}C NMR (175 MHz, $CDCl_3$) δ 166.17 (N-*C*=N), 154.44 (Ar*C*), 147.80 (Ar*C*), 131.87 (Ar*C*), 128.79 (Ar*C*), 123.03 (Ar*C*) (Ar*C*H), 121.27 (Ar*C*), 120.04 (Ar*C*H), 113.45 (Ar-*C*N), 50.07 (pyrrolidinyl-*C*), 25.83 (pyrrolidinyl-*C*). HRMS (ESI^+) Calcd. for $C_{13}H_{11}N_4S_2$ $[M + H]^+$ 287.0425, found 287.0427.

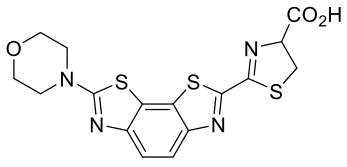

349a

2-(7-morpholinobenzo[1,2-d:4,3-d']bis(thiazole)-2-yl)-4,5-dihydrothiazole-4-carboxylic acid (**349a**)

A solution of 7-morpholinobenzo[1,2-d:4,3-d']bis(thiazole)-2-carbonitrile (**352a**) (0.01 g, 0.03 mmol), $NaHCO_3$ (0.06 g, 0.04 mmol) and DL-cysteine (0.05 g, 0.04 mmol) in DCM

(0.5 mL) and water (0.5 mL) was stirred at rt under N_2 for 2 days. After the solvents were removed *in vacuo*, the crude product was further sonicated with H_2O (1 mL) and $CHCl_3$ (1 mL). After filtration, the desired product **349a** was collected as a yellow solid (12.1 mg, 90%). mp. 164 °C (dec.); IR υ_{max} (solid): 3343 (COOH), 2922 (C-H), 2853 (C-H) cm^{-1}. ^1H NMR (700 MHz, Methanol-d_4) δ 7.99 (1H, d, *J* = 8.8 Hz, Ar*H*), 7.68 (1H, d, *J* = 8.8 Hz, Ar*H*), 5.22 (1H, app t, *J* = 9.2 Hz, C*H*(COOH)), 3.85 – 3.83 (4H, m, O(CH_2)$_2$), 3.74 (2H, dd, *J* = 9.3, 7.5 Hz, CH_2S), 3.69 – 3.66 (4H, m, N(CH_2)$_2$). ^{13}C NMR (175 MHz, Methanol-d_4) δ 177.1(*C*OOH), 171.2 (*C*N(CH_3)$_2$), 160.0 (S*C*N), 153.3 (Ar*C*), 150.4 (Ar*C*), 129.9 (Ar*C*), 126.3 (Ar*C*), 122.8 (Ar*C*H), 119.8 (Ar*C*H), 83.0 (N*C*H), 67.2 O(*C*H_2)$_2$, 49.9 N(*C*H_2)$_2$, 37.4 (S*C*H_2). HRMS (ESI^+) Calcd. for $C_{16}H_{15}N_4O_3S_3$ $[M + H]^+$ 407.0301, found 407.0309.

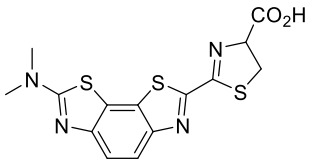

349b

2-(7-(dimethylamino)benzo[1,2-d:4,3-d']bis(thiazole)-2-yl)-4,5-dihydrothiazole-4-carboxylic acid (**349b**)

Compound **352b** (10.0 mg, 0.04 mmol) was subjected to condensation conditions as for the preparation of **349a**. The desired product **349b** was obtained as a yellow solid (15.0 mg, 69%). mp. 166 °C (dec.); IR υ_{max} (solid): 3394 (COOH), 3041 (C-H), 2918 (C-H), 1709 (C=O) cm^{-1}. ^1H NMR (700 MHz, Methanol-d_4) δ 7.95 (1H, d, *J* = 8.8, Ar*H*), 7.63 (1H, d, *J* = 8.8, Ar*H*), 5.22 (app t, *J* = 9.3, 1H, C*H*(COOH)), 3.74 (2H, dd, *J* = 9.3, 7.4, CH_2S), 3.25 (6H, s, N(CH_3)$_2$). ^{13}C NMR (176 MHz, Methanol-d_4) δ 177.0 (*C*OOH), 170.8 (*C*N(CH_3)$_2$), 165.1 (*C*=NCH), 159.4 (S*C*N), 153.7 (Ar*C*), 149.8 (Ar*C*), 129.7 (Ar*C*), 123.7 (Ar*C*), 122.9 (Ar*C*H), 119.1 (Ar*C*H), 82.8 (N*C*H(COOH), 40.6 (N(*C*H_3)$_2$), 37.2 (S*C*H_2). HRMS (ESI^+) Calcd. for $C_{14}H_{13}N_4O_2S_3$ $[M + H]^+$ 365.0195, found 365.0814.

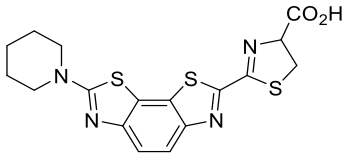

349c

2-(7-(piperidin-1-yl)benzo[1,2-d:4,3-d']bis(thiazole)-2-yl)-4,5-dihydrothiazole-4-carboxylic acid (**349c**)

Compound **352c** (10.0 mg, 0.03 mmol) was subjected to condensation conditions as for the preparation of **349a**. The desired product **349c** was obtained as a yellow solid (10.0 mg, 75%). mp. 189 °C (dec.); IR υ_{max} (solid): 3379 (COOH), 2930 (C-H), 2850 (C-H), 1740 (C=O) cm^{-1}. ^{1}H NMR (700 MHz, Methanol-d_4) δ 7.94 (1H, d, *J* = 8.8 Hz, Ar*H*), 7.60 (1H, d, *J* = 8.8 Hz, Ar*H*), 5.20 (1H, app t, *J* = 9.3 Hz, C*H*(COOH)), 3.73 (2H, dd, *J* = 9.3, 6.6 Hz, CH_2S), 3.65 (4H, bs, piperidinyl-*H*), 1.73 (6H, m, piperidinyl-*H*). ^{13}C NMR (176 MHz, Methanol-d_4) δ 177.3 (*C*OOH), 170.7 (*C*N$(CH_3)_2$), 164.8 (*C*=NCH), 161.4 (S*C*N), 159.6 (Ar*C*), 153.5 (Ar*C*), 149.9 (Ar*C*), 129.6 (Ar*C*), 122.9 (Ar*C*H), 119.2 (Ar*C*H), 83.1 (N*C*H), 50.9 (piperidinyl-*C*), 37.4 (S*C*H_2), 26.3 (piperidinyl-*C*), 25.0 (piperidinyl-*C*). HRMS (ESI^+) Calcd. for $C_{17}H_{16}N_4O_2S_3$ $[M + H]^+$ 405.0508, found 405.0514.

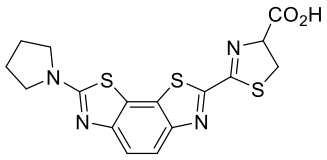

349d

2-(7-(pyrrolidin-1-yl)benzo[1,2-d:4,3-d']bis(thiazole)-2-yl)-4,5-dihydrothiazole-4-carboxylic acid (**349d**)

Compound **352d** (10.0 mg, 0.04 mmol) was subjected to condensation conditions as for the preparation of **349a**. The desired product **349d** was obtained as a yellow solid (12.1 mg, 90%). mp. 183 °C (dec.); IR υ_{max} (solid): 3378 (COOH), 2925 (C-H), 2925 (C-H), 2825 (C-H), 1727 (C=O) cm^{-1}. ^{1}H NMR (400 MHz, DMSO-d_6) δ 8.05 (1H, d, *J* = 8.7 Hz, Ar*H*), 7.70 (1H, d, *J* = 8.7 Hz, Ar*H*), 5.42 (app t, *J* = 9.2 Hz, 1H), 3.85 – 3.68 (2H, dd, *J* = 9.2, 7.5 Hz, CH_2S), 3.55 (4H, bs, pyrrolidinyl-*H*), 2.04 (4H, bs, pyrrolidinyl-*H*). ^{13}C NMR (176 MHz, DMSO) δ 171.2 (*C*OOH), 170.1 (*C*N$(CH_3)_2$), 165.0 (S*C*N), 164.2 (Ar*C*), 153.1 (Ar*C*), 147.8 (Ar*C*), 128.1 (Ar*C*), 122.2 (Ar*C*), 121.2 (Ar*C*H), 118.5 (Ar*C*H), 78.1, 49.7 (pyrrolidinyl-*C*), 34.9 (S*C*H_2), 25.2 (pyrrolidinyl-*C*). HRMS (ESI^+) Calcd. for $C_{16}H_{15}N_4O_2S_3$ $[M + H]^+$ 391.0352, found 391.0350.

Gaussian input File

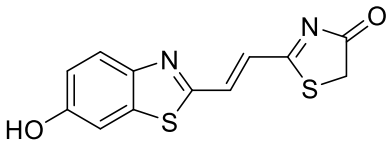

322

Compound **322**

Oxy infra-luciferins oxy-iLH$_2$ **322** was calculated by density functional calculations (DFT) at the B3LYP/6-311++G(3df,3pd) level

Input file:

%chk=EXP565.chk
opt b3lyp/6-311++g(3df,3pd) geom=connectivity

EXP565

0 1

C	-2.74814100	0.92796100	-0.00025000
C	-2.94397400	-0.48064700	0.00006700
C	-4.21747600	-1.04801900	0.00032600
C	-5.31195400	-0.18164400	0.00017800
C	-5.13965100	1.22034200	-0.00019900
C	-3.86935600	1.77558400	-0.00038600
C	-0.60982700	0.33566100	-0.00018900
H	-4.38193400	-2.11952700	0.00063700
H	-6.01430600	1.86621900	-0.00036200
H	-3.72522000	2.85070600	-0.00064300
C	0.82317400	0.51688800	-0.00023500
H	1.14954200	1.55352300	-0.00013200
C	1.75040600	-0.46949500	-0.00022100
H	1.46034500	-1.51723300	-0.00019100
C	3.17528100	-0.18681400	-0.00007600
N	-1.43879000	1.34493800	-0.00033400
N	3.68391000	1.00675000	0.00032000
S	-1.38846600	-1.27693800	0.00015100
S	4.29247200	-1.58258300	-0.00045100
C	5.08317200	1.00172500	0.00029700
O	5.78132900	1.99370500	0.00046500
C	5.69310900	-0.42219700	0.00023300
H	6.31294700	-0.55730800	0.88953800
H	6.31387300	-0.55729900	-0.88838500
O	-6.55211400	-0.75505600	0.00029100
H	-7.23747300	-0.07382600	0.00112700

1 2 1.5 6 1.5 16 1.5
2 3 1.5 18 1.0
3 4 1.5 8 1.0
4 5 1.5 25 1.0
5 6 1.5 9 1.0
6 10 1.0
7 11 1.5 16 2.0 18 1.0
8
9
10
11 12 1.0 13 2.0
12
13 14 1.0 15 1.0
14
15 17 2.0 19 1.0
16
17 20 1.0
18
19 22 1.0
20 21 2.0 22 1.0
21
22 23 1.0 24 1.0
23
24
25 26 1.0
26

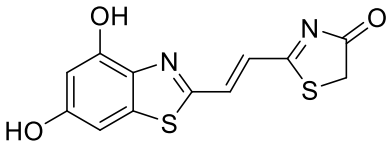

323

Compound **323**

Oxy-**323** was calculated by density functional calculations (DFT) at the B3LYP/6-311++G(3df,3pd) level

Input file

%chk=EXP548.chk
opt b3lyp/6-311++g(3df,3pd) geom=connectivity

EXP548

0 1

C	-4.09342183	2.52520602	0.53003043
C	-2.75727325	2.46267712	-0.01867170
C	-2.16327611	3.59340541	-0.54205804
C	-2.88686732	4.79754953	-0.52705528
C	-4.17138787	4.85768884	0.00056900
C	-4.79061004	3.71643958	0.53714239
C	-3.32992757	0.34331964	0.73382488
H	-2.42378645	5.70551642	-0.94144578
H	-5.80670405	3.78029226	0.95070342
C	-3.26299868	-1.15858807	1.06758192
H	-4.09719602	-1.63853292	1.53520113
C	-2.15118156	-1.87448287	0.77106150
H	-1.31391152	-1.40010425	0.30325406
C	-2.09259479	-3.37590348	1.10855781
C	-1.34091824	-5.56130442	1.31853144
O	-4.88103435	6.09918059	0.00087833
H	-4.31934307	6.78944991	-0.35916497
O	-0.84286676	3.55250561	-1.08954901
H	-0.59454676	4.42873639	-1.39312237
O	-0.86192071	-6.70972812	1.00947194
C	-2.67739602	-5.49038786	1.86540887
H	-2.66259992	-5.77027756	2.89804764
H	-3.32841583	-6.14716221	1.32715181
N	-2.30219333	1.08514703	0.12143245
N	-0.99909662	-4.22345055	0.85153025
S	-4.42759337	1.18443508	0.99419395
S	-3.12495515	-4.11078271	1.72154609

1 2 1.0 6 2.0 26 1.0

2 3 2.0 24 1.0
3 4 1.0 18 1.0
4 5 2.0 8 1.0
5 6 1.0 16 1.0
6 9 1.0
7 10 1.0 24 2.0 26 1.0
8
9
10 11 1.0 12 2.0
11
12 13 1.0 14 1.0
13
14 25 2.0 27 1.0
15 20 2.0 21 1.0 25 1.0
16 17 1.0
17
18 19 1.0
19
20
21 22 1.0 23 1.0 27 1.0
22
23
24
25
26
27

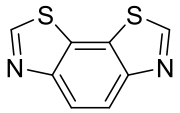

350

Core **350**

Core structures **350** was conducted by time-dependent density functional theory (TD-DFT) at the level td B3LYP/6-311++G(d).

Input file

```
%chk=benzodithiazole.chk
# opt td b3lyp/6-311++g(d) geom=connectivity

EXP637

0 1
 C              -1.39201400    1.00502000    0.00004200
 C              -0.69856000   -0.22465000   -0.00001900
 C               0.69879900   -0.22518200    0.00004900
 C               1.39247800    1.00457600    0.00021600
 C               0.68993100    2.22761700    0.00026000
 C              -0.68896700    2.22781600    0.00016400
 C              -3.13615700   -0.34194000   -0.00020100
 H               1.25425700    3.15279100    0.00047100
 H              -1.25312500    3.15312300    0.00024700
 H              -4.16815700   -0.67079200   -0.00031500
 C               3.13627500   -0.34260900   -0.00013900
 H               4.16799400   -0.67227600   -0.00023700
 N              -2.77329900    0.89275800   -0.00001100
 N               2.77374100    0.89208600    0.00063800
 S               1.84179700   -1.54511100   -0.00017400
 S              -1.84272000   -1.54492800   -0.00025000

 1 2 1.5 6 1.5 13 1.0
 2 3 1.5 16 1.0
 3 4 1.5 15 1.0
 4 5 1.5 14 1.0
 5 6 2.0 8 1.0
 6 9 1.0
 7 10 1.0 13 2.0 16 1.0
 8
 9
 10
 11 12 1.0 14 2.0 15 1.0
 12
```

13
14
15
16

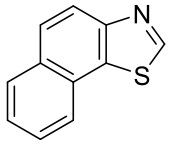

351

Core **351**

Core structures **351** was conducted by time-dependent density functional theory (TD-DFT) at the level td B3LYP/6-311++G(d).

Input file

%chk=EXP638.chk
opt td b3lyp/6-311++g(d) geom=connectivity

Title Card Required

0 1

C	0.68859800	2.19144900	-0.00032000
C	-0.66688300	-0.33437500	0.00023100
C	-1.38808100	0.90292400	0.00001300
C	-0.67835800	2.14330300	0.00003500
C	-2.80421900	0.85959300	-0.00023800
H	-3.35393900	1.79627700	-0.00063100
C	-3.48062100	-0.33915700	-0.00008900
C	-2.76484200	-1.55559000	0.00031000
C	-1.38825000	-1.55261200	0.00036200
H	1.22756900	3.13207100	0.00026600
H	-1.25329900	3.06423800	0.00018100
H	-4.56559200	-0.35212100	-0.00030400
H	-3.30318900	-2.49772400	0.00048100
H	-0.84552300	-2.49287800	0.00060200
C	0.75293400	-0.24703300	-0.00013700
C	1.42503600	0.97900900	-0.00021400
C	3.19712800	-0.32390600	0.00010100
N	2.80804800	0.90531700	0.00077600
S	1.92794900	-1.54360100	-0.00041900
H	4.23580000	-0.63110700	0.00034700

1 4 2.0 10 1.0 16 1.5
2 3 1.5 9 1.5 15 1.5
3 4 1.5 5 1.5
4 11 1.0
5 6 1.0 7 2.0
6
7 8 1.5 12 1.0

8 9 2.0 13 1.0
9 14 1.0
10
11
12
13
14
15 16 1.5 19 1.0
16 18 1.0
17 18 2.0 19 1.0 20 1.0
18
19
20

References

[1] Lee. J. W., *Bioluminescence, the Nature of the Light*., The University of Georgia. **2015**.

[2] Darwin, C., *D. Applet. Co*. **1859**.

[3] Dubois, R. La Vie et la Lumiere. Librairie Felix Alcan, Paris. **1914**.

[4] Shimomura, O., *Bioluminescence: Chemical Principles and Methods.* World Scientific, Singapore. **2006**.

[5] (a) Herring, P. J., *J. Biolumin. Chemilumin.*, **1987**, *1*, 147–163. (b) Haddock, S. H. D.; Moline M. A.; Case J. F., *Ann. Rev. Mar. Sci*., **2010**, *2*, 443–493. (c) Oba, Y.; Schultz D. T., *Adv. Biochem. Eng. Biotechnol*., **2014**, *144*, 3–36.

[6] (a) White, E. H.; McCapra, F.; Field, G. F.; McElroy, W. D., *J. Am. Chem. Soc.*, **1961**, *83*, 2402–2403. (b) Seliger, H. H.; McCapra, F.; Field, G. F.; McElroy, W. D., *Proc. Natl. Acad. Sci*., **1961**, *47*, 1129–1134.

[7] Shimomura, O.; Johnson, F. H., *Proc. Natl. Acad. Sci*. USA., **1975**, *72*, 1546–1549.

[8] Dunlap, J. C.; Hastings, J. W.; Shimomura, O., *Proc. Natl. Acad. Sci*., **1980**, *77*, 1394–1397.

[9] Shimomura, O.; Johnson, F. H., *Biochemistry*, **1968**, *7*, 1734–1738.

[10] Konstantin, V. P.; Valentin N. P.; Mikhail, S. B.; Konstantin, S. M.; Natalja, S. R.; Zinaida, M. K.; Aleksandra, S. T.; Alexei, I. P.; Vladimir, S. B.; Emma, K. R.; Svetlana, E. M.; Yuichi, O.; Yumiko, O.; Alexander, S. A.; Sergey, L.; Josef, I. G.; Ilia, V. Y., *Angew. Chemie Int. Ed.*, **2015**, *54*, 8124–8128.

[11] Ohtsuka, H.; Rudie, N. G.; Wampler, J. E., *Biochemistry*, **1976**, *15*, 1001–1004.

[12] Kishi, T.; Goto, T.; Hirata, Y.; Shimomura, O.; Johnson, F. H., *Tetrahedron Lett*., **1966**, *7*, 3427–3436.

[13] (a) Kurfürst, M.; Ghisla, S.; Hastings, J. W. *Biochemistry*, **1983**, *22*, 1521–1525. (b) Tan, S. L. J.; Kan, J. M.; Webster, R. D., *J. Phys. Chem. B*, **2013**, *117*, 13755−13766. (c) Kurfürst, M.; Ghisla, S.; Presswood, R.; Hasttngs, J. W., *Eur. J. Biochem.*, **1982**, *123*, 355–361.

[14] McElroy, W. D., *Proc. Natl. Acad. Sci*. USA., **1947**, *33*, 342–345

[15] Green, A. A.; McElroy, W. D., *Biochim. Biophys. ACTA*, **1956**, *20*, 170–176.

[16] Conti, E.; Franks, N. P.; Brick, P., *Structure*, **1996**, *4*, 287-298.

[17] Oba, Y.; Stevani, C.V.; Oliveira, A. G.; Tsarkova, A. S.; Chepurnykh, T.V.; Yampolsky, I. V., *Photochem. Photobiol.*, **2017**, *93*, 405–415.

[18] Bai, H.; Zhu, P.; Wu, W.; Li, J.; Ma, Z.; Zhang, W.; Cheng, Y.; Du, L.; Li, M., *Med. Chem. Commun.*, **2015**, *6*, 418–424.

[19] (a) White, E. H.; Miano, J. D.; Umbreit, M. *J. Am. Chem. Soc.* **1975**, *97*, 1982−2000. (b) White, E. H.; Rapaport, E.; Seliger, H. H.; Hopkins, T. A., *Biochemistry*, **1971**, *1*, 92–122.

[20] Branchini, B. R.; Behney, C. E.; Southworth, T. L.; Fontaine, D. M.; Gulick, A. M.; Vinyard, D. J.; Brudvig, G. W., *J. Am. Chem. Soc.*, **2015**, *137*, 7592−7595.

[21] Koo, J. Y.; Schmidt, S. P.; Schuster, G. B., *Proc. Natl. Acad. Sci. USA.*, **1978**, *75*, 30–33.

[22] (a) Fraga, H.; Fernandes, D.; Novotny, J.; Fontes, R.; Esteves Da Silva, J. C. G., *ChemBioChem*, **2006**, *7*, 929–935. (b) Navizet, I.; Liu, Y. J.; Ferré, N.; Roca-Sanjuán, D.; Lindh, R., *ChemPhysChem*, **2011**, *12*, 3064–3076.

[23] Seliger, H. H.; McElroy, W. D., *Proc. Natl. Acad. Sci*., **1964**, *52*, 75–81.

[24] Wood, K.V; Lam, Y. A.; Seliger, H. H.; McElroy, W. D., *Science*, **1989**, *244*, 700–702.

[25] Naumov, P.; Ozawa, Y.; Ohkubo, K.; Fukuzumi, S., *J. Am. Chem. Soc.*, **2009**, *131*, 11590–11605.

[26] Contag, C. H.; Contag, P. R.; Mullins, J. I.; Spilman, S. D.; Stevenson, D. K; Benaron, D. A., *Mol. Microbiol.*, **1995**, *18*, 593–603.

[27] Prescher, J. A.; Contag, C. H., *Curr. Opin. Chem. Biol*., **2010**, *14*, 80–89.

[28] Jensen, E. C., *The Anatomical record*, **2012**, *295*, 2031–2036.

[29] Weissleder, R.; Ntziachristos, V., *Nat. Med*., **2003**, *9*, 123–128.

[30] Berger, F.; Paulmurugan, R.; Bhaumik, S.; Gambhir, S. S., *Eur. J. Nucl. Med. Mol. Imaging*, **2008**, *35*, 2275–2285.

[31] Iwano, S.; Sugiyama, M.; Hama, H.; Watakabe, A.; Hasegawa, N.; Kuchimaru, T.; Tanaka, K. Z.; Takahashi, M.; Ishida, Y.; Hata, J.; Shimozono, S.; Namiki, K.; Fukano, T.; Kiyama, M.; Okano, H.; Kizaka-kondoh, S.; Mchugh, T. J.; Yamamori, T.; Hioki, H.; Maki, S.; Miyawaki, A., *Science*, **2018**, *359*, 935–939.

[32] Viviani, V. R.; Prado, R. A.; Neves, D. R.; Kato, D.; Barbosa, J. A., *Biochemistry*, **2013**, *52*, 3963−3973.

[33] (a) Ugarova, N. N.; Brovko, L. Y., *Luminescence*, **2002**, *17*, 321–330. (b) Branchini, B. R.; Ablamsky, D. M.; Davis, A. L.; Southworth, T. L.; Butler, B.; Fan, F.; Jathoul, A. P.; Pule, M. A., *Anal. Biochem.*, **2010**, *396*, 290–297. (c) Branchini, B. R.; Southworth, T. L.; Murtiashaw, M. H.; Magyar, R. A.; Gonzalez, S. A.; Ruggiero, M.

C.; Stroh, J. G., *Biochemistry*, **2004**, *43*, 7255–7262. (d) Zomer, G.; Hastings, J. W.; Berthold, F.; Lundin, A.; Garcia Campana, A. M.; Niessner, R.; Christolous, T. K.; Lowik, C.; Branchini, B. R.; Daunert, S.; Blum, L.; Kricka, L. J.; Roda, A., *Chemiluminescence and Bioluminescence*, *The Royal Society of Chemistry*. **2011**.

[34] Okada, K.; Lio, H.; Kubota, I.; Goto, T., *Tetrahedron Lett*., **1974**, 15, 2771–2774.

[35] Kanie, S.; Nishikawa, T.; Ojika, M.; Oba, Y., *Sci. Rep.*, **2016**, 6. 24794.

[36] (a) Kanie, S.; Nakai, R.; Ojika, M.; Oba, Y., *Bioorg. Chem.*, **2018**, *80*, 223–229. (b) Oba, Y.; Yoshida, N.; Kanie, S.; Ojika, M.; Inouye, S., *LoS ONE*, **2013**, *8*, e84023.

[37] Appel, R.; Janssen, H.; Siray, M.; Knoch, F., *Chem. Ber*., **1985**, *118*, 1632–1643.

[38] Besson, T.; Guillard, J.; Rees, C. W., *J. Chem. Soc., Perkin Trans*., **2000**, *1*, 563–566.

[39] McCutcheon, D. C.; Paley, M. A.; Steinhardt, R. C.; Prescher, J. A., *J. Am. Chem. Soc.*, **2012**, *134*, 7604–7607.

[40] McCutcheon, D. C.; Porterfield, W. B.; Prescher, J. A., *Org. Biomol. Chem.*, **2015**, *13*, 2117–2121.

[41] Miller, S. C.; Mofford, D. M.; Adams, S. T., *ACS Chem. Biol*., **2018**, *13*, 1734–1740.

[42] Ikeda, Y.; Saitoh, T.; Niwa, K.; Nakajima, T.; Kitada, N.; Maki, S. A. Sato, M.; Citterio, D.; Nishiyama, S.; Suzuki, K., *Chem. Commun*., **2018**, *54*, 1774–1777.

[43] Podsiadły, R.; Grzelakowska, A.; Modrzejewska, J.; Siarkiewicz, P.; Słowiński, D.; Szala, M.; Świerczyńska, M., *Dyes and Pigments*, **2019**, *170*, 1076272.

[44] White, E. H.; Wörther, H.; Field, G. F.; McElroy, W. D., *J. Org. Chem*., **1965**, *30*, 2344–2348.

[45] White, E. H.; Wörther, H, *J. Org. Chem*., **1966**, *31*, 1484–1488.

[46] White, E. H.; Wörther, H.; Seliger, H. H.; McElroy, W. D., *J. Am. Chem. Soc.*, **1966**, *88*, 2015–219.

[47] Reddy, G. R.; Thompson, W. C.; Miller, S. C. *J. Am. Chem. Soc.*, **2010**, *132*, 13586–13587.

[48] Mofford, D. M.; Reddy, G. R.; Miller, S. C., *J. Am. Chem. Soc.*, **2014**, *136*, 13277–13282.

[49] Takakura, H.; Kojima, R.; Urano, Y.; Terai, T.; Hanaoka, K.; Nagano, T., *Chem. Asian J*., **2011**, *6*, 1800–1810.

[50] Kojima, R.; Takakura, H.; Ozawa, T.; Tada, Y.; Nagano, T.; Urano, Y., *Angew. Chem. Int. Ed.*, **2013**, *52*, 1175–1179.

[51] Wu, W.; Su, J.; Tang, C.; Bai, H.; Ma, Z.; Zhang, T.; Yuan, Z.; Li, Z.; Zhou, W.; Zhang, H.; Liu, Z.; Wang, Y.; Zhou, Y.; Du, L.; Gu, L.; Li, M., *Anal. Chem.*, **2017**, *89*, 4808−4816.

[52] Sharma, D. K.; Adams, S. T.; Liebmann, K. L.; Miller, S. C., *Org. Lett*., **2017**, *19*, 5836–5839.

[53] (a) Paul, F.; Patt, J.; Hartwig, J. F., *J. Am. Chem. Soc*., **1994**, *116*, 5969−5970. (b) Guram, A. S.; Buchwald, S. L., *J. Am. Chem. Soc*., **1994**, *116*, 7901−7902.

[54] Sharma, D. K.; Adams, S. T.; Liebmann, K. L.; Choi, A.; Miller, S. C., *Org. Lett*., **2019**, *21*, 1641–1644.

[55] Farace, C.; Blanchot, B.; Champiat, D.; Couble, P.; Declercq, G.; Millet, J. L., *J. Clin. Chem. Clin. Biochem.*, **1990**, *28*, 471–474.

[56] Pirrung, M. C.; Biswas, G.; Howitt, N. D.; Liao, J., *Bioorg. Med. Chem. Lett*., **2014**, *24*, 4881–4883.

[57] Steinhardt, R. C.; O'Neill, J. M.; Rathbun, C. M.; McCutcheon, D. C.; Paley, M. A.; Prescher, J. A., *Chem. Eur. J*., **2016**, *22*, 3671–3675.

[58] Steinhardt, R. C.; Rathbun, C. M.; Krull, B. T.; Yu, J. M.; Yang, Y.; Nguyen, B. D.; Kwon, J.; McCutcheon, D. C.; Jones, K. A.; Furche, F.; Prescher, J. A., *ChemBioChem*, **2017**, *18*, 96–100.

[59] Jones, K. A.; Porterfield, W. B.; Rathbun, C. M.; McCutcheon, D. C.; Paley, M. A.; Prescher, J., A. *J. Am. Chem. Soc.*, **2017**, *139*, 2351–2358.

[60] Takakura, H.; Kojima, R.; Ozawa, T.; Nagano, T.; Urano, Y., *ChemBioChem*, **2012**, *13*, 1424–1427.

[61] Ikeda, Y.; Saitoh, T.; Niwa, K.; Nakajima, T.; Kitada, N.; Maki, S. A.; Sato, M. Citterio, D.; Nishiyama, S.; Suzuki, K., *Chem. Commun*., **2018**, *54*, 1774–1777.

[62] Woodroofe, C. C.; Meisenheimer, P. L.; Klaubert, D. H.; Kovic, Y.; Rosenberg, J. C.; Behney, C. E.; Southworth, T. L.; Branchini, B. R., *Biochemistry*, **2012**, *51*, 9807−9813.

[63] Branchini, B. R.; Hayward, M. M.; Bamford, S.; Brennan, P. M.; Lajiness, E. J., *Photochem. Photobiol*., **1989**, *49*, 689–695.

[64] Takakura, H.; Sasakura, K.; Ueno, T.; Urano, Y.; Terai, T.; Hanaoka, K.; Tsuboi, T.; Nagano, T., *Chem. Asian J*., **2010**, *5*, 2053–2061.

[65] (a) Zhang, B. S.; Jones, K. A.; McCutcheon, D. C.; Prescher, J. A., *ChemBioChem*, **2018**, *19*,470–477. (b) Li, B.; Xue, S.; Yang, Y.; Feng, J.; Liu, P.; Zhang, Y.; Zhu, J.; Xu, Z.; Hall, A.; Zhao, B.; Shi, J.; Zhu, W., *Sci. Rep*., **2016**, *7*, 60–62 .

[66] Hall, M. P.; Woodroofe, C. C.; Wood, M. G.; Que, I.; Van'T Root, M.; Ridwan, Y.; Shi, C.; Kirkland, T. A.; Encell, L. P.; Wood, K. V.; Löwik, C.; Mezzanotte, L., *Nat. Commun.*, **2018**, *9*, 132–143.

[67] McCutcheon, D. C.; Paley, M. A.; Steinhardt, R. C.; Prescher, J. A., *J. Am. Chem. Soc.*, **2012**, *134*, 7604–7607.

[68] Conley, N. R.; Dragulescu-Andrasi, A.; Rao, J.; Moerner, W. E., *Angew. Chem. Int. Ed.*, **2012**, *51*, 3350–3353.

[69] Ioka, S.; Saitoh, T.; Iwano, S.; Suzuki, K.; Maki, S. A.; Miyawaki, A.; Imoto, M.; Nishiyama, S., *Chem. Eur. J.*, **2016**, *22*, 9330–9337.

[70] Miura, C.; Kiyama, M.; Iwano, S.; Ito, K.; Obata, R.; Hirano, T.; Maki, S.; Niwa, H., *Tetrahedron*, **2013**, *69*, 9726–9734.

[71] Iwano, S.; Obata, R.; Miura, C.; Kiyama, M.; Hama, K.; Nakamura, M.; Amano, Y.; Kojima, S.; Hirano, T.; Maki, S.; Niwa, H., *Tetrahedron*, **2013**, *69*, 3847–3856.

[72] Kuchimaru, T.; Iwano, S.; Kiyama, M.; Mitsumata, S.; Kadonosono, T.; Niwa, H.; Maki, S.; Kizaka-Kondoh, S., *Nat. Commun.*, **2016**, *7*, 11856.

[73] Ribeiro, C.; Esteves da Silva, J. C. G., *Photochem. Photobiol. Sci.*, **2008**, *7*, 1085–1090.

[74] Kitada, N.; Saitoh, T.; Ikeda, Y.; Iwano, S.; Obata, R.; Niwa, H.; Hirano, T.; Miyawaki, A.; Suzuki, K.; Nishiyama, S.; Maki, S. A., *Tetrahedron Lett.*, **2018**, *59*, 1087–1090.

[75] Kiyama, M.; Iwano, S.; Otsuka, S.; Lu, S. W.; Obata, R.; Miyawaki, A.; Hirano, T.; Maki, S. A., *Tetrahedron*, **2018**, *74*, 652–660.

[76] Jathoul, A. P.; Grounds, H.; Anderson, J. C.; Pule, M. A., *Angew. Chem. Int. Ed.*, **2014**, *53*, 13059–13063.

[77] Anderson, J. C.; Grounds, H.; Jathoul, A.; Murray, J.; Pacman, S.; Tisi, L., *RSC Adv.*, **2017**, *7*, 3975–3982.

[78] Nicolaou, K. C.; Nevalainen, M.; Zak, M.; Bulat, S.; Bella, M.; Safina, B. S., *Angew. Chem., Int. Ed.*, **2003**, *42*, 3418–3424.

[79] Anderson, J. C.; Chang, C.-H.; Jathoul, A. P.; Syed, A. J., *Tetrahedron*, **2019**, *75*, 347–356.

[80] Ikeda, Y.; Nomoto, T.; Hiruta, Y.; Nishiyama, N.; Citterio, D., *Anal. Chem.*, **2020**, *92*, 4235–4243.

[81] Ando, Y.; Niwa, K.; Yamada, N.; Enomoto, T.; Irie, T.; Kubota, H.; Ohmiya, Y.; Akiyama, H., *Nat. Photonics*, **2008**, *2*, 44−47.

[82] (a) Maity, A.; Sarkar, A.; Sil, A.; Shivakiran, S. B.; Patra, S. K., *New J. Chem*., **2017**, *41*, 2296–2308. (b) Wang, J. B.; Fang, X. Q.; Pan, X.; Dai, S. Y.; Song, Q. H., *Chem. Asian J*., **2012**, *7*, 696–700.

[83] (a) Bixon, M.; Jortner, J.; Cortes, J.; Heitele, H.; Michel-Beyerle, M. E., *J. Phys. Chem.*, **1994**, *98*,1289–7299. (b) Lee, W. W. H.; Zhao, Z.; Cai, Y.; Xu, Z.; Yu, Y.; Xiong, Y.; Kwok, R. T. K.; Chen, Y.; Leung, N. L. C.; Ma, D.; Lam, J. W. Y.; Qin, A.; Tang, B. Z., *Chem. Sci*., **2018**, *9*, 6118–6125. (c) Turro, N. J.; Ramamurthy, V.; Scaiano, J. C., *Modern Molecular Photochemistry of Organic Molecules*. University Science Book. **2010**, 1st Edition. (d) Hanson, K., *Lecture Note, CHM 5175: Part 2.7*, Slide 58, Florida State University.

[84] Lakowicz, J. R., *Principles of Fluorescence Spectroscopy*. **2010**, 3rd Edition, *Chapter 9*, 334.

[85] Kautsky, H., *Trans. Faraday Soc.*, **1939**, *35*, 216–219.

[86] (a) Eftink, M. R.; Ghiron, C., *Anal Biochem*, **1981**, *114*, 199–227. (b) Eftink, M. R., *Biophysical and biochemical aspects of fluorescence spectroscopy*, **1991**, Ed TG Dewey. Plenum Press, New York. 1–44. (c) Eftink, M. R., *Topics in fluorescence spectroscopy*, **1911**, Ed JR Lakowicz. Plenum Press, New York. 53–126.

[87] Knibbe, H.; Rehm, D.; Weller, A., *Ber Bunsenges Phys Chem*, **1968**, *72*, 257–263.

[88] Al-Kindy, S. M. Z.; Miller, J. N., *Luminescence*, **2011**, *26*, 148–152.

[89] Chevalier, A.; Renard, P. Y., Romieu, A., *Org. Lett*., **2014**, *16*, 3946−3949.

[90] Tanner, P. A; Zhou, L.; Duan, C; Wong, K, *Chem. Soc. Rev*., **2018**, *47*, 5234−5265.

[91] Takakura, H.; Kojima, R.; Kamiya, M.; Kobayashi, E.; Komatsu, T.; Ueno, T.; Terai, T.; Hanaoka, K.; Nagano, T.; Urano, Y., *J. Am. Chem. Soc*., **2015**, *137*, 4010−4013.

[92] Pirrung, M. C.; Dorsey, A.; Howitt, N. D.; Liao, J., *Chemistry Open*, **2017**, *6*, 697–700.

[93] (a) Chen, J.; Burghart, A.; Wan, C.-W.; Thai, L.; Ortiz, C.; Reibenspies, J.; Burgess, K., *Tetrahedron Lett.*, **2000**, *41*, 2303–2307. (b) Liu, S.-F.; Wu, Q.; Schmider, H. L.; Aziz, H.; Hu, N.-X.; Popovic, Z.; Wang, S., *J. Am. Chem. Soc.*, **2000**, *122*, 3671–3678. (c) Liu, Q.-D.; Mudadu, M. S.; Thummel, R.; Tao, Y.; Wang, S., *AdV. Funct. Mater.*, **2005**, *15*, 143–154. (d) Huenig, S.; Wehner, I., *Heterocycles*, **1989**, *28*, 359–363.

[94] (a) Dennis D.; Stanford Jnr R. H., *Acta Cryst.*, **1973**. *B29*, 1053–1058. (b) Nakatsu, T., Ichiyama, S., Hiratake, J., Saldanha, A., Kobashi, N.'Sakata, K., Kato, H., *Nature*, **2006**, 372–376.

[95] Koutentis, P., *Molecules*, **2005**, *10*, 346–359.

[96] (a) Leyva, S.; Hernández, H., *J. Fluor. Chem.*, **2010**, *131*, 982–988. (b) Lin, L.; Zhai, Y.; Wang, D.; Yin, G.; Fan, L.; Hu, Y., *J. Fluor. Chem.*, **2016**, *182*, 7–11. (c) VanLeeuwen, S. H.; Quaedflieg, P. J. L. M.; Broxterman, Q. B.; Milhajlovic, Y.; Liskamp, R. M. J., *Tetrahedron Lett.*, **2005**, *46*, 653–656.

[97] Kleiman, R.; Spencer, G. F.; Earle, F. R., *Lipids*., **1969**, *4*, 118-122.

[98] (a) Nosova, E. V.; Moshkina, T. N.; Lipunova, G. N.; Baklanova, I. V.; Slepukhin, P. A.; Charushin, V. N., *J. Fluor. Chem.*, **2015**, *175*, 145–151. (b) Frath, D.; Azizi, S.; Ulrich, G.; Retailleau, P.; Ziessel, R., *Org. Lett.*, **2011**, *13*, 3414–3417.

[99] (a) Chen, Y.; Qi, D.; Zhao, L.; Cao, W.; Huang, C.; Jiang, Ji., *Chem. Eur. J.*, **2013**, *19*, 7342–7347. (b) Kilic, A.; Aydemir, M.; Durgun, M.; Meriç, N.; Ocak, Y. S.; Keles, A.; Temel, H., *J. Fluor. Chem.*, **2014**, *162*, 9–16.

[100] Zeng, X.; Qian, M.; Hu, Q.; Negishi, E., *Angew. Chem., Int. Ed.*, **2004**, *43*, 2259–2263.

[101] (a) Aziz, K. Final year MSci Project Report. UCL Chemistry Department. **2015**. (b) Pumpianskii, M. Final year MSci Project Report. UCL Chemistry Department. **2017**.

[102] (a) Padalkar, V. S.; Seki, S., *Chem. Soc. Rev*., **2016**, *45*, 169–202. (b) Demchenko, A. P.; Tang, K.-C.; Chou, P.-T., *Chem*. *Soc. Rev*., **2013**, *42*, 1379–1408.

[103] (a) Park, S.; Ji, E. K.; Se, H. K.; Seo, J.; Chung, K.; Park, S. Y.; Jang, D. J.; Medina, B. M.; Gierschner, J.; Soo, Y. P., *J. Am. Chem. Soc*., **2009**, *131*, 14043–14049. (b) Tang, K.-C.; Chang, M.-J.; Lin, T.-Y.; Pan, H.-A.; Fang, T.-C.; Chen, K.-Y.; Hung, W.-Y.; Hsu, Y.-H.; Chou, P.-T., *J. Am. Chem. Soc*., **2011**, *133*, 17738–17745.

[104] Gu, B.; Huang, L.; Mi, N.; Yin, P.; Zhang, Y.; Tu, X.; Luo, X.; Luo, S.; Yao, S., *Analyst*, **2015**, *140*, 2778–2784.

[105] Padalkar, V. S.; Sakamaki, D.; Tohnai, N.; Akutagawa, T.; Sakai, K. I.; Seki, S., *RSC Adv.*, **2015**, *5*,80283–80296.

[106] Maltsev, O. V.; Walter, V.; Brandl, M. J.; Hintermann, L. *Synthesis.*, **2013**, *45*, 2763–2767.

[107] Treibs, A; Kreuzer, B, F., *Justus Liebigs Ann. Der Chemie*, **1968**, *718*, 208–223.

[108] Tram, K.; Yan, H.; Jenkins, H. A.; Vassiliev, S.; Bruce, D., *Dye. Pigment*., **2009**, *82*,

392–395.

[109] (a) Komatsu, T.; Urano, Y.; Fujikawa, Y.; Kobayashi, T.; Kojima, H.; Terai, T.; Hanaoka, K.; Nagano, T., *Chem. Commun*., **2009**, 7015–7017. (b) Liao, J.; Zhao, H.; Xu, Y.; Zhou, W.; Peng, F.; Wang, Y., *RSC Adv.*, **2017**, *7*, 33975–33985. (c) Kaur, P.; Singh, K., *J. Mater. Chem. C*, **2019**, *7*, 11361—11405.

[110] Loudet, A; Burgess, K., *Chem. Soc. Rev*., **2007**, *107*, 4891–4932.

[111] Sritharan, S. R.; Hussein, B. A.; Machin, D. D.; El-Aooiti, M. A.; Adjei, J. A.; Singh, J. K.; Pau, J. T. H.; Dhindsa, J. S.; Lough, A. J.; Koivisto, B. D., *RSC Adv*., **2017**, *7*, 8922–8926.

[112] Vilsmeier, A.; Haack, A, *Ber. Dtsch. Chem. Ges*., **1927**, *60*, 119–122.

[113] Al-Warhi, T. I.; Al-Hazimi, H. M. A.; El-Faham, A., *J. Saudi Chem. Soc.*, **2012**, *16*, 97–116.

[114] Braslau, R.; Rivera, F.; Tansakul, C., *Reactive & Functional Polymers*, **2013**, *73*, 624–633.

[115] Wang, H.; Fronczek, F. R.; Vicente, M. G. H.; Smith, K. M., *J. Org. Chem.*, **2014**, *79*, 10342−10352.

[116] Bonnier, C.; MacHin, D. D.; Abdi, O.; Koivisto, B. D., *Org. Biomol. Chem*., **2013**, *11*, 3756–3760.

[117] (a) Milstein, D.; Stille, J. K., *J. Am. Chem. Soc*., **1979**, *101*, 4981–4991. (b) Milstein, D.; Stille, J. K., *J. Am. Chem. Soc*., **1979**, *101*, 4992–4998.

[118] Heck, R. F., *J. Am. Chem. Soc*., **1968**, *90*, 5518–5526.

[119] (a) Hendrickson, J. B.; Schwartzman, S. M., *Tetrahedron Lett.*, **1975**, *16*, 277–280. (b) Hendrickson, J. B.; Hussoin, Md. S., *J. Org. Chem.*, **1987**, *52*, 4137–4139.

[120] Sun, H.; Liu, D.; Wang, T.; Li, P.; Bridgmohan, C. N.; Li, W.; Lu, T.; Hu, W.; Wang, L.; Zhou, X., *Organic Electronics*, **2018**, *61*, 35–45.

[121] Kim, M. J.; Lee, Y. S.; Shin, S. C.; Kim, Y. H., *J Polym Sci A Polym Chem*, **2016**, *54*, 525–531.

[122] Tang, W.; Dai, Y.; Gu, B.; Liu, M.; Yi, Z.; Li, Z.; Zhang, Z.; He, H.; Zeng, R., *Analyst*, **2020**, *145*,1427–1432.

[123] (a) Galievsky, V. A.; Zachariasse, K. A., *Acta Physica Polonica A*, **2007**, *112*, S39–S 56. (b) Ramprasad, M.; Bhattacharyya, S., *Introduction to Intramolecular Charge Transfer*, **2018**, Wiley-VCH Verlag GmbH & Co. KGaA.

[124] (a) Lou, A. J.-T.; Righetto, S.; Barger, C.; Zuccaccia, C.; Cariati, E.; Macchioni, A.; Marks, T. J., *J. Am. Chem. Soc.*, **2018**, *140*, 8746–8755. (b) Chung, P.-H.; Tregidgo,

C.; Suhling, K., *Methods Appl. Fluoresc.*, **2016**, *4*, 045001. (c) Liu, Y.; Yang, L.; Ma, C.; Tang, A., *Dyes and Pigments*, **2020**, *173*, 107981.

[125] Fairchild, J. Masters Project Report. UCL Chemistry Department. **2018**.

[126] Hirose, W.; Sato, K.; Matsuda, A., *Eur. J. Org. Chem*. **2011**, *31*, 6206–6217.

[127] Hou**,** C.; Ren, Y.; Lang, R.; Hu, X.; Xia, C.; Li, F., *Chem. Commun*., **2012**, *42*, 5181–5183.

[128] Do, H-Q.; Daugulis, O., *Org. Lett*., **2009**, *11*, 421–423.

[129] Farràs, J.; Serra, C.; Vilarrasa, J., *Tetrahedron Lett*., **1998**, *39*, 324–330.

[130] Mukherjee, R., *IJSRR*, **2018**, *7*, 1050–1069.

[131] (a) Conboy, G.; Taylor, R. G. D.; Findlay, N. J.; Kanibolotsky, A. L.; Inigo, A. R.; Ghosh, S. S.; Ebenhoch, B.; Jagadamma, L. Krishnan.; Thalluri, G. K. V. V.; Sajjad, M. T.; Samuel, I. D. W.; Skabara, P. J., *J. Mater. Chem. C*, **2017**, *5*, 11927–11936. (b) McEntee, G. J.; Vilela, F.; Skabara, P. J.; Anthopoulos, T. D.; Labram, J. G.; Tierney, S.; Harrington, R. W.; Clegg, W., *J. Mater. Chem*., **2011**, *21*, 2091–2097.

[132] Hrobárik, P.; Hrobáriková, V.; Semak, V.; Kasák, P.; Rakovský, E.; Polyzos, I.; Fakis, M.; Persephonis, P., *Org. Lett*. **2014**, *16*, 6358−6361.

[133] Prak, K.; Janos, K-V.; Chan, A. W. E.; Christin, L.; Costa, J. R.; Pengo, N.; Ketteler, R., *Biochemistry*, **2016**, *55*, 608−617.

[134] Liu, B.; You, Q. D.; Li, Z. Y., *Chinese Chem Lett*, **2010**, *21*, 554–557.

[135] Gaussian 09, Revision D.01, Frisch, M. J.; Trucks, G. W.; Schlegel, H. B.; Scuseria, G. E.; Robb, M. A.; Cheeseman, J. R. Scalmani, G.; Barone, V.; Mennucci, B.; Petersson, G. A.; Nakatsuji, H.; Caricato, M.; Li, X.; Hratchian, H. P.; Izmaylov, A. F.; Bloino, J.; Zheng, G.; Sonnenberg, J. L.; Hada, M.; Ehara, M.; Toyota, K.; Fukuda, R.; Hasegawa, J.; Ishida, M.; Nakajima, T.; Honda, Y.; Kitao, O.; Nakai, H.; Vreven, T.; Montgomery, Jr. J. A.; Peralta, J. E.; Ogliaro, F.; Bearpark, M.; Heyd,J.; Brothers, J. E.; Kudin, K. N.; Staroverov, V. N.; Keith, T.; Kobayashi, R.; Normand, J.; Raghavachari, K.; Rendell, A.; Burant, J. C.; Iyengar, S. S.; Tomasi, J.; Cossi, M.; Rega, N.; Millam, J. M.; Klene, M. Knox, J. E.; Cross, J. B.; Bakken, V.; Adamo, C.; Jaramillo, J.; Gomperts, R.; Stratmann, R. E.; Yazyev, O.; Austin, A. J.; Cammi, R.; Pomelli, C.; Ochterski, J. W.; Martin, R. L.; Morokuma, K.; Zakrzewski, V. G.; Voth, G. A.; Salvador, P.; Dannenberg, J. J.; Dapprich, S.; Daniels, A. D.; Farkas, O.; Foresman, J. B.; Ortiz, J. V.; Cioslowski, J.; Fox, D. J. Gaussian, Inc., Wallingford CT, **2013**.

[136] Appel, R.; Janssen, H.; Siray, M., *Chem. Ber*. **1985**, *118*, 1632−1643.

[137] Xie, A.; Cao, M.; Liu, Y.; Feng, L.; Hu, X.; Dong, W., *Eur. J. Org. Chem*. **2014**, *2*, 436−441.

[138] Suzuki, N.; Sato, M.; Okada, K.; Goto, T., Tetrahedron, **1972**, *28*, 4059−4064.

[139] Yoshikawa, K.; Yoshino, T.; Yokomizo, Y.; Uoto, K.; Naito, H.; Kawakami, K.; Mochizuki, A.; Nagata, T.; Suzuki, M.; Kanno, H.; Takemura, M.; Ohta, T., *Bioorg. Med. Chem. Lett*., **2011**, *21*, 2133–2140.

[140] Hauser, J. R.; Beard, H. A.; Bayana, M. E.; Jolley, K. E.; Warriner, S. L.; Bon, R. S., *Beilstein J. Org. Chem*., **2016**, *12*, 2019–2025.

[141] Zhu, H.; Zhang, S. B.; Liu, X.; Cheng, Y.; Peng, H. Y.; Dong, Z. B., *Eur. J. Org. Chem*., **2018**, 5711–5716.

[142] Katz, L., *Am. Chem. Soc.*, **1951**, *73*, 4007–4010.